To the Graduate Council:

We are submitting herewith a thesis written by Weiju Ren entitled "Time-Dependent Fracture Mechanics Characterization of Haynes HR160 Superalloy". We have examined the final copy of this thesis for form and content and recommend that it be accepted in partial fulfillment of the requirements for the degree of Doctor of Philosophy, with a major in Metallurgical Engineering.

Peter K. Liaw, Thomas T. Meek, Chairpersons

We have read this thesis
and recommend its acceptance:

Charlie R. Brooks

Carl J. McHargue

John D. Landes

Accepted for the Council:

Associate Vice Chancellor
and Dean of The Graduate School

TIME-DEPENDENT FRACTURE MECHANICS CHARACTERIZATION OF HAYNES HR160 SUPERALLOY

A Dissertation

Presented for the

Doctor of Philosophy

Degree

The University of Tennessee, Knoxville

Weiju Ren

May 1995

DEDICATION

Two awards have been granted to the published papers extracted from this dissertation

Outstanding Student Award

from the International Precious Metals Institute, Inc.

and

ASME 95 PVP International Student Paper Competition Finalist Award

from the American Society of Mechanical Engineers Pressure Vessels and Piping Division

This dissertation and the honors granted to this dissertation

are hereby

dedicated to my parents

Mr. Boli Ren

and

Mrs. Yongcui Li

who gave me invaluable educational opportunities

during the difficulty days of their lives

ACKNOWLEDGMENTS

I would like to express my sincere gratitude to my advisors, Dr. Peter K. Liaw for his guidance and help, and Dr. Thomas T. Meek for his constant concerns and encouragement, during the process of this research. I would like to thank senior research staff Mr. Robert W. Swindeman and Dr. Brian G. Gieseke, of the Metals and Ceramics Division, Oak Ridge National Laboratory (ORNL), and Dr. George Y. Lai, group leader of the High Temperature Alloys, Haynes International Inc., for their help with my conducting the experiments. I would also like to thank my other committee members, Dr. Carl J McHargue, Dr. Charlie R. Brooks and Dr. John D. Landes for their friendly advice and consultation in preparing the proposal for this investigation.

My thanks also go to the SURA/ORAU/ORNL Summer Cooperative Program, Division of Materials Science, Department of Energy, and the Scholarly Activities Incentive Fund (SAIF) of the University of Tennessee, Dr. Joseph E. Spruiell, head of the Materials Science and Engineering Department and Dr. Carl J. McHargue, director of the Materials Processing Center, the University of Tennessee, Dr. George Y. Lai, group leader and Dr. D. Klarstrom, vice president of technology of Haynes International Inc., for their financial support; Mr. Michael Tuck, the Manager, and his coworkers, Michael Pelfrey and Ernie Webb, of the Manufacturing Demonstration Center, Y-12 Plant of ORNL, for their assistance in machining my specimens; Dr. Charles Brinkman, group leader of the creep laboratory of ORNL, for allowing me to conduct testing in his laboratory; Mr. Hurley Upton for his help in the creep experiment, and many other creep laboratory staff members of ORNL for their constant help whenever I needed; Mrs. Shelly X. Ren, my lovely wife, for her much wise advice and help with my computer programming and microstructural analyses; Dr. C. T. Liu for allowing me to use his equipment; and Professor A. Saxena for many constructive comments and suggestions during the course of this investigation.

The author is indebted to many professors, staff members and his fellow graduate students in the Department of Materials Science and Engineering, the University of Tennessee, and to many staff members of the Oak Ridge National Laboratory for their generous support and encouragement in the pursuit of this degree.

ABSTRACT

The time-dependent fracture mechanics properties of HAYNES® HR160™ at temperatures up to 950°C (1742°F) were investigated for the next generation of fossil energy systems. The material characterization with the time-dependent fracture mechanics parameters were studied under different testing conditions such as temperature, load level and specimen size; different material conditions such as heat, the as-received, coarse grain size, aged and welded conditions; different fatigue conditions such as with and without various hold times. The creep crack and creep-fatigue crack propagation mechanisms were studied through microstructural characterizations. Theoretical modeling was conducted on the dynamic process of creep crack propagation.

The results show that creep crack propagation rate can be uniquely correlated to the time-dependent fracture mechanics parameter, $C^*(t)$, in the form of $da/dt = A[C^*(t)]^q$. This correlation is independent of temperature, load level, and specimen size. Desired data can be obtained by manipulating these parameters to save testing time and materials. Under the conditions of this study, the creep crack propagation rate of HR160 is not affected by heat difference, grain coarsening and aging, but increased approximately 15 times by welding, which causes a casting structure lack of creep ductility in the material.

The creep-fatigue crack propagation behavior was successfully correlated to the creep crack propagation behavior. The creep zone at the crack tip was found to accumulatively expand during the hold time, and the average value of $C^*(t)$ was proposed for characterizing the creep-fatigue crack propagation rate beyond the accumulative transition time. Decreasing hold time during creep-fatigue tests increases the average crack propagation rate. Therefore, increasing shut-downs or stress fluctuations in high temperature components decreases their lives.

Microstructural analyses show that creep cracks propagate mainly in an intergranular mode by the coalescence of creep cavities which occur along grain boundaries and twin boundaries. Load cycling causes a transgranular crack propagation mode within the creep zone, induces a mixed intergranular and transgranular crack propagation, and increases the total crack propagation rate.

A model has been established to show that the creep crack propagation rate depends on the creep rate at the crack tip, the creep zone geometry and the rupture strain of the material. The rate estimation number, R_{en}, has been introduced and uniquely correlated to the minimum creep rate. The q' in this correlation is numerically close to the q in the da/dt versus C*(t) relationship for superalloy HR160 and can be used as a reference for q when long-term test results are predicted from short-term tests.

TABLE OF CONTENTS

LIST OF TABLES

LIST OF FIGURES

NOMENCLATURE

Term	Description
A	Coefficient of $C^*(t)$ (mm/hr)$(m^2 \cdot hr/kilo\ joules)^q$
A_1	Primary creep coefficient $(MPa^{-n_1(1-p)} \cdot hr^{-1})$
A_2	Secondary creep coefficient $(MPa^{-n} \cdot hr^{-1})$
a	Crack length (mm)
$\dot{a}$	Creep crack growth rate, da/dt, (mm/hr)
a_h	Half crack length (mm)
a_o	Initial crack length (mm)
B	(1) Thickness of the cracked body specimen (mm) (2) Dimensionless coefficient of rupture strain versus minimum creep rate equation
B_N	Net specimen thickness, distance between the roots of the side grooves in side-grooved specimens (mm)
C	(1) Elastic compliance (2) Fatigue coefficient $(mm)/(MPa.m^{1/2})^{n_f}$
C^*	Path-independent integral characterizing the crack tip singularity under extensive secondary creep conditions $(kJ/m^2 \cdot hr)$
C_h^*	Stress-dependent part of the path-independent integral $C^*(t)$ under extensive pure primary creep conditions $(kJ/m^2 \cdot hr)$
C_s^*	The value of C^* when the pure secondary creep condition is emphasized $(kJ/m^2 \cdot hr)$
C_t	Instantaneous stress-power input uniquely related to the rate of expansion of the creep zone size under small-scale creep conditions $(kJ/m^2 \cdot hr)$

$C(t)$	Integral with the path within the crack tip creep zone characterizing the crack tip singularity under small-scale creep conditions ($kJ/m^2 \cdot hr$)
$(C_t)_{ssc}$	The value of C_t when small-scale creep condition is emphasized ($kJ/m^2 \cdot hr$)
D	(1) Plasticity coefficient (MPa^{-m}) (2) Material constant for rupture time equation
D_b	Grain boundary diffusion constant (cm^2/s)
$\left(\frac{da}{dt}\right)_{avg}$	Average creep-fatigue crack growth rate (mm/hr)
$\left(\frac{da}{dN}\right)_m$	Measured creep-fatigue crack growth rate (mm/cycle)
$\left(\frac{da}{dN}\right)_{tr}$	Fatigue crack growth rate under triangular waveform loading (mm/cycle)
ds	Increment of the contour path (mm)
E	Young's Modulus (MPa)
e	Engineering strain
e_c	Critical strain
e_r	Rupture strain
$\dot{e}$	Engineering creep strain rate (1/hr)
F	K-calibration factor, $F = (K/P)BW^{1/2}$
F'	a/W derivative of K-calibration factor F, $F' = dF/d(a/W)$
h_1	Function of a/W and strain-hardening exponent, m
I_n	Dimensionless factor dependent upon n in expressions for the crack tip stress field under extensive secondary creep condition
I_{n_1}	Nondimentional factor dependent upon n_1
J	Path-independent integral under nonlinear elastic or equivalent conditions ($kN \cdot m/m^2$)

ΔJ_c	Time integral of C* or J* over the hold time (t_h) of a trapezoidal waveform ($kN \cdot m/m^2$)
ΔJ_f	Cycle-dependent integral associated with time-independent plasticity ($kN \cdot m/m^2$)
ΔJ_T	Total J-integral consisted of $\Delta J_c + \Delta J_f$ ($kN \cdot m/m^2$)
J_p	Fully plastic component of the J-integral ($kN \cdot m/m^2$)
K	Stress intensity factor ($MPa \cdot m^{1/2}$)
K_{eff}	Effective stress intensity factor ($MPa \cdot m^{1/2}$)
ΔK	Range of stress intensity factor ($MPa \cdot m^{1/2}$)
k	Boltzmann's constant (1.38×10^{-23} J/°C)
m	Strain-hardening exponent
m'	Cyclic strain-hardening exponent
N	Number of fatigue cycles
n	Secondary creep exponent
n_1	Primary creep exponent
n_f	Fatigue exponent
P	Applied load (N)
ΔP	Applied load range in a fatigue test (N)
p	Primary creep exponent
q	Exponent of C*(t)
q'	Exponent of the rate estimation number R_{en}
r	Distance form the crack tip in a polar coordinate system (mm)
r_c	The size of the process zone at the crack tip (mm)
R_{en}	Rate Estimation Number ($watt/m^3$)
s	Engineering stress, nominal stress (MPa)
$\dot{s}$	Applied engineering stress rate (MPa/hr)

T	Temperature (°C)
T_i	Outward traction (stress) vector acting on the contour around the crack
t	Time (hr)
t_h	Hold time at maximum load in trapezoidal loading waveform (s)
t_{pl}	Factor added to account for retardation in the creep zone expansion rate due to cyclic plasticity
t_r	Rupture time (s)
t_T	Transition time from small-scale creep to extensive creep (hr)
t_{TP}	Transition time from small-scale primary creep to extensive primary creep (hr)
t_2	Time of transition from extensive primary creep to extensive secondary creep (hr)
U^*	Power or energy input rate into the cracked body (watt/m^2)
u_i	Displacement vector
$\dot{u}_i$	Displacement rate vector
$\dot{V}$	Loadline deflection rate (mm/hr)
$\dot{V}_c$	Loadline deflection rate due to creep (mm/hr)
ΔV_c	Loadline deflection due to creep during the hold-time period (mm/hr)
W	Width of the compact-tension specimen (C(T) specimen) (mm)
w	Half width of the crack in the grain boundary separation model (mm)
W_s	Strain energy at a crack tip per unit volume due to loading (J/m^2)
W_s^*	Strain energy rate per unit volume (watt/m^2)
$W^*(t)$	Instantaneous strain energy rate per unit volume (watt/m^2)
x, y, z	Cartesian coordinates
y_o	Half of the distance between two output electric potential leads on a C(T) specimen (mm)

α	(1) Dimensionless constant dependent on n
	(2) Growth rate of the fingers in diffusive separation model (mm/hr)
β	(1) Constant depending on cavity conditions in cavity coalescence model
	(2) Scaling factor in diffusive separation model
$\dot{\gamma}_c$	Rate of the expansion of creep zone size
$\tilde{\dot{\gamma}}_c(\theta)$	Dimensionless function defining creep zone shape
γ_s	Surface free energy (J/m^2)
Γ	Counter-clockwise contour of the integral which encloses the crack tip
Γ_s	Counter-clockwise contour of the integral which encloses the crack within the crack tip creep zone
δ	Output electric potential of C(T) specimen (μV)
δ_b	Width of grain boundary diffusion path (m)
δ_o	Initial output electric potential of C(T) specimen (μV)
ε_A	Average creep deformation rate
ε_f	Failure strain, creep ductility
ε_{ij}	Strain tensor
$\dot{\varepsilon}_{ij}$	Strain rate tensor
$\tilde{\dot{\varepsilon}}_{ij}(\theta;n)$	Dimensionless strain rate angular distribution
$\dot{\varepsilon}_o$	Material constant at constant temperature
ε_{of}	Creep ductility at σ_o
η	A function of crack length, exponent on stress in Norton's creep equation and specimen geometry
θ	Angular coordinate in polar coordinate system at the crack tip
ν	Poisson's ratio
ρ	Cavity size (μm)

$\dot{\rho}$	Cavity size growth rate (μm/s)
σ_a	Applied remote stress (MPa)
σ_x, σ_y	True stresses in x and y directions (MPa)
σ_{ij}	Stress tensor
$\tilde{\sigma}_{ij}(\theta;n)$	Dimensionless stress angular distribution
σ_{YS}^c	Cyclic yield strength determined as the stress amplitude ($\Delta\sigma/2$) corresponding to a plastic strain amplitude ($\Delta\varepsilon_p/2$) of 0.2%
σ_o	Material constant at constant temperature
τ	Specimen-dependent function for fully plastic integral calculations
τ_{xy}	Shear stress on xy plane (MPa)
υ	Material constant in rupture time equation
ϕ	Function relating cavity growth rate to the stress
Ω	Atomic volume (m^3)

CHAPTER I

INTRODUCTION

At present, a majority of fossil energy systems and chemical and petroleum plants throughout the world have reached their designed service lives of 30 to 40 years [1-26]. In the fossil energy generation industry, while many of these systems are, and will still be in operation because of economic considerations, the design of the next generation of fossil energy systems is gradually coming into consideration. With all the achievements and rapid developments in sciences and engineering after the World War II, the expertise and technologies available for such tasks are obviously very different from those employed decades ago. This is also true about the requirements and design philosophy for the new generation of fossil energy systems. In order to increase efficiency, the operating temperatures will be greatly increased. In some components, such as heat exchangers, turbine blades, steam headers and turbine rotors, the temperatures are expected to be raised to around 1000°C (1832°F), almost doubling the conventional operating temperatures of approximately 538°C (1000°F), at which many of the current systems are running. The corrosion resistance of the new energy systems is also required to be much higher than that of the current ones in order to stand dirty environments, cut down the fuel cost and survive the worsening energy crisis. Furthermore, the designed service lives of the new components are demanded to be long and accurately predicted. To meet these requirements, a very decisive step is to choose the right materials of construction.

The research presented herein is a part of the efforts at selecting the materials for the next generation of fossil energy systems. The candidate material studied in this investigation was HAYNES® HR160™, a Ni-Co-Cr-Si superalloy newly developed and

introduced into the marketplace by Haynes International, Inc.. **The first goal of this research was to study the mechanical behavior of HR160 at elevated temperatures and provide a sound database for the material selection campaign.**

The requirements for the database needed for such a selection depend mainly on the design philosophy. One of the most important changes in recent decades in the design philosophy for pressure vessels and piping operating at elevated temperatures is that the occurrence of cracks in a component is no longer considered to be the end of the component's life.

During their long-term service periods, components of fossil energy systems inevitably become aged at elevated temperatures. Their microstructures and chemical properties become degraded. Creep damage gradually deteriorates their mechanical properties. Eventually, microcrack initiation can be induced by the accumulation of creep deformation damage in stress concentration areas. On the other hand, pre-existing flaws, such as microcracks, are commonly found in engineering materials. These pre-existing microcracks may result from crystal or material processing defects. The resulting stress concentration at these microcrack tips may induce localized creep deformation when exposed to elevated temperatures even under very low applied load levels. As time elapses, these microcracks may grow by a process of coalescence of creep cavities near crack tips. Because this process can occur for the combinations of temperature and net section stress where creep would not normally be of concern, conventional designs based upon creep rupture data may not be suitable.

It has been realized that although cracks can pre-exist and initiate in a component during its service at elevated temperatures, a large portion of the component's life may be spent in crack propagation [27]. Today, in the energy generation industry, many components are still operating safely with cracks nucleating and propagating at elevated service temperatures because of the development of this new concept of service life. The

recognition of the time a component spends in creep crack growth as a portion of the service life obviously brings great economic benefits to the power generation industry.

However, this concept of service life has also raised serious concerns about the safety of such systems. With this concept, the lives of elevated-temperature structural components often depend on their crack growth rates [28, 29]. Most failure of these components resulted from the rupture that occurred when the cracks had grown to a critical size. Failure in these components usually cause a great loss of human lives and millions of dollars. For more than 19 years, efforts have been made to develop a life prediction methodology to cope with this problem. This methodology, based on characterizing with different parameters the stress field, strain rate field and the stress-power dissipation rate at the tips of cracks introduced by creep damage accumulation or the combination of creep and fatigue damage accumulation, is expected to estimate the propagation rate of the cracks, and thus, help establish the correct inspection intervals and predict the life of the component. Several time-dependent fracture mechanics parameters have been proposed for this purpose. The development of this methodology makes the data pertaining to time-dependent fracture mechanics become important parameters for high-temperature life prediction analyses. The candidate material, HAYNES® HR160™, newly introduced into the marketplace, is not provided with these data which are very important for the changed design philosophy. The present research has focused on studying the time-dependent fracture mechanics properties of this candidate material, meanwhile, it has provided a good opportunity for investigating the proposed time-dependent fracture mechanics parameters and the life prediction methodology. **To reach the second goal of this investigation, the application of some proposed time-dependent fracture mechanics parameters has been studied under various testing conditions.** The time-dependent fracture parameters were applied to a high alloy for the

first time and verified within a higher temperature range than ever did before with testing condition variations in temperature, static loading level and sample size.

In addition to the deterioration caused by creep phenomenon, the structural materials operating at elevated temperatures also suffer from fatigue damage. As a matter of fact, fossil energy systems are rarely operated under steady-state conditions for extended periods of time. Many factors, such as the fluctuations of demands for energy, shut-downs for safety inspections, etc., can introduce a thermal-mechanical fatigue process in the components. This further complicates the situation because the fatigue processes can induce a redistribution of crack-tip stresses and affect the creep zone growth behavior [30], and it can also change the creep crack propagation mechanisms [31]. Attempts have been made to correlate the material behavior under creep-fatigue conditions to experimental and analytical results obtained under creep conditions. It has been shown that for the creep-ductile materials, reasonable results have been obtained for such a correlation. However, more experimental data are needed from different materials before such a correlation method can be confirmed and generalized. **The third goal of this research was to study the creep-fatigue crack propagation behavior of HR160 and its relationship with the creep crack propagation behavior.**

It is well known that the properties of a material depend on its microstructure and chemical composition. These factors can be changed during material processing or service aging. The major subject studied in the materials science and engineering can be briefly described with the "relationship triangle" of structure, property and behavior. The approaches adopted in this research for studying these changes followed this triangle principle. In this research, mechanical properties such as tensile, creep deformation, creep rupture, creep crack growth rate and creep-fatigue crack growth rate of HR160 have been tested and a database of these properties has been established at different temperatures and stress levels. To investigate the effects of structures on these

mechanical properties, several treatments have been conducted to change the microstructure of this material. Beside the as-received condition, the material has been tested under conditions of different heats, aging, coarse grain size and welding. Therefore, **as the fourth goal of this research, the effects of material treatments and chemical composition on the time-dependent fracture mechanics behavior of HR160 were studied through the comparison of the properties under these different material conditions.**

The fifth goal of this research was to study the creep crack and creep-fatigue crack propagation mechanisms of HR160 and understand the relationship between the microstructures and the properties. Some of the tested samples have been characterized with microanalysis techniques such as optical microscopy (OP), scanning electron microscopy (SEM), and X-ray diffraction (XRD). These analyses have provided a fundamental understanding of the mechanisms of the material behavior and the relationship between the properties and microstructures introduced through different material treatments. With this fundamental understanding of the mechanisms, properties and structures, the behavior of this candidate material can be predicted with confidence.

In studying a dynamic process such as creep crack propagation, theoretical modeling is usually desired because it simulates the process mathematically, and if a model is correctly established, it provides a mechanistic understanding of the process under investigation. Furthermore, in the case of creep crack propagation, testing can be very time consuming, modeling may provide new methods to save the experimental time and materials. In this research, attempts have been made to model and predict some material behavior at elevated temperatures. **This was the sixth goal: conducting theoretical modeling and predicting the material behavior at elevated temperatures.**

This research has provided us with a sound database of mechanical properties of HR160 at elevated temperatures, an in-depth understanding of the proposed time-

dependent fracture mechanics parameters, useful knowledge of the properties and material treatments of HR160, an insight of the relationship between the microstructures and properties of HR160, and finally, some useful modeling equations for understanding and predicting the material behavior. These results can not only facilitate the material selection campaign for the next generation of fossil energy systems, but also contribute to the development of the time-dependent fracture mechanics and the life prediction methodology, which is highly desirable for the determination of the remaining lives of the structural components of many aged fossil energy systems still in operation. In addition, the database generated through this research will benefit the nuclear energy generation industry, chemical processing industry and waste incineration industry where superalloy HR160 can find its vast applications.

CHAPTER II

LITERATURE REVIEW

This research has involved the investigation of the mechanical properties of Haynes superalloy HR160, characterization of cracked bodies, life prediction methodology, microstructure analysis of crept materials and theoretical modeling of creep crack propagation process. The literature review has been conducted in these areas.

Because a significant number of symbols are encountered in the literature regarding these areas, especially the characterization of cracked bodies, each symbol will only be defined or explained the first time it appears in order to reduce the volume of this dissertation. All the symbols used in this review are listed in the nomenclature for reference.

2.1 High-Temperature Corrosion Resistant Superalloy HAYNES® HR160™

The material selected for this research, HAYNES® HR160™ superalloy, is one of the newly commercialized superalloys designed for high-temperature and corrosive-environment applications [32]. There are a limited number of engineering alloys that can resist high-temperature corrosion attack in "dirty" environments commonly found in chemical processing, waste incineration, and fossil energy industries. These environments have a strong potential for sulfidation, chloride attack, carburization and oxidation. Stainless steels, iron-nickel-chromium alloys, and nickel-base alloys are commonly used for these applications. These alloys have limitations, especially in environments where both sulfidation and chloride attack are operating. High nickel-containing alloys are generally not good in sulfidizing environments because of the formation of low-melting point nickel sulfide eutectics. Iron-based alloys, on the other

hand, perform poorly in chloride or chlorine-bearing environments because of the formation of highly volatile iron chlorides, particularly, $FeCl_3$. These limitations in corrosion resistance, combined with the stress effects at elevated temperatures, such as creep deformation and creep-fatigue damage, are most likely to induce crack initiation and propagation in these materials.

The proposed material, HAYNES® HR160™, is a new solid-solution-strengthened, high-temperature alloy which is very resistant to both sulfidation and chloride attack over a wide temperature range. This alloy is based on a Ni-Co-Cr-Si system. The nominal chemical composition in weight percent is shown in Table 2.1-1.

The combination of high chromium and silicon in HR160 forms a very protective surface scale. Cobalt as a matrix element also enhances sulfidation resistance. Nickel imparts resistance to chloride attack and carburization, and at 37 weight percentage, does not adversely affect sulfidation resistance due to the high chromium and silicon. The alloy also attributes the good resistance to chloride attack to its low iron content. The high level of combined cobalt and nickel yields a stable austenitic structure with good thermal stability. With such composition, HR160 is extremely resistant to high-temperature corrosion attack in environments containing sulfur, chlorine, vapors of chlorides and sulfates, chloride and sulfate deposits and ash deposits, such as those found in coal combustion and conversion, chemical processing, waste incineration and others. Both laboratory and field tests have shown that in different corrosive gas mixtures and various industrial environments containing both chlorine (chloride) and sulfur which are commonly found in coal-fired boilers, petrochemical processes, fuel furnaces and many other conditions, HR160 is significantly better than many current commercial alloys. In many cases, it outperformed some current alloys by a factor of 10 in corrosion resistance. The detailed information about corrosion resistance properties of HAYNES® HR160™ can be found in reference [32].

Table 2.1-1 Nominal Composition (wt%) of Haynes HR160

Ni	Co	Cr	Fe	Si	Mn	Ti	C	Mo	W	Cb
Bal	30	28	3.5	2.75	0.5	0.5	0.05	1.0*	1.0*	1.0*

* maximum

Metallurgically, HAYNES® HR160™ has a stable austenitic structure and exhibits no sigma or mu phases after long-term aging. In the annealed condition, the alloy exhibits a clean microstructure. X-ray diffraction analysis of an annealed sample showed TiN phases with some $Cr_{23}C_6$. The grain size typically varies from ASTM No. 1 to No. 4 for sheets, plates and bars. The alloy is non-magnetic in both annealed and cold-worked conditions.

The thermal stability is indicated by room temperature tensile elongation before and after aging for 8000 hours at 870°C (1600°F) causing only a decrease from 68% to 20%. Electrolytically extracted residues obtained from an aged sample indicated that during long-term aging at 870°C (1600°F), the precipitated phases formed were $Cr_{23}C_6$ (major) and G phase (medium). The G phase is $N_{16}Ti_6Si_7$. The morphologies of both carbides and G phases are similar under an optical microscope. Thus, G phase is not considered to be more detrimental than carbides in causing ductility drop upon long-term aging.

Some basic mechanical property data of HR160 can be found in reference [32]. The creep-rupture data can be well fit by the Larson-Miller Parameter (LMP) equation as:

$$LMP = T(14.1 + \log t)/1000 \qquad (2.1\text{-}1)$$

where, T = temperature (°R)

t = time

The creep deformation data plotted as stress versus minimum creep strain rate in logarithm in form show that the isothermal line fittings are straight and essentially parallel until 980°C (1800°F) when slight divergence begins to occur [32].

2.2 Characterization of a Cracked Body

2.2.1 Brief Introduction

The main purpose of fracture mechanics is to predict the behavior of cracks in cracked bodies. In order to do this, the first step is to be able to correctly describe the state of the object, i.e., to characterize the mechanics of a cracked body with appropriate correlating parameters, and relate these parameters to quantities which can be measured experimentally in specimens, and then, conduct experiments to obtain data for these measurable quantities. With the correlating parameters and the experimental results from the specimens, the behavior of the cracks in the cracked body can be predicted.

In this process, the first step, to determine the appropriate correlating parameters, is the most important one. Tremendous efforts have been devoted to this area and many references can be found in the literature.

In order to accurately characterize the crack in a cracked body and predict its behavior, fracture mechanics has been divided into several categories according to the conditions the cracked body is subjected to and the response of the cracked body to these conditions because under different conditions, the state of a cracked body and its response to the imposed conditions are different.

From the "time" point of view, the mechanics of a cracked body is briefly divided into two categories: time-independent and time-dependent fracture mechanics. Time-independent fracture mechanics deals with the mechanical behavior of a cracked body relatively independent of time. Crack behavior under elastic and plastic conditions falls into this category. In contrast, time-dependent fracture mechanics deals with the mechanical behavior of a cracked body as a function of time. Crack behavior under anelastic conditions, such as creep, belongs to this category. Creep is a phenomenon commonly found in the components of fossil energy systems.

From the "load" point of view, the fracture mechanics can be divided into static and cyclic loading categories. Under static loading conditions, the load is kept constant as time elapses, while under cyclic loading conditions, the constant load is periodically interrupted by unloading and reloading.

Static and cyclic loadings are common phenomena in fossil energy systems and other engineering structures. For a fossil energy system, a long-term operation with a constant pressure and temperature is a case of static loading, and periodic shut-downs for safety inspections or fluctuations of pressure and temperature due to changes in output energy demands can be considered as an example of cyclic loading. The interruption of a constant load in such a case usually induces changes in a cracked body's response to the working conditions and also in the accumulated damage of the cracked body.

Since this research was devoted to evaluating HR160 as a candidate material for the next generation of fossil energy systems which would operate at elevated temperatures and be subject to fluctuations of temperature and pressure for the reasons mentioned above, the mechanics part of this survey emphasizes on the time-dependent fracture mechanics under both static and cyclic loading conditions. The time-independent fracture mechanics is only briefly addressed.

According to the relative directions of the applied stress and the crack surfaces, a crack can be in the crack-opening, the forward shear and the parallel shear modes represented by Mode I, II and III, respectively. The crack-opening mode, mode I, is the most commonly found one in engineering applications [33].

2.2.2 Time-Independent Fracture Mechanics

Two important parameters have been developed for the time-independent fracture mechanics: the linear elastic stress intensity factor K and the path-independent integral J. They apply to elastic and plastic conditions respectively.

When a cracked body is being loaded slightly or upon being loaded heavily, the response of the material is mainly elastic, and the stress field at the crack tip can be described by:

$$\sigma_x = \frac{K}{\sqrt{2\pi r}}\left[\cos\frac{\theta}{2}\left(1-\sin\frac{\theta}{2}\sin\frac{3\theta}{2}\right)\right]$$

$$\sigma_y = \frac{K}{\sqrt{2\pi r}}\left[\cos\frac{\theta}{2}\left(1+\cos\frac{\theta}{2}\sin\frac{3\theta}{2}\right)\right] \qquad (2.2\text{-}1)$$

$$\tau_{xy} = \frac{K}{\sqrt{2\pi r}}\left(\sin\frac{\theta}{2}\cos\frac{\theta}{2}\cos\frac{3\theta}{2}\right)$$

where, σ_x = true stress in x direction

σ_y = true stress in y direction

τ_{xy} = shear stress on xy plane

K = the stress intensity factor which relates the stress field at the crack tip to the nominal stress applied to the cracked body.

r = distance from the crack tip in a polar coordinate system

θ = angular coordinate in a polar coordinate system at the crack tip

K is defined as:

$$K = \alpha s\sqrt{\pi a_h} \qquad (2.2\text{-}2)$$

where, α = parameter that depends on the geometry of the cracked body and the crack.

s = nominal stress

a_h = the half crack length.

When the cracked body is heavily loaded so that plastic deformation at the crack tip becomes significant, as is usually in case of low-strength ductile materials, the crack tip state is better described by the path-independent line integral J [34] [35], which is related to the energy in the vicinity of a crack and defined as:

$$J = \int_{\Gamma}\left(W_s dy - T_i \frac{\partial u_i}{\partial x} ds \right) \qquad (2.2\text{-}3)$$

where,

J = path-independent integral under nonlinear elastic or equivalent conditions

W_s = strain energy per unit volume due to loading, $W_s = \int_0^{\varepsilon_{ij}} \sigma_{ij} d\varepsilon_{ij}$

σ_{ij} = stress tensor

ε_{ij} = strain tensor

Γ = counter-clockwise contour of the integral which encloses the crack tip

T_i = outward traction (stress) vector acting on the contour around the crack

u_i = displacement vector

ds = increment of the contour path

x, y = the rectangular coordinates

It is obvious that J is a calculation of the energy input in the crack tip area enclosed by Γ.

The stress intensity factor (K) contains the information of the nominal stress and the geometry of the cracked body, while J is the energy input in the crack tip area. For materials of interest, critical values, K_{Ic} and J_{Ic}, independent of specimen geometry are determined experimentally, above which rupture is to occur.

2.2.3 Basic Concepts of Time-Dependent Fracture Mechanics

At elevated temperatures, materials experience time-dependent anelastic deformation called creep even though they may be loaded at a stress far below the yield stress at such temperatures. At a given temperature, the higher the stress, the more severe the creep deformation. When a cracked body is loaded at elevated temperatures, creep deformation begins to occur at the crack tip because of the stress concentration. As time elapses, creep deformation accumulates, the stress at the crack tip relaxes and the creep zone expands outwards. Since the deformation is of anelastic nature as a function of time, such behavior can not be described by time-independent elastic or plastic fracture mechanics any more. More appropriate methods should be used to deal with such cases. For more than 19 years, efforts have been made to develop a methodology based on time-dependent fracture mechanics to predict the crack behavior in such a situation. Because many factors are involved in these cases, and several concepts and parameters have been introduced to describe the phenomena, furthermore, these concepts and parameters have been evolving over years of development, confusion some times happens even among professional researchers, causing misuse of equations [36]. Therefore, it is necessary herein to review some basic concepts involved in this area.

The Scale of a Creep Zone

The scale of a creep zone can be divided into three regimes according to the relative sizes of the zone and the uncracked ligament in the body[37]. When the creep zone size is small in comparison to pertinent body dimensions, the small-scale creep (SSC) is said to exist. This is an analogy to small-scale yielding in linear elastic fracture mechanics. When the creep zone has expanded through the entire remaining uncracked ligament, the extensive creep (EC) condition is considered to exist. The situation where the creep zone size is between those of small-scale creep and extensive creep conditions

is called the transition creep condition (TC). These conditions are schematically shown in Figure 2.2-1.

The Level of Load

The level of load can also be divided into three regimes according to the response of the loaded body. When elastic deformation occurs upon loading, the elastic loading (EL) condition is said to exist. When a large plastic zone appears, the plastic loading (PL) condition is considered to be present. The situation between these two is called the elastic-plastic (EL-PL) condition.

The Stage of Creep Deformation

The creep deformation under static loading can be divided into three regimes according to the creep rate variation in a creep strain versus time plot developed from a constant load creep deformation test. The first portion of high creep rate in the curve is defined as the primary creep (PC). This portion is usually small in the curve. For some materials this portion may not exist. The second portion of the curve, the part with minimum creep rate, is called the secondary creep (SC) or minimum rate creep. This is usually the largest portion of the curve, and thus, the most important part of the curve. The third portion is the tertiary creep. In many materials, this occurs when rupture is about to take place and therefore, the time duration is generally short. These three portions are presented in Figure 2.2-2.

The Combination of the Conditions

All the conditions discussed above are summarized in Table 2.2-1. In this review, the scale of a creep zone, the level of load and the stage of creep deformation are numbered as I, II and III, respectively. Each of the three regimes in the scale of a creep

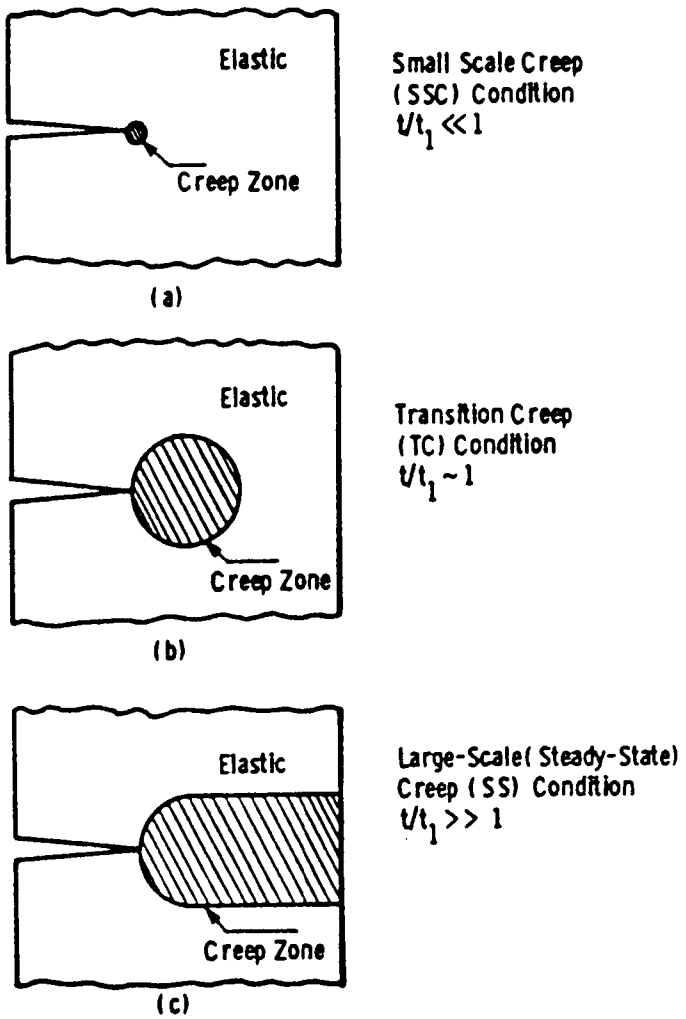

Figure 2.2-1 Schematic of the Scale of Creep Deformation:
a) Small-Scale Creep (SCC); b) Transition Creep (TC);
c) Extensive Creep (EC)

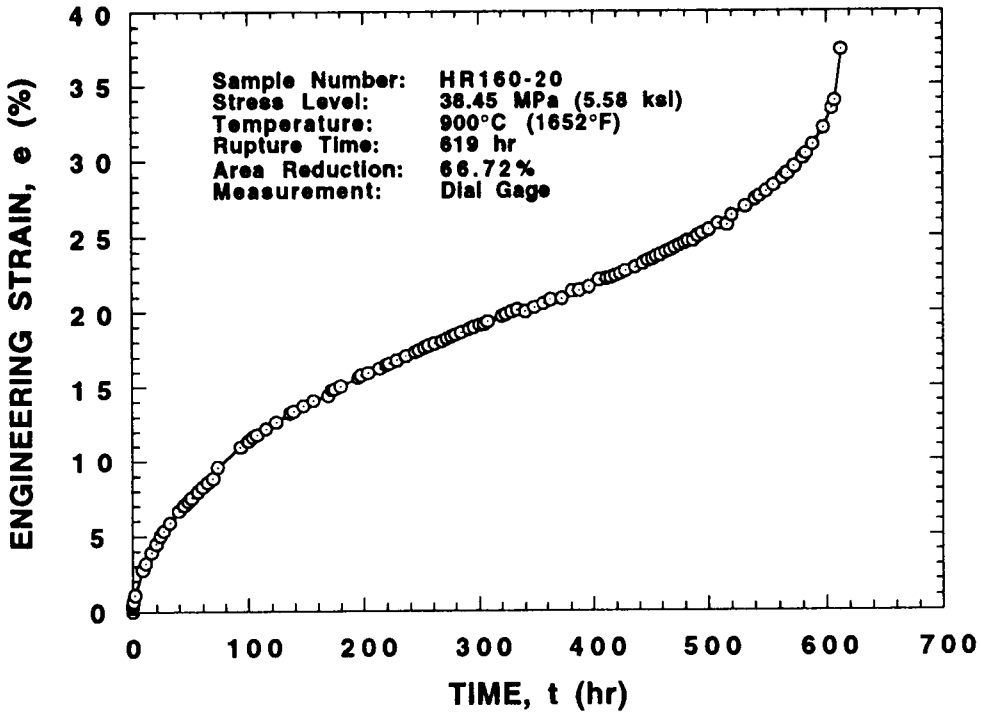

Figure 2.2-2 A Creep Deformation Curve of HR160
Resulting from a Constant Load Test

Table 2.2-1 Summary of the Conditions in the Time-Dependent Fracture Mechanics

I	II	III
Scale of Creep	Level of Load	Stage of Creep Deformation
Small-Scale Creep (SSC)	Elastic Loading (EL)	Primary Creep (PC)
Transition Creep (TC)	Elastic-Plastic Loading (EL-PL)	Secondary Creep (SC)
Extensive Creep (EC)	Plastic Loading (PL)	Tertiary Creep (TC)

zone, the level of load and the stage of creep deformation may combine with one another and complicate the situation. Therefore, before any discussions, the condition equation in the form of I-II-III will be clearly identified. For example, we may have a situation with I = extensive creep scale, II = elastic-plastic loading and III = secondary creep deformation, i.e., EC-EL-PL-SC conditions, or I = transition creep scale, II = either elastic or plastic loading and III = primary creep deformation, i.e., TC-II-PC conditions. The condition number II is put in for the conditions which are not specified.

Beside these basic concepts, the terms, large-scale creep and steady-state creep, also frequently appear in literature. Large-scale creep usually is an alternative term for extensive creep. Steady-state creep often refers to the situation where a fully developed creep stress distribution has been produced around the crack tip [38]. This concept is frequently not distinguished from the extensive creep in some of the published papers.

Thanks to years of efforts, the behavior of cracked bodies under some of these different conditions has been successfully described with various mathematical models which apply to a number of engineering materials. Because different combinations of these conditions can cause different responses from cracked bodies, and thus, have a great influence on the nature of the solutions for the crack-tip stress and strain rate fields, it is very important that the conditions of interest are clearly identified before a mathematical model is applied or developed.

2.2.4 Time-Dependent Fracture Mechanics Parameters for Static Loading

Creep Constitutive Equation Parameters

To characterize the creep crack behavior in a cracked body, the creep deformation behavior and the relationship among creep strain, stress and strain rate should first be studied. In the stress analysis of cracks in creeping solids under static loading, the most commonly used equation for this relationship is given as the following [36]:

$$\dot{e} = \frac{\dot{s}}{E} + A_1 e^{-p} s^{n_1(1+p)} + A_2 s^n \qquad (2.2\text{-}4)$$

where,

$\dot{e}$	=	engineering creep strain rate
$\dot{s}$	=	applied engineering stress rate
e	=	engineering strain
s	=	engineering stress, nominal stress
E	=	Young's Modulus
A_1	=	primary creep coefficient
p	=	primary creep exponent
n_1	=	primary creep exponent
A_2	=	secondary creep coefficient
n	=	secondary creep exponent

The first term on the right-hand side is due to the elastic strain rate, which is significant only during small-scale creep when the stress redistribution is taking place. Under extensive creep conditions, it can be neglected.

The second term on the right-hand side is due to the primary creep. Under extensive primary creep conditions, Equation (2.2-4) reduces to:

$$\dot{e} = A_1 e^{-p} s^{n_1(1+p)} \qquad (2.2\text{-}5)$$

The third term on the right-hand side is due to the secondary creep. Under extensive secondary creep conditions, Equation (2.2-4) reduces to:

$$\dot{e} = A_2 s^n \qquad (2.2\text{-}6)$$

Coefficients and exponents in Equation (2.2-5) and Equation (2.2-6) can be obtained from creep deformation test results.

C^* Parameter

The conditions for the application of C^* can be expressed as EC-II-SC, i.e., the extensive secondary creep conditions. C_s^* is sometimes used for C^* when the **pure** secondary creep condition is emphasized. Under the extensive creep conditions, the creep strain rate dominates the elastic or plastic strain rate throughout the cracked body, and condition II usually has a negligible effect on the material behavior. Furthermore, under extensive secondary creep conditions, a unique power-law strain rate and stress relationship exists in the cracked body as given in Equation (2.2-6)

The C^* parameter is an analogy of the path-independent J-integral in Equation (2.2-3) used in time-independent fracture mechanics. In Japanese literature, the same parameter is also known as J^*. The fundamental definition of C^* is given by Landes and Begley [39], Nikbin [40], et al. and Taira, et al. [41] as:

$$C^* = \int_\Gamma \left(W_s^* dy - T_i \frac{\partial \dot{u}_i}{\partial x} ds \right) \qquad (2.2\text{-}7)$$

where, C^* = path-independent integral characterizing the crack tip singularity under extensive secondary creep conditions

W_s^* = strain energy rate density, $W_s^* = \int_0^{\dot{\varepsilon}_{mn}} \sigma_{ij} d\dot{\varepsilon}_{ij}$

$\dot{u}_i$ = displacement rate vector

Like the J-integral which is a calculation of the energy input in the crack tip area enclosed by Γ, C^* is a calculation of the energy input rate (power input) in the crack tip area enclosed by Γ, or the stress-power dissipation rate in the cracked body [39].

A method for estimating C^* uses the EPRI (Electric Power Research Institute) Handbook Solution. C^* is indirectly calculated from the material power-law creep constants, A_2 and n, by making use of Equation (2.2-7). For the compact-tension (C(T)) specimens under plain strain conditions, the equation is given as the following:

$$C^* = \frac{A}{(W-a)^n} h_1\left(\frac{a}{W}, n\right)\left(\frac{P}{1.445\zeta B}\right)^{n+1} \qquad (2.2\text{-}8)$$

with

$$\zeta = \left[\left(\frac{2a}{W-a}\right)^2 + 2\left(\frac{2a}{W-a}\right) + 2\right]^{\frac{1}{2}} - \left(\frac{2a}{W-a}\right) - 1 \qquad (2.2\text{-}9)$$

where,

- W = compact-tension specimen width
- a = crack length
- P = applied load
- B = thickness of the cracked body
- h_1 = function of a/W and strain-hardening exponent. Numerical values of h_1 can be found in Reference [42].

C^* can also be interpreted as the energy input rate difference between two identically loaded bodies with incrementally differing crack length (da):

$$C^* = -\frac{1}{B}\frac{dU^*}{da} \qquad (2.2\text{-}10)$$

where, U^* = power input in the cracked body

From Equation (2.2-10), an expression for experimentally measuring C* has been derived as:

$$C^* = \frac{P\dot{V}_c}{B_N W}\eta(n, \frac{a}{W}) \qquad (2.2\text{-}11)$$

where, $\dot{V}_c$ = loadline deflection rate due to creep

B_N = net specimen thickness, the distance between the roots of the side grooves in side-grooved specimens

η = a function of crack length, exponent on stress in Norton's creep equation and specimen geometry

Since the cracked body is under extensive secondary creep conditions and the stress and strain rates of the cracked body are related by Equation (2.2-6), the crack tip stress and strain rate fields can be described with C* as [43, 44]:

$$\sigma_{ij} = (\frac{C^*}{I_n A_2 r})^{\frac{1}{(n+1)}} \tilde{\sigma}_{ij}(\theta; n) \qquad (2.2\text{-}12)$$

$$\dot{\varepsilon}_{ij} = (\frac{C^*}{I_n A_2 r})^{\frac{n}{(n+1)}} \tilde{\dot{\varepsilon}}_{ij}(\theta; n) \qquad (2.2\text{-}13)$$

where, I_n = dimensionless factor [45]

$\tilde{\sigma}_{ij}(\theta; n)$ = dimensionless stress angular distribution [45]

$\dot{\varepsilon}_{ij}$ = strain rate tensor

$\dot{\varepsilon}_{ij}(\theta;n)$ = dimensionless strain rate angular distribution

$C^*(t)$ Parameter

The conditions for $C^*(t)$ can be expressed as EC-II-III, i.e., the extensive primary and/or secondary creep conditions. Tertiary creep is not found to be considered in literature for the $C^*(t)$ parameter. Condition II has little effect on the material behavior due to the domination of the creep strain rate over the elastic or plastic strain rate throughout the cracked body under extensive creep conditions. $C^*(t)$ is the extension of C^* from extensive secondary creep conditions into extensive primary creep conditions. It is defined as:

$$C^*(t) = \int_\Gamma \left[W^*(t)dy - T_i \frac{\partial \dot{u}_i}{\partial x} ds \right] \qquad (2.2\text{-}14)$$

where, $W^*(t)$ = instantaneous stress-power or energy rate per unit volume

It is evident in Equation (2.2-14) that under extensive, pure secondary creep conditions, $W^*(t)$ is replaced by W_s^*, and thus, $C^*(t)$ equals to C^*, as expressed in Equation (2.2-7). Under extensive, pure primary creep conditions, i.e., EC-II-PC, the strain rate and stress relationship in the cracked body is given by Equation (2.2-5). Integrating Equation (2.2-5) in time (t) and substituting the resulting strain (e) back into Equation (2.2-5) yields:

$$\dot{e} = \frac{[A_1(1+p)]^{1/(1+p)}}{(1+p)t^{p/(1+p)}} s^{n_1} \qquad (2.2\text{-}15)$$

To simplify the equation, let:

$$A(t) = \frac{[A_1(1+p)]^{1/(1+p)}}{(1+p)t^{p/(1+p)}} \tag{2.2-16}$$

Equation (2.2-15) has the form:

$$\dot{e} = A(t)s^{n_1} \tag{2.2-17}$$

Equation (2.2-17) resembles Equation (2.2-6) in form except that A_2 and n have been replaced by A(t) and n_1, respectively. The creep coefficient, A(t), in Equation (2.2-17) is a function of time. This means that under extensive primary creep conditions, the time and stress dependence of strain rate in the constitutive law is separable. At a fixed time, $t = t_o$, we have $A(t) = A(t_o)$, and $C^*(t) = C^*(t_o)$, and C(t) has all the features of C^* such as path-independent when integrated with Equation (2.2-14).

Extensive creep conditions are not always associated with pure secondary or pure primary creep. A mixture of primary and secondary creep associated with extensive creep conditions is commonly found. Under such conditions (EC-II-PC-SC), the separable single-value time and stress function as shown in Equation (2.2-17) does not exist any more, therefore, the $C^*(t)$ integral is no longer path-independent. However, it has been shown that an approximation of $C^*(t)$ can still be calculated path-independently with an error of 2% [46].

The value of $C^*(t)$ under extensive primary-secondary creep conditions can also be approximated by the sum of $C^*(t)$ under extensive primary creep conditions and $C^*(t)$ or C^* under extensive secondary creep conditions. The approximation is given as:

$$C^*(t) \approx \frac{C_h^*}{(1+p)t^{p/(1+p)}} + C_s^* \qquad (2.2\text{-}18)$$

where, C_h^* = stress-dependent part of the path-independent integral $C^*(t)$ under extensive primary creep conditions

The first term on the right-hand side is the $C^*(t)$ value under extensive pure primary creep conditions, while the second term is the $C^*(t)$ or C^* value under extensive pure secondary creep conditions. An equivalent expression of Equation (2.2-18) is:

$$C^*(t) \approx [1+(t_2/t)^{p/(1+p)}]C_s^* \qquad (2.2\text{-}19)$$

where, t_2 = time of transition from extensive primary creep to extensive secondary creep

t_2 can be determined as:

$$t_2 = \left[\frac{C_h^*}{(1+p)C_s^*}\right]^{(1+p)/p} \qquad (2.2\text{-}20)$$

As C^* can be experimentally estimated from Equation (2.2-11), $C^*(t)$ can also be measured in test specimens under extensive creep conditions (EC-II-III) with the following equation:

$$C^*(t) = \frac{P\dot{V}_c}{B_N W}\eta(n_1, n, \frac{a}{W}) \qquad (2.2\text{-}21)$$

The only difference between Equation (2.2-11) and Equation (2.2-21) is that in Equation (2.2-21), the function, η, is also a function of the primary creep exponent (n_1) in addition to the secondary creep exponent (n) and the crack size to specimen width ratio (a/W). The expression for η is given as [47]:

$$\eta = \left[\frac{n}{n+1}\frac{t}{t_2} + \frac{n_1}{n_1+1}\left(1-\frac{t}{t_2}\right)\right]\left(\frac{2}{1-a/W} + 0.522\right) \qquad (2.2\text{-}22)$$

It has been shown that for C(T) specimens, the dependency of η on n and n_1 is weak. Therefore, it is recommended that for C(T) specimens, η can be approximated by the following equation [48]:

$$\eta = \frac{n}{n+1}\left(\frac{2}{1-a/W} + 0.522\right) \qquad (2.2\text{-}23)$$

Equation (2.2-23) has been adopted by ASTM standard E1457 entitled "Standard Test Method for Measurement of Creep Crack Growth Rates in Metals"[38].

C_h^* Parameter

The conditions for C_h^* can be expressed as EC-II-PC, i.e., extensive primary creep conditions. It has been shown in Equation (2.2-17) that under extensive primary creep conditions, the time and stress dependence of strain rate in the constitutive law is separable. And also at a fixed time t_o, the $C^*(t)$ integral under extensive primary creep conditions is path-independent. Based on these facts, Riedel defined C_h^* as a path-independent integral [49]. $C^*(t)$ can be formulated with separable single-value time-dependent and stress-dependent functions. C_h^* is the stress-dependent part of $C^*(t)$ under extensive primary creep conditions shown as the following:

$$C^*(t) = \frac{C_h^*}{(1+p)t^{p/(1+p)}} \tag{2.2-24}$$

C_h^* can be determined by the equation:

$$C_h^* = \frac{[A_1(1+p)]^{1/(1+p)}}{(W-a)^{n_1}} h_1\left(\frac{a}{W}, n_1\right)\left(\frac{P}{1.445\zeta B}\right)^{n_1} \tag{2.2-25}$$

C(t) Parameter

The conditions for C(t) can be described as SSC-EL-III, i.e., small-scale, elastic, primary and/or secondary creep conditions. Such conditions are very common at the crack tip of practical engineering structural components. Ohji et al. [50], Bassani and McClintock [51], and Ehlers and Riedel [52] studied the crack tip stress fields under these conditions and defined C(t) integral as the following:

$$C(t) = \int_{\Gamma s}\left(W_s^* dy - T_i \frac{\partial \dot{u}_i}{\partial x} ds\right) \tag{2.2-26}$$

where, Γ_s = counter-clockwise contour of the integral which encloses the crack within the crack tip creep zone

Equation (2.2-26) differs from Equation (2.2-7) in the counter-clockwise contour of the integral. In Equation (2.2-7), the contour of the integral is not limited to the crack tip creep zone. The reason for restricting the integral path within the small-scale creep zone in Equation (2.2-26) is that only in the creep zone, can the creep strain rate dominate the elastic strain rate. Condition II is restricted to elastic loading for C(t) because under

small-scale creep zone conditions, the creep strain rate may not be able to dominate the plastic strain rate since the plastic zone size may be larger than the creep zone size. It is obvious from its definition that in the cases that the creep zone scale changes from small to extensive conditions, i.e., from SSC-EL-III to EC-II-III, C(t) becomes identical to C*(t).

Under SSC-EL-SC conditions, i.e., the small-scale, elastic, secondary creep conditions, for a plane strain case, the value of C(t) can be approximated by the following equation [50-52]:

$$C(t) \approx \frac{K^2(1-\nu^2)}{(n+1)Et} \qquad (2.2\text{-}27)$$

where, ν = Poisson's ratio

Another approximation for C(t) under SSC-EL-SC conditions is given as the following [52]:

$$C(t) = [1 + t_T / t]C_s^* \qquad (2.2\text{-}28)$$

where, t_T = transition time from small-scale creep to extensive creep

t_T is determined as:

$$t_T = \frac{K^2(1-\nu^2)}{E(n+1)C_s^*} \qquad (2.2\text{-}29)$$

Several numerical studies have confirmed that the approximations from Equation (2.2-28) are reasonably accurate [46, 55].

Under SSC-EL-PC-SC conditions, i.e., the small-scale, elastic, primary and/or secondary creep conditions, C(t) can be approximated as follows [46, 53]:

$$C(t) = \left[1 + t_{TP} / t + (t_2 / t)^{p/(1+p)}\right] C_s^* \qquad (2.2\text{-}30)$$

where, t_{TP} = transition time from small-scale primary creep to extensive primary creep

t_{TP} is determined as:

$$t_{TP} = \left[\frac{K^2(1-\nu^2)}{EC_s^*}\right]^{1+p} \frac{1}{1+n_1} \qquad (2.2\text{-}31)$$

Over the range of creep deformation SSC-TC-EC-II-III, i.e., from small-scale creep to extensive creep, Riedel and Ehlers [52] proposed that C(t) can be determined with the sum of the small-scale and extensive creep solutions as the following:

$$C(t) = \frac{K^2(1-\nu^2)}{(n+1)Et} + C^* \qquad (2.2\text{-}32)$$

Analytical work conducted by Riedel and Ehlers [52] and Ohji et al. [50] has shown that like C^* for the EC-II-SC conditions, C(t) can be used to describe the crack tip stress and strain rate fields under the SSC-EL-III conditions:

$$\sigma_{ij} = \left[\frac{C(t)}{I_n A_2 r}\right]^{\frac{1}{(n+1)}} \tilde{\sigma}_{ij}(\theta; n) \qquad (2.2\text{-}33)$$

$$\dot{\varepsilon}_{ij} = \left[\frac{C(t)}{I_n A_2 r}\right]^{\frac{n}{(n+1)}} \tilde{\dot{\varepsilon}}_{ij}(\theta; n) \qquad (2.2\text{-}34)$$

Although C(t) can be applied to small-scale creep conditions and extended to extensive creep conditions, i.e., I-II-III, it has a significant disadvantage. The values of C(t) can only be calculated with the equations given above. It can not be experimentally measured as in the cases of C^* and $C^*(t)$. This greatly limits its applications. Furthermore, the accuracy of the calculated C(t) values significantly depends on the accuracy of the constitutive equations employed for the calculation.

$C_{st}(t)$ Parameter

The conditions for $C_{st}(t)$ can be described as SSC-EL-III plus $t_2 >> t > t_1$, i.e., small-scale, elastic, primary and/or secondary creep conditions during the time shortly after t_1 and long before t_2 is reached. t_1 is the transition time from small-scale primary creep in the elastic field to extensive primary creep conditions. It has been shown by McDowell et al. [54] that in a C(T) specimen C(t) becomes essentially path-independent during this period of time, because a stationary stress field is achieved across the remaining ligament. C(t) under such conditions is defined as $C_{st}(t)$. It can be determined by the following equation:

$$C_{st}(t) = [1 + (t_2 / t)^{p/(1+p)}]C_s^* \qquad (2.2\text{-}35)$$

It is not hard to see that $C_{st}(t)$ is actually the first and third terms of Equation (2.2-30).

C_t Parameter

The conditions for C_t can be described as SSC-TC-EL-III, i.e., small-scale or transition, elastic, primary and/or secondary creep conditions. C_t was proposed by Saxena [37] to overcome the disadvantage of C(t) which can not be experimentally measured. C_t is essentially the extension of the C^* integral into the small-scale and transition creep regions. Like the $C^*(t)$ parameter, C_t approaches the value of $C^*(t)$ under extensive creep conditions. However, under small-scale conditions, C_t is different from C(t). Equation (2.2-33) and Equation (2.2-34) show that C(t) is the amplitude of the crack tip stress field. C_t, as defined by Saxena, is uniquely related to the rate of expansion of the creep zone size under small-scale creep conditions [55]:

$$(C_t)_{ssc} = \frac{2}{3}(1-\nu^2)\frac{K^2}{EW}(F'/F)\beta\dot{\gamma}_c \qquad (2.2\text{-}36)$$

where, $(C_t)_{ssc}$ = the value of C_t when the small-scale creep condition is emphasized

F = K-calibration factor, $F = (K/P)BW^{1/2}$

F' = a/W derivative of F, $F' = dF/d(a/W)$

$\dot{\gamma}_c$ = the rate of expansion of the creep zone size

Expressions for the rate of expansion of the creep zone size ($\dot{\gamma}_c$) have been derived for elastic, primary creep and elastic, secondary creep conditions [47, 55]. Analytical estimation of $(C_t)_{ssc}$ can be obtained by substituting the corresponding $\dot{\gamma}_c$ expressions into Equation (2.2-36).

Under SSC-EL-PC, i.e., small-scale, elastic primary creep conditions, the rate of expansion of the creep zone size is given as:

$$\dot{\gamma}_c = \frac{K^2}{2\pi}\left[\frac{I_{n_1} E}{2\pi(1-\nu^2)}\right]^{2/(n_1-1)} \times\left[(1+n_1)(1+p)A_1\right]^{2/(1+p)(n_1-1)}$$

$$\times\left[\frac{\tilde{\gamma}_c(\theta)}{1+p}\right]\times\left[\frac{2}{n_1-1}\right] t^{[2/(1+p)(n_1-1)-1]} \qquad (2.2\text{-}37)$$

where, I_{n_1} = nondimentional factor dependent upon n_1

$\tilde{\gamma}_c(\theta)$ = dimensionless function defining the creep zone shape

Under SSC-EL-SC, i.e., small-scale, elastic secondary creep conditions, the rate of expansion of the creep zone size is given as:

$$\dot{\gamma}_c = \frac{2\alpha}{n-1} K^2 t^{-(n-3)/(n-1)} (EA)^{2/(n-1)} \tilde{\gamma}_c(\theta) \qquad (2.2\text{-}38)$$

where, α = dimensionless constant dependent on n

Over the range from small-scale creep to extensive creep, C_t can be estimated from the following equation [46]:

$$C_t = (C_t)_{ssc} + C^*(t) \qquad (2.2\text{-}39)$$

where $(C_t)_{ssc}$ and $C^*(t)$ are both calculated values rather than experimentally measured values. As mentioned before, C_t from Equation (2.2-39) changes from $(C_t)_{ssc}$ to $C^*(t)$ as the conditions change from small-scale creep to extensive creep.

To experimentally measure C_t under small-scale creep conditions, the following equation should be used:

$$(C_t)_{ssc} = \frac{P\dot{V}_c}{\sqrt{B_N BW}}(F'/F) \qquad (2.2\text{-}40)$$

Equation (2.2-40) has been adopted into ASTM "Standard Test Method for Measurement of Creep Crack Growth Rates in Metals" [38].

2.2.5 Time-Dependent Fracture Mechanics Parameters for Cyclic Loading

ΔJ_c Parameter

The ΔJ_c parameter is a time integral of C^* or J^* over the hold time (t_h) of a trapezoidal waveform loading. The ΔJ_c parameter was first used by Jaske and Begley [56], and Taira, Ohtani and Komatsu [57] to correlate with the time-dependent creep crack growth during a trapezoidal waveform loading at elevated temperatures. It is defined as [58-61]:

$$\Delta J_c = \int_0^{t_h} C^* dt \qquad (2.2\text{-}41)$$

where, t_h = hold time at maximum load in a trapezoidal waveform loading

Under a trapezoidal waveform loading, the material's response can be divided into two categories for discussion, the loading portion and the hold time portion. Creep deformation can occur at the crack tip during the hold time (t_h) as well as during the loading portion of the cycle. Integrated over the hold time, the ΔJ_c parameter gives the total energy input in the crack tip area due to creep deformation during the hold time. For

the loading portion, the magnitude of creep deformation depends on the rate of loading. For fast loading, creep deformation is relatively small compared to elastic and plastic deformation. Therefore, it is usually negligible and no time-dependent fracture mechanics parameter has been defined for such cases. For slow loading, creep deformation may dominant over elastic and plastic deformation. A method of estimating the ΔJ_c parameter has been proposed by Ohtani et al.[58] and other researchers [59-61] with a basic built-in assumption that the creep deformation occurs under extensive creep conditions.

Since elastic and plastic deformations are involved during a trapezoidal waveform loading, the total energy input for a whole cycle should be the sum of cycle-dependent and time-dependent contributions. Therefore, ΔJ_c can be integrated into the total J-integral (ΔJ_T) which is defined as [35, 57]:

$$\Delta J_T = \Delta J_f + \Delta J_c \tag{2.2-42}$$

where, ΔJ_f = cycle-dependent integral associated with time-independent plasticity.

$(C_t)_{avg}$ Parameter

The $(C_t)_{avg}$ parameter is the average value of the C_t parameter during the hold time of a trapezoidal waveform loading. The $(C_t)_{avg}$ parameter was defined by Saxena and Gieseke as [26, 62, 63]:

$$(C_t)_{avg} = \frac{1}{t_h}\int_0^{t_h} C_t dt \tag{2.2-43}$$

Unlike ΔJ_f, the $(C_t)_{avg}$ parameter is not defined for the loading portion in a trapezoidal waveform even if the loading rate is very slow. The $(C_t)_{avg}$ parameter given in Equation (2.2-43) is defined only for creep deformation occurring during the hold time (t_h). During the hold time, creep deformation is usually accompanied by elastic deformation due to the stress relaxation process. If the hold time is sufficiently long, the creep zone size will develop from small-scale creep to extensive creep, and the elastic deformation will finally become negligible. From the definition, it is not hard to see that as the creep zone develops from small-scale creep to extensive creep and C_t approaches C^*, $t_h \cdot (C_t)_{avg}$ becomes equal to ΔJ_c. However, under small-scale creep conditions, $t_h \cdot (C_t)_{avg}$ and ΔJ_c will be different especially when they are calculated rather than experimentally determined.

The value of $(C_t)_{avg}$ is usually determined in two ways depending on how the deflection rate of the crack body is estimated. For those conditions where both load and loadline deflection as functions of time can be experimentally measured, as in the case of a C(T) specimen test, the value of $(C_t)_{avg}$ is determined by experimental measurements. For those conditions where the deflection rate can only be analytically predicted, as in the case of a cracked component, the value of $(C_t)_{avg}$ is determined by calculation.

When $(C_t)_{avg}$ is determined experimentally, the value can be obtained from the following equation:

$$(C_t)_{avg} = \frac{\Delta P \Delta V_c}{B W t_h} \frac{F'}{F} - C^* \left(\frac{F'}{F} \frac{1}{\eta} - 1 \right) \qquad (2.2\text{-}44)$$

where, ΔP = applied load range

ΔV_c = loadline deflection due to creep during the hold period

C^* and η can be determined from Equation (2.2-11) and Equation (2.2-23), respectively.

When $(C_t)_{avg}$ is determined analytically, the equations employed depend on the material conditions. For materials with low resistance to cyclic plasticity such that the cyclic plastic zone is larger than the creep zone that develops during the hold time, the value can be calculated as elastic-cyclic plastic-secondary creep conditions (EL-CPL-SC) from the following equation [62]:

$$(C_t)_{avg} = \frac{2\alpha\beta\tilde{\gamma}_c(\theta)}{E}(1-\nu^2)\frac{\Delta K^4}{W}\frac{F}{F}(EA_2)^{\frac{2}{n-1}}$$

$$\times\left[\frac{(t_h + t_{pl})^{\frac{2}{n-1}} - (t_{pl})^{\frac{2}{n-1}}}{t_h}\right] + C^* \qquad (2.2\text{-}45)$$

where, ΔK = range of stress intensity factor

t_{pl} = factor added to account for retardation in the creep zone expansion rate due to cyclic plasticity

α, β = constants

t_{pl} can be estimated as:

$$t_{pl} = \frac{1}{EA_2}\left[\xi\left(\frac{m'-1}{m'+1}\right)\left(\frac{1}{2\sigma_{YS}^c}\right)^2 \frac{1}{\alpha\tilde{\gamma}_c(90°)}\right]^{\frac{n-1}{2}} \qquad (2.2\text{-}46)$$

where, m' = cyclic strain-hardening exponent

σ_{YS}^c = cyclic yield strength determined as the stress amplitude ($\Delta\sigma/2$) corresponding to a plastic strain amplitude ($\Delta\varepsilon_p/2$) of 0.2%

ξ = constant

For materials with high resistance to cyclic deformation such that the creep rates are high and the creep zone size very quickly exceeds the cyclic plastic zone size, the value can be calculated from the following equation [64]:

$$(C_t)_{avg} = \frac{4\alpha n\beta \tilde{\gamma}_c(\theta)}{EW}(1-\nu^2)$$

$$\times \Delta K^4 \frac{F'}{F}(EA_2)^{\frac{2}{n-1}}(Nt_h)^{-\frac{n-1}{n-3}} + C^* \qquad (2.2\text{-}47)$$

where, N = number of fatigue cycles

The details of Equation (2.2-46) and Equation (2.2-47) can be found in References [62] and [64].

2.3 Life Prediction Methodology

With appropriate time-dependent fracture mechanics parameters, the crack propagation rate of a component containing cracks operating at elevated temperatures can be estimated, the intervals for inspections can be set with confidence, and the remaining life of such a component can thus be predicted with a life prediction methodology proposed by Saxena and Liaw [65].

The life prediction methodology is divided into three steps: In the first step, the material is tested to obtain its creep deformation and creep crack or creep-fatigue crack propagation properties with specimens in a laboratory. Then, the developed creep or creep-fatigue crack propagation rates from the test data are correlated to a parameter C. Here C represents any of the appropriate time-dependent fracture mechanics parameters. In the second step, the state of the crack in an engineering component containing cracks

operating at elevated temperatures is characterized with the same appropriate time-dependent fracture mechanics parameter C. In the third step, with the time-dependent fracture mechanics parameter C related to the crack in the component and the crack propagation rate in the test specimen, the crack propagation rate in the cracked component can be estimated. Once the final crack length at which the failure of the component occurs is known, the remaining life of the cracked component can be determined by integrating the crack length increment represented by the time-dependent fracture mechanics parameter equation on the time axis. This life prediction methodology is summarized in Figure 2.3-1.

The most critical step in accurately predicting the crack propagation rate or the remaining life of a cracked component is the second step. Appropriate expressions for the time-dependent fracture mechanics parameters in the cracked component must be developed and the final crack length beyond which failure occurs must be determined. These two tasks are very challenging. Over-conservative life predictions may cause unnecessary financial waste, while over-risky predictions may cause loss of human lives. At present, a limited number of expressions for calculating the time-dependent fracture mechanics parameters have been developed for certain component geometry [2, 23, 65]. Approximation equations can be derived from these expressions for similar component geometry. However, in some cases, the finite element analysis has to be employed to develop appropriate time-dependent fracture mechanics parameter expressions for a certain component geometry.

2.4 Microscopic Models of Creep Crack Growth

2.4.1 Fundamental Mechanisms of Creep

Since the crack growth phenomenon at elevated temperatures is resulted from creep, it is necessary to first briefly review the creep phenomenon when the study on

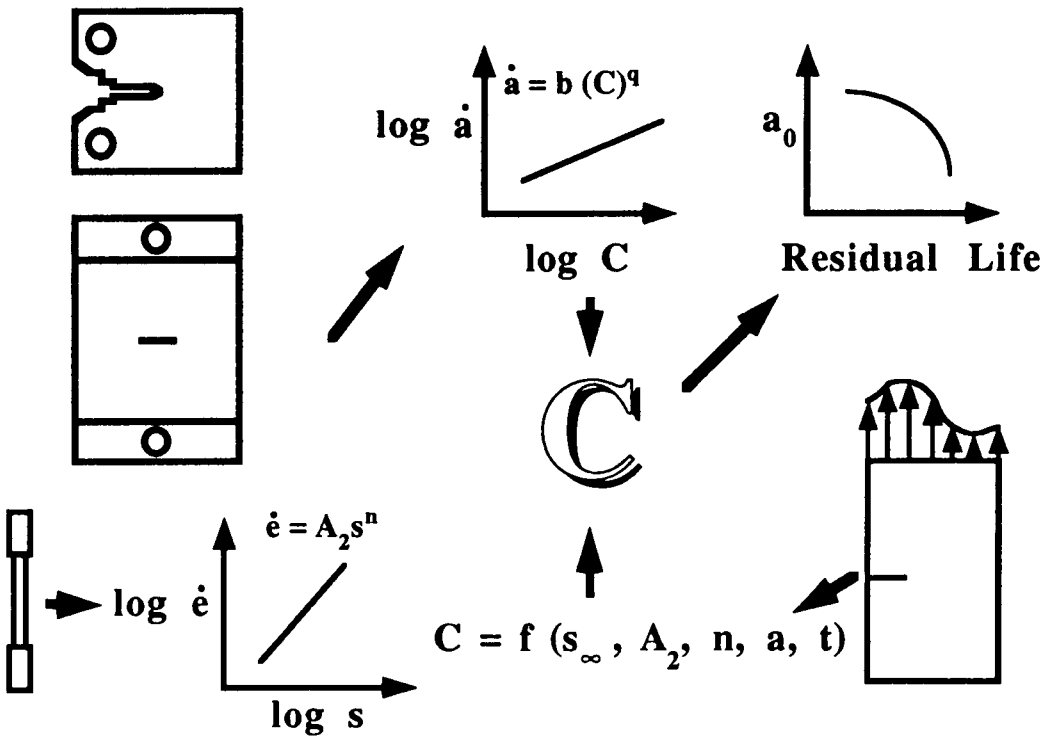

Figure 2.3-1 Methodology for Predicting the Remaining Life of a Cracked Component Operating at Elevated Temperatures.

creep crack growth mechanisms is persued.

In 1954, Orr et al. [66, 67] introduced the concept that the activation energy for creep and diffusion is the same for an appreciable number of metals. This is an indication that creep is related to diffusion processes in some materials. Many other researchers who studied the creep mechanisms concluded that there are mainly four kinds of fundamental mechanisms for creep: diffusion creep, dislocation creep, dislocation glide and grain boundary sliding. Most of these creep mechanisms depend on diffusion processes. In the diffusion creep mechanisms, several dynamic processes have been proposed, the flux of vacancies inside a grain can produce an increase in the length of the grain along the direction of applied tensile stresses [68, 69], the diffusion in grain boundaries instead of the bulk can result in sliding of the grain boundaries[70], and dislocations can climb exclusively by vacancy diffusion between sources and sinks [71, 72]. In the dislocation creep mechanism, creep is considered to occur by dislocation glide aided by vacancy diffusion when an obstacle is to be overcome [73, 74]. In the grain boundary sliding mechanism, the sliding is thought to occur with a diffusional flow transporting material or vacancies, generating fracture at grain boundaries by nucleation and growth of voids [75, 76].

Since most of the creep mechanisms are related to diffusion phenomenon, the magnitude of creep largely depends on the rate of diffusion or the diffusion coefficient. Many experimental results indicate that the diffusion coefficient of grain boundaries is usually several orders greater than that of the bulk within certain temperature ranges [77]. This means that under creep conditions, the grain boundaries are relatively weak in many materials because of the high grain boundary diffusion rates. Previous studies have shown that creep cavities nucleate more easily and grow more rapidly at grain boundaries than inside the grains because of higher grain boundary diffusion rates [80], and the creep cracks propagate mainly in an intergranular mode. The mechanism for creep crack

growth is considered to be composed of three steps: the nucleation, growth and coalescence of grain boundary cavities [39, 40, 78, 79]. Of the three steps, the nucleation and coalescence of grain boundary cavities are relatively less understood. Assumption has been made that the coalescence process occurs when the remaining ligaments between adjoining cavities can not bear the load any more and rupture takes place. For creep crack growth, a significant amount of work has been done to understand its mechanisms. Some models have been developed to describe the microscopic process of creep crack growth.

2.4.2 Grain Boundary Cavity Coalescence Model

For many metals, the examination of creep crack fracture surfaces reveals that the crack growth is a result of grain boundary cavitation [76]. Many models have been proposed for describing the creep crack propagation process in these metals [82-85]. One of these models proposed by Bassani and Vitek [84] is reviewed here, which provides some valuable insights into the creep crack propagation process and incorporates microstructural parameters into a relationship between the creep crack growth rate, da/dt, and an appropriate time-dependent fracture mechanics parameter.

The grain boundary cavity coalescence model proposed by Bassani and Vitek is schematically shown in Figure 2.4-1. In this model, it is assumed that there is an array of N growing grain boundary cavities at the crack tip spaced a distance 2b apart. The size of the cavities decreases with increased distance from the crack tip and the most distant cavity has a size equal to the critical size r_N for nucleation. All the cavities are assumed to grow according to the same growth law given as:

$$\dot{\rho} = \phi(\rho, b)\sigma^{\beta} \qquad (2.4\text{-}1)$$

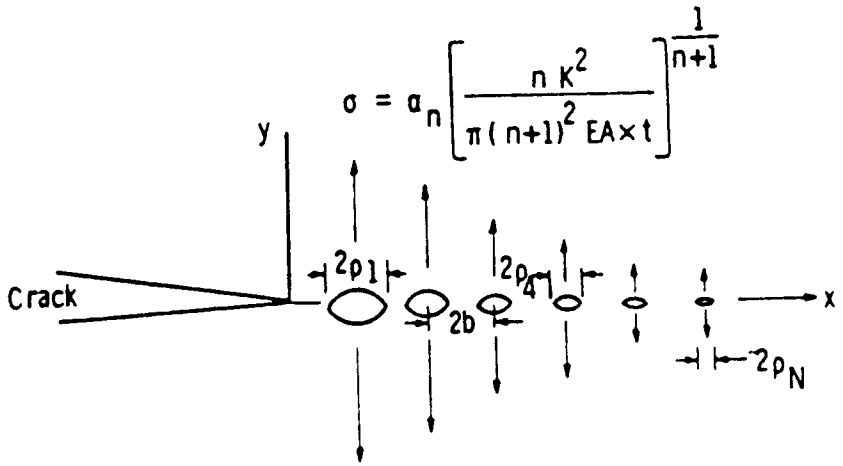

Figure 2.4-1 The Grain Boundary Cavity Coalescence Model Proposed by Bassani and Vitek (Courtesy of Basani et al. [84])

where, ρ = cavity size

$\dot{\rho}$ = cavity growth rate

β = constant depending on cavity conditions: β is 1 for diffusive spherical cavity growth, 3 for diffusive crack-like cavity growth and n for constrained cavity growth

ϕ = function of ρ and 2b, depending on the exact mechanism

This model correlates a time-dependent fracture mechanics parameter to the stress field in which the cavities grow by the following equation:

$$\sigma = \left[\frac{C(t)}{x}\right]^{\alpha} \qquad (2.4\text{-}2)$$

The analysis is restricted to one dimension. It is assumed that during an interval of time Δt, the cavity nearest to the crack tip reaches a critical size ρ_c and coalesces with the crack tip, and the crack length is then increased by a distance of 2b. The average crack growth rate (da/dt) can be calculated as:

$$\frac{da}{dt} = \frac{2b}{\Delta t} \qquad (2.4\text{-}3)$$

At the same time, each cavity is assumed to grow to the size of the cavity immediately preceding it. Thus, the second cavity with radius ρ_2 grows to radius ρ_1, the third cavity grows to size ρ_2, ..., and so forth. To establish a steady-state crack growth process, a new cavity of radius ρ_N nucleates at a distance 2bN ahead of the crack tip, replacing the first cavity.

The time interval Δt in Equation (2.4-3) can be determined by solving N simultaneous equations involving $\rho_c, \rho_1, ..., \rho_N$, given by:

$$\Delta t = \int_{\rho_m}^{\rho_{m-1}} \frac{d\rho}{\dot{\rho}} \qquad \text{for } m = 1, 2, ..., N \tag{2.4-4}$$

With the solution of the time interval, the crack growth rate can be expressed as:

$$\frac{da}{dt} = \left[\frac{(2b)^{1-\frac{\alpha}{n+1}}}{(\psi_0 - \psi_N) \sum_{m=1}^{N} (m)^{\frac{\alpha}{n+1}}} \right] \left[\frac{C(t)}{I_n A_2} \right]^{\frac{\alpha}{n+1}} \tag{2.4-5}$$

To relate this expression to the cavity sizes, Jani and Saxena [27] used a relationship for the cavity growth rate supplied by Rice [86] to obtain an expression for $\psi(\rho, b)$ function. Inserting their expression into Equation (2.4-5) they showed that:

$$\frac{da}{dt} = \left[\frac{(2b)^{\frac{2n+3}{n+1}} 3dA_2^{\frac{1}{n+1}}}{2.5(\rho_0^3 - \rho_N^3) \sum_{m=1}^{N} (m)^{\frac{\alpha}{n+1}}} \right] \left[\frac{C^*}{I_n A_2} \right]^{\frac{1}{n+1}} \tag{2.4-6}$$

It can be seen from this equation that the creep crack growth rate (da/dt) is not very sensitive to changes in A_2 which varies significantly with the temperature. Equation (2.4-6) shows that the correlation between the time-dependent fracture mechanics parameters and the creep crack growth rate is not sensitive to temperature [27], and the

creep crack growth rate is sensitive to changes in the nucleation size (ρ_N), the critical cavity size (ρ_c) and the inter-cavity spacing (2b).

Since the application of the time-dependent fracture mechanics parameters depends on the combination of the crack body conditions, C^* may not be appropriate in Equation (2.4-6) under certain conditions. Other time-dependent fracture mechanics parameters might be more appropriate in some cases [87].

2.4.3 Grain Boundary Separation Model

It was observed in iron [88, 89] and tungsten [90, 91] that at high strain rates or at low temperatures, the shape of creep cavities becomes crack-like, elongated and often directionally aligned [92]. Sometimes, the periphery of the cavity breaks up into fingers which tunnel down the grain boundaries ahead of a general crack front [92]. This phenomenon seems to be limited essentially to pure alloys or single-phase, solid solutions which are devoid of grain boundary precipitates. This intergranular crack growth mechanism has been modeled by Fields and Ashby [93] as the diffusive separation of grain boundaries. It is analogous to the peeling of a layer of tape from a smooth surface. The model is schematically shown in Figure 2.4-2. With this model, the creep crack growth rate of a crack of width 2w growing along a grain boundary by grain boundary diffusion can be expressed as:

$$\frac{da}{dt} = \frac{\pi\beta^2\alpha}{8}\frac{D_b\delta_b\sigma_a^2\Omega}{kTw\gamma_s}\left[1-\frac{\gamma_s}{\beta\sigma_a w}\right]^2 \qquad (2.4\text{-}7)$$

where, α = growth rate of fingers

β = scaling factor

D_b = grain boundary diffusion constant

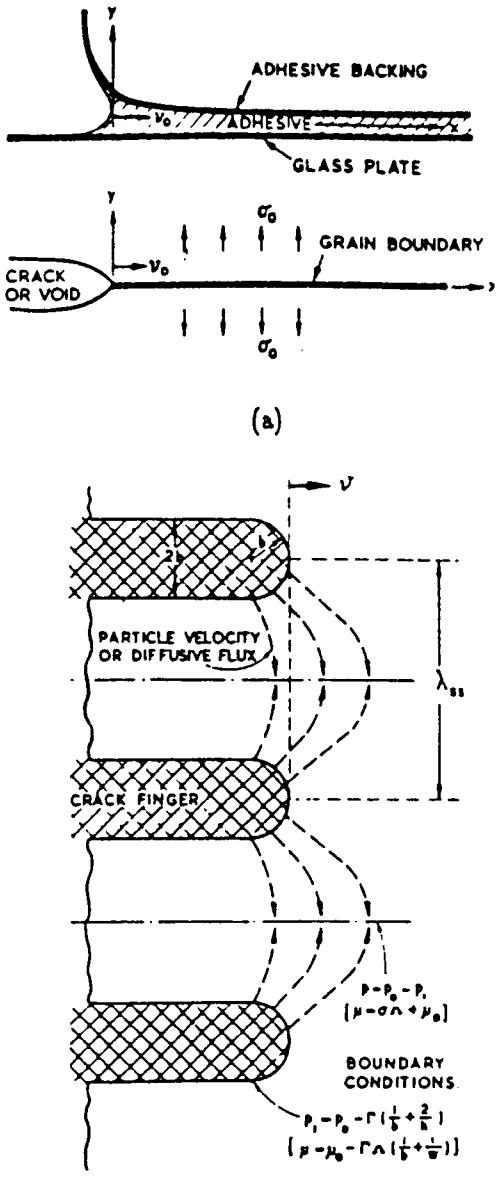

Figure 2.4-2 Schematic of Finger-Like Crack Growth Model,
a) The Process of Peeling Tape off a Smooth Surface,
b) The Assumed Shape of the Finger-Like Crack
Front (Courtesy of Fields et al. [93])

δ_b = width of grain boundary diffusion path

Ω = atomic volume

k = Boltzmann's constant

γ_s = surface free energy

σ_a = applied remote stress

w = half width of the crack

This equation relates the crack growth rate to the applied remote stress based on a mechanism that does not require the presence of creep cavities.

2.5 Macroscopic Models of Creep Crack Growth

In order to have an in-depth understanding of the dynamic process of creep crack propagation, and provide methods to save experimental time and materials for predicting the creep crack propagation rate, mathematical modeling of the creep crack propagation process is always desirable. For these purposes, Nikbin, Webster et al. [94, 95], and Cocks and Ashby [96] proposed a model which is shown in Figure 2.5-1. In this model, a process zone of size r_c is postulated at the crack tip. It is assumed that this zone encompasses the region over which creep damage accumulates locally at the crack tip. An element of material first experiences creep damage when it enters this zone at $r = r_c$ and accumulates creep strain ε_{ij} by the time it is a distance r from the crack tip such that:

$$\varepsilon_{ij} = \int_{r_c}^{r} \dot{\varepsilon}_{ij}\, dt \qquad (2.5\text{-}1)$$

To simplify the calculation, the three stages of creep deformation are treated in an approximate manner by defining an average creep rate which can be obtained from the

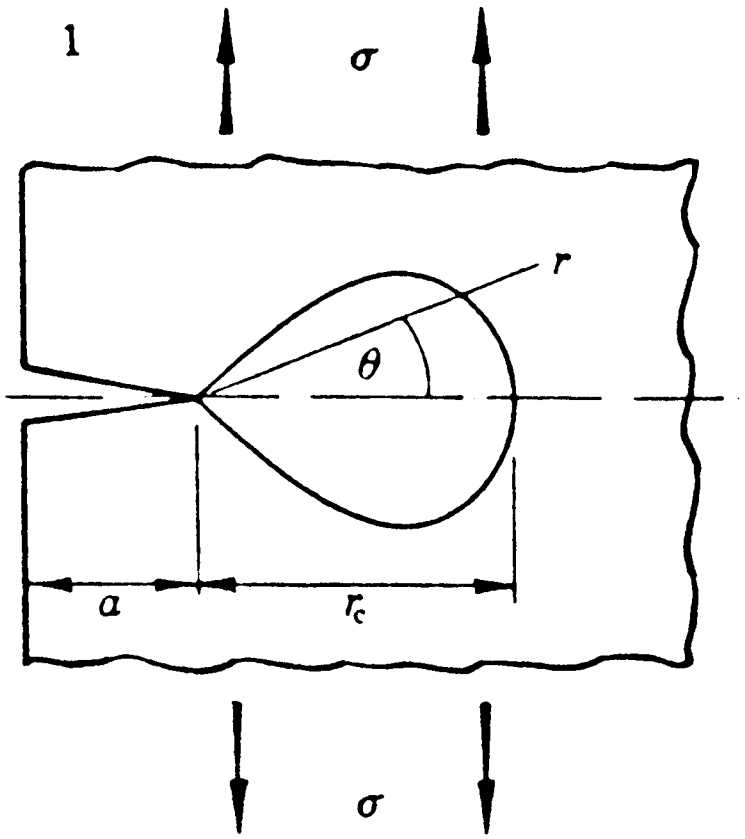

Figure 2.5-1 Process Zone Model for Predicting the Creep Crack Growth Rate (Courtesy of Austin and Webster [94])

rupture data as shown in Figure 2.5-2. The value of the average creep rate is calculated as:

$$\dot{\varepsilon}_A = \varepsilon_f / t_r \qquad (2.5\text{-}2)$$

where, $\dot{\varepsilon}_A$ = average creep deformation rate

ε_f = failure strain, creep ductility

t_r = rupture time

The rupture time is stress-dependent and can be expressed as:

$$t_r = D / \sigma^{\upsilon} \qquad (2.5\text{-}3)$$

where, D, υ = material constants

For creep failure under variable load conditions, several cumulative damage models have been proposed [97] such as the strain fraction, life fraction and Rabotnov damage laws [98]. In the strain fraction law, failure occurs when:

$$\int d\varepsilon_{ij} / \varepsilon_f = 1 \qquad (2.5\text{-}4)$$

In the life fraction rule, failure takes place when:

$$\int dt / t_r = 1 \qquad (2.5\text{-}5)$$

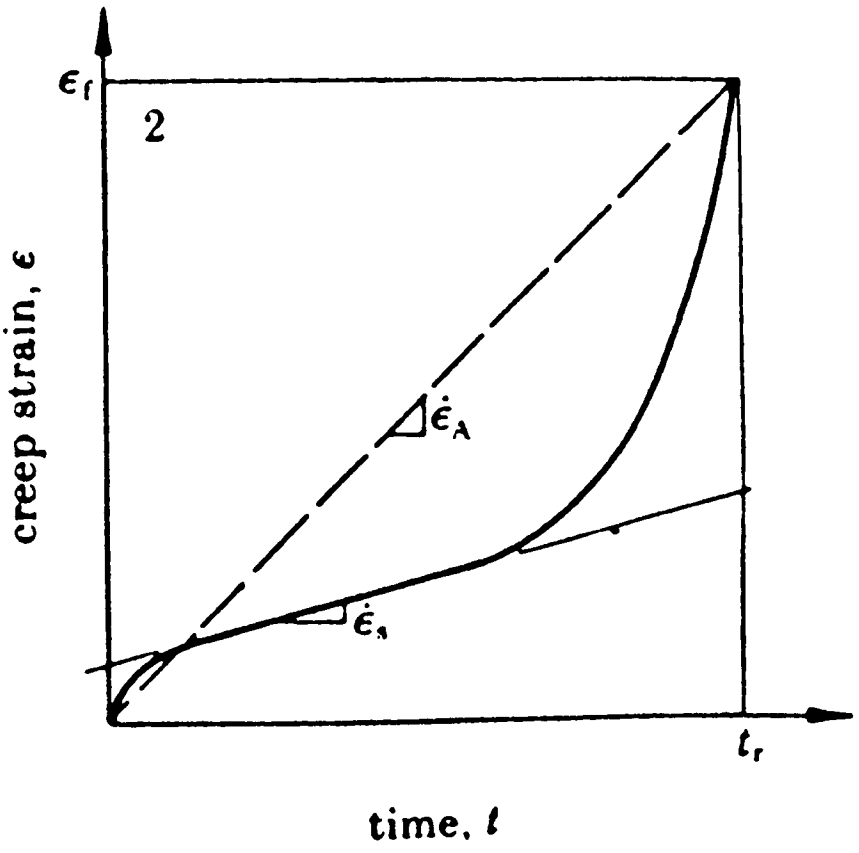

Figure 2.5-2 Simplification of Primary, Secondary and Tertiary Creep to an Average Creep Rate.

By inserting Equations (2.2-12) and (2.5-3) into Equation (2.5-5), the creep crack growth rate expression can be derived as:

$$\dot{a} = \left(\frac{n+1}{n+1-\upsilon}\right)\frac{\dot{\varepsilon}_o}{\varepsilon_{fo}}\left(\frac{C^*}{I_n \sigma_o \dot{\varepsilon}_o}\right)^{\frac{\upsilon}{(n+1)}} \times r_c^{(n+1-\upsilon)/(n+1)} \qquad (2.5\text{-}6)$$

where, $\dot{a}$ = creep crack growth rate, da/dt

$\dot{\varepsilon}_o$, σ_o = material constants at a given temperature

e_{fo} = creep ductility at σ_o

This model allows all stages of creep deformation to be incorporated in an approximate manner, and creep ductility to be stress and stress-state sensitive. Good agreement has been obtained with experimental crack growth data on materials such as low alloy steels, stainless steels, aluminum alloys and nickel-base superalloys. It is evident from Equation (2.5-6) that the creep crack growth rate is sensitive to the size of creep process zone but inversely proportional to creep ductility. This model has been modified over the years, and the details can be found in references [99-102].

CHAPTER III

EXPERIMENTAL PROCEDURES

As introduced in Chapter I, six goals were set for this study.

1. To evaluate the mechanical properties of HR160 at elevated temperatures and generate a sound database for the material selection campaign for the next generation of fossil energy systems.
2. To study the effects of various testing conditions such as temperature, load level and specimen size on the application of the time-dependent fracture mechanics parameters
3. To study the effects of chemical compositions and material treatments such as grain size coarsening, aging and welding, on the time-dependent fracture mechanics behavior of HR160 through testing and comparing the properties in these different material conditions.
4. To investigate the creep-fatigue crack propagation behavior of HR160 and its relationship with the creep crack propagation behavior.
5. To study the creep crack and creep-fatigue crack propagation mechanisms of HR160 and understand the relationship between the microstructures and the properties.
6. To develop theoretical models for an in-depth understanding of the dynamics of creep crack propagation and provide possible methods for the prediction of the creep crack behavior at elevated temperatures.

In order to reach these goals, specimens of HR160 in different material conditions were prepared for this investigation. Mechanical testing was first performed on these specimens. The mechanical tests included tensile tests, creep deformation tests, creep

crack growth tests and creep-fatigue crack growth tests. The results of these tests have formed a sound database for the material selection purpose for the next generation of fossil energy systems. Meanwhile, the data generated from these tests were used for the model development and the study of the applications of the time-dependent fracture mechanics parameters under different conditions. Then tested samples were used to investigate the mechanisms of creep deformation, creep crack and creep-fatigue crack propagation. The details of the experimental procedures are described as follows.

3.1. Material Conditions

The material studied in this investigation was a Ni-Co-Cr-Si superalloy, HAYNES® HR160™. The nominal composition of HR160 has been given in Table 2.1-1. The material was studied on two different heats and in four different conditions listed below:

heat 7011
heat 7507
as-received condition
coarse grain size condition
aged condition
welded condition

The compositions of the two heats are shown in Table 3.1-1. The as-received material was annealed at 1093°C (2000°F). The microstructure of the as-received HR160 was a clean austenitic structure with a grain size of ASTM No. 3. The coarse grain size was obtained from heat 7507 by re-annealing at 1204°C (2200°F) for 20 minutes followed by water quench. The resulting material had a grain size of ASTM No. 00. The aged

Table 3.1-1 Compositions of Haynes HR160 for the Present Study

Heat	Ni	Co	Cr	Si	Mn	Ti	Al	Fe
7011	37.40	29.0	27.90	2.78	0.40	0.46	-	1.64
7507	37.87	29.93	27.67	2.72	0.43	0.46	0.16	0.13
Heat	W	Mo	C	Cb	Cu	P	S	N
7011	-	-	0.05	-	-	< 0.001	0.006	0.0026
7505	< 0.1	0.06	0.05	< 0.05	0.01	< 0.002	< 0.002	-

material was also obtained from heat 7507 by re-annealing at 649°C (1200°F) for 1000 hours followed by air cooling. In the welded condition, the base metal was the as-received heat 7507 HR160 and the filler metal was also made of HR160 with the same nominal chemical composition from heat 7544. The welds were made with double V grooves by using TIG (tungsten inert gas) welding method.

3.2 Test Matrix for Mechanical Property Evaluation

3.2.1 Tensile Tests

Tensile tests were conducted to obtain the plasticity exponent (m) and the plasticity coefficient (D) of the Ramberg-Osgood stress and strain equation. These two parameters were used for the calculation of the time-dependent fracture mechanics parameters. Meanwhile, conventional tensile property parameters such as the yield strength (s_y), Young's Modulus (E) etc., were also developed.

Tensile tests were performed on HR160 in the as-received, coarse grain size, aged and welded conditions for heat 7507, and the as-received condition for heat 7011. For each condition, tests were conducted at temperatures ranging from 23 to 950°C (73.4 to 1742°F). The detailed conditions for tensile tests are summarized in Table 3.2-1. Totally 12 tensile tests were conducted in this investigation.

3.2.2 Creep Deformation Tests

Creep deformation tests were performed to generate creep deformation and rupture property data for the calculation of the time-dependent fracture mechanics parameters. These data were also used for the model development. Furthermore, the tested samples provided the material for microstructural characterization, and thus, the understanding of the relationships among properties, structures and performance of HR160.

Table 3.2-1 Tensile Test Conditions for HR160

Material Condition	Temperature							
	°C	°F	°C	°F	°C	°F	°C	°F
Heat 7011								
As-Received	23	73.4	-	-	900	1652	-	-
Heat 7507								
As-Received	23	73.4	850	1562	900	1652	950	1742
Coarse Grain	23	73.4	850	1562	-	-	-	-
Aged	23	73.4	850	1562	-	-	-	-
Weldment	23	73.4	850	1562	-	-	-	-

Creep deformation tests were conducted on HR160 in the as-received, coarse grain size, aged and welded conditions for heat 7507, and the as-received condition for heat 7011. The tests were conducted at three different temperatures ranging form 850°C to 950°C (1562°F to 1742°F) and four different initial stress levels ranging from 13.78 MPa to 82.68 MPa (2.0 ksi to 12.0 ksi) as shown in Table 3.2-2. Some tests were repeated to generate samples for microstructural characterization by interrupting the testing at certain points. Totally, 45 creep deformation tests were conducted in this investigation.

3.2.3 Creep Crack Growth Tests

Creep crack growth tests were conducted to provide a sound database for design and life prediction. Meanwhile, this database was used to study the characterization of the creep crack growth rate with time-dependent fracture mechanics parameters and time-independent fracture mechanics parameter, i.e., the stress intensity factor, K. It was also used to study the effects of load level, temperature and sample size on the creep crack growth behavior and the time-dependent fracture mechanics methodology.

For the as-received HR160, the test conditions composed of temperature 850°C (1562°F), load level 2326.3 N (523 lb) and sample width 50.8 mm (2 in) were chosen as the baseline for the test matrix. Based on these conditions, the temperature was varied to 900°C (1652°F) and 950°C (1742°F) to study the temperature effect with three different temperatures, the load level was changed to 1579 N (355 lb) and 3031 N (681 lb) to investigate the load effect with three different load levels, and the sample width was reduced to 25.4 mm (1 in) to show the sample size effect with two different sample sizes. Because of the limited material source, the half-size C(T) samples were made of HR160 from heat 7011 while the full-size C(T) samples were made of heat 7505. This also provided an opportunity for observing the heat effect, if any, on the creep crack

Table 3.2-2 Creep Deformation Test Conditions for HR160

T		S_1		S_2		S_3		S_4	
°C	°F	MPa	ksi	MPa	ksi	MPa	ksi	MPa	ksi
As-received Heat 7011									
900	1652	115.3	16.73	89.57	13.0	64.08	9.3	38.45	5.58
1000	1832	-	-	38.45	5.58	24.12	3.5	13.78	2.0
As-received Heat 7507									
850	1562	82.68	12.0	64.08	9.3	48.23	7.0	38.45	5.58
900	1652	64.08	9.3	48.23	7.0	38.45	5.58	24.12	3.5
950	1742	48.23	7.0	38.45	5.58	24.12	3.5	13.78	2.0
Coarse Grain Size Heat 7507									
850	1562	82.68	12.0	64.08	9.3	48.23	7.0	38.45	5.58
900	1652	64.08	9.3	48.23	7.0	38.45	5.58	24.12	3.5
950	1742	48.23	7.0	38.45	5.58	24.12	3.5	13.78	2.0
Aged Heat 7507									
850	1562	82.68	12.0	64.08	9.3	48.23	7.0	-	-
Weldment of Heat 7507 Base Metal + Heat 7544 Weld Wire									
850	1562	82.68	12.0	64.08	9.3	48.23	7.0	-	-

propagation behavior. These testing conditions are given in Table 3.2-3, Table 3.2-4 and Table 3.2-5, respectively. For the coarse grain size and welded HR160, the tests were carried out under the baseline conditions at the temperature of 850°C (1562°F) and load level of 2326.3 N (523 lb), plus a load level of 3030.6 N (681 lb). For the aged HR160, the tests were conducted under the baseline condition at the temperature of 800°C (1562°F) and load level of 2326.3 N (523 lb), plus a load level of 1881.5 N (423 lb). These testing conditions are shown in Table 3.2-3. The load form of the creep crack growth tests is as shown in Figure 3.2-1. Same as in creep deformation tests, some creep crack growth tests were repeated to generate samples for microstructural characterization by interrupting the testing at certain points. Totally, 20 creep crack growth tests were conducted in this investigation.

3.2.4 Creep-Fatigue Crack Growth Tests

Creep-fatigue crack growth tests were conducted to study the fatigue effect on the creep crack growth behavior and the characterization of the creep-fatigue crack growth rate with the time-dependent fracture mechanics parameters. It was expected that a correlation between the creep crack growth and the creep-fatigue crack growth results could be found, and thus, the creep-fatigue crack growth behavior of the tests with different hold times could be estimated from the combination of the results of triangular wavefrom loading tests and creep crack growth tests. This could not only expand the database without doing a large number of tests, but also provide a better understanding of the fatigue effect on creep crack growth behavior. In addition to generating a database for simulating the periodic thermal and load cycling in fossil energy generation systems caused by reasons such as operation variations, interruptions for maintenance and power demand fluctuations, the tests provided tested samples for microstructural

Table 3.2-3 Different Load Levels and Material Conditions of Creep Crack Growth Tests on HR160

T		K		P	
°C	°F	MPa$\sqrt{m}$	ksi$\sqrt{in}$	N	lb
As-received Heat 7507					
850	1562	7.1	6.5	1579	355
		11	10	2326.3	523
		14.3	13	3030.6	681
		Coarse Grain Size Heat 7507			
850	1562	11	10	2326.3	523
		14.3	13	3030.6	681
		Aged Heat 7507			
850	1562	9	8.2	1881.5	423
		11	10	2326.3	523
		Weldment of Heat 7507 Base Metal/Heat 7544 Weld Wire			
850	1562	11	10	2326.3	523
		14.3	13	3030.6	681

Table 3.2-4 Creep Crack Growth Test Conditions for Temperature Effect Study on the As-Received HR160

K		P		T	
$MPa\sqrt{m}$	$ksi\sqrt{in}$	N	lb	℃	℉
11	10	2326.3	523	850	1562
				900	1652
				950	1742

Table 3.2-5 Creep Crack Growth Test Conditions for Sample Size Effect Study on the As-Received HR160

T		K		P		W	
℃	℉	MPa$\sqrt{m}$	ksi$\sqrt{in}$	N	lb	mm	in
900	1652	4.4	4	645	145	25.4	1.0
		8.2	7.5	1134.2	255	25.4	1.0
		11	10	2326.3	523	50.8	2.0

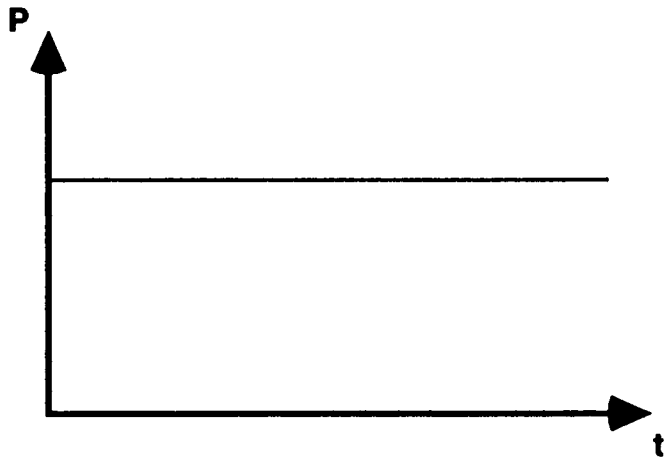

Figure 3.2-1 Loading Form for Creep Crack Growth Tests

characterization, and thus, a mechanistic understanding of the material behavior in such circumstances.

Creep-fatigue tests were conducted on the as-received HR160 from heat 7507. The baseline conditions for the creep crack growth tests, i.e., the temperature of 850°C (1562°F), the load level of 2326.3 N (523 lb) and the sample width of 50.8 mm (2.0 in), were employed for the creep-fatigue tests with the load level of 2326.3 N (523 lb) as the maximum load (P_{max}). These tests were conducted with four different hold times (t_h) ranging from 0 to 3600 seconds at the maximum load. All the tests were performed with a frequency of 0.5 Hz and a minimum to maximum load ratio of 0.1. The conditions for the creep-fatigue crack growth tests are summarized in Table 3.2-6, and the loading waveforms employed are as shown in Figure 3.2-2. The frequency of the trapezoidal waveform in this study means the frequency of the loading and unloading portions excluding the hold time. The frequency of 0.5 Hz for all the tests ensured that the samples were loaded and unloaded at the same rate in all the creep-fatigue tests. Totally, 8 creep-fatigue crack growth tests were conducted including the interrupted tests for generating samples for microstructural characterization.

3.3 Test Procedures and Data Reduction

3.3.1 Tensile Tests

The samples for tensile and creep deformation tests had a gage length of 31.75 mm (1.25 in) and a diameter of 6.35 mm (0.25 in) as shown in Figure 3.3-1. The samples were machined parallel to the rolling direction. For tests on welded HR160, two plates having a nominal thickness of 12.7 mm (0.5 in) were first welded with double-V grooves, the tensile and creep deformation test samples were machined perpendicularly to the weld of the welded plates as shown in Figure 3.3-2. The gage length section of the samples contained the weld, HAZ and base metal with weld in the middle of the samples.

Table 3.2-6 Creep-Fatigue Crack Growth Test Conditions
on the As-Received HR160

T		K		P_{max}		t_h
°C	°F	MPa$\sqrt{m}$	ksi$\sqrt{in}$	N	lb	sec
850	1562	11	10	2326.3	523	0
						10
						100
						3600

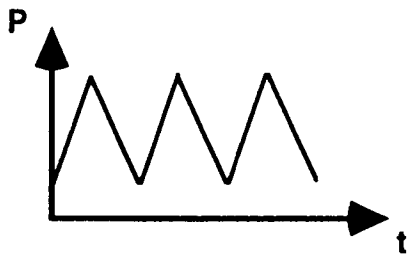

a) Without Hold Time

b) With Hold Time

Figure 3.2-2 Loading Waveforms for Creep-Fatigue Crack Growth Tests

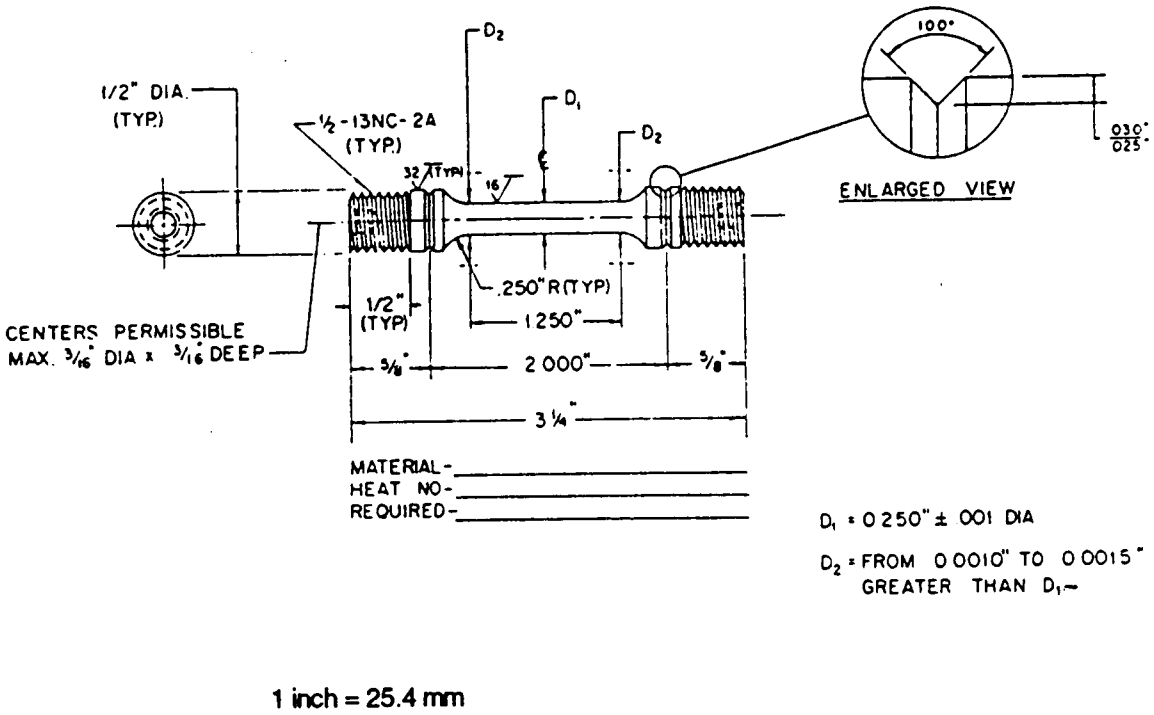

1 inch = 25.4 mm

Figure 3.3-1 Geometry of Tensile and Creep Deformation Specimens

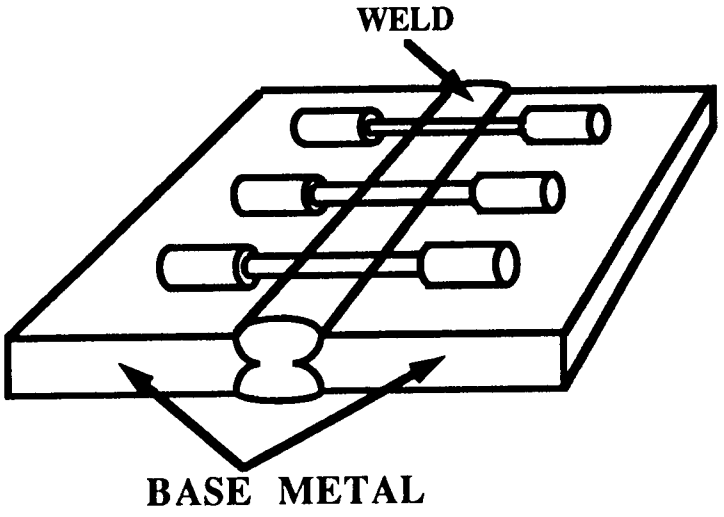

Figure 3.3-2 The Preparation of Tensile and Creep Deformation Specimens of the Welded Condition

The tensile tests were conducted on a screw driven tensile test machine. Load versus elongation curves were recorded in two ways. An X-Y recorder was employed to record the signal from an extensometer attached to a 25.4 mm (1 in) gage length section of the specimen. A chart recorder was also used to record the displacement of the crosshead. Complete stress versus strain data curves were obtained from these two recordings. The developed true stress-strain curves were then fitted into the Ramberg-Osgood stress and strain equation:

$$\varepsilon = \frac{\sigma}{E} + D\sigma^{m} \qquad (3.3\text{-}1)$$

where, D = plasticity coefficient

m = plasticity exponent

The values of plasticity coefficient (D) and plasticity exponent (m) were required in the calculations of creep crack growth rate correlating parameters.

3.3.2 Creep Deformation Tests

Creep deformation tests were performed in accordance with the ASTM standard E139-83 entitled "Standard Practice for Conducting Creep, Creep Rupture, and Stress-Rupture Tests of Metallic Materials" [103]. The samples for creep deformation tests were identical to the tensile test samples as shown in Figure 3.3-1. Lever-arm machines were employed to conduct the creep deformation tests. The furnace temperatures were controlled within ±2°C (3.6°F) of the prescribed test temperatures. In each test, creep deformation was recorded across the shoulders of the sample with a dial gage and a linear variable differential transformer (LVDT) or a continuous chart recorder, depending on the duration of the test. The engineering creep strain versus time curve was developed from

the recorded deformation data. Then, the curve of the creep rate versus time was developed by a seven-point incremental polynomial method. A typical curve of creep rate versus time is given in Figure 3.3-3. The minimum creep rate ($\dot{e}$) was determined by fitting a straight line to the lower portion of the creep rate versus time curve as shown in Figure 3.3-3. The minimum creep rate was directly read from the intersection of the straight line with the ordinate $\dot{e}$. The rupture strain and rupture time were also recorded for each test. The minimum values of the creep rate ($\dot{e}$) and the initial engineering stress (s) were fitted into Equation (2.2-6):

$$\dot{e} = A_2 s^n \qquad (2.2\text{-}6)$$

The creep coefficient (A_2) and the creep exponent (n) were obtained from a linear regression analysis of the test data. The values of A_2 and n were subsequently used for calculating the creep crack growth rate correlating parameters. The creep deformation data were also used in the theoretical model development.

3.3.3 Creep Crack Growth Tests

Compact-tension (C(T)) samples, as shown in Figure 3.3-4, were used for creep crack growth tests. The C(T) samples were machined with the notch perpendicular to the rolling direction. For the welded condition, each C(T) sample was machined from the welded plates with the notch cutting through the weld and HAZ as shown in Figure 3.3-5. The weld was then ground to the thickness of the base metal. All the creep crack growth test samples had the as-received thickness of 12.7 mm (0.5 in).

The tests were conducted in accordance with ASTM standard E1457 entitled "Standard Test Method for Measurement of Creep Crack Growth Rates in Metals" [38]. Prior to creep crack propagation testing, the C(T) samples were fatigue-precracked at

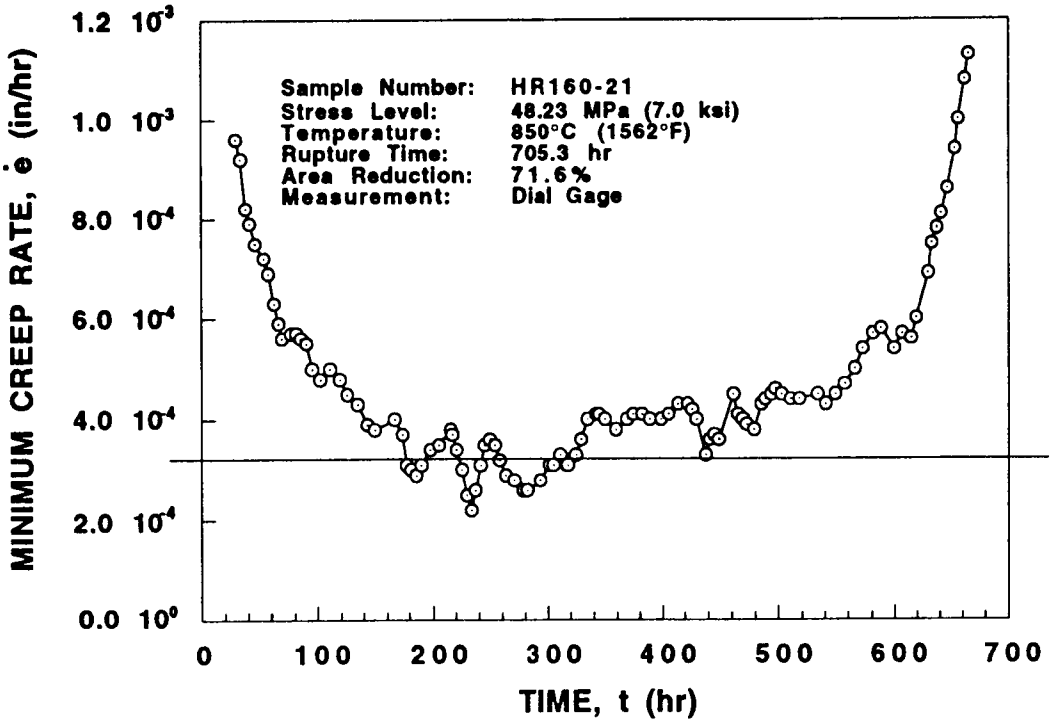

Figure 3.3-3 A Typical Creep Rate Versus Time Plot. (The Straight Line Is Drawn to Fit the Lower Portion of the Curve and Obtain the Minimum Creep Rate)

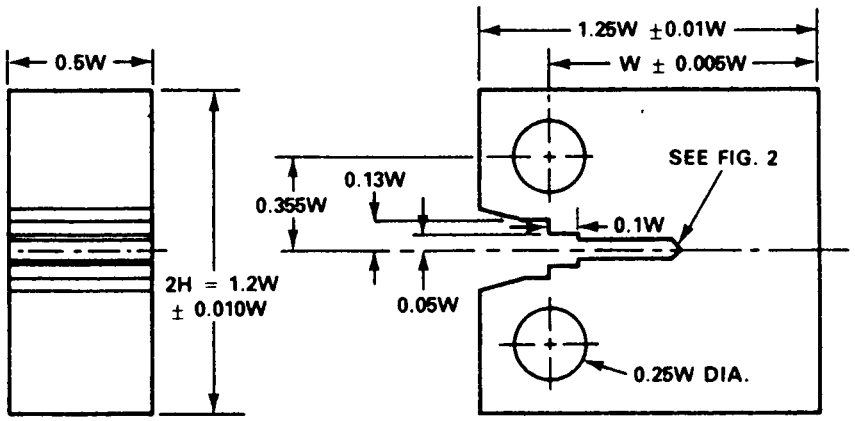

COMPACT TEST SPECIMEN FOR PIN OF 0.24W (+0.000W/−0.005W) DIAMETER

Drawing of a Standard C(T) Specimen

Figure 3.3-4 Geometry of Compact-Tension (C(T)) Specimens for Creep Crack Growth and Creep-Fatigue Crack Growth Tests

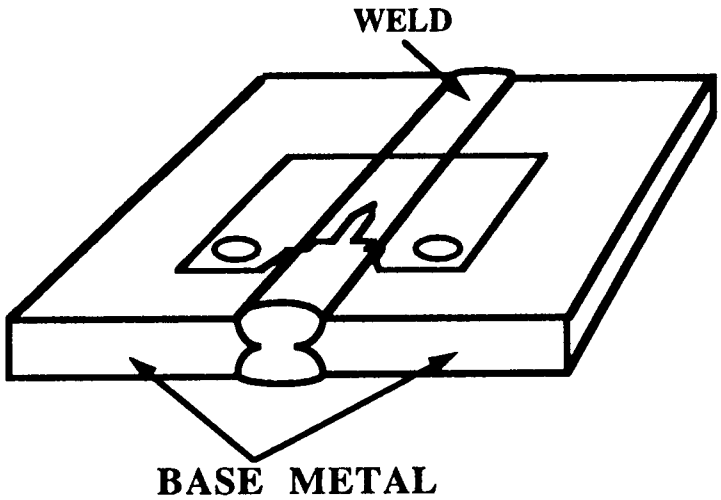

Figure 3.3-5 The Preparation of C(T) Specimens for the Study of Welded Condition

room temperature. Each fatigue crack was controlled to extend from the machined notch no less than 5% of the total crack length (a_o) and not less than 1.3 mm (0.005 in). The samples were side-grooved to 10% of the thickness on each side to minimize crack tunneling.

In order to measure the crack length during testing with the D.C. potential drop technique, two heavy duty input wires were TIG (tungsten inert gas welding) welded on the top and the bottom of each sample at the points 0.5W (W = sample width) away from the non-notched side on the mid-thickness line, another two output leads were spot welded to the upper and lower edges of the machined notch opening.

For the two different sample sizes employed, the full-size samples contained a width of W = 50.8 mm (2 in) and the half-size samples of W = 25.4 mm (1 in). The actual samples are shown in Figure 3.3-6. In each test, a sample was mounted on a creep machine, heated up to the desired temperature in a resistance-type furnace, and then loaded through the lever arm or with dead weight. The test temperature was controlled within ±2°C (3.6°F) of the prescribed temperatures, as it was in tensile and creep deformation tests. A constant 10 ampere D.C. current was passed through the C(T) sample via the heavy duty wires. The output voltage was monitored with a digital voltmeter capable of reading accurately in one microvolt range. The no-current voltage was also measured periodically to determine the thermal voltage so that the output voltage could be compensated accordingly. The crack length was then determined from the potential drop data with the following Johnson's formula [104]:

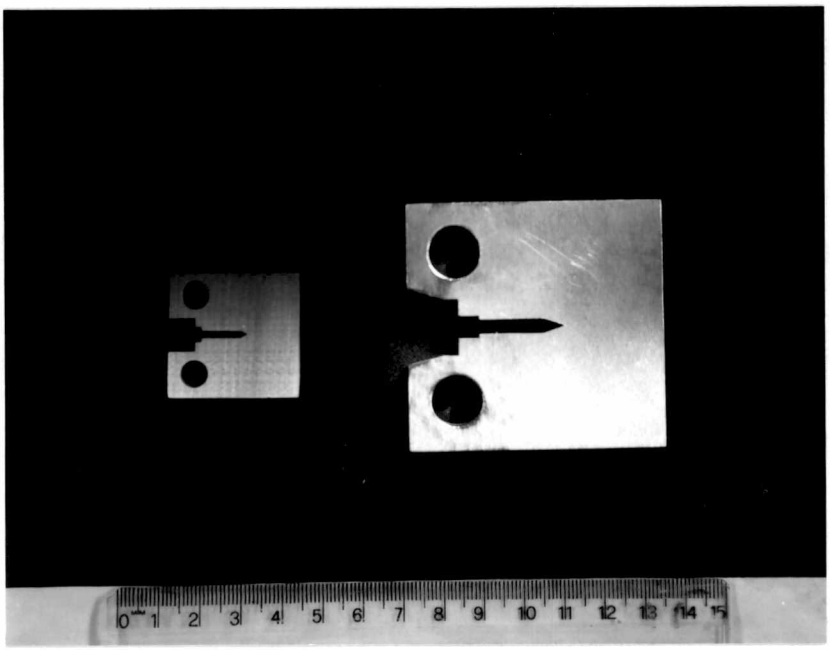

Figure 3.3-6 Full-Size and Half-Size Creep Crack Growth Specimens

$$\frac{a}{W} = \frac{2}{\pi}\cos^{-1}\left\{\frac{\cosh\frac{\pi y_o}{2W}}{\cosh\left[\frac{\delta}{\delta_o}\cosh^{-1}\left[\frac{\cosh\frac{\pi y_o}{2W}}{\cos\frac{\pi a_o}{2W}}\right]\right]}\right\} \qquad (3.3\text{-}2)$$

where, y_o = half of the distance between two output electric potential leads

δ = output electric potential

δ_o = initial output electric potential

a_o = initial crack length

The loadline deflection (V) was measured as a function of time with a dial gage and/or a LVDT. The data obtained from a creep crack growth test consisted of crack length and loadline deflection as functions of time. These data were processed numerically to obtain their respective rates [da/dt or $(\dot{a})$ and dV/dt or $(\dot{V})$] by using the seven-point incremental polynomial technique.

The creep crack growth rate correlating parameters, $C^*(t)$ and C_t, valid for extensive creep and small-scale creep conditions respectively, were calculated according to the following equations:

$$C^*(t) = \frac{P\dot{V}_c}{B_N(W-a)}\frac{n}{n+1}\left(2+0.522\frac{W-a}{W}\right) \qquad (3.3\text{-}3)$$

$$C_t = \frac{P\dot{V}_c}{\sqrt{BB_N}W}(F'/F) \qquad (2.2\text{-}40)$$

where the loadline deflection rate due to creep ($\dot{V}_c$) was determined from the total deflection rate ($\dot{V}$) as the following:

$$\dot{V}_c = \dot{V} - \frac{\dot{a} B_N}{P}\left[\frac{2K^2}{E} + (m+1)J_p\right] \tag{3.3-4}$$

K was estimated as:

$$K = \frac{P}{\sqrt{BB_N}W^{1/2}} \frac{2 + a/W}{(1 - a/W)^{3/2}} f(a/W) \tag{3.3-5}$$

where,

$$f(a/W) = 0.886 + 4.64(a/W) - 13.32(a/W)^2 + 14.72(a/W)^3 - 5.6(a/W)^4 \tag{3.3-6}$$

J_p was estimated as:

$$J_P = \frac{Dh_1(a/W, m)}{(W - a)^m}\left(\frac{P}{1.455B_N a}\right)^{m+1} \tag{3.3-7}$$

where,

$$\alpha = (\phi^2 + 2\phi + 2)^{1/2} - (\phi + 1)$$

$$\phi = 2a/(W - a)$$

F'/F in Equation (2.2-40) was estimated as:

$$F'/F = \left[\frac{1}{2 + a/W} + \frac{3}{2(1 - a/W)}\right] + \frac{f'}{f} \qquad (3.3\text{-}8)$$

where, f' = the derivative of f(a/W) with respect to a/W

The criterion for extensive creep or small-scale creep conditions was determined by the transition time (t_T) of Equation (2.2-29) in the following form:

$$t_T = \frac{K^2(1-\nu^2)}{E(n+1)C^*(t_T)} \qquad (3.3\text{-}9)$$

where, $C^*(t_T)$ = the value of C^* at the transition time t_T.

For the time (t) corresponding to each data point, t'_T was calculated from Equation (3.3-9) but substituting $C^*(t)$ for $C^*(t_T)$. t_T was then the largest value of t'_T in the entire data set. The creep zone would be considered to be extensive and the creep crack growth rate data would be correlated by Equation (3.3-3) when the time exceeded the transition time, i.e., $t > t_T$. Otherwise, the creep crack growth rate data would be correlated by Equation (2.2-40). Details of the calculations involved in this section can be found in Reference [38].

3.3.4 Creep-Fatigue Crack Growth Tests

The specimens for creep-fatigue crack growth tests were identical to the full-size C(T) specimens used for creep crack growth tests. The tests were conducted on a servo hydraulic MTS fatigue machine. The setup for the crack length measurement was essentially the same as that for creep crack growth tests except that the potential drop was measured continuously with a YOKOGAWA chart recorder instead of a microvolt meter.

The loadline deflection was also continuously measured with the YOKOGAWA chart recorder. For creep-fatigue tests with short hold times, an additional X-Y recorder of high resolution was employed to periodically record the loadline deflection.

The average crack growth rate $(da/dt)_{avg}$ during the hold time was calculated from the creep-fatigue test data with the following equation:

$$\left(\frac{da}{dt}\right)_{avg} = \frac{1}{t_h}\left[\left(\frac{da}{dN}\right)_m - \left(\frac{da}{dN}\right)_{tr}\right]_{\Delta K} \qquad (3.3\text{-}10)$$

where, t_h = hold time

$\left(\frac{da}{dN}\right)_m$ = measured creep-fatigue crack growth rate

$\left(\frac{da}{dN}\right)_{tr}$ = crack growth rate under triangular waveform loading

The subscript, ΔK, in Equation (3.3-10) indicates that the subtraction between the measured creep-fatigue crack growth rate and the crack growth rate under triangular waveform loading was conducted at the same values of the stress intensity factor range. In order to simplify the calculation, the data of triangular waveform loading tests were represented by the Paris law. The parameters C and n_f in the Paris law were obtained by fitting the data of triangular waveform loading into the Paris law as the following:

$$\left(\frac{da}{dN}\right)_{tr} = C(\Delta K)^{n_f} \qquad (3.3\text{-}11)$$

where, C = fatigue coefficient

n_f = fatigue exponent

In order to find the relationship between the creep crack propagation behavior and the creep-fatigue crack growth behavior, the average creep-fatigue crack growth rate was characterized with the average time-dependent fracture mechanics parameter during the hold time $(C_t)_{avg}$ in many literature papers [26, 62, 63]. In this investigation, the average value of the C*(t) parameter during the hold time, $[C^*(t)]_{avg}$ was compared with $(C_t)_{avg}$ for discussion. Furthermore, the values of C_t and C*(t) at the half hold time, $(C_t)_{0.5th}$ and $[C^*(t)]_{0.5th}$, were proposed to approximate $(C_t)_{avg}$ and $[C^*(t)]_{avg}$, respectively. The details for calculating the proposed parameters, $[C^*(t)]_{avg}$, $(C_t)_{0.5th}$ and $[C^*(t)]_{0.5th}$ are discussed in the next chapter.

3.3.5 Programming

Several EXCEL worksheets were customized for processing the original readings from all the tests. Four FORTRAN programs were written for the final data processing. The seven-point incremental polynomial method and the differentiation of the polynomial were used in these programs. In the program for processing the creep crack growth data, the procedures given in ASTM standard E1457 [38] were followed so that each step of the calculation can be easily tracked and understood. However, the subroutine suggested in the appendix of the standard was not adopted because of its somewhat tediousness. The programs for processing the data of triangular waveform loading tests and creep-fatigue tests were obtained by modifying the program for creep crack growth data processing. All these programs are given in the Appendices.

3.4 Microstructural Characterization

3.4.1 Tensile and Creep Deformation Specimens

Microstructural characterizations with optical microscopy (OP), scanning electron microscopy (SEM) and X-ray Diffraction (XRD) were conducted on the tested creep

deformation specimens before and after the testing to provide a mechanistic understanding of the creep deformation behavior of HR160. The creep deformation samples for microstructural characterization were obtained at the four different creep stages: the as-received, primary creep, secondary creep and tertiary creep stages. Some tested tensile specimens were also characterized for comparison. Machining of the tested tensile and creep deformation samples was conducted to provide cross sections for microstructural characterization perpendicular and parallel to the loading direction respectively. The specimens were sliced, mounted in epoxy, polished and electrolytically etched for observation. The etching was conducted in a solution of 75 ml hydrogen chloride acid (HCl) and 25 ml glycerol [$C_3H_5(OH)_3$] with the voltage range from 0.1 to 5 volts. The voltage was manually controlled to obtain the optimal etching effect.

3.4.2 Creep Crack and Creep-Fatigue Crack Growth Specimens

The tested creep crack and creep-fatigue crack growth samples were prepared for microstructural characterizations in two fashions. A tested C(T) sample was first sectioned with an electrical discharge machine (EDM) through the middle of the specimen thickness. Then, one half of the sectioned sample was polished and etched for crack tip characterizations with OP and SEM. The first three samples were observed and photographed before and after etching so that the effect of etching on creep cavity size, if any, could be identified. The other half of the tested C(T) sample was fractured by fatigue at room temperature on a fatigue machine to avoid further plastic deformation. The initial and final crack lengths were measured on this half, and the fracture surface was observed with SEM. For comparison, samples of fracture surface produced by fatigue or tensile overloading at room temperature were prepared from the as-received HR160. To check for the possible uneven crack fronts, most tested samples were fractured by fatigue without being sectioned through the middle of the specimen

thickness. A few sectioned half samples were also fractured by fatigue after the crack tip characterization. No obvious uneven crack fronts has been found.

CHAPTER IV

RESULTS AND DISCUSSION

4.1 Tensile and Creep Deformation Properties and Microstructures

Tensile and creep deformation test results are presented and discussed first in this chapter, because these results are needed for the calculation of the time-dependent fracture mechanics parameters, and the microstructures of the tested specimens can provide insights for understanding the microstructural evolution during the exposure to the elevated temperatures and applied stresses.

4.1.1 Tensile Test Results

The results of tensile tests of the as-received HR160 are listed in Table 4.1-1, and those of the aged, coarse grain size and welded HR160 are given in Table 4.1-2.

A comparison of the results from different heats in Table 4.1-1 shows that there is no obvious heat effect on the tensile properties of this material. For heat 7011, sample No. 1 and No. 2 were tested at 23°C (73.4°F) and 900°C (1652°F), respectively. Their corresponding samples from heat 7507 were No. 13 and No. 15. All the tensile property parameters listed in Table 4.1-1, the yield strength, the ultimate tensile strength, the rupture strain and the reduction in area are close in values under the same test conditions in spite of the heats. The maximum difference between the counterpart values is approximately 10%, which can be considered as the scattering of data.

It is also evident in Table 4.1-1 that temperature has a great effect on tensile properties. As the temperature changes from 850°C (1562°F) to 950°C (1742°F), the yield strength drops approximately 46%. In case of creep crack propagation, this can greatly increase the size of the plastic zone at the crack tip and thus, increases the creep

Table 4.1-1 Tensile Test Results of the As-Received HR160

Sample No.	Temperature		0.2% Yield Strength		Ultimate Tensile Strength		Rupture Strain	Reduction in Area	D		m
	℃	℉	MPa	ksi	MPa	ksi	%	%	MPa^{-m}	ksi^{-m}	
Heat 7011											
1	23	73.4	349.5	50.72	792.4	115	83.4	73.5	7.25×10^{-9}	9.80×10^{-7}	2.54
2	900	1652	115.6	16.8	133.6	19.4	158.4	99.2	1.49×10^{-30}	1.68×10^{-19}	13.19
Heat 7507											
13	23	73.4	313.3	45.5	771.7	112	83.7	73.6	2.17×10^{-7}	1.16×10^{-5}	2.06
14	850	1562	157.4	23.9	185.6	26.9	132.4	84.5	2.91×10^{-54}	3.6×10^{-35}	22.77
15	900	1652	119.3	17.3	136.4	19.8	146.2	97.9	1.6×10^{-27}	1.19×10^{-17}	11.78
16	950	1742	84.7	12.3	97.4	14.1	147.8	95.7	1.6×10^{-22}	4.19×10^{-14}	10.04

Table 4.1-2 Tensile Test Results of HR160 Under Different Material Conditions

Sample Designation	0.2% Yield Strength		Ultimate Tensile Strength		Rupture Strain	Reduction in Area	D		m
	MPa	ksi	MPa	ksi	%	%	MPa^{-m}	ksi^{-m}	
Temperature: 23°C (73.4°F)									
As-received	313.3	45.5	771.7	112	83.7	73.6	2.17×10^{-7}	1.16×10^{-5}	2.06
Coarse Grain	250.2	36.3	614.8	89.2	87.3	73.8	4.3×10^{-8}	4.08×10^{-6}	2.36
Weldment	317.9	46.1	598.3	86.8	32.9	17	1.4×10^{-13}	5.39×10^{-10}	4.28
Aged	253.5	36.8	475.1	69	16	13.3	3.5×10^{-14}	2.4×10^{-10}	4.58
Temperature: 850°C (1562°F)									
As-received	157.4	23.9	185.6	26.9	132.4	84.5	2.91×10^{-54}	3.6×10^{-35}	22.8
Coarse Grain	129.8	18.8	144.1	20.9	110.1	74.1	4.38×10^{-32}	1.51×10^{-20}	13.8
Weldment	134.5	19.5	151.6	22.0	50.2	60.6	9.25×10^{-49}	5.27×10^{-31}	21.2
Aged	137.1	19.9	152.9	22.2	115.3	88.3	1.30×10^{-28}	1.56×10^{-18}	12.0

crack growth rate. However, the ductility is increased with temperature. This may help decrease the creep crack growth rate. The details about the effect of ductility on creep crack growth behavior are discussed in Section 4.5.

In Table 4.1-2, the data show that grain coarsening, aging and welding slightly decrease the strength of the material, especially at the elevated temperature. The most obvious effect of the material condition on the tensile properties is the drop of ductility in the weld, at both room and elevated temperatures. At room temperature, the rupture strain decreases approximately 60%, and at 850°C (1562°F) it drops about 62%. Later discussion in Section 4.5 shows that the decrease in ductility of the weld makes it a weak part against creep crack propagation.

In both Table 4.1-1 and Table 4.1-2, changes in the strain hardening exponent (m) and the plasticity coefficient (D) from room temperature to elevated temperatures are obvious. The strain hardening exponent (m) increases while the plasticity coefficient (D) decreases as the temperature changes from room temperature to elevated temperatures. However, their values at the elevated temperatures, especially the values of the plasticity coefficient (D), show great variations without obvious correlation with the temperatures or the material conditions. It is possible that the effects of temperature and material condition on m and D under these circumstances are so small that they are covered by the scattering of the data. In mechanical test results, the scattering of data is commonly found. In this study, the way these data were processed to obtain the values of m and D may have worsened the situation. The values of m and D have been obtained by processing the developed true stress and true strain data on a logarithmic base and then converted to the present values. Many factors, such as the scattering in the original data, the number of the data points used for curve fitting, and their distribution on the coordinate system can greatly affect the final values. Fortunately, further calculation did not show evident effects resulting from the variations in the values of m and D on the

time-dependent fracture mechanics parameters. It seems that the time-dependent fracture mechanics parameters are insensitive to these two tensile property parameters. This is reasonable because the time-dependent fracture mechanics parameters are designed to describe the phenomena under creep conditions.

Since the accuracy of using the Ramberg-Osgood stress and strain equation to represent the tensile behavior of a material increases with the plasticity of the material, the experimental data were plotted with the calculated curves from the equation to verify the m and D values obtained. The results showed that all the calculated curves matched the experimental data with reasonable accuracy except those at room temperature 23°C (73.4°F). Two of these plots, one at 23°C (73.4°F) and the other at 850°C (1562°F) respectively, are presented in Figure 4.1-1 and Figure 4.1-2. Obviously, at 850°C (1562°F), the material displays enough plasticity to be accurately represented by the equation. In this investigation, 850°C (1562°F) was the lowest temperature employed for time-dependent fracture mechanics characterization. Since the test results in Table 4.1-1 and Table 4.1-2 show that the ductility and plasticity increase with temperature, the m and D values obtained at these temperatures can truly describe the tensile deformation of the material and be used in the time-dependent fracture mechanics characterization.

4.1.2 Creep Deformation Test Results

A typical creep strain versus time curve resulting from a creep deformation test of the as-received HR160 is given in Figure 4.1-3. The test temperature was 850°C (1562°F) and the load level was 38.45 MPa (5.58 ksi). It is observed that the curve has a primary creep strain of about 10% even at the high temperature of 850°C (1562°F) with the rupture time of 4,109 hours. Another test at 900°C (1652°F) with the rupture time of more than 5,000 hours also shows obvious primary creep strain. This is not commonly found in many materials when exposed to such temperatures for such a long time. The

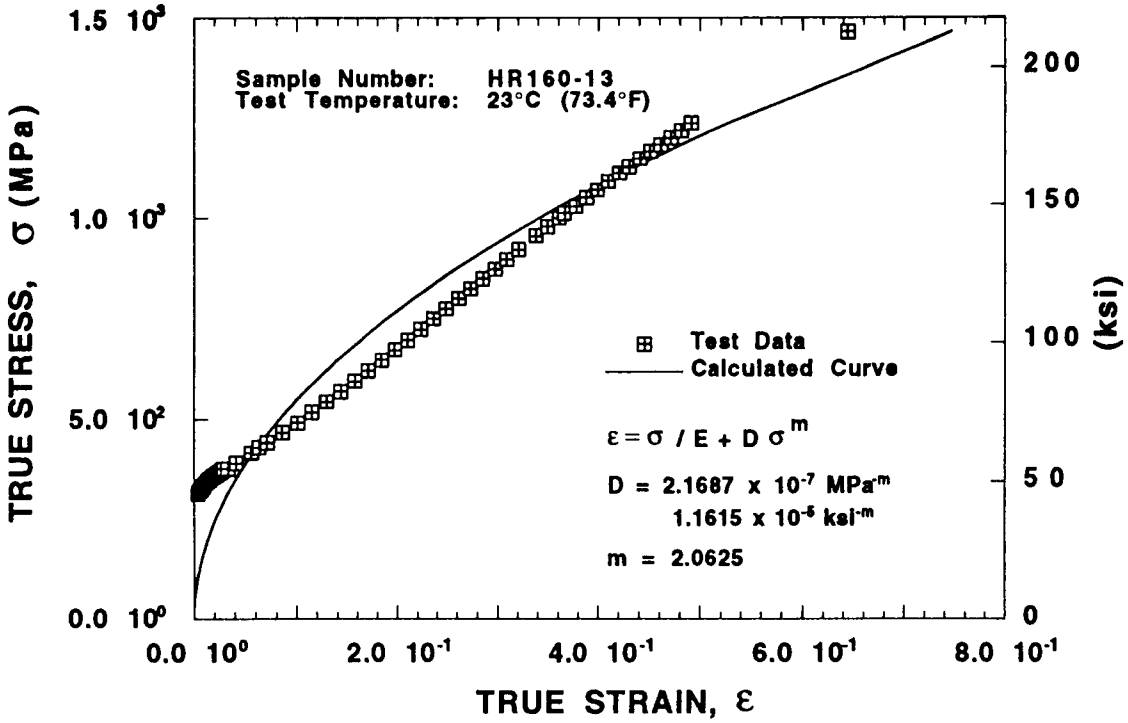

Figure 4.1-1 Calculated and Experimental True Stress Versus True Strain Curves of HR160 at 23°C (73.4°F)

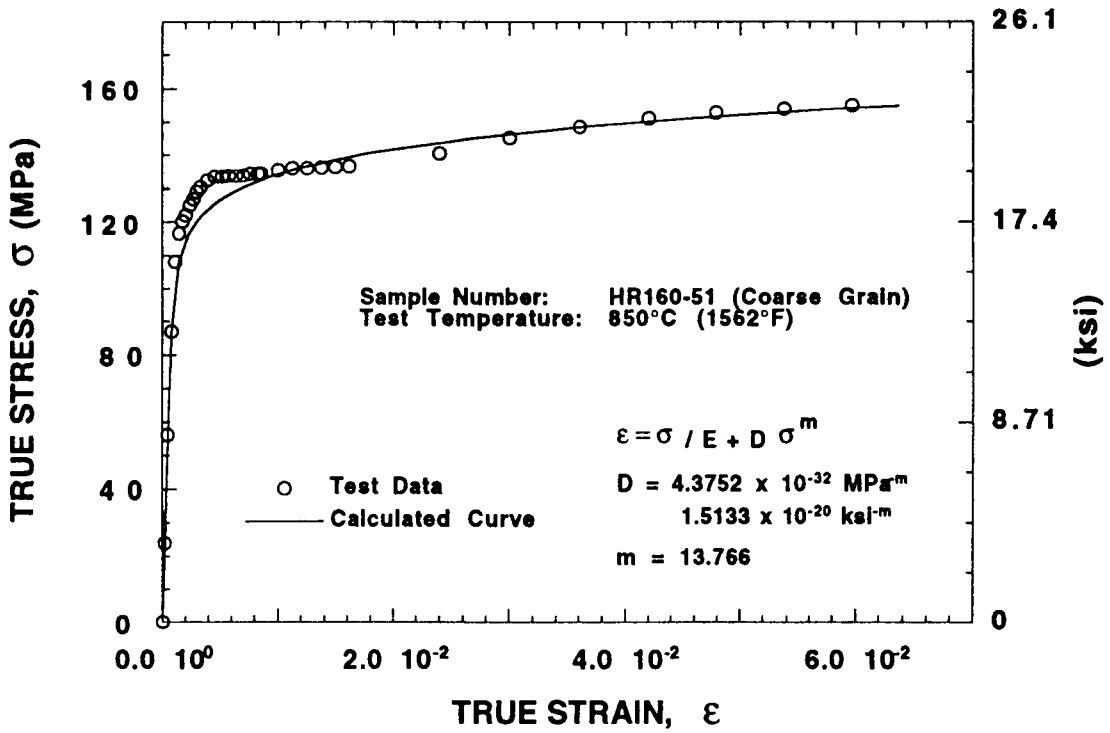

Figure 4.1-2 Calculated and Experimental True Stress Versus True Strain Curves of HR160 at 850°C (1562°F)

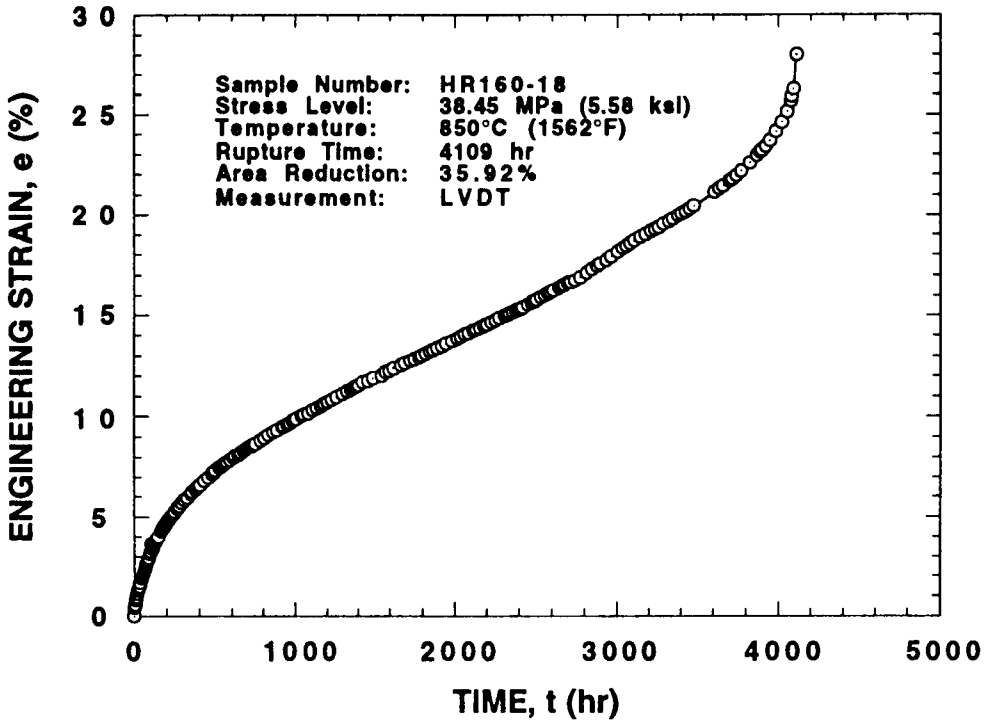

Figure 4.1-3 Typical Creep Strain Versus Time Curve of the As-Received HR160 Showing Significant Primary Creep.

reason for this phenomenon is not well understood so far. This large primary strain of HR160 can be an advantage or disadvantage, depending on the application requirements. When the dimensions of a structure serving at elevated temperatures are strictly required, the large primary creep strain may soon disqualify its components made of HR160. However, in case that the dimensions of the structure are not very important, the large portion of primary creep strain may help relax the stress concentration at a creep crack tip and thus, tend to increase creep crack resistance.

All the creep deformation test results obtained in this investigation are given in three tables. The results of the as-received HR160 is given in Table 4.1-3, coarse grain size in Table 4.1-4, a comparison of the as-received, coarse grain size, aged and welded conditions in Table 4.1-5. The shortest rupture time shown in these tables is approximately 10 hours and the longest is about 5,415 hours. Two tests with the lowest load level have lasted for more than 5,500 hours and are still running. The minimum creep rates in these tables cover a range from 10^{-2} to 10^{-5} 1/hr. All these test results have been plotted as minimum creep engineering strain rate ($\dot{e}$) versus initial engineering stress (s) and are given in four figures. The results from the as-received are given in Figure 4.1-4. The values of A_2 and n of the as-received are listed in this figure. The values of A_2 range from 10^{-19} to 10^{-8} ($MPa^{-n} \cdot hr^{-1}$), while those of n remain approximately 8. For comparison purpose, the results of the two different heats are presented in Figure 4.1-5, the as-received and the coarse grain size in Figure 4.1-6, and the as-received, coarse grain size, aged and welded in Figure 4.1-7. The values of A_2 and n of all the tests including the as-received, coarse grain size, aged and welded are listed in Table 4.1-6.

It is shown in Figure 4.1-4 that at each temperature, there is a linear relationship between $\log(\dot{e})$ and log(s), which can be described by Equation (2.2-6). Obvious temperature effect on the minimum creep rate can be seen in this figure, i.e., at a given

Table 4.1-3 Creep Deformation Test Results of the As-Received HR160

Sample No.	Temperature		Applied Stress		Creep Rate	Rupture Strain	Reduction in Area	Rupture Time
	°C	°F	MPa	ksi	1/hr	%	%	hr
AR18	850	1562	38.45	5.58	3.95×10^{-5}	30	35.9	4109
AR21	850	1562	48.23	7.0	2.98×10^{-4}	48	71.6	705
AR22	850	1562	64.1	9.3	1.61×10^{-3}	53	75.0	208
AR30	850	1562	82.68	12.0	3.60×10^{-2}	87	90.3	10.7
AR17	900	1652	24.12	3.5	3.05×10^{-5}	25	26.3	5415
AR20	900	1652	38.45	5.58	3.06×10^{-4}	42	66.7	619
AR23	900	1652	48.23	7.0	2.87×10^{-3}	70	91.8	98.4
AR32	900	1652	64.1	9.3	2.81×10^{-2}	88	97.1	14.6
AR16	950	1742	13.78	2.0	-	-	-	> 5,500
AR19	950	1742	24.12	3.5	1.99×10^{-4}	40	93.5	783.7
AR24	950	1742	38.45	5.58	5.58×10^{-3}	74	96.7	46.9
AR31	950	1742	48.23	7.0	2.59×10^{-2}	75	98.9	11.7

Table 4.1-4 Creep Deformation Test Results of Coarse Grain Size HR160

Sample No.	Temperature		Applied Stress		Creep Rate	Rupture Strain	Reduction in Area	Rupture Time
	℃	℉	MPa	ksi	1/hr	%	%	hr
CGS45	850	1562	38.45	5.58	4.49×10^{-5}	26.7	20.7	3556.6
CGS42	850	1562	48.23	7.0	3.89×10^{-4}	39.8	42.4	588.7
CGS39	850	1562	64.1	9.3	5.58×10^{-3}	67.4	67.4	77
CGS38	850	1562	82.68	12.0	3.96×10^{-2}	91.6	66.5	12.8
CGS37	900	1652	24.12	3.5	3.01×10^{-5}	-	-	-
CGS40	900	1652	38.45	5.58	6.12×10^{-4}	38.7	40.4	331.6
CGS43	900	1652	48.23	7.0	3.72×10^{-3}	55.8	77.5	104.3
CGS46	900	1652	64.1	9.3	5.07×10^{-2}	84.4	79.7	10.5
CGS47	950	1742	13.78	2.0	-	-	-	> 5,500
CGS41	950	1742	24.12	3.5	1.31×10^{-4}	30.8	52.4	1007.7
CGS44	950	1742	38.45	5.58	3.96×10^{-3}	52.7	84.1	55.8
CGS49	950	1742	48.23	7.0	6.12×10^{-2}	68.4	75.9	5.8

Table 4.1-5 Creep Deformation Test Results of the As-Received (AR), Coarse Grain Size (CGS), Aged (AD) and Welded (WD) HR160

Sample No	Temperature		Applied Stress		Creep Rate	Rupture Strain	Reduction in Area	Rupture Time
	℃	℉	MPa	ksi	1/hr	%	%	hr
AR21	850	1562	48.23	7.0	$2.98x10^{-4}$	48.0	71.6	705
CGS42	850	1562	48.23	7.0	$3.89x10^{-4}$	39.8	42.4	588.7
AD03	850	1562	48.23	7.0	$4.60X10^{-4}$	64.8	86.4	615.3
WD01	850	1562	48.23	7.0	$9.78X10^{-5}$	18.1	9.5	720.2
AR22	850	1562	64.1	9.3	$1.61x10^{-3}$	53.0	75.0	208
CGS39	850	1562	64.1	9.3	$5.58x10^{-3}$	67.4	67.4	77
AD02	850	1562	64.1	9.3	$1.65X10^{-2}$	93.0	92.5	24
WD02	850	1562	64.1	9.3	$2.16X10^{-3}$	32.6	82.8	81.9
AR30	850	1562	82.68	12.0	$3.60x10^{-2}$	87	90.3	10.7
CGS38	850	1562	82.68	12.0	$3.96x10^{-2}$	91.6	66.5	12.8
AD01	850	1562	82.68	12.0	$2.91X10^{-2}$	99.1	91.4	12
WD03	850	1562	82.68	12.0	$9.89X10^{-3}$	45.6	84.3	24.9

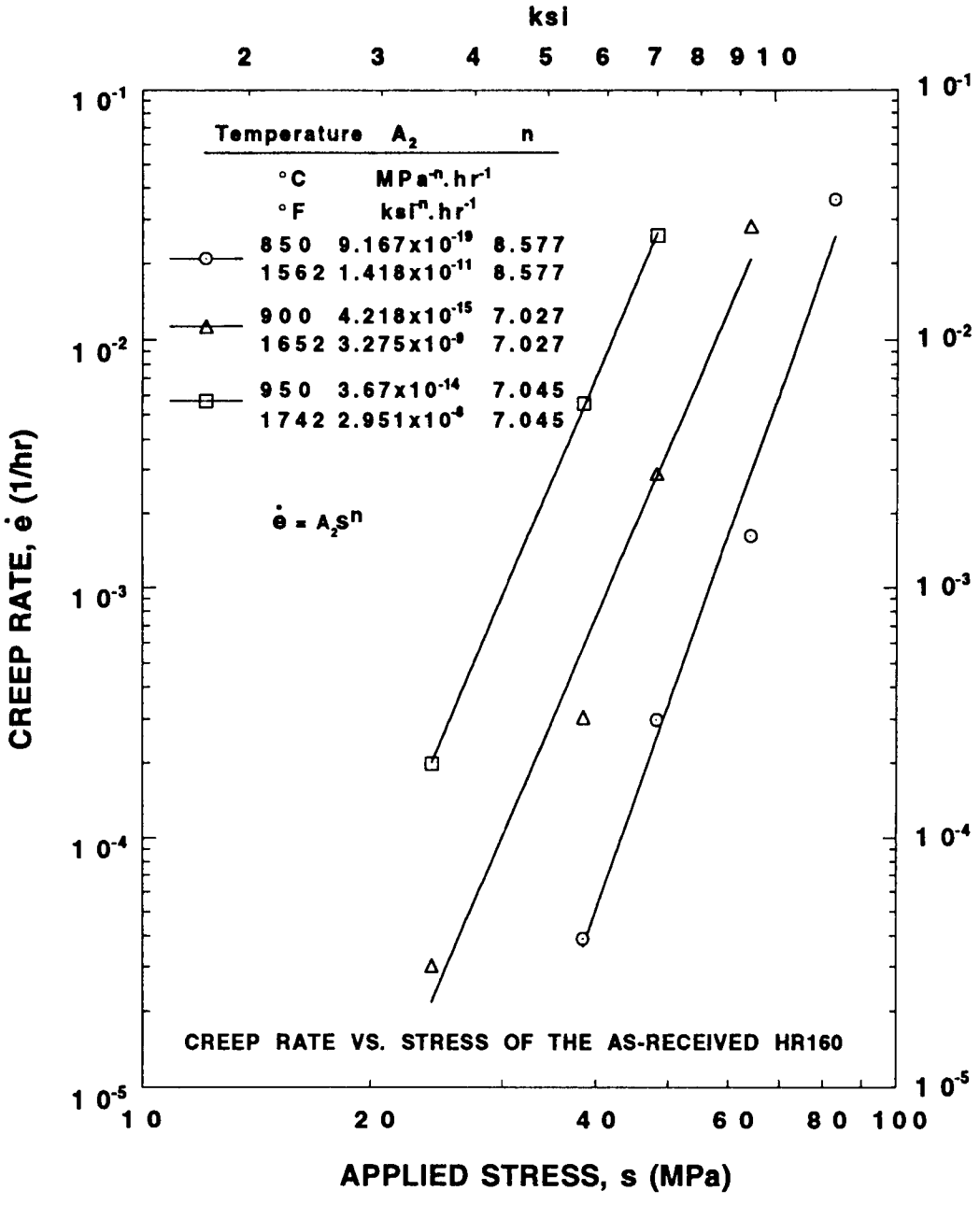

Figure 4.1-4 Minimum Creep Engineering Strain Rate Versus Applied Stress of the As-Received HR160 at Temperatures of 850, 900 and 950°C (1562, 1652 and 1742°F)

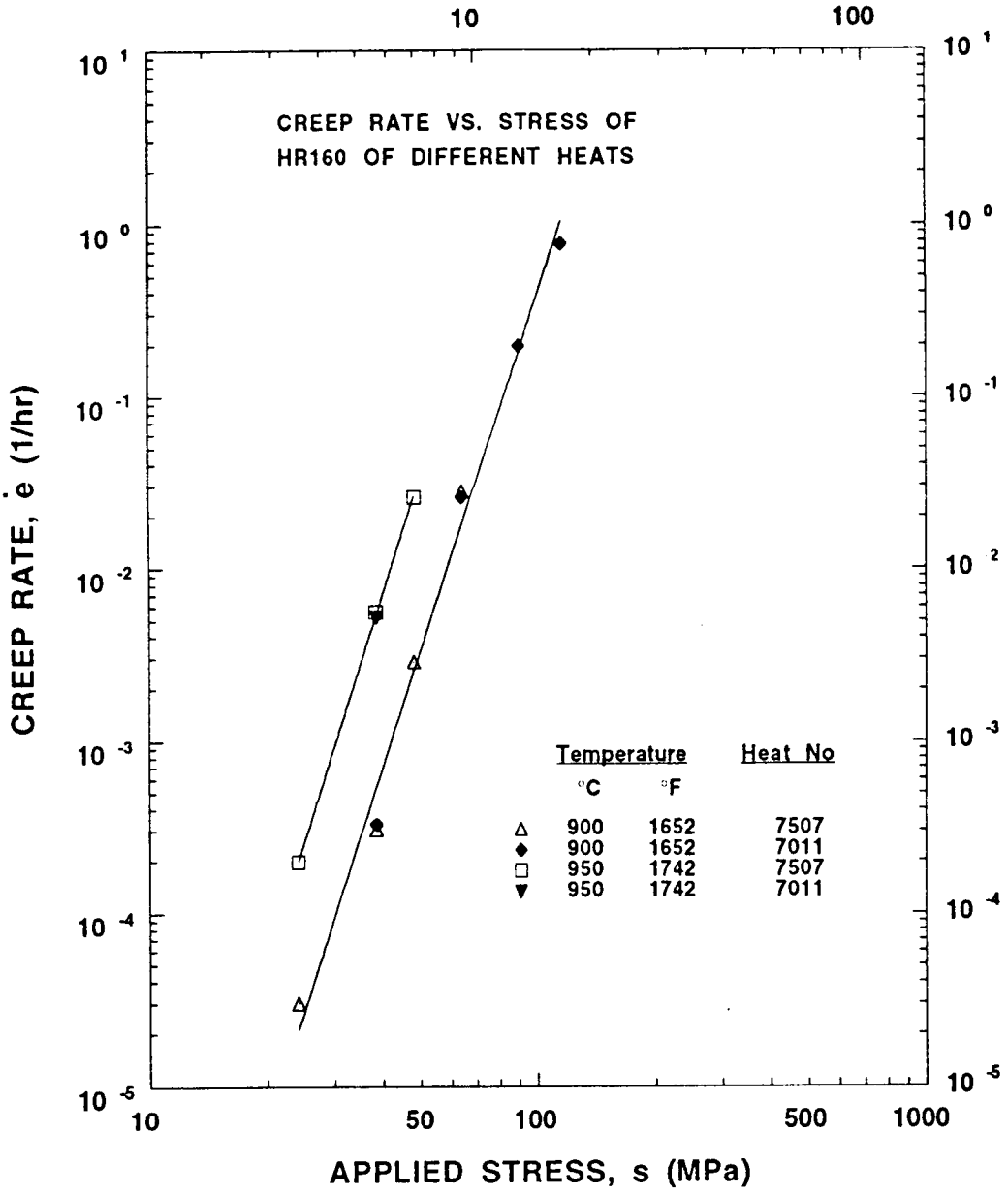

Figure 4.1-5 Minimum Creep Engineering Strain Rate Versus Applied Stress of the Different Heats of the As-Received HR160 at Temperatures of 900 and 950°C (1652 and 1742°F)

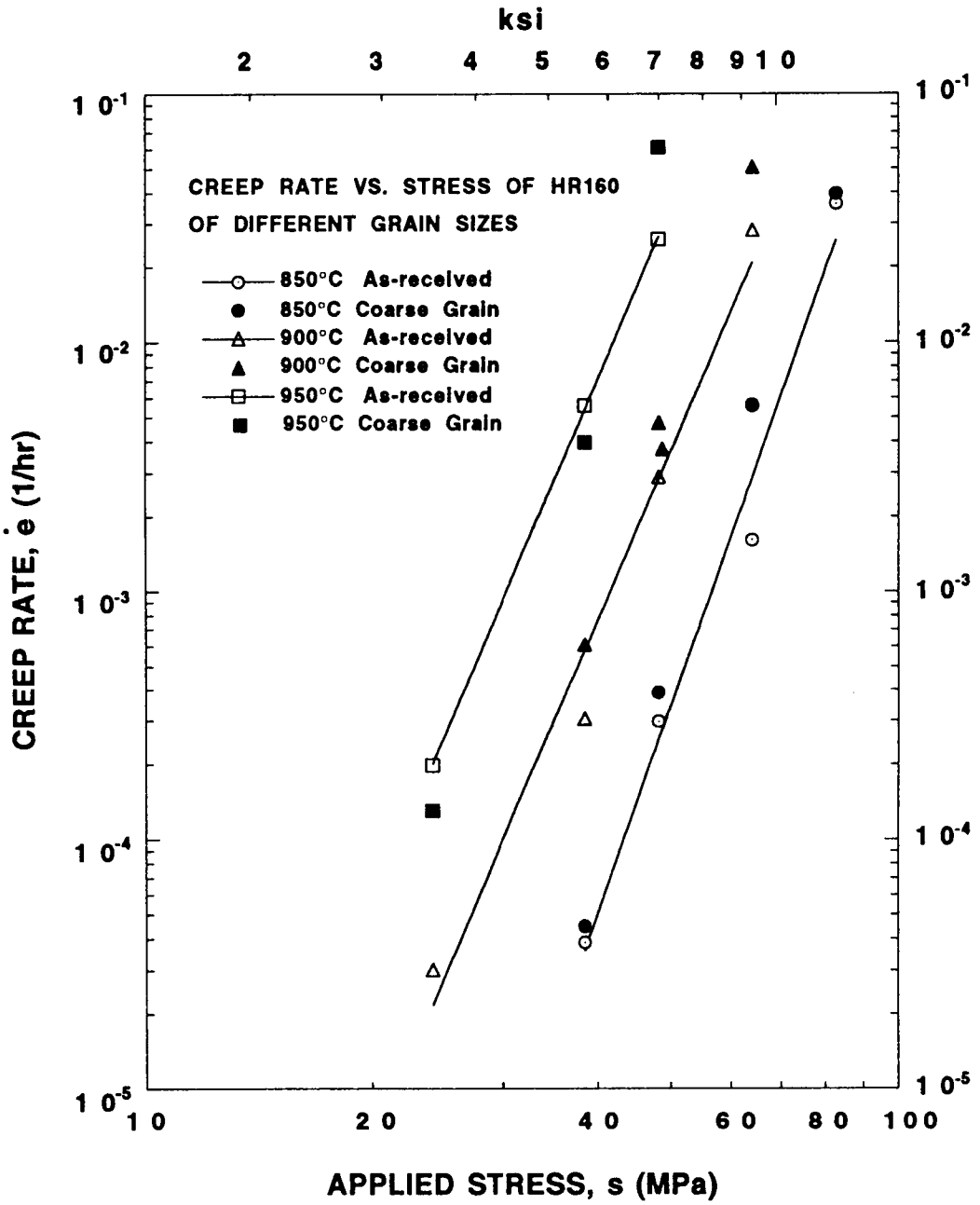

Figure 4.1-6 Minimum Creep Engineering Strain Rate Versus Applied Stress of the As-Received and Coarse Grain Size HR160 at Temperatures of 850, 900 and 950°C (1562, 1652 and 1742°F)

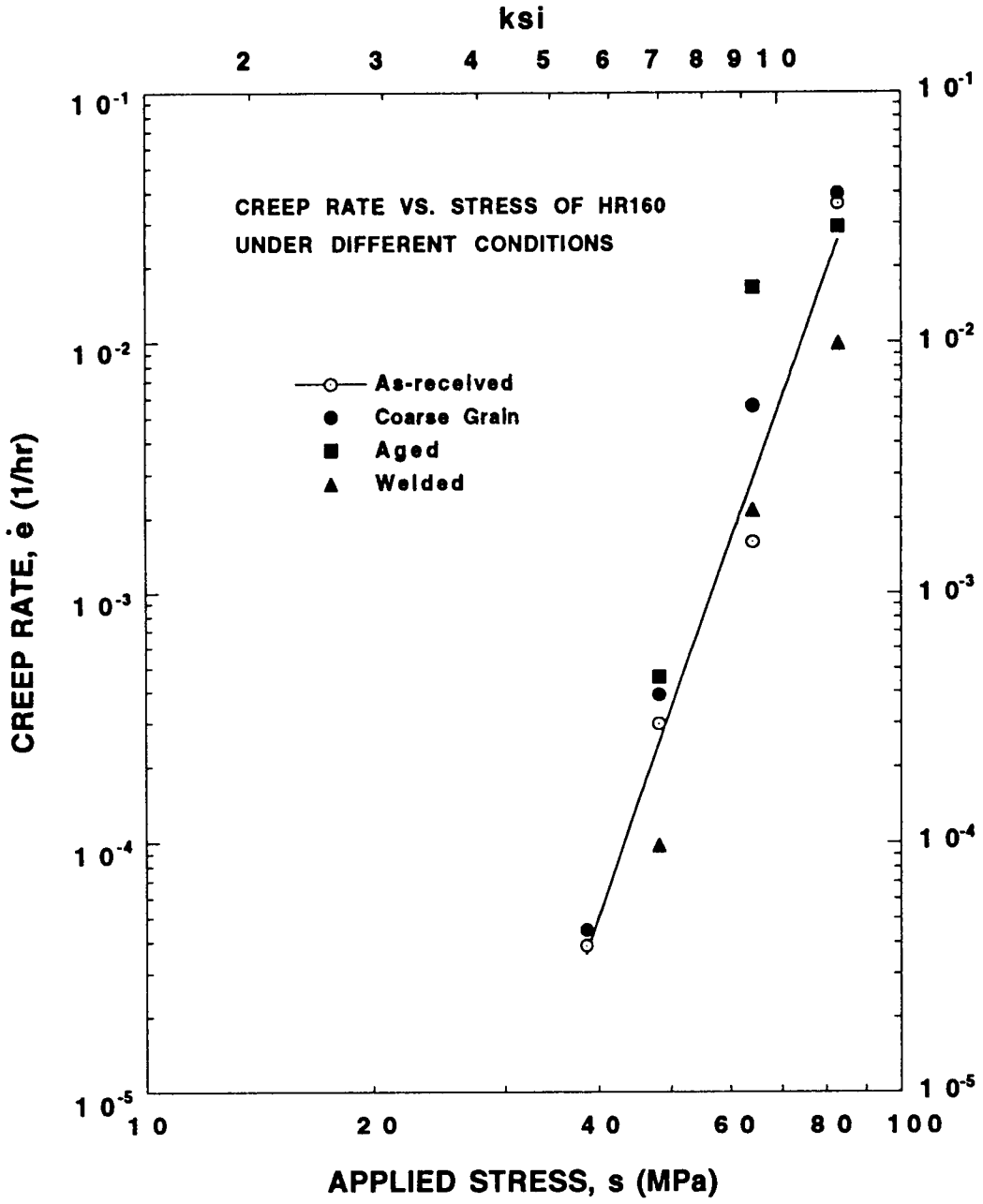

Figure 4.1-7 Minimum Creep Engineering Strain Rate Versus Applied Stress of the As-Received, Coarse Grain Size, Aged and Welded HR160 at the Temperature of 850°C (1562°F)

Table 4.1-6 The Values of Secondary Creep Coefficient and Exponent of HR160 Under Different Material Conditions

Condition	Temperature		A_2		n
	℃	℉	$MPa^{-n}hr^{-1}$	$ksi^{-n}hr^{-1}$	
As-received	850	1562	9.167×10^{-19}	1.418×10^{-11}	8.577
Coarse Grain	850	1562	3.741×10^{-19}	1.098×10^{-11}	8.909
Aged	850	1562	5.487×10^{-17}	1.862×10^{-10}	7.791
Welded	850	1562	3.872×10^{-19}	6.370×10^{-12}	8.609
All	850	1562	1.273×10^{-18}	1.805×10^{-11}	8.532
As-received	900	1652	4.218×10^{-15}	3.275×10^{-9}	7.027
Coarse Grain	900	1652	1.190×10^{-17}	2.083×10^{-10}	8.641
As-received	950	1742	3.670×10^{-14}	2.951×10^{-8}	7.045
Coarse Grain	950	1742	1.302×10^{-16}	2.252×10^{-9}	8.635

stress level, increasing the temperature increases the minimum creep rate. This trend can also be seen in the fact that the coefficient A_2 becomes greater as the temperature increases. However, n is not sensitive to temperature.

In Figure 4.1-5, the straight lines are the fit lines based on the test results of the as-received heat 7507 which are represented by the clear symbols. The solid symbols represent the test results of the as-received heat 7011. At the same temperatures and applied stress levels, the data points of heat 7011 overlap those of heat 7507. Under the conditions of the same temperature but different applied stress levels, the data points of heat 7011 fall on the fit line of heat 7507. This trend indicates that there is no heat effects in the creep deformation behavior of the material investigated.

In Figure 4.1-6, the straight lines are the fit lines based on the as-received data points represented by the clear symbols. It can be seen that, at the same temperatures and applied stress levels, the data points of the coarse grain size represented by solid symbols do not overlap the as-received points as those of heat 7011 did in Figure 4.1-5. However, they fall near the fit lines of the as-received data. It is obvious that the change of grain size may have some effects on the creep deformation behavior, but the change from ASTM No. 3 to No. 00 in this investigation is not great enough to bring about obvious effects. Since the coarse grain size ASTM No. 00 in this investigation is the largest grain size which was achieved with great difficulties, a conclusion can be drawn at this point that the grain size of HR160 is quite stable when exposed to elevated temperatures, and the grown grain size has little effect on its minimum creep rate. Therefore, HR160 is a stable material when the relationship between grain size and creep deformation rate is concerned.

In Figure 4.1-7, the results of the coarse grain size, aged and welded HR160 are plotted with a set of as-received data points and its fit line. These data are obtained from the tests at the same temperature. Obviously, as in Figure 4.1-6, the different material

conditions such as coarse grain size, aged and welded structures have little effect on the minimum creep rate of the material. All the data points fall near the fit line developed from the as-received material. Therefore, HR160 is quite stable in the minimum creep rate under these different material conditions tested in this investigation.

Although different material conditions such as heat, coarse grain size, the aged and the welded did not show obvious effects on the relationship between the minimum creep rate and the applied stress, a great effect of welding has been found on the stage of creep deformation. Figure 4.1-8 a) and Figure 4.1-8 b) show the curves of creep strain versus time of the as-received and the welded HR160, respectively. Both tests were conducted at a temperature of 850°C (1562°F) and a stress level of 64.1 MPa (9.3 ksi). It is obvious that the as-received curve has a significant amount of primary creep, while the welded curve starts directly from the secondary creep stage. This explains why the welded HR160 has much less creep ductility as indicated by the rupture strain and the reduction in area presented in Table 4.1-6. In the case of creep crack propagation, the great primary creep in the base metal and the lack of primary creep and creep ductility in the weld may increase the stress concentration at the crack tip in the weld area, making the weld a weak part against creep crack propagation.

4.1.3 Microstructural Characterization of Tensile and Creep Deformation Test Samples

Figure 4.1-9 shows the unetched cross section of a tested creep deformation sample (Figure 4.1-9 a) and that of a tested tensile sample (Figure 4.1-9 b). These cross sections are parallel to the applied stress direction. Both samples have been tested at 850°C (1562°F). The creep deformation test sample in Figure 4.1-9 a) shows small surface grain boundary cracks, while the tensile test sample in Figure 4.1-9 b) shows no such cracks. It is believed that those surface cracks in the creep sample were caused by the combination of stress and oxidation at elevated temperatures. Weakened grain

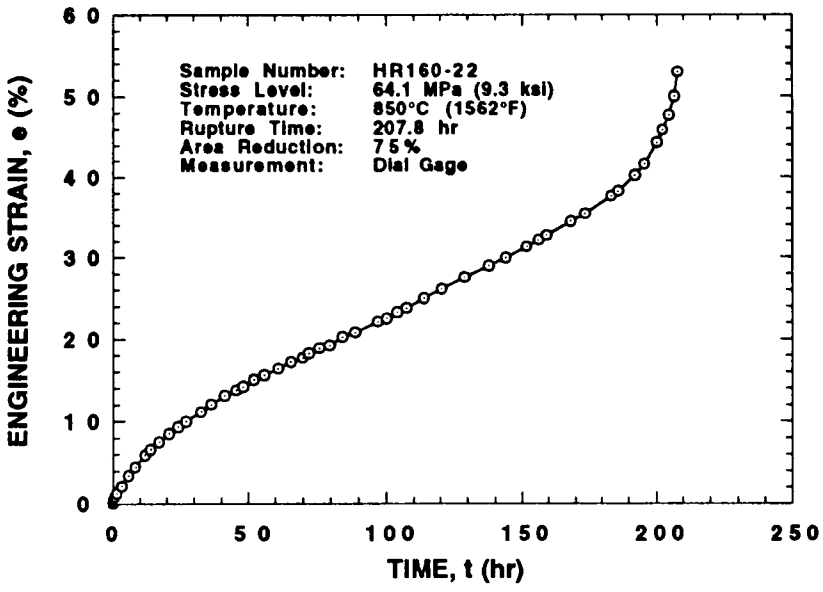

a) The As-Received HR160

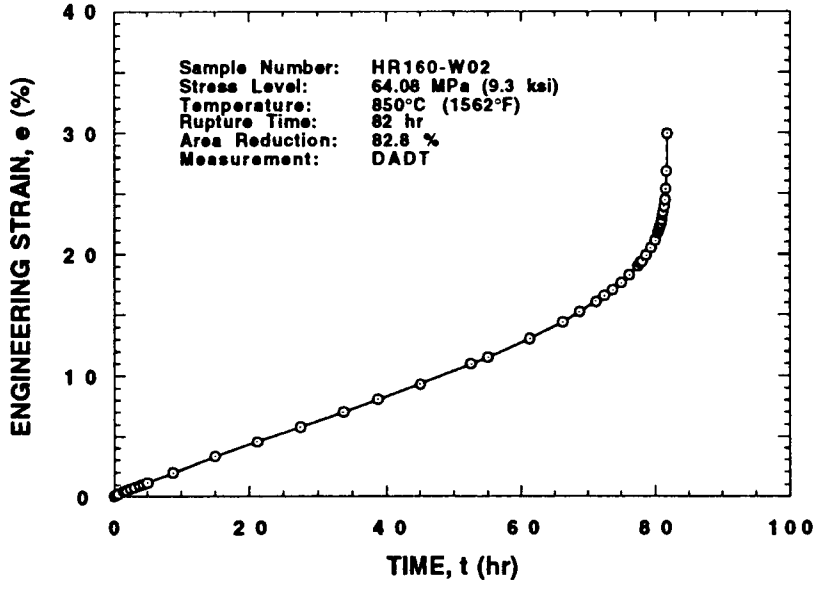

b) The Welded HR160

Figure 4.1-8 Creep Strain Versus Time Curves of the As-Received and Welded HR160 at a Temperature of 850°C (1562°) and a Stress Level of 64.1 MPa (9.3 ksi)

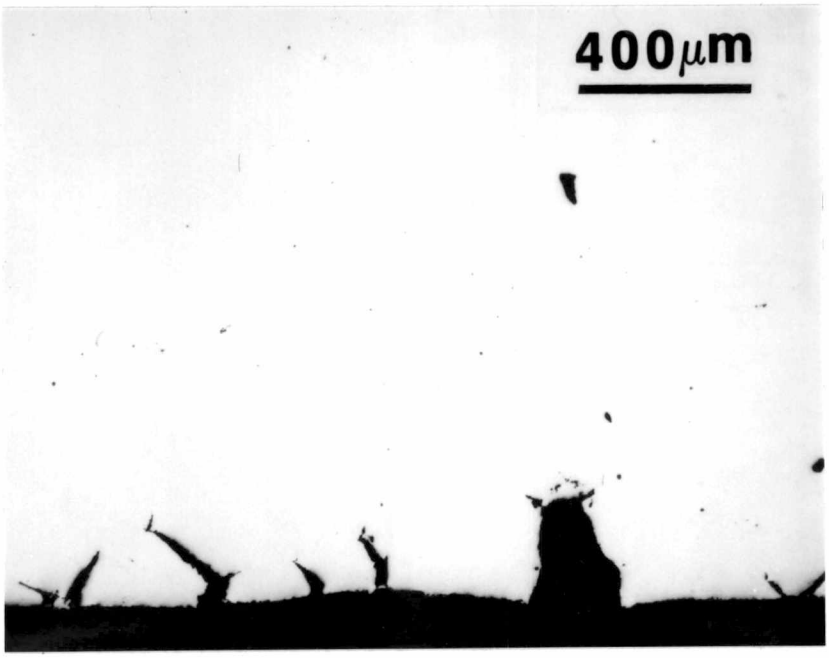

a) The Tested Creep Specimen Showing Deep Surface Cracks

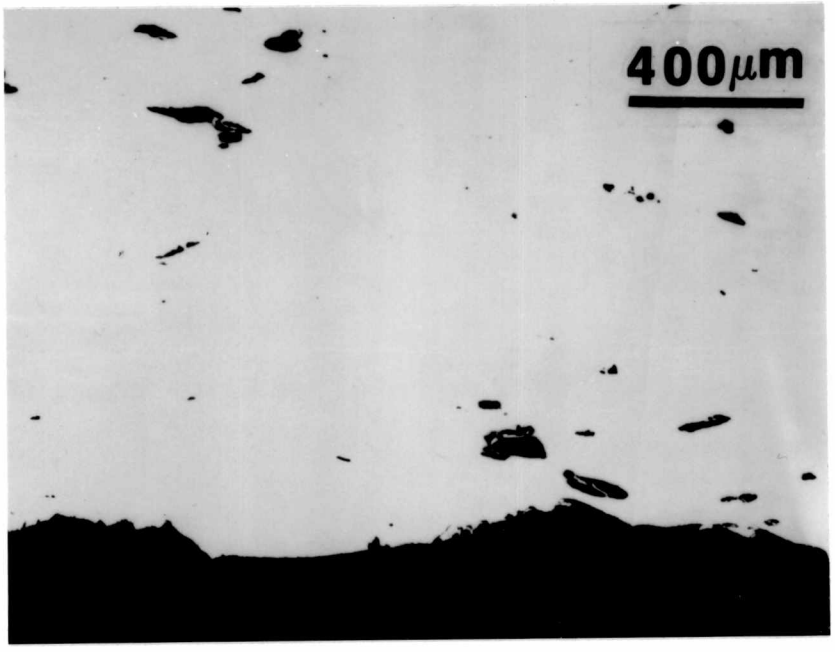

b) The Tested Tensile Specimen Showing A Rough Surface Without Deep Cracks

Figure 4.1-9 A Comparison Between the Unetched Cross Sections of a Tested Creep and a Tested Tensile Specimens Parallel to the Applied Stress Direction

boundaries resulting from creep might also have worsened the situation. In the tensile test case, there was not enough time for these combined mechanisms to occur.

The microanalyses of the creep deformation process were conducted on a test with the applied stress level of 48.23 MPa (7.0 ksi) and the testing temperature of 850°C (1562°F) as shown in Figure 4.1-10. The large circles on the creep curve in this figure represent the non-creep (as-received), primary creep, secondary creep (minimum rate creep), and tertiary creep stages, at which microanalyses have been conducted. The microstructures of these four stages are shown in Figure 4.1-11. The horizontal direction is the direction of applied stress except in the as-received condition. Figure 4.1-11 a) shows that the as-received condition is a clean, annealed austenitic structure with a grain size of ASTM No. 3. After exposure to 850°C (1562°F) for 40 hours with a strain of approximately 5%, the primary creep structure (Figure 4.1-11 b) shows some grain growth. (Note the different scales in figures a) and b).) Some cracks can be observed along the grain boundaries near the specimen surface. Little grain deformation can be observed at this stage. The structure in the secondary creep region (Figure 4.1-11 c), having exposed to 850°C for 400 hours with a strain of approximately 18%, shows more grain growth and obvious grain deformation along the direction of applied stress. The surface grain boundary cracks are deeper. At a strain of 42%, the tertiary creep structure (Figure 4.2-11 d) shows a significant amount of creep cavitation and grain deformation. Recrystallization seems to have occurred along the deformed grain boundaries. These new recrystallized grains, free of strain, may help slow down the creep cavity growth and increase creep crack resistance.

Another phenomenon observed from the different creep stages is that as the test time elapsed, precipitation occurred along grain boundaries, twin boundaries and precipitation habit planes. This phenomenon is shown clearly in Figure 4.1-12 which exhibits the corresponding microstructures of Figure 4.1-11 at higher magnifications.

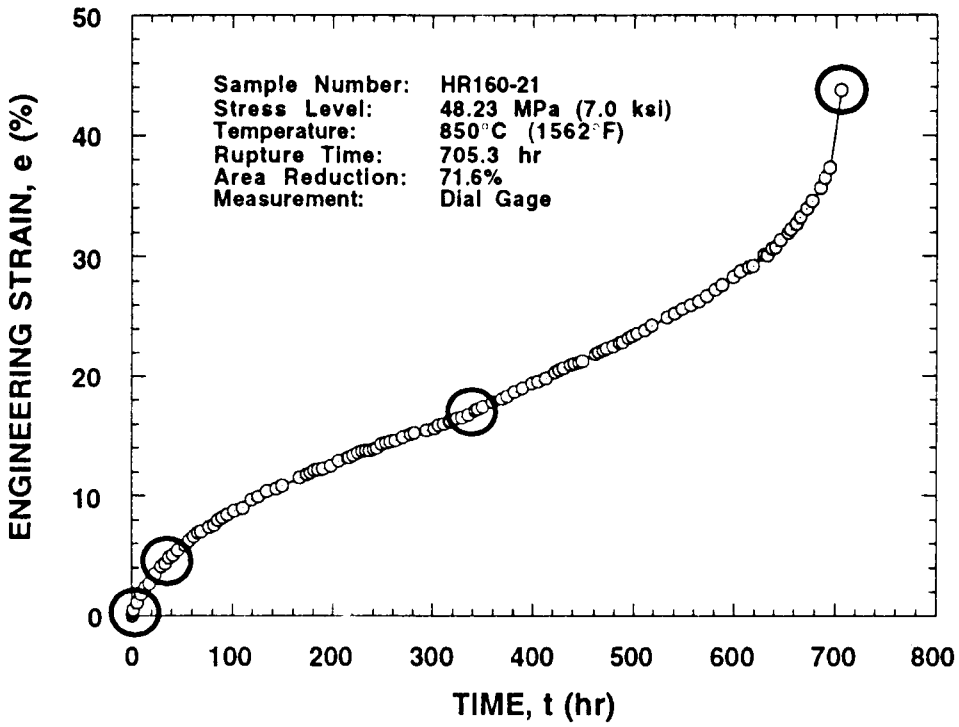

Figure 4.1-10 Large Circles on the Creep Curve Showing the Creep Deformation Stages at Which Microstructural Analyses Were Conducted: Non-Creep (the As-Received), Primary Creep, Secondary Creep (Minimum Rate Creep) and Tertiary Creep

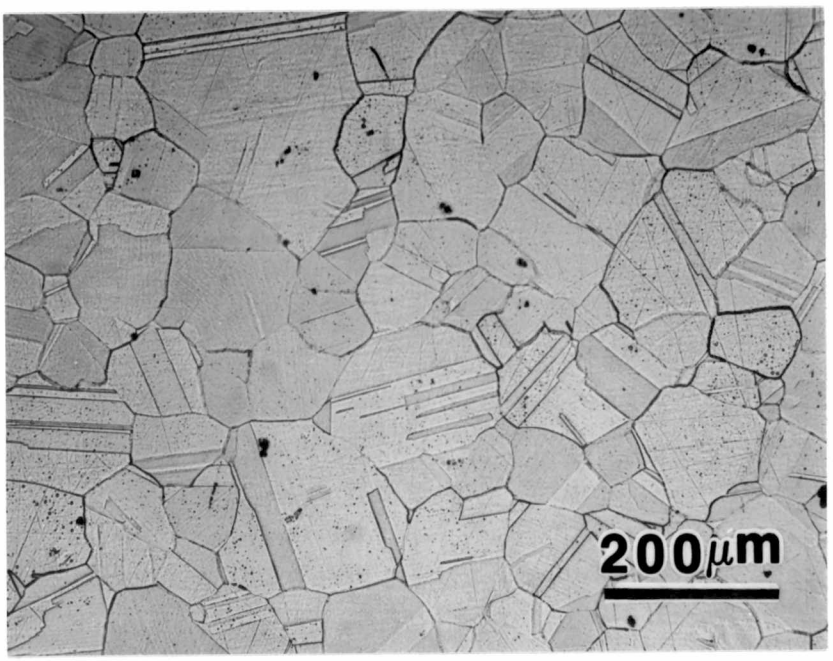

a) The As-Received Condition

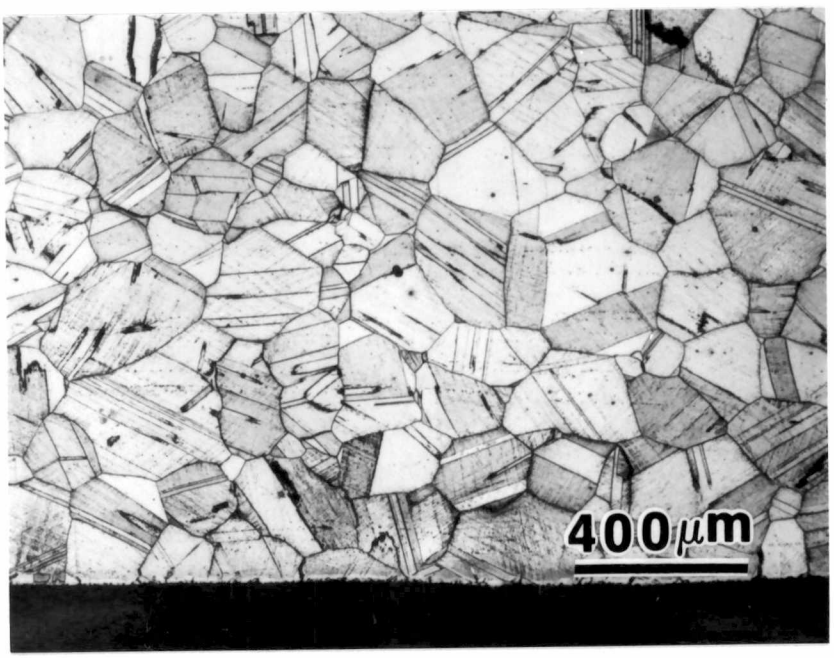

b) After Some Primary Creep at 850°C (1562°F)

Figure 4.1-11 Microstructures of Haynes HR160 at Different Creep Stages

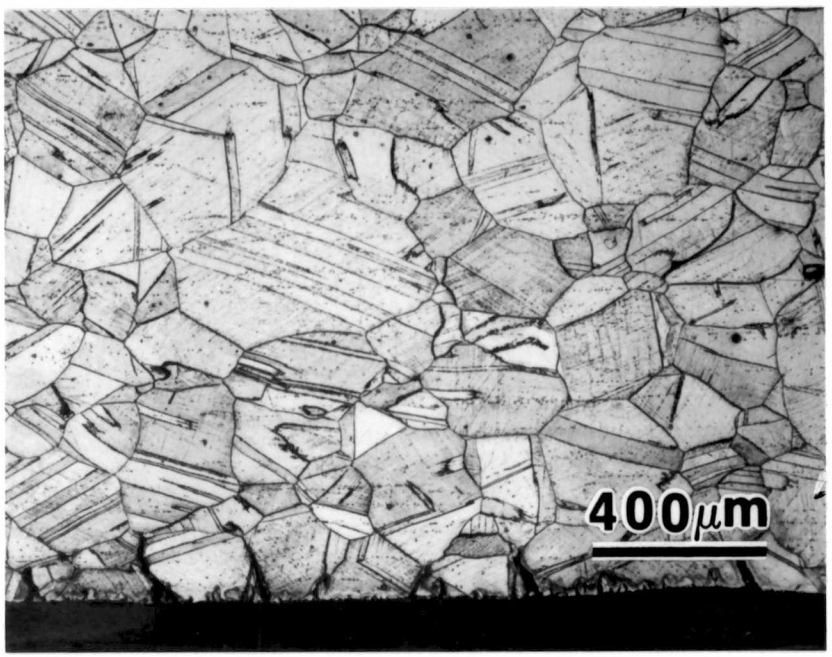

c) After a Period of Secondary Creep at 850°C (1652°F)

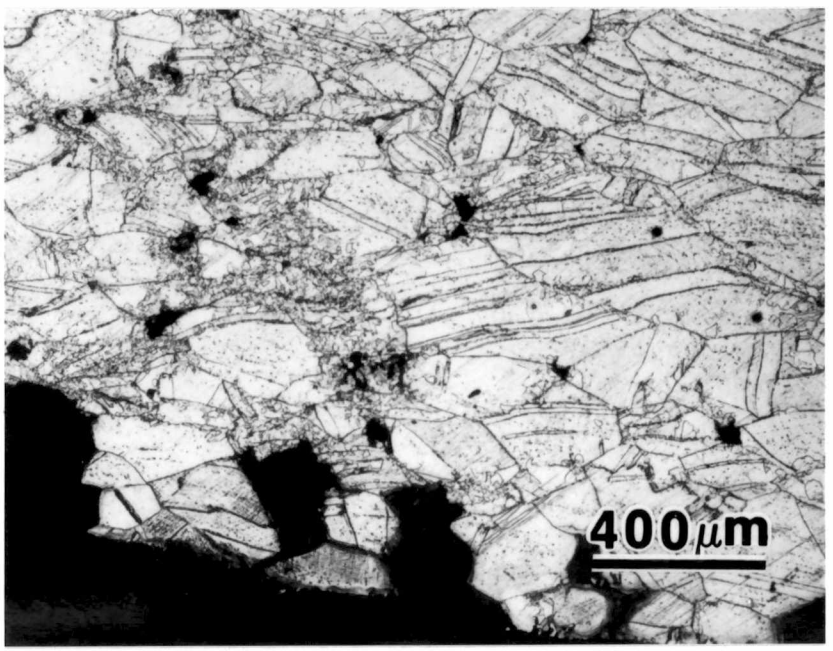

d) Ruptured After Tertiary Creep at 850°C (1562°F)

Figure 4.1-11 (Continued)

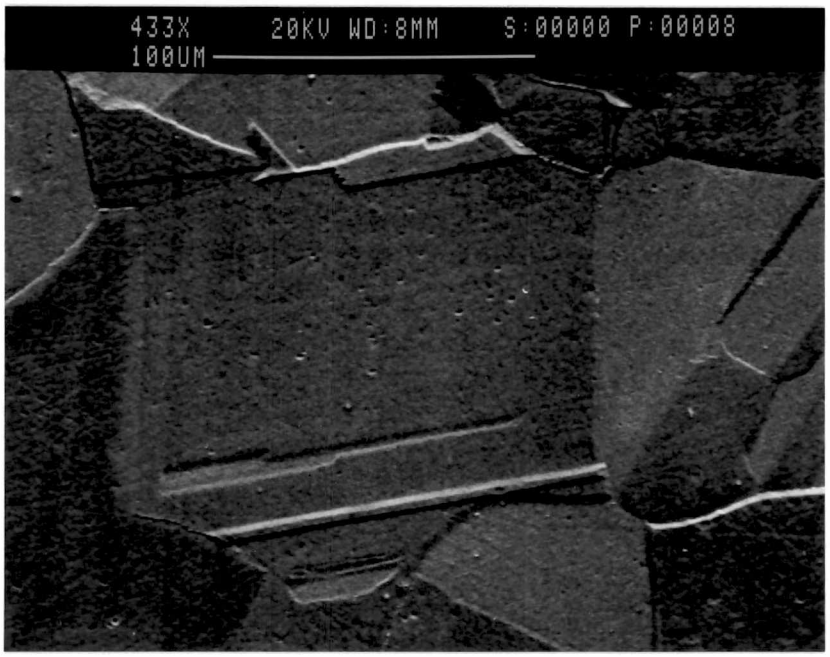

a) The As-Received Condition

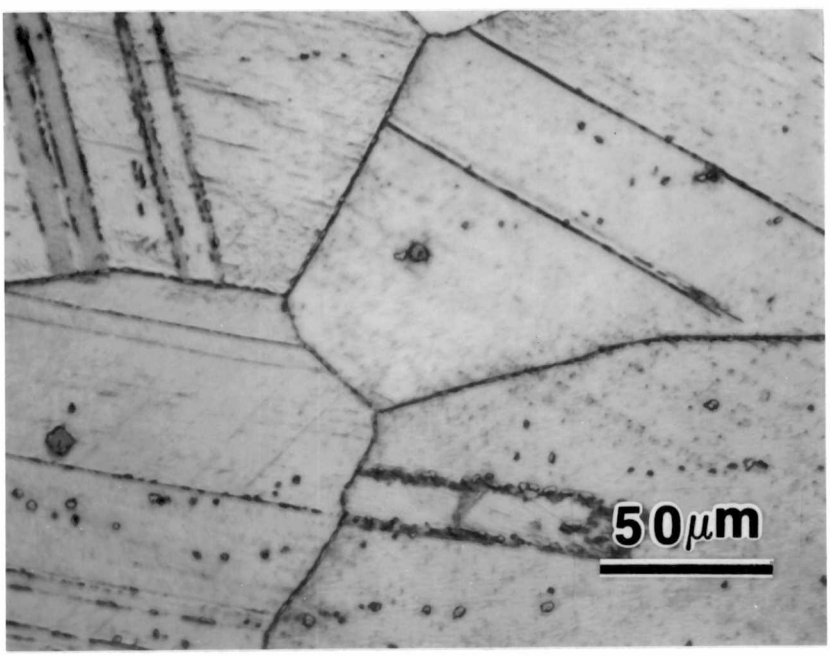

b) Primary Creep

Figure 4.1-12 High Magnification Micrograph of Figure 4.1-11 Showing the Precipitation Process of HR160 During Creep Deformation Tests at 850°C (1562°F)

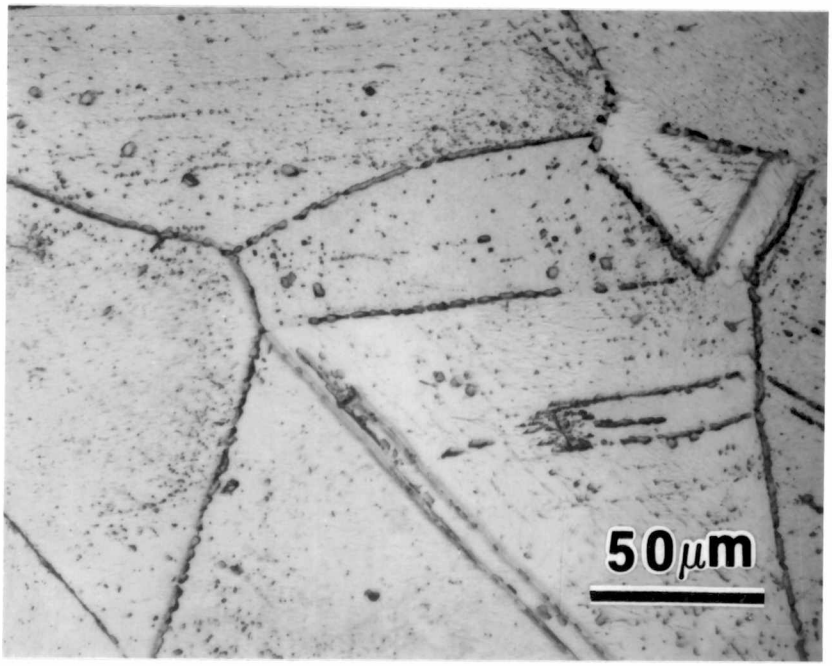

c) Secondary Creep

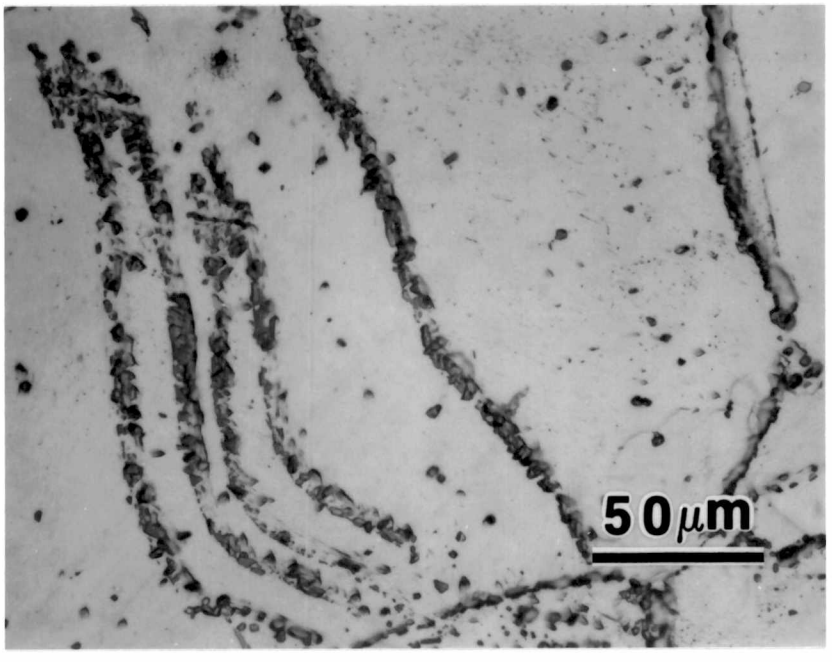

d) Tertiary Creep

Figure 4.1-12 (Continued)

Figure 4.1-12 a) shows that the grain boundaries of the as-received HR160 are almost free of precipitates. X-ray diffraction analysis of extracted residues reveals that the little precipitates found in the as-received HR160 are mainly TiN and some $Cr_{23}C_6$. As the elapse of time, more and more precipitates appeared (figures b, c, & d). X-ray diffraction analysis of extracted residues from the sample tested at 850°C (1562°F) for 705 hours as shown in Figure 4.1-12 d) shows that Cr_2C_3 appears as the major precipitates with medium G phase and minor $Cr_{23}C_6$ under this condition. The G phase has been determined to have the composition of $Ni_{16}Ti_6Si_7$. No TiN has been detected after being tested at 850°C (1562°F) for 705 hours.

4.2 Time-Dependent Fracture Mechanics Characterization Under Different Testing Conditions

4.2.1 Observation of Creep Crack Propagation Process

A typical curve of creep crack length versus time obtained in the tests of the as-received HR160 is given in Figure 4.2-1. It is obvious that the shape of the curve resembles that of a typical creep strain versus time curve presented in Figure 4.1-3. This implies that the three stages of creep deformation of a material, or, in other words, the shape of the creep strain versus time curve, may greatly affect the creep crack propagation process. The feature of this process is more evidently presented by its creep crack growth rate versus time curve. Such a curve for the test presented in Figure 4.2-1 is given in Figure 4.2-2 a). It exhibits a high initial creep crack propagation rate followed by a decrease and then an increase in the crack propagation rate. This trend is also reflected in the measured loadline deflection rates as shown in Figure 4.2-2 b).

The reasons for this trend observed in these figures are discussed as follows.

At the beginning of a test, the crack started to grow from the precrack produced by fatigue at room temperature. Because of the fatigue damage at the precrack tip

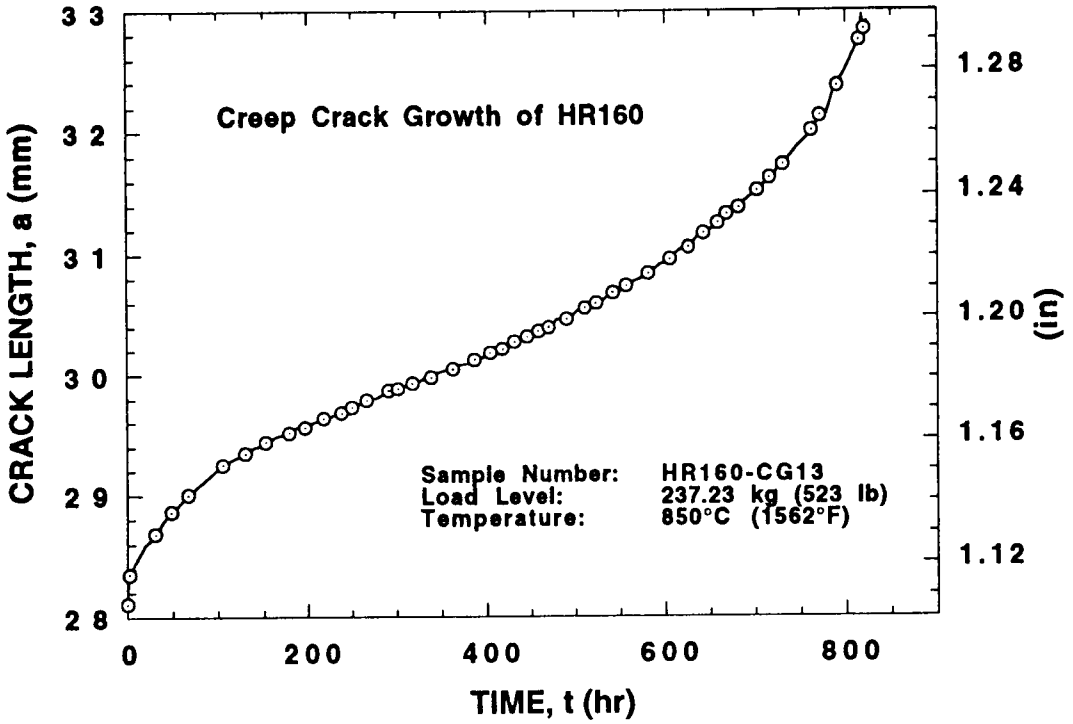

Figure 4.2-1 A Typical Curve of Creep Crack Length Versus Time Obtained from the Tests on the As-Received HR160

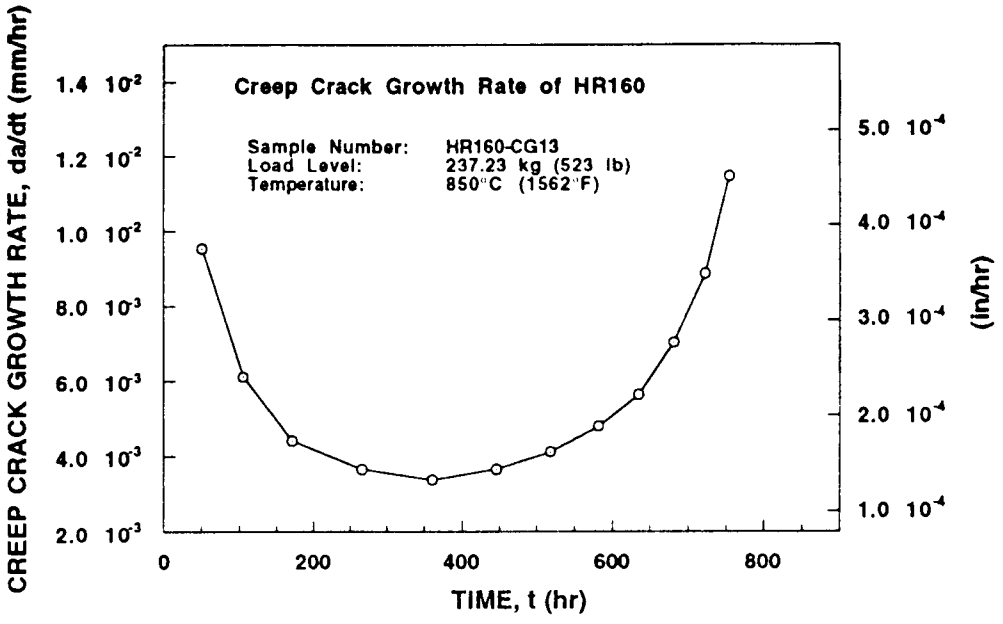

a) Creep Crack Growth Rate Versus Time

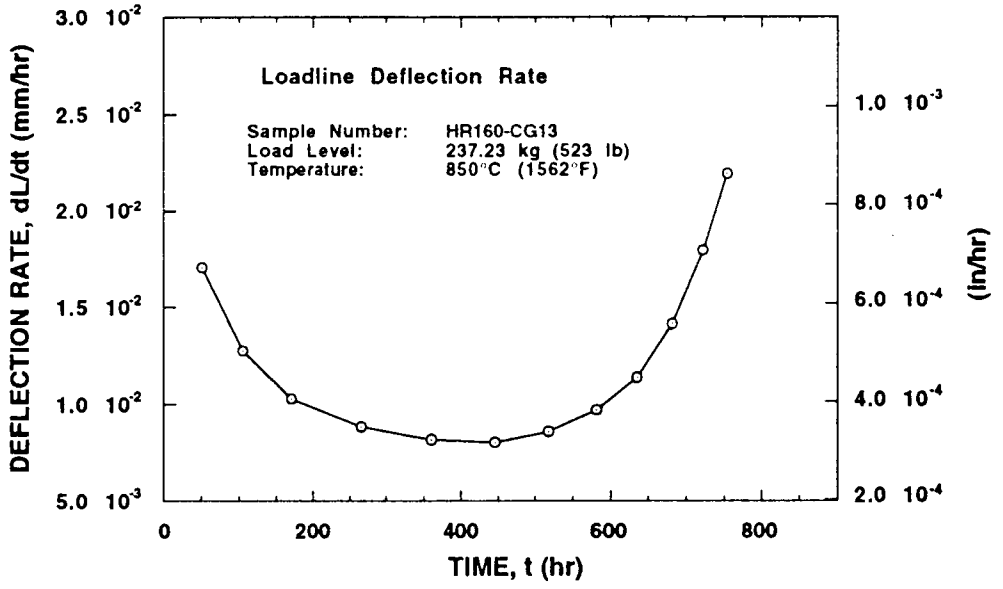

b) Loadline Deflection Rate Versus Time

Figure 4.2-2 Creep Crack Growth and Loadline Deflection Rates of HR160 as Functions of Time

introduced during the precracking process, the local material at the precrack tip was weakened. Moreover, the stress concentration caused by the sharp fatigue precrack tip provided a high driving force for the crack growth. This explains the high creep crack growth rate at the beginning of the test. As the time elapsed, the sharp precrack tip became blunted and the creep crack growth rate was decreased. When the crack grew out of the fatigue damaged region, the crack growth rate stopped decreasing. Then, as the crack became longer and longer, the uncracked load-bearing area became smaller and smaller, and the crack growth rate started to increase.

Another reason for this trend can be found in Figure 4.1-3 of the creep strain versus time data. In Figure 4.1-3, the creep deformation rate as a function of time can be obtained from the tangent of the creep strain versus time curve. At the beginning of the test, the primary creep deformation occurred at a high deformation rate. Calculation shows that extensive creep condition occurred in this creep crack propagation test in less than 1 hour. This implies that soon after loading, the creep zone in the C(T) sample spread over the entire uncracked ligament and deformed at high primary creep rates. Under this condition, two mechanisms could have occurred. First, the local material at the sharp precrack tip elongated in the loading direction during the fast primary creep process. To keep a constant bulk volume during the elongation, the elongating material had to reduce its cross section area, as a tensile bar or a creep deformation test specimen does on loading. In other words, lateral contraction had to occur to compensate the elongation. Since the thickness of the C(T) specimen and its uncracked ligament constrained such reduction, the lateral contraction could only occur at the precrack tip. Thus, the precrack tip material moved rapidly toward the uncracked ligament direction at a rate related to its primary creep rate. During this process, the precrack tip did not only become blunted, but also moved toward the uncracked ligament direction without any rupture taking place in the local material. Since the technique employed to measure the

crack length actually measured the potential drop across the uncracked ligament of the C(T) specimen, such lateral contraction of the uncracked ligament at the precrack tip was recorded as crack propagation. The crack indeed became longer in this process, but no rupture of the crack tip material was involved. The extension of the crack in such a manner depended on the primary creep rate of the precrack tip material. This high primary creep rate at the beginning of the test is also indicated by the measured loadline deflection rate given in Figure 4.2-2 b), which shows a high initial loadline deflection rate. In order to confirm this argument, one of the tests was stopped during the stage of the high initial deflection rate. The sample was examined with an optical microscope. The result strongly supports the above argument that the high primary creep rate caused the high initial crack propagation rate. The results from this examination is discussed in Section 4.2.4 with micrographs. After the blunting of the precrack tip, another mechanism occurred to maintain the high initial crack propagation. Because the high primary deformation rate of the entire uncracked ligament kept the crack tip highly stressed, the creep ductility was soon exhausted after certain amount of creep deformation, the local material at the crack tip reached its rupture strain in a short time, and the crack propagated at a high rate by the rupture of the local material at the crack tip. Thus, the creep crack propagation rate was high. The creep crack propagation rate gradually decreased as the creep zone entered the secondary creep stage and the creep rate became lower. It finally picked up the speed when the uncracked ligament became smaller and smaller.

From the above analysis, a prediction can be made that the creep crack propagation of a weld specimen will not have a high initial rate because the creep deformation of the weld does not have the primary creep stage as shown in Figure 4.1-8 b) discussed in Section 4.1.2.

4.2.2 Effects of Different Testing Conditions on the Time-Dependent Fracture Mechanics Characterization

Data analyses of the creep crack growth tests of the as-received HR160 show that all the developed data points exceed the transition time t_T. Therefore, only C*(t) was used to characterize the creep crack growth test results in this investigation. A typical plot of the creep crack propagation rate versus the time-dependent fracture mechanics parameter C*(t) for HR160 developed from the test data of one of the full-size samples is shown in Figure 4.2-3 a). The arrow shows a beginning point of the developed test data. The same creep crack propagation trend observed in Figure 4.2-2 a) is also shown in this figure. At the beginning, the rate was high, it decreased and then increased for the same reasons described in Figure 4.2-2 a). Note that unlike time (t) in Figure 4.2-2 a), C*(t) in Figure 4.2-3 a) also decreases and increases with the creep crack propagation rate. Admitted to the statistical scattering nature of mechanical property data, each C*(t) value generally corresponds to only one creep crack propagation rate. This trend indicates that C*(t) is a good parameter for characterizing the rate of creep crack propagation. The somewhat scattering nature of the first point as arrowed in this figure can be considered as being resulted from a different material, because it is from the crack tip material damaged by fatigue precracking.

To contrast the uniqueness of the correlation of the creep crack propagation rate with the time-dependent fracture mechanics parameter C*(t), the stress intensity factor, K, was also calculated for the same set of test data and correlated to the creep crack propagation rate for comparison. The correlation of K and da/dt is plotted in Figure 4.2-3 b). It can be seen that same creep crack growth rate at different time of the test can be related to different K values, and a unique correlation between da/dt and K can not be found. This trend further suggests that C*(t) is an effective means in uniquely correlating the creep crack propagation rate of HR160 rather than K.

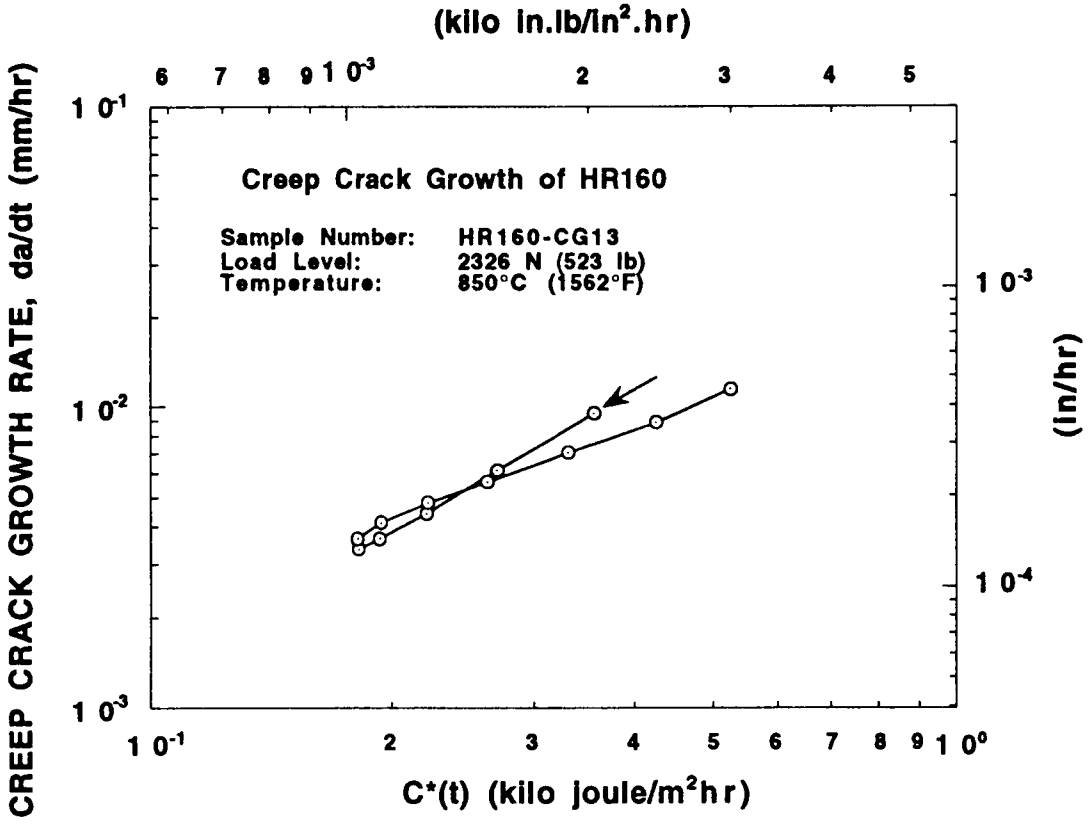

a) The Creep Crack Propagation Rate Versus the Time-Dependent Fracture Mechanics Parameter C*(t)

Figure 4.2-3 Fracture Mechanics Characterization of the Creep Crack Propagation Rate of a Full-Size Specimen for HR160 (W = 50.8 mm, 2.0 in)

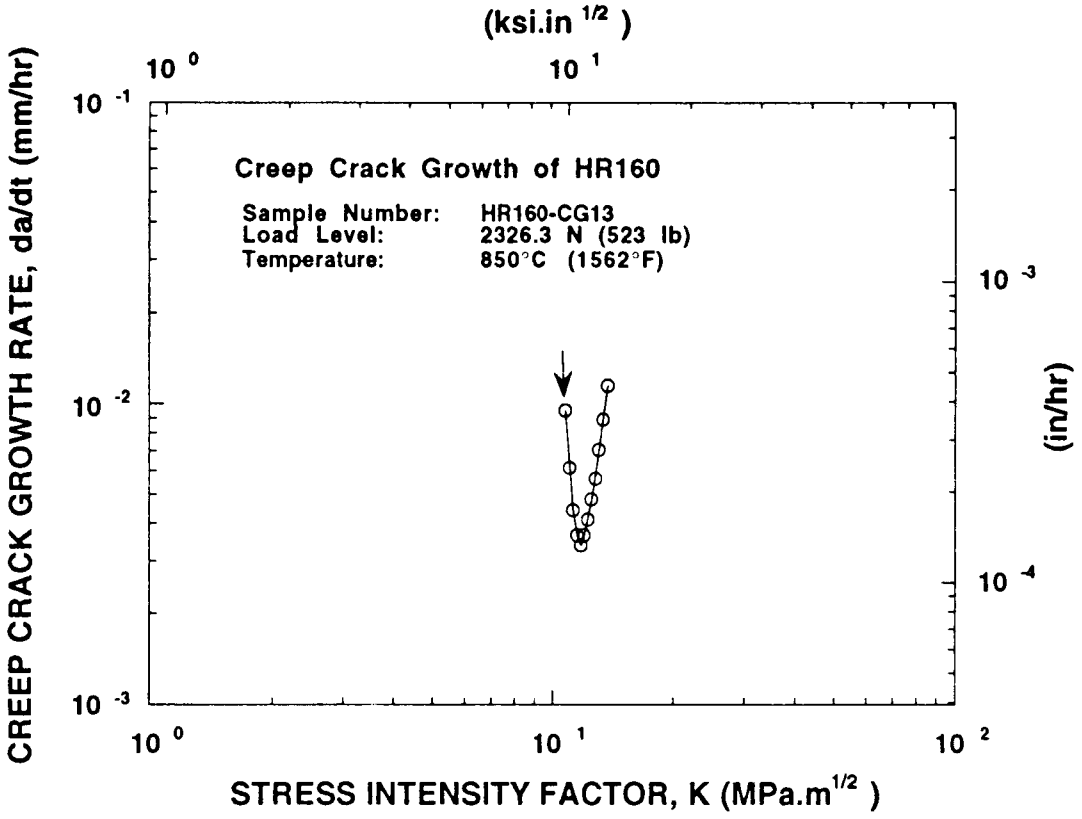

b) The Creep Crack Propagation Rate Versus the Stress Intensity Factor K

Figure 4.2-3 (Continued)

To examine the effect of load levels on the creep crack growth behavior and the characterization of the creep crack propagation rate with the time-dependent fracture mechanics parameter C*(t), all the test data generated for the as-received HR160 at 850°C (1562°F) under different load levels characterized with C*(t) are presented in Figure 4.2-4 a). They all fall in the same trend and can be well presented with the fit line and the equation given below:

$$da/dt = A[C^*(t)]^q \qquad (4.2\text{-}1)$$

where, A = coefficient of C*(t)

q = exponent of C*(t)

The change of load level only shifts the result data points up or down along the straight fit line of da/dt versus C*(t). The data of the lowest load level, 1579 N (355 lb), show a pattern different from those of the other two tests of higher load levels though they all fall in the same trend. There are at least two reasons for the data obtained from the test under the lowest load level to show a pattern different from the others. Because the load level of this test was very low, it is possible that the test was still in its primary creep stage when it was stopped for data processing. This is supported by the decreasing trend of the data points shown in the plot. Another reason is that the strange pattern may be caused by the error introduce by small variations of the testing equipment during the long testing time. These three tests of load levels of 3030.6 N (681 lb), 2326.3 N (523 lb) and 1579 N (355 lb) lasted for 169, 698 and 7,059 hours, respectively. During the 7,059 hours of testing, several kinds of variations in the testing equipment system could have occurred. The electronic components such as power supply and amplifiers could drift, the mechanical parts such as the pulling rods could vary the lengths because of relaxation, or

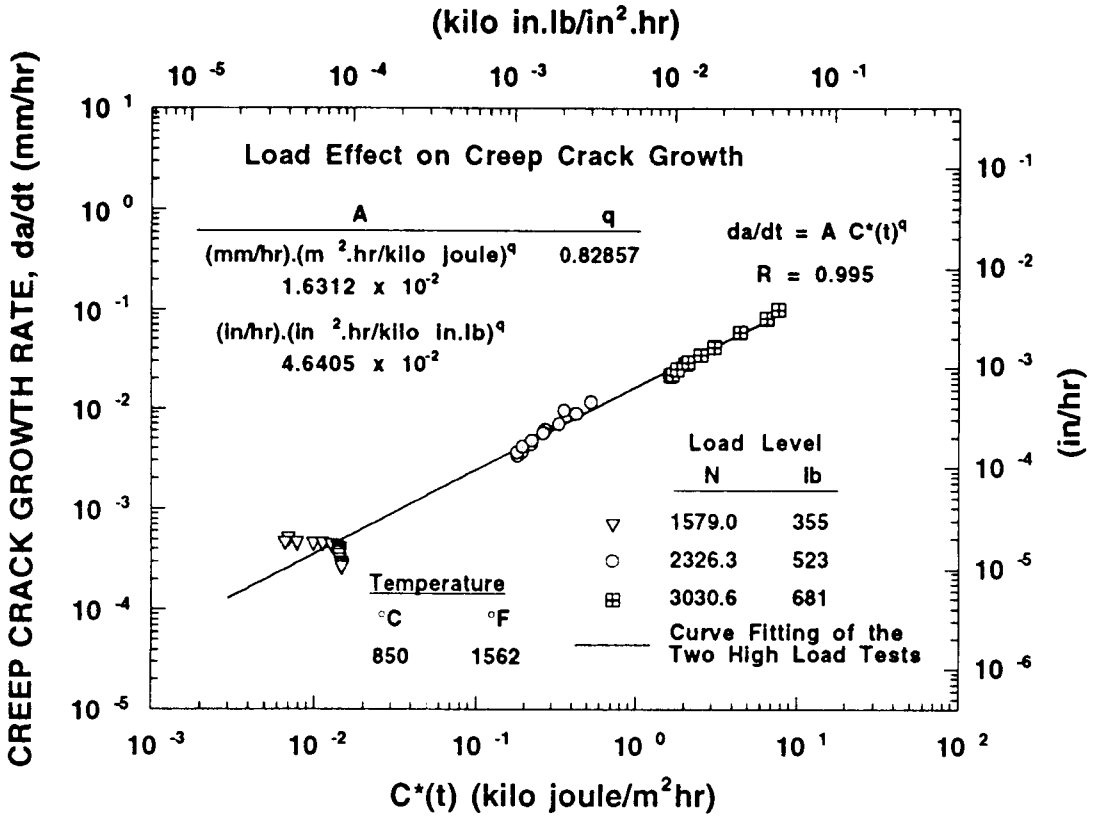

a) The Creep Crack Propagation Rate of HR160 as a Function of the Time-Dependent Fracture Mechanics Parameter C*(t)

Figure 4.2-4 The Load Level Effect on the Creep Crack Propagation Rate of HR160 at 850°C (1562°F)

shrinkage and expansion as the temperature changed with the seasons. From this stand point of view, it is not very practical to run a creep crack growth test over a long period of time. However, the creep crack propagation rates that can be obtained under long-time test conditions are usually within the range found in real engineering components, and therefore, highly desired by the industries. The feature of straight fit line in the characterization of creep crack propagation rate with the time-dependent fracture mechanics parameter C*(t) obviously provides a means to overcome the possible equipment problems and meet the industrial needs. From the results presented above, it can be predicted that all the data points of the tests under different load levels fall on a single straight fit line. Since the other two tests under higher load levels shown in Figure 4.2-4 a) lasted for only 169 and 698 hours respectively, the straight fit line can be obtained from these two tests. The results of tests under lower load levels can thus be predicted with the extended straight fit line on the left lower part of the figure. This straight-line feature of the characterization gives us a way to speed up the test by increasing the load level and extrapolating the fit line to obtain the creep crack growth rates at low load levels and C*(t) values. This application makes the time-dependent fracture mechanics parameter C*(t) a very useful parameter in dealing with such problems. For a comparison purpose, the results of the same three tests are also characterized with the stress intensity factor (K) and shown in Figure 4.2-4 b). It is obvious that no unique relationship can be found between the creep crack propagation rate and the stress intensity factor.

The developed test data at the three different temperatures of 850, 900 and 950°C (1562, 1652 and 1742°F) characterized with the time-dependent fracture mechanics parameter C*(t) and the stress intensity factor K are presented in Figure 4.2-5 a) and Figure 4.2-5 b), respectively. In the time-dependent fracture mechanics parameter characterization shown in Figure 4.2-5 a), all the data fall into the same trend and can be

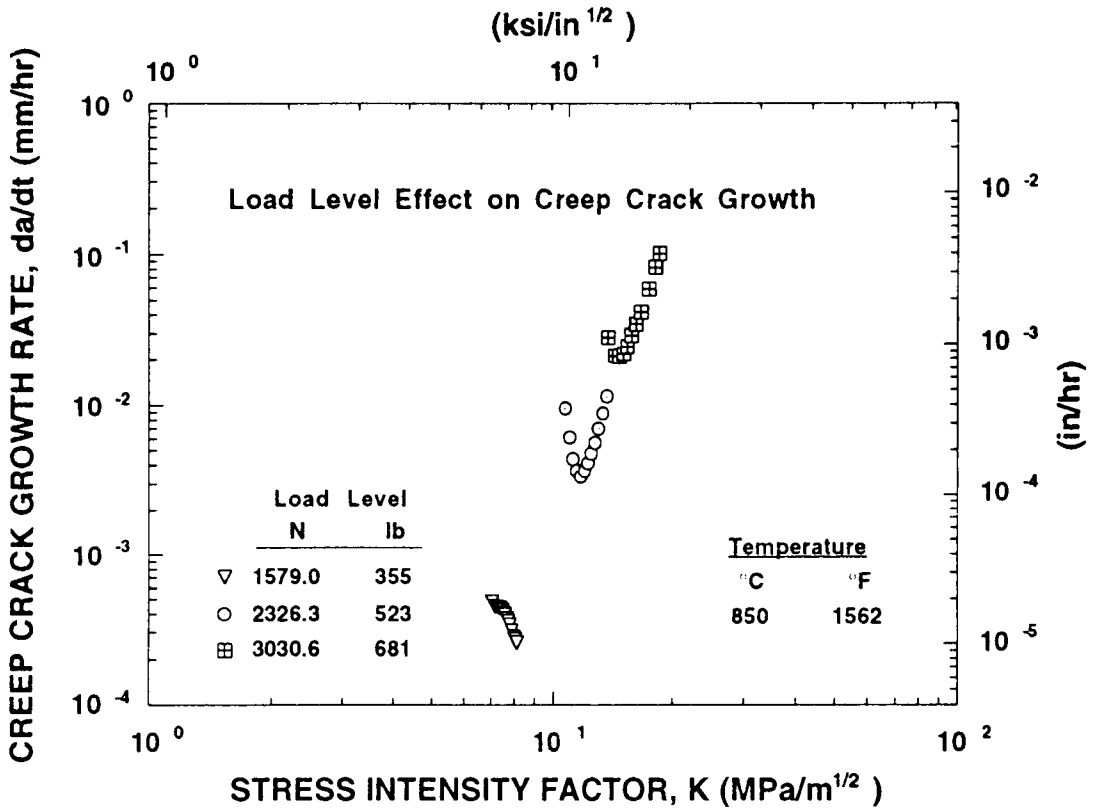

b) The Creep Crack Propagation Rate of HR160 as a Function of the Stress Intensity Factor K

Figure 4.2-4 (Continued)

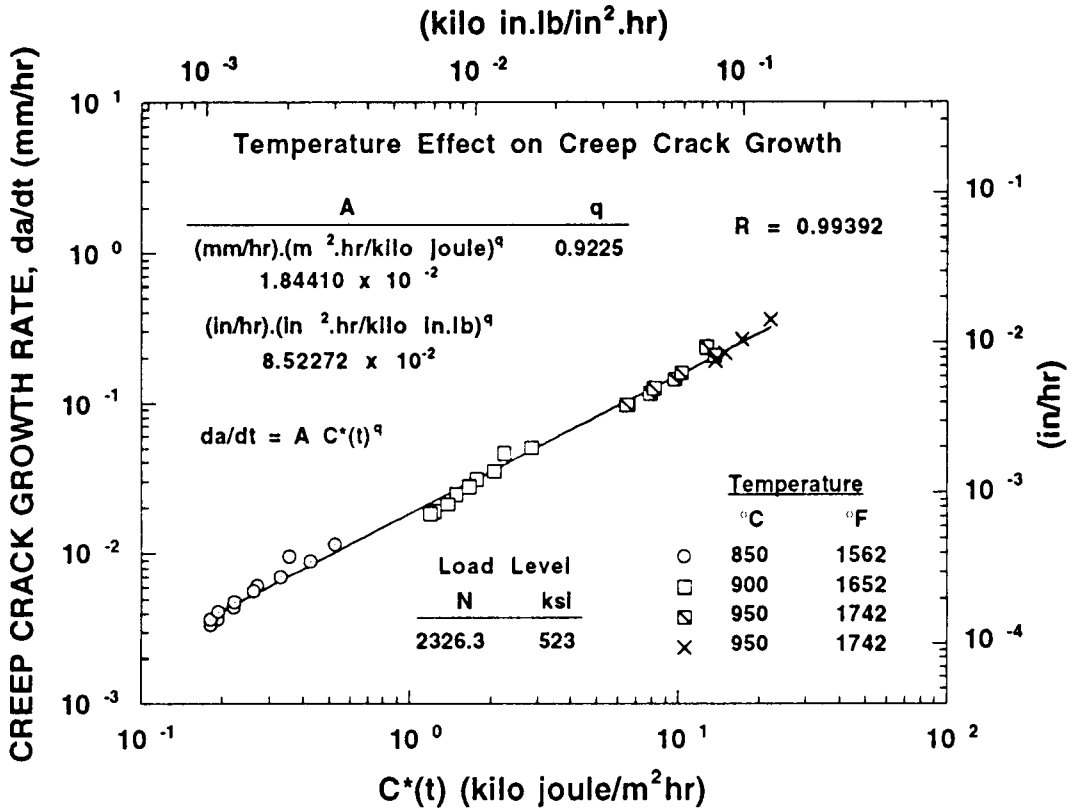

a) The Creep Crack Propagation Rate of HR160 as a Function of the Time-Dependent Fracture Mechanics Parameter C*(t)

Figure 4.2-5 The Temperature Effect on the Creep Crack Propagation Rate of HR160 at a Load Level of 2326.3 N (523 lb)

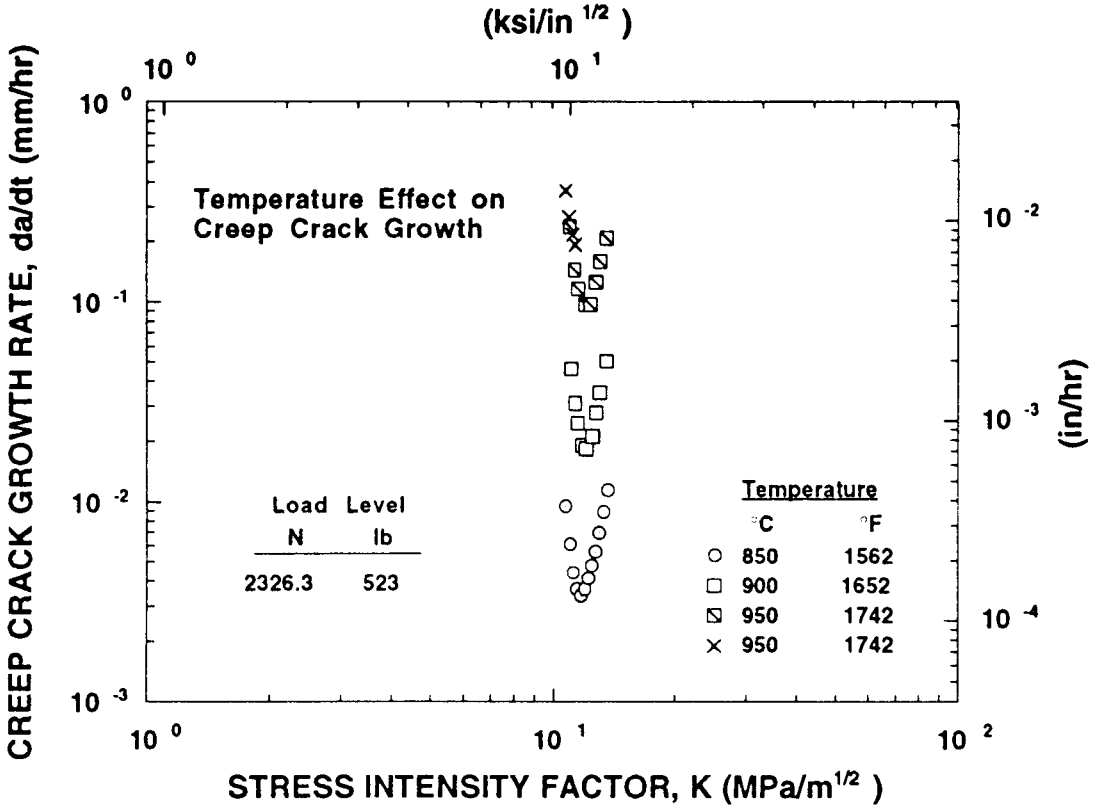

b) The Creep Crack Propagation Rate of HR160 as a Function of the Stress Intensity Factor K

Figure 4.2-5 (Continued)

well presented by the straight fit line and Equation (4.2-1). On contrast, no unique relationship between da/dt and K can be found in the stress intensity factor characterization. The C*(t) parameter seems to normalize the effect of temperature on creep crack propagation rates. This strongly supports the model expressed by Equation (2.4-6) discussed in Section 2.4.2. Equation (2.4-6) shows that the creep crack propagation rate is not very sensitive to changes of the creep coefficient A_2 which varies significantly with temperature, therefore, the correlation between the time-dependent fracture mechanics parameter and the creep crack propagation rate is not sensitive to temperature.

However, the normalization of the temperature effect by using C*(t) found in this investigation is different from the results of some early work [105]. Temperature was found slightly affecting the characterization of type 316 stainless steel. Care must be exercised when new materials are characterized.

For HR160 studied in this investigation, the change of test temperature only shifts the data points up or down along the straight fit line, like in the case of the load level effect. This feature gives another way to speed up the test, i. e., increasing the test temperature and obtaining the crack propagation rate results at lower temperatures by extrapolating higher temperature test results along the linear fit line of da/dt versus C*(t). On the other hand, in case that the equipment does not allow high-temperature testing, data can be obtained by testing at the allowable temperature range of the equipment and then conducting extrapolation in data processing to obtain the values needed at higher temperatures.

Figure 4.2-6 shows the creep crack propagation rates from a half-size sample characterized by the time-dependent fracture mechanics parameter C*(t). It gives the unique trend of da/dt versus C*(t) as shown by the full-size sample in Figure 4.2-3 a). This trend indicates that reducing the sample to half size does not affect the

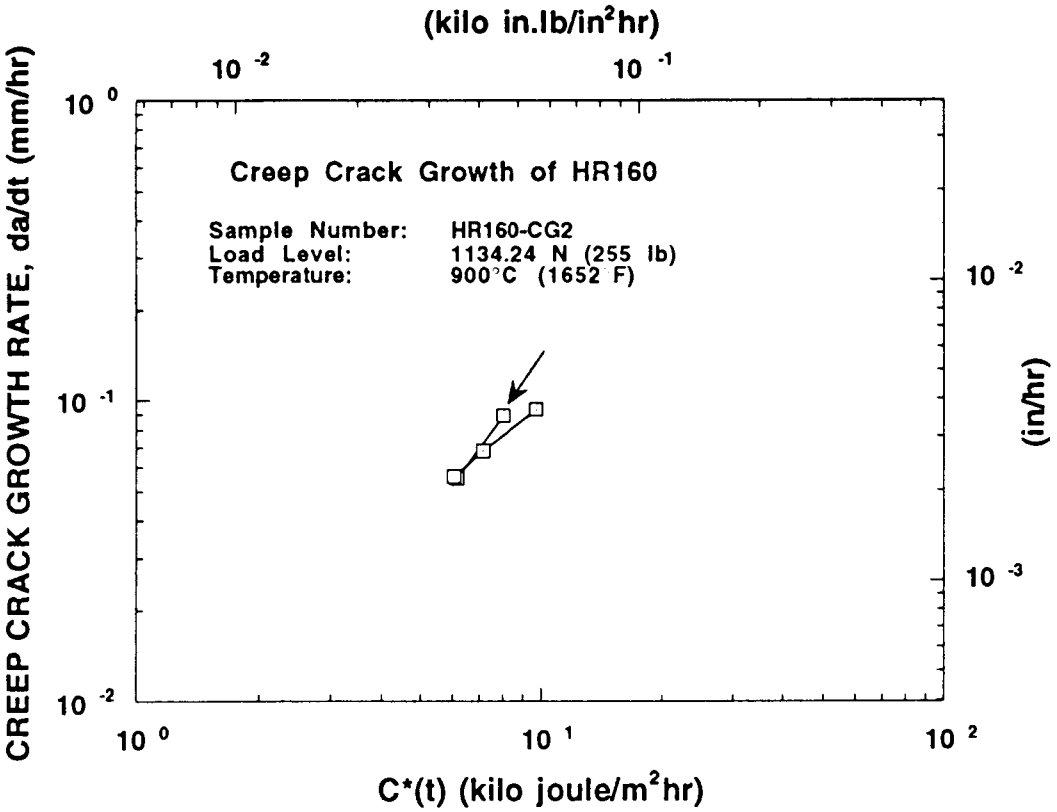

Figure 4.2-6 The Creep Crack Propagation Rate Versus the Time-Dependent Fracture Mechanics Parameter C*(t) of a Half-Size Specimen for HR160 (W = 25.4 mm, 1.0 in)

characterization of creep crack growth rates with C*(t). Recall that the half-size samples were made of HR160 from the other heat, there is no heat effect on the creep crack propagation rate behavior either.

The effects of testing conditions on the time-dependent fracture mechanics characterization are summarized in Figure 4.2-7 a). Figure 4.2-7 a) shows all the developed creep crack propagation data from the tests of the as-received HR160 under conditions of different load levels, temperatures and sample sizes. They all fall into the same trend and can be presented by Equation (4.2-1) with A = 1.7464 x 10^{-2} (mm/hr)·(m^2·hr/kilo joules)^q, i. e., 6.06696 x 10^{-2} (in/hr)·(in^2hr/kilo in·lb)^q and q = 0.86734. The up-triangles and up-crosses represent the results developed from the tests on half-size samples. Their fitting into the linear fit line clearly shows that reducing the samples to half size does not affect the test results and the characterization. Whether there is a limit beyond which the sample size starts to affect the creep crack growth rate results is not known from this investigation. However, the results from these half-size tests in this research are very valuable, when the test material source is limited, especially when the test materials have to be obtained by cutting from some components still in operation. It is worth mentioning that the shortest testing time among all the tests in Figure 4.2-7 a) is the one at 900°C with a half-size test sample loaded at 1134 N (255 lb). It lasted only about 35 hours. This confirms that by using the results of short time and half-size specimen tests, the crack propagation rates of long time and full-size specimen tests can be estimated from the straight line relationship of da/dt versus C*(t).

The same creep crack growth rate data presented in Figure 4.2-7 a) are also correlated to the stress intensity factor K as shown in Figure 4.2-7 b). The same symbols are used for each test condition as in Figure 4.2-7 a). It is more obvious in this figure than the previous ones that no unique correlation between da/dt and K can be found. It is clear that the stress intensity factor K can not be used to characterize the

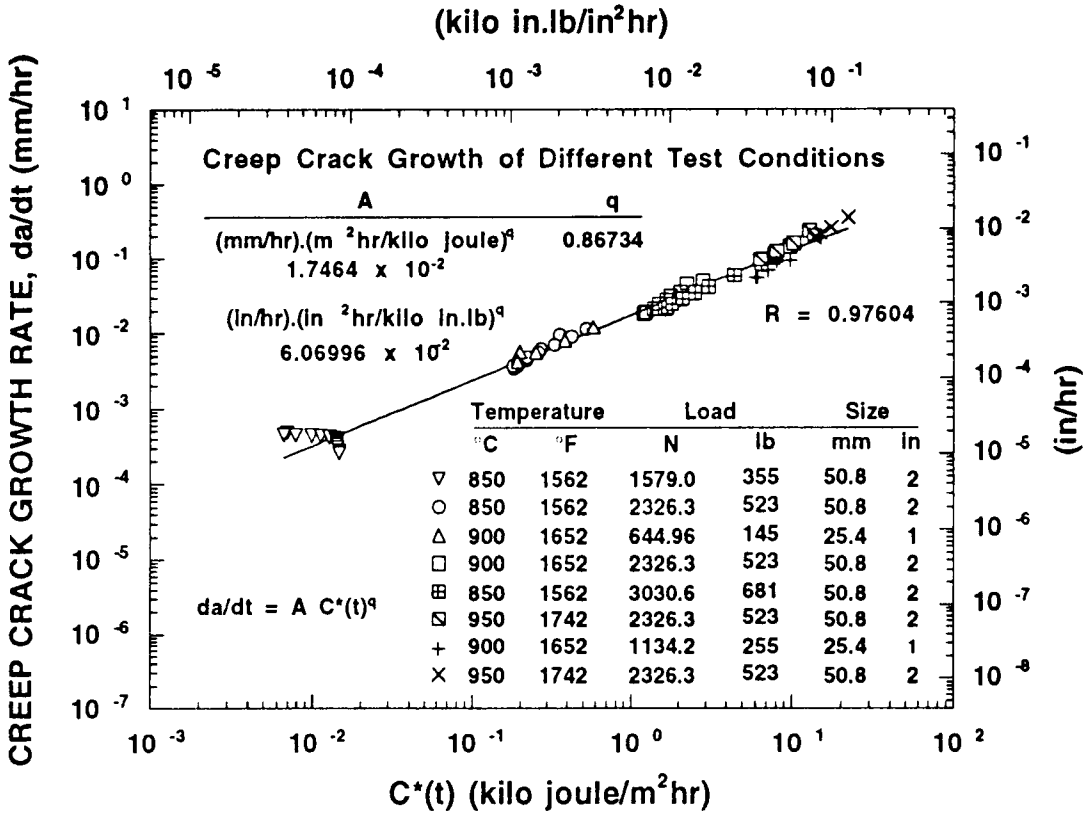

a) The Creep Crack Propagation Rate of HR160 as a Function of the Time-Dependent Fracture Mechanics Parameter C*(t)

Figure 4.2-7 Effect of Different Testing Conditions on the Creep Crack Propagation Rate of the As-Received HR160

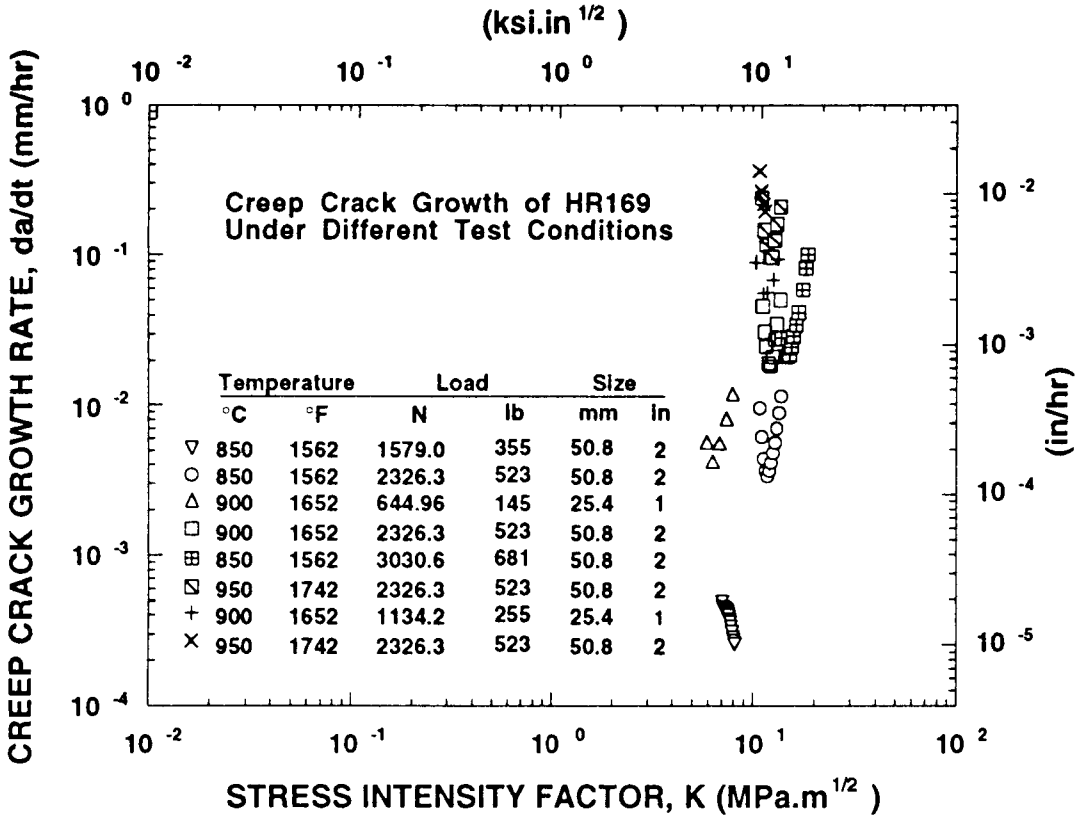

b) The Creep Crack Propagation Rate of HR160 as a Function of the Stress Intensity Factor K

Figure 4.2-7 (Continued)

creep crack propagation rate at elevated temperatures. The C*(t) parameter can normalize the effects of load level, test temperature and specimen size on creep crack propagation rates. Thus, C*(t) is a better creep crack growth rate correlating parameter rather than K.

4.2.3 Short-Term Estimation of the q Value

As discussed in last section, the coefficient A and exponent q in Equation (4.2-1) can be obtained from short-term tests to estimate long-term test results by extrapolation. This is highly desired because the required testing program, which includes tensile, creep deformation and crack growth tests, is very time consuming and expensive. The extrapolation can obviously save the time for experiments. However, this can also sometimes introduce significant error when the short-term tests do not cover a reasonable range of C*(t).

Table 4.2-1 gives the values of A and q for the tests presented in Figure 4.2-7 a) except the first one with the lowest load level of 1579.0 N (335 lb). All the tests listed in Table 4.2-1 lasted for less than 1,000 hours. The values were obtained by conducting curve fitting with data for these tests individually. The tests are numbered in the same sequence as presented in Figure 4.2-7 a). It is evident from Table 4.2-1 that the individual fitting values of A and q can be quite different from those obtained from all these test data points as a whole. The equation, $da/dt = AC^*(t)^q$, is plotted on logarithmic coordinates in Figure 4.2-7 a). The coefficient A is actually the da/dt at unit C*(t), and q is the slope of the fit line. In Table 4.2-1, the largest A and q values for the individual fit lines are 2.5572×10^{-2} (mm/hr)·(m2·hr/KJ)^q and 1.3252, respectively, and the smallest 5.9984×10^{-3} (mm/hr)·(m2·hr/KJ)^q and 0.82691, respectively, while the A and q values for all of these tests as a whole are 1.7389×10^{-2} (mm/hr)·(m2·hr/KJ)^q and 0.87719. It can be seen that the individual values of A and q can be different from those obtained

Table 4.2-1 Parameters A and q of $da/dt = AC^*(t)^q$ for Individual Creep Crack Growth Tests on the As-Received HR160

Test No.	A		q
	$(mm/hr)\cdot(m^2\cdot hr/KJ)^q$	$(in/hr)\cdot(in^2 hr/K\ in.lb)^q$	
2	2.5572×10^{-2}	3.6672×10^{-1}	1.1417
3	1.8429×10^{-2}	5.1980×10^{-2}	0.82691
4	1.4823×10^{-2}	3.5707×10^{-1}	1.2421
5	1.3544×10^{-2}	8.3685×10^{-2}	0.97871
6	1.1038×10^{-2}	1.6868×10^{-1}	1.154
7	6.3727×10^{-3}	1.2992×10^{-1}	1.2098
8	5.9984×10^{-3}	2.2197×10^{-1}	1.3252
All	1.7389×10^{-2}	6.35939×10^{-2}	0.87719

from all of these test data points as a whole, which are very close to the values from all the tests including the one of the lowest load level, i.e., 1.7464×10^{-2} $(mm/hr)\cdot(m2\cdot hr/KJ)^q$ and 0.86734, as listed in Figure 4.2-7 a). The scattering of the values from individual tests is believed to be caused by the effects of primary creep deformation and the precrack damage on the crack propagation under different test conditions and sample geometry. When results are obtained from two or more tests with reasonable spans between their individual covering range of C*(t), the scattering of A and q can be normalized. However, when extrapolation is conducted based on A and q values obtained from an individual short-term test result, this scattering, especially the scattering in the slope, q, can sometimes cause a significant error when the extrapolation covers a great span of C*(t). Caution must be taken when such an extrapolation is performed. A possible way to overcome this problem is discussed Section 4.5.

4.2.4 Microstructural Characterization of the Creep Crack Propagation Process of the As-Received HR160

It has been discussed in Section 4.2.1 that the high initial crack propagation rate as shown in Figure 4.2-1 and Figure 4.2-2 a) is attributed to the precracking damage and the blunting at the precrack tip caused by the high rate primary creep. This is fully supported by the microstructural analysis results. Figure 4.2-8 shows a precrack introduced by fatigue at room temperature from the machined notch. Figure 4.2-9 shows this precrack at high magnification. It is evident in these figures that the crack tip is sharp, and the fatigue precrack propagated mainly in a transgranular mode. The remaining fatigue precracking damage, i.e., the slip bands formed at the crack tip during the precrack propagation process, can be clearly observed. As discussed in Section 4.2.1, when the sample was loaded and exposed to an elevated temperature, the sharp precrack material started to creep at a high primary creep rate. Because of

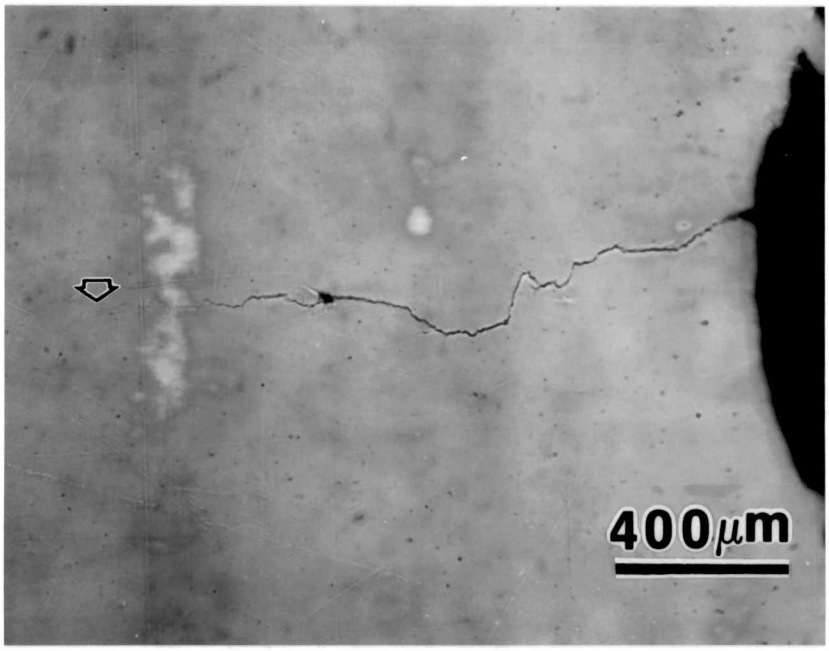

Figure 4.2-8 A Precrack Produced by Fatigue at Room Temperature
(The Arrow Indicates the Location of the Crack Tip)

Figure 4.2-9 A Precrack Produced by Fatigue at Room Temperature Showing the Remaining Crack Tip Damage Along the Crack Sides

constraint on the three sides, the lateral contraction which had to occur to keep the constant volume of the creeping bulk material could only take place at the precrack tip, making the tip move toward the uncracked direction while becoming blunted. The resulting blunted precrack tip is shown in Figure 4.2-10. The same scale is used in Figure 4.2-8 and Figure 4.2-10. The arrows in both figures point to the same spot. No rupture of the local crack tip material can be observed in Figure 4.2-10. However, the potential drop showed high rate crack propagation at this point because of the lateral contraction caused by the high rate primary creep.

It can also be observed in Figure 4.2-10 that the local creep deformation resulting from stress concentration at the crack tip caused tremendous creep cavitation in the creep zone. These creep cavities would become greater and greater as the test time elapsed, finally they would coalesce and the crack would propagate by the coalescence of these creep cavities. The result of such a process is shown in Figure 4.2-11.

Figure 4.2-11 shows a creep crack propagated by the rupture of the local material at the crack tip. It is observed that the crack propagated mainly in an intergranular mode. This is completely different from the transgranular mode of the precrack produced by fatigue at room temperature as shown in Figure 4.2-9. Along the creep crack, a few grains are found elongated but no recrystallization is observed. This observation is very different from the large grain deformation and massive recrystallization found at the tertiary creep stage in the creep deformation tests. This difference probably resulted from the fact that the constraint in C(T) samples prohibited large grain deformation and thus recrystallization. The expected mechanism in which recrystallization decreases crack propagation did not work in this situation.

However, another mechanism is observed which may help slow down creep crack growth. Figure 4.2-12 shows creep cavities along the grain boundary at the crack tip. The arrows indicate the points where the creep cavity growth was deflected from the

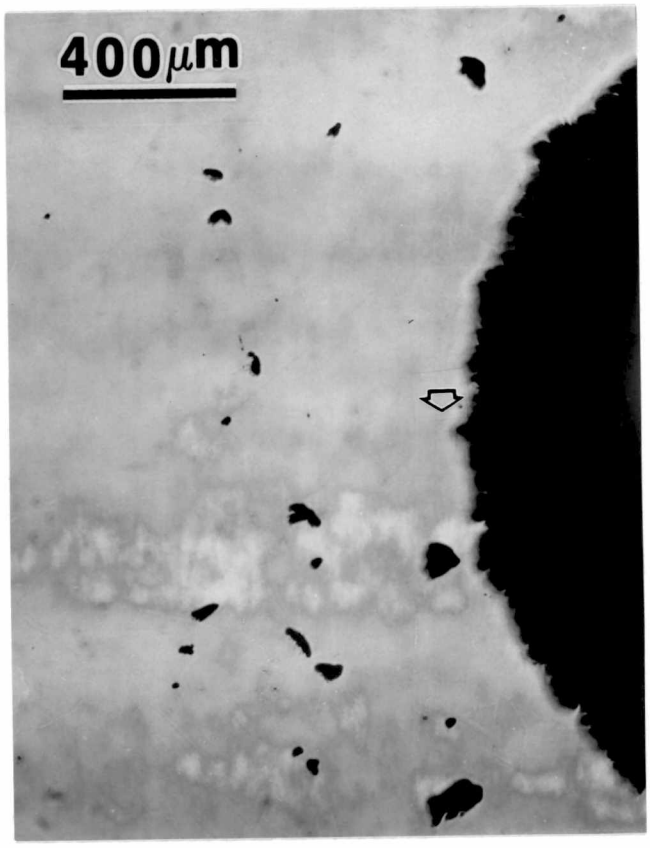

Figure 4.2-10 A Blunted Precrack and Creep Cavitation in the Creep Zone at the Crack Tip (The Arrow Indicates the Location of the Crack Tip as Shown in Figure 4.2-8)

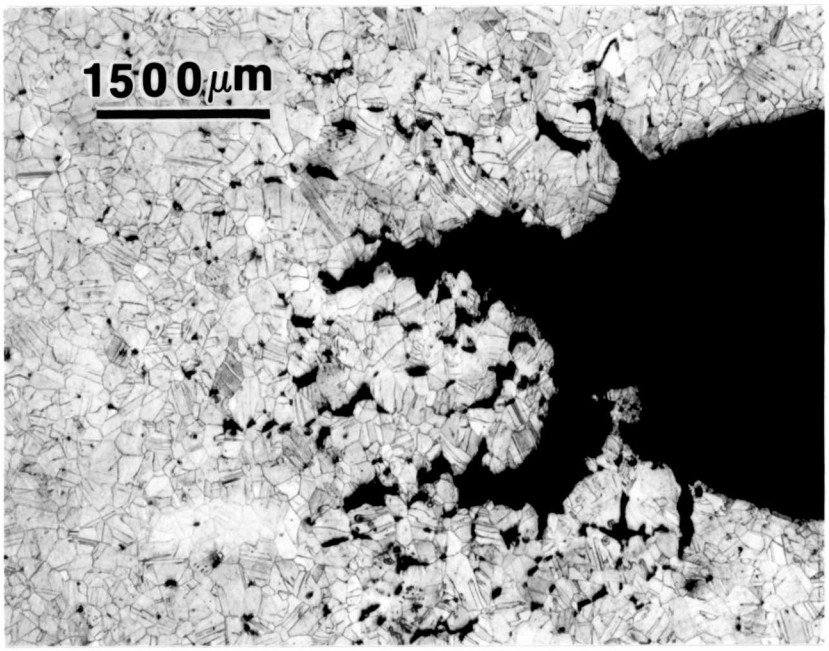

Figure 4.2-11 A Micrograph Showing Intergranular Nature of Creep Crack Growth in Haynes HR160 Tested at 850°C (1562°F).
(Crack Growth Direction is from the Right to the Left.)

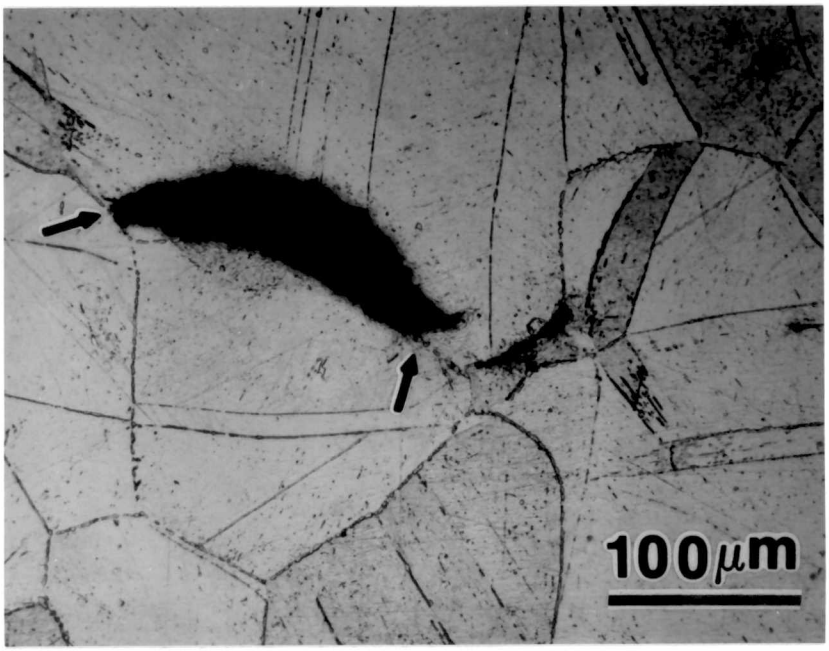

Figure 4.2-12 A High Magnification Micrograph Showing a Crack Deflected off the Grain Boundary by Grain Boundary Precipitates

grain boundary into the grain by grain boundary precipitates. Because the creep deformation is more likely to occur at the grain boundaries, this mechanism makes the cavity growth deflect into difficult growing areas and have to take a longer route to coalesce, therefore, it may decrease the creep crack propagation rate. Note that in the as-received condition, few precipitates were found. Whether an optimal precipitate size and density exist for the best creep crack growth resistance requires further study.

In order to provide a better understanding of the entire process for creep crack propagation in HR160, the entire fracture surface of a creep crack growth test sample after being tested at 900°C (1652°F) was analyzed with a scanning electron microscope (SEM). This fracture surface is given in Figure 4.2-13. There are four regions from the left to the right: precrack growth region, creep crack growth region, crack tip region and uncracked region. The uncracked region was obtained by interrupting the test in progress and fatigue-rupturing the tested C(T) sample at room temperature. These four regions are shown at high magnifications and discussed in details. The precrack structure at high magnification is shown in Figure 4.2-14. The fracture is a flat transgranular surface covered with oxide. Surface cracks in the oxide scales can be observed. Figure 4.2-15 shows the creep crack fracture surface. The morphology consists of grain boundary surfaces covered with fine oxide scales. This confirms the observation at the crack tip of the sectioned half sample in Figure 4.2-11 that the creep crack propagated intergranularly. Figure 4.2-16 shows a high magnification view of the fine oxide scales on the grain boundary surfaces. It is believed that the fine oxide scales can protect the material from further oxidation [32]. Figure 4.2-17 shows the fracture of the untested as-received HR160 prepared by overloading at room temperature. The surface shows a typical ductile fracture with many ductile dimples. No feature of intergranular fracture is observed. This proves that the intergranular crack propagation mode in the creep crack fracture region shown in Figure 4.2-15 is a result of creep damage at elevated

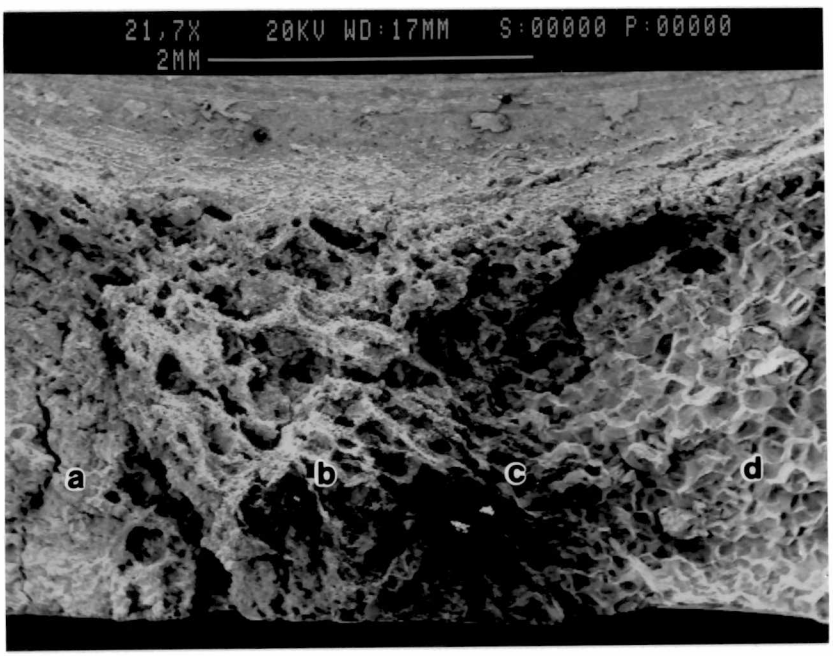

Figure 4.2-13 An Overall View of the Fracture Surface of a Creep Crack Growth Test Speimen; The Crack Grew from the Left to the Right; a) Precrack Growth Region, b) Creep Crack Growth Region, c) Crack Tip, d) Uncracked Region

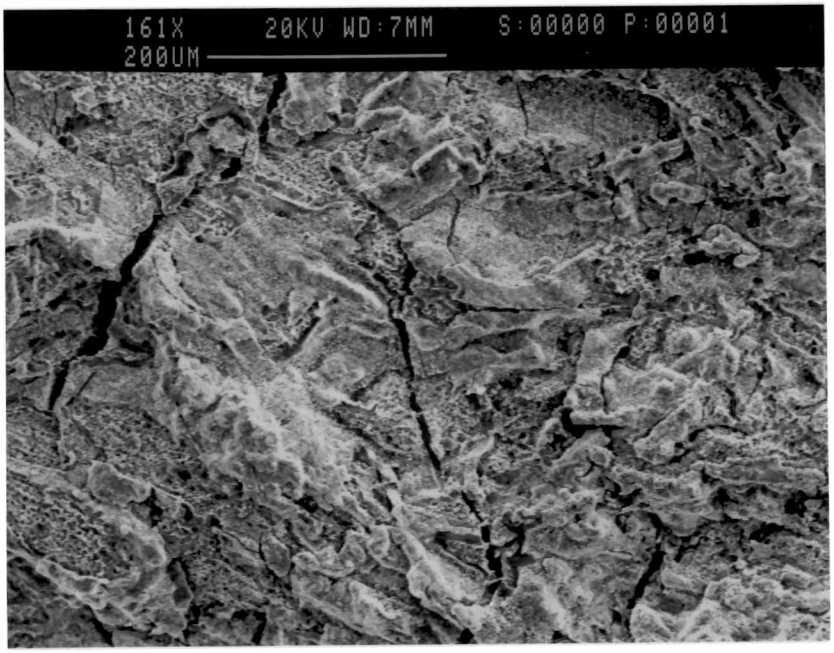

Figure 4.2-14 A High Magnification Micrograph Showing Fracture Surface in the Precrack Region

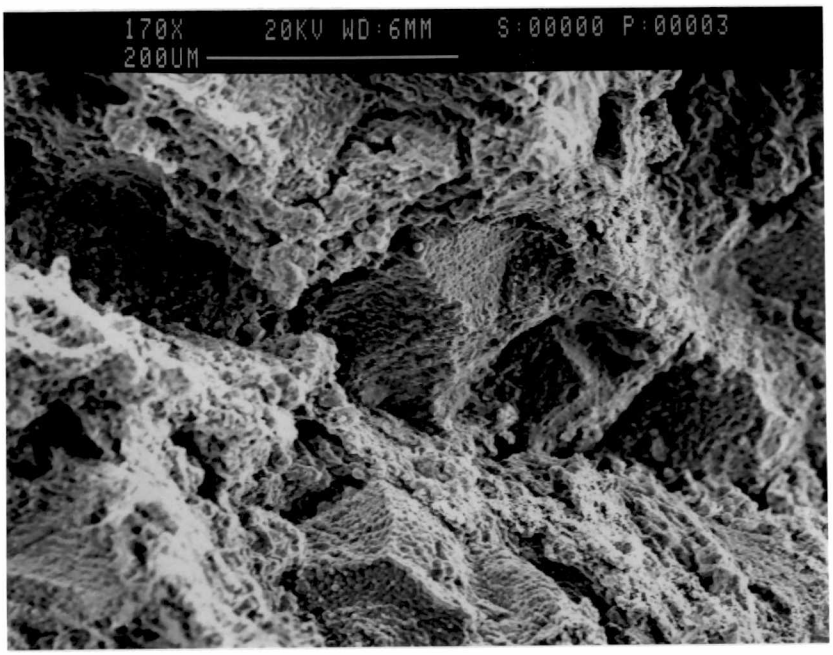

Figure 4.2-15 A High Magnification Micrograph Showing Fracture Surface in the Creep Crack Growth Region; Note the Grain Boundary Surfaces Indicating Intergranular Nature of Crack Growth.

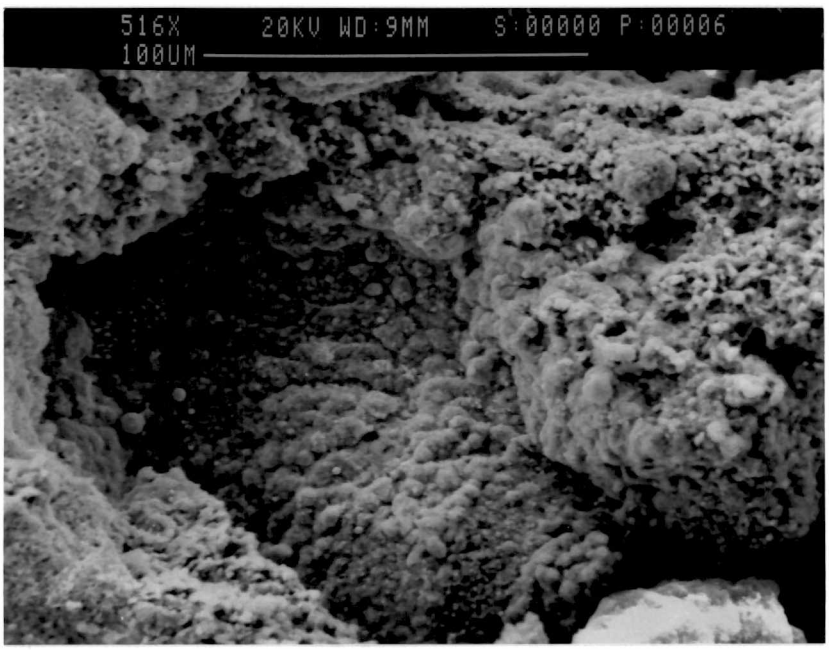

Figure 4.2-16 A High Magnification Micrograph Showing the Fine Oxide Scales on the Grain Boundary Surfaces in the Creep Crack Growth Region

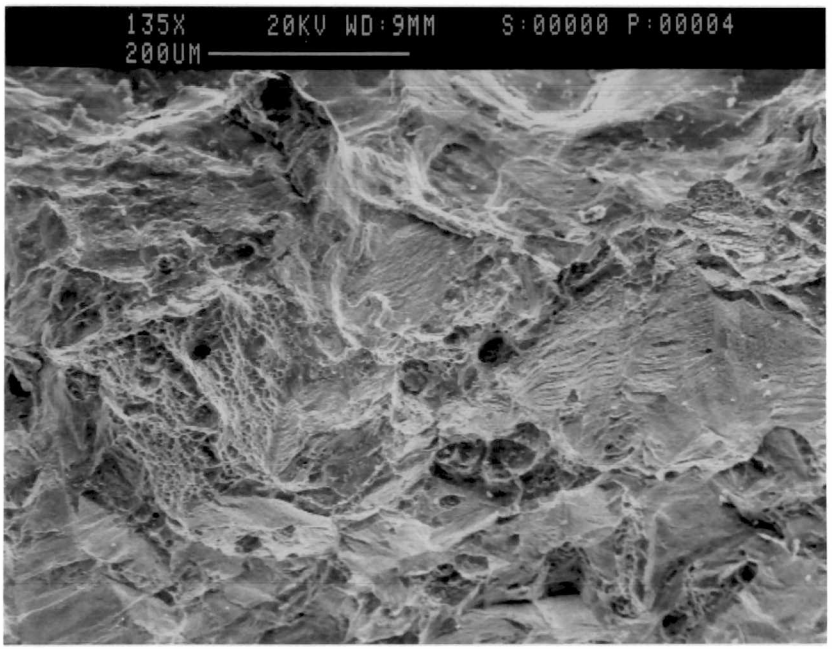

Figure 4.2-17 The Fracture Surface of the As-Received HR160 Prepared by Overload at Room Temperature

temperature. The crack tip region is shown in Figure 4.2-18. This area is a zone of only a few grain width. It can be seen that the grain boundaries are covered with a light layer of oxide. Since it was the uncracked region right in front of the crack tip, grain boundary cavities must have existed to allow the air to get into this region and form high temperature oxides. A high magnification view of the light oxide layer is shown in Figure 4.2-19. Comparing with the fine oxide scales on the grain boundary surfaces of the creep crack growth region as shown in Figure 4.2-15, Figure 4.2-19 shows a network structure on the crept grain boundary surfaces, which is the remaining morphology from the creep cavitation along the grain boundaries. Figure 4.2-20 is the morphology of the uncracked region fractured by fatigue at room temperature after the testing. Different from the transgranular fracture morphology usually found in a fatigue fracture of the as-received condition as shown in Figure 4.2-21, this fracture surface shows mainly intergranular morphology. A high magnification micrograph of the grain boundary surfaces of the uncracked ligament area given in Figure 4.2-22 shows a network structure formed by micro creep cavitation. The dimples were formed by grain and twin boundary creep cavitation at the elevated testing temperature. When the sample was ruptured by fatigue at room temperature after creep crack growth testing, the "walls" between the micro creep cavities easily broke and the network remained from these broken "walls". The micro creep cavitation formed microcracks not only along grain boundaries, but also along twin boundaries as shown in Figure 4.2-23. These results further suggest the following mechanism for creep crack growth of HR160: Around the creep crack tip, creep cavities form along the grain and twin boundaries. These cavities grow and coalesce, and the creep crack extends. Thus, the extension of a creep crack in HR160 is strongly related to the nucleation, growth and coalescence of creep cavities along grain and twin boundaries.

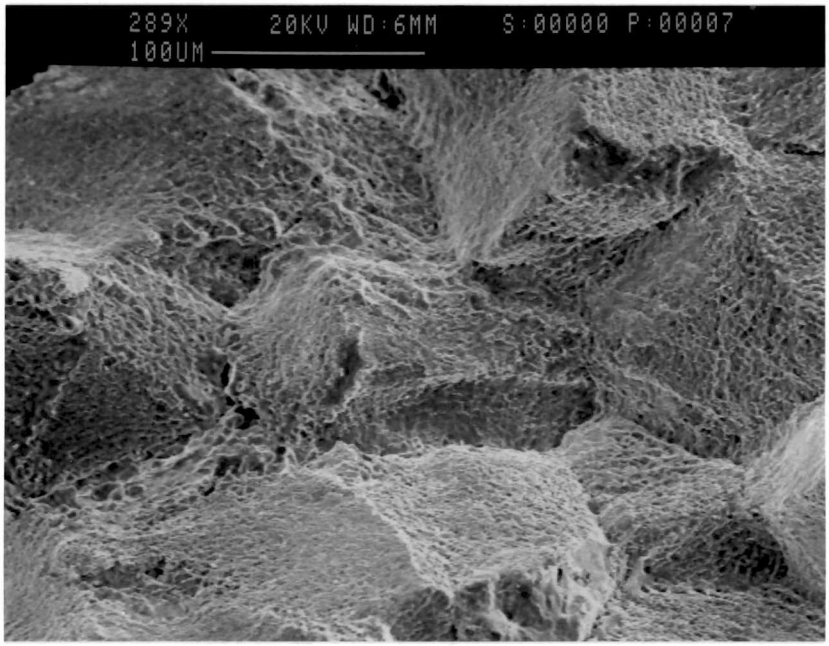

Figure 4.2-18 A High Magnification Micrograph Showing the Fracture Surface of the Crack Tip Region; Note the Intergranular Nature of the Crack Path.

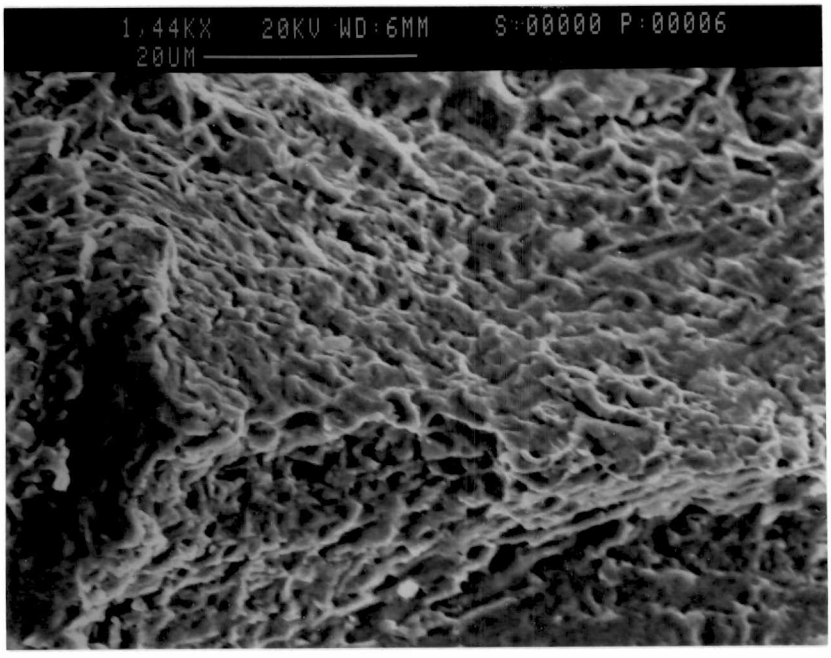

Figure 4.2-19 A High Magnification Micrograph Showing a Light Oxide Layer on the Grain Boundary Surfaces in the Crack Tip Region

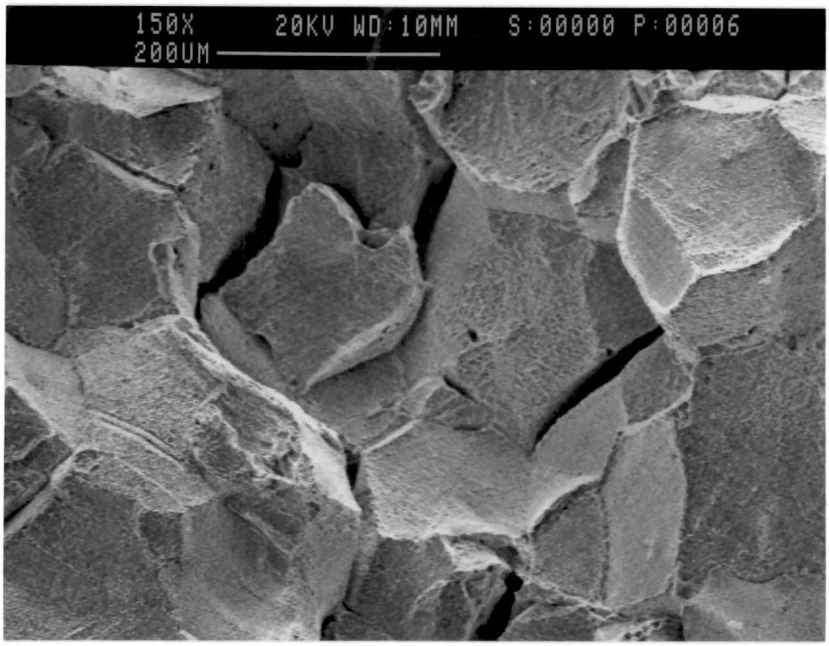

Figure 4.2-20 A High Magnification Micrograph Showing the Uncracked Region Ruptured by Fatigue at Room Temperature

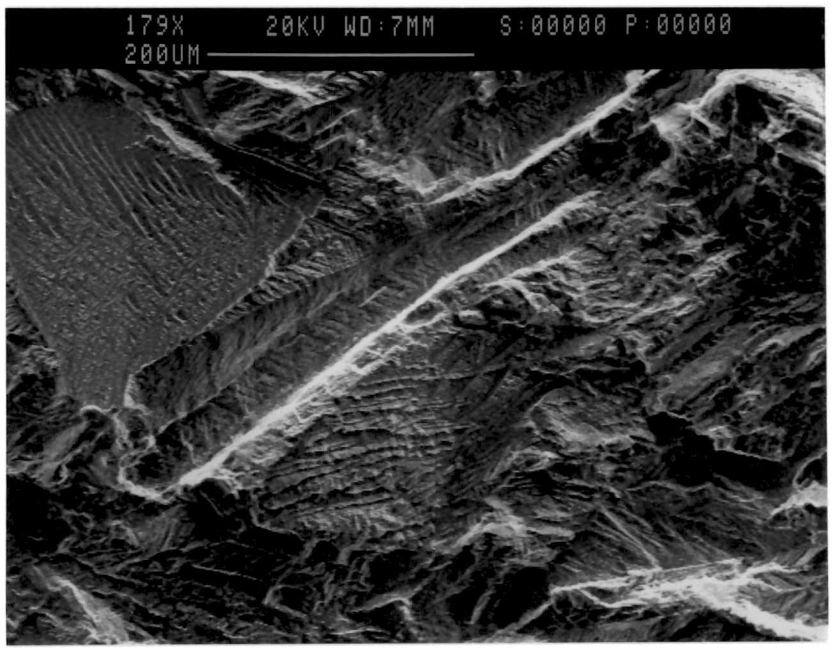

Figure 4.2-21 A Micrograph Showing the Morphology of the Fracture Surface of the As-Received HR160 Ruptured by Fatigue at Room Temperature

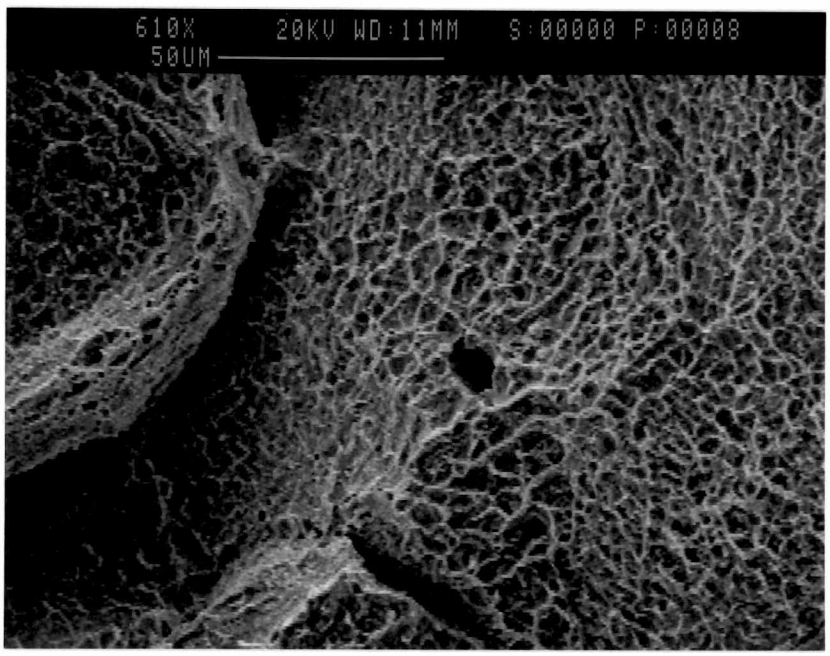

Figure 4.2-22 A High Magnification Micrograph Showing a Net Structure Formed by Creep Cavitation on Grain Boundary Surfaces in the Uncracked Region

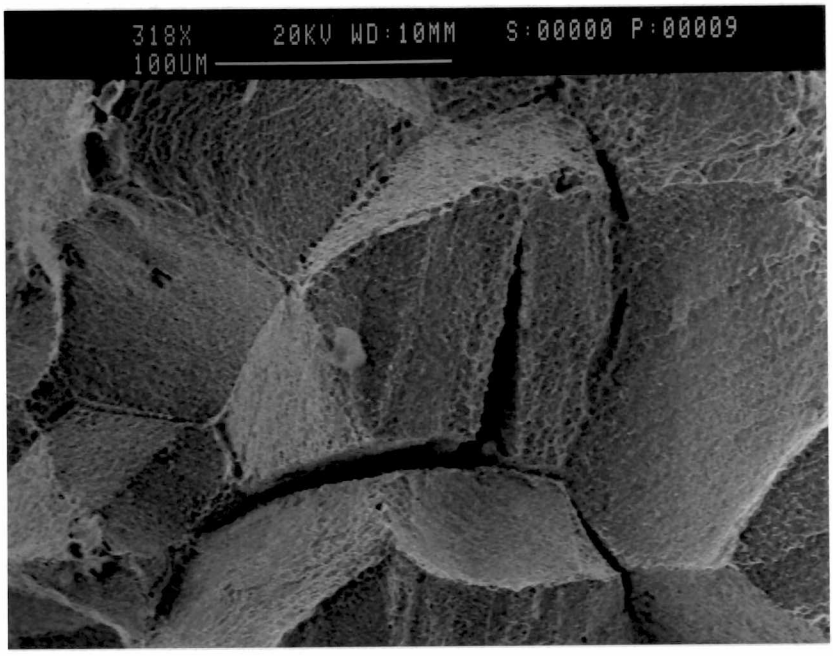

Figure 4.2-23 A Micrograph Showing a Microcrack Formed by the Coalescence of Creep Cavities Along a Twin Boundary in the Uncracked Region Ruptured by Fatigue at Room Temperature

4.3 Time-Dependent Fracture Mechanics Characterization Under Different Material Conditions

4.3.1 Coarse Grain Size Condition

A typical plot of the creep crack propagation rate of the coarse grain size HR160 characterized with the time-dependent fracture mechanics parameter C*(t) is given in Figure 4.3-1. It has the same trend of that of the as-received HR160. The crack propagation started at a high initial rate because of the primary creep, slowed down in the secondary creep stage and picked up the speed when the load bearing area became smaller and smaller. An interesting phenomenon that can be observed from this plot is that at the end of the test, the rate increased with a great drop in C*(t) value. This was caused by the tensile rupture of the small remaining uncracked ligament. Usually at the end of a creep propagation test, the plastic zone becomes large enough to engulf the creep zone. Since C*(t) is a measure of the creep energy dissipation rate, its values decrease as the creep zone disappears. Mathematically, this means that the crack propagation rate ($\dot{a}$) in Equation (3.3-4) becomes too large so that the second term approaches the first term $\dot{V}$, and the creep deflection rate, $\dot{V}_c$, becomes smaller and smaller. Therefore, C*(t) decreases.

Figure 4.3-2 shows the developed linear relationship between the creep crack propagation rate of the coarse grain size HR160 and the time-dependent fracture mechanics parameter C*(t). The fit line is in the same da/dt versus C*(t) range of that of the as-received HR160. This trend can be seen more obviously in Figure 4.3-3. The results of the as-received and the coarse grain size HR160 tested at same temperatures and load levels are plotted in this figure. All the data points fall in the same trend and cover the entire tested C*(t) range. This indicates that the coarse grain size of HR160 tested in this investigation has no obvious effect on the creep crack propagation rate, as it was predicted in the discussion of the creep deformation test results. Since the coarse

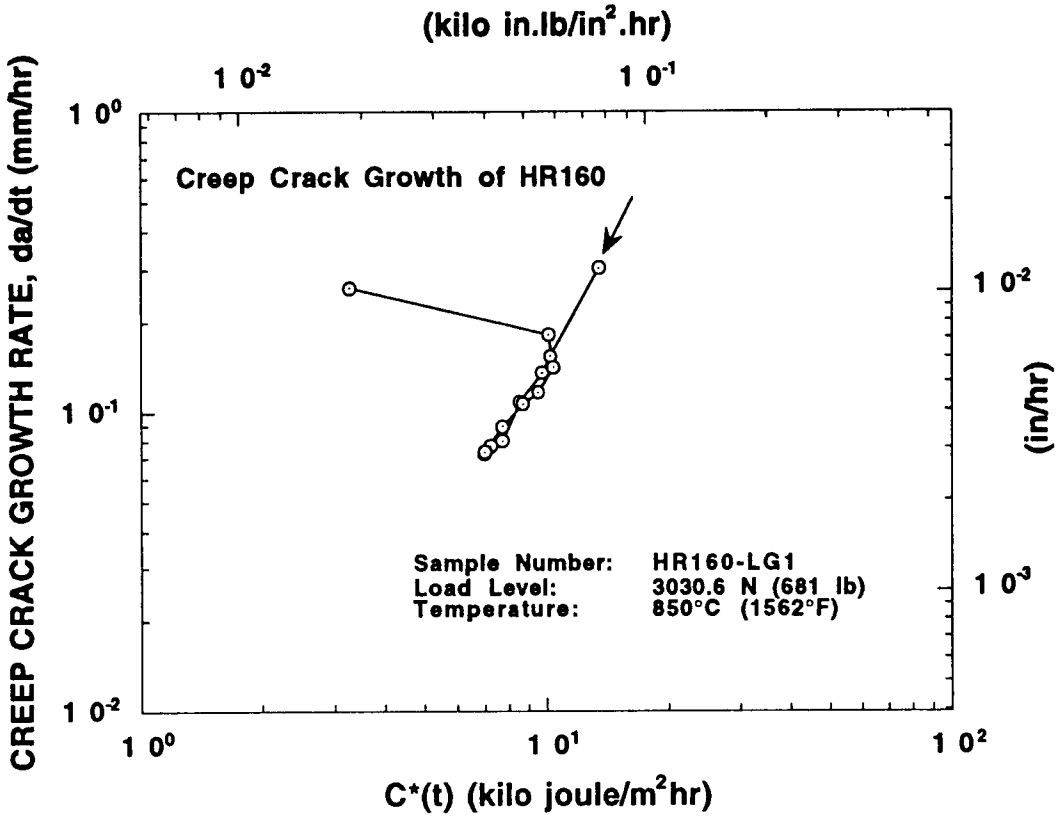

Figure 4.3-1 A Typical Plot of the Creep Crack Propagation Rate of the Coarse Grain Size HR160 Characterized with the Time-Dependent Fracture Mechanics Parameter C*(t)

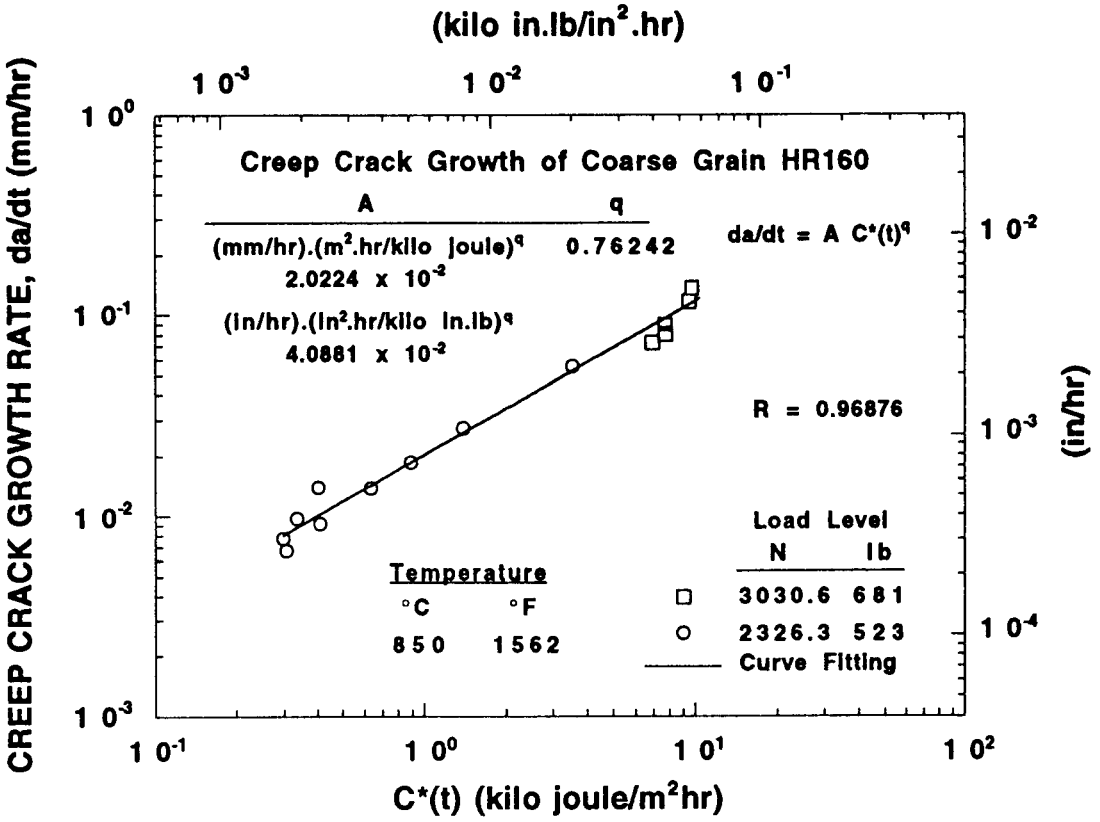

Figure 4.3-2 The Unique Correlation Between the Creep Crack Propagation Rate of Coarse Grain Size HR160 and the Time-Dependent Fracture Mechanics Parameter C*(t).

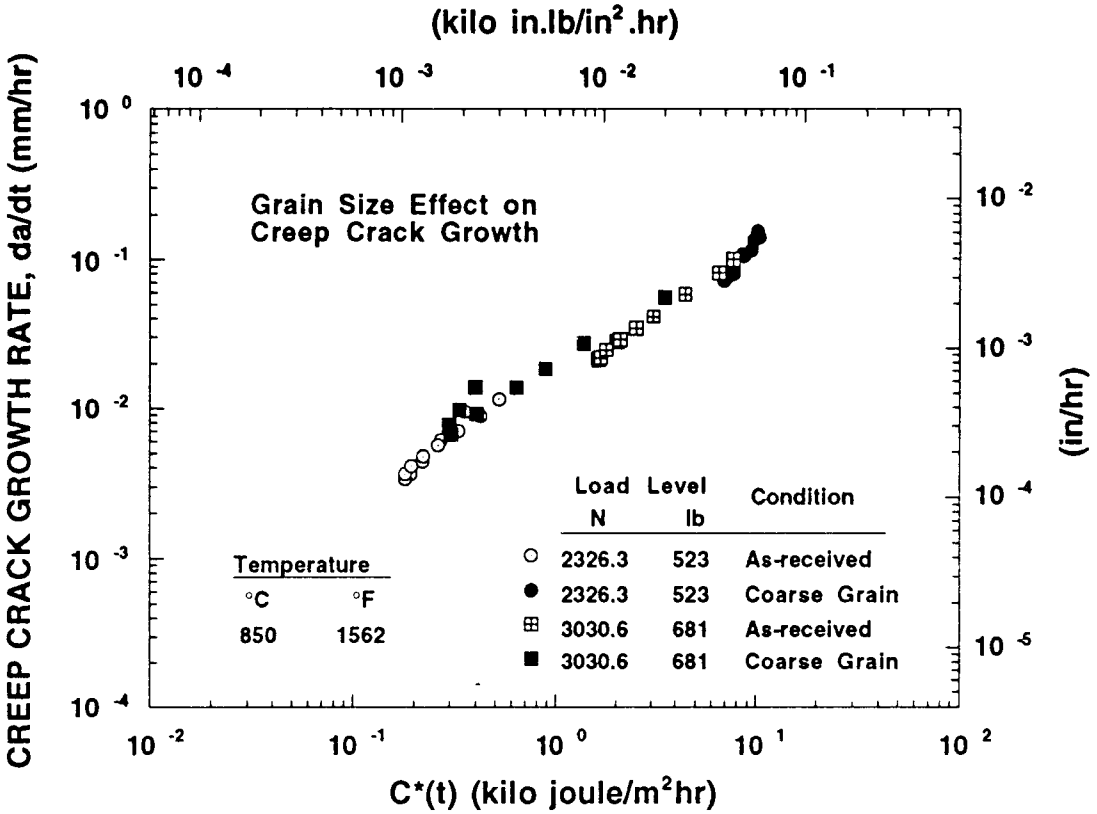

Figure 4.3-3 A Comparison Between the Creep Crack Propagation Rates of the Coarse Grain Size and the As-received HR160 Characterized with the Time-Dependent Fracture Mechanics Parameter C*(t)

grain size tested in this investigation was ASTM No. 00, the coarsest one which was obtained in this material, and no effect on the creep crack propagation rate has been observed, HR160 can be considered as a very stable material from the standpoint of grain size and creep crack growth resistance.

4.3.2 Aged Condition

A typical plot of the creep crack propagation rate of the aged HR160 characterized with the time-dependent fracture mechanics parameter C*(t) is given in Figure 4.3-4. It also has the same trend of that of the as-received HR160, starting at a high initial rate because of the primary creep, slowing down in the secondary creep stage and picking up the speed with the decreasing load bearing area. Figure 4.3-5 shows the developed linear relationship between the creep crack propagation rate of the aged HR160 and the time-dependent fracture mechanics parameter C*(t). Again, the fit line is in the same da/dt versus C*(t) range of that of the as-received HR160. The comparison of the results between the aged and as-received HR160 is given in Figure 4.3-6. All the tests were conducted at the same temperature and one pair of the tests were also at the same load level. In this figure, all the data points fall in the same trend and cover the entire tested C*(t) range. This indicates that the aging process of HR160 tested in this investigation has no obvious effect on the creep crack propagation rate of HR160, as it was predicted in the discussion of the creep deformation test results.

Usually, when a material is aged, its properties are deteriorated because of microstructural changes. The aged HR160 studied in this investigation has been aged at 649°C (1200°F) for 1,000 hours followed by air cooling. No obvious effect on its creep crack propagation resistance has been found. Moreover, the sample of the creep crack propagation test at the temperature of 850°C (1562°F) and the load level of 1579 N (355

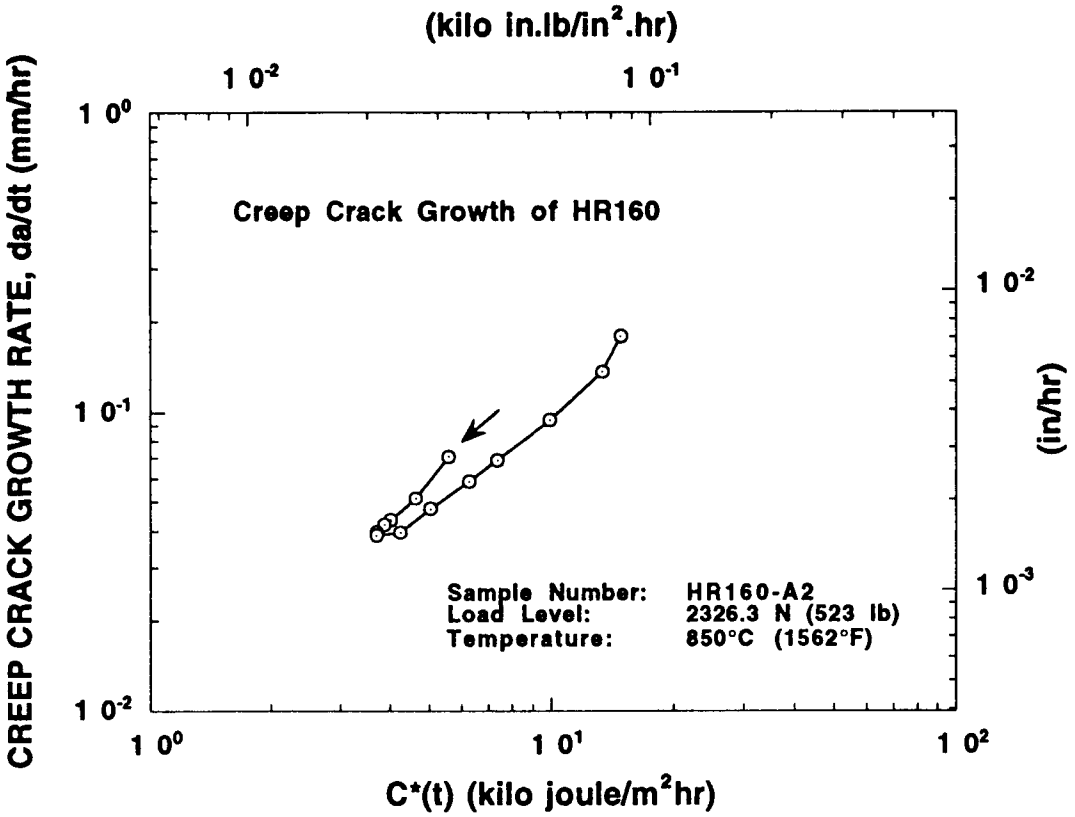

Figure 4.3-4 A Typical Plot of the Creep Crack Propagation Rate of the Aged HR160 Characterized with the Time-Dependent Fracture Mechanics Parameter C*(t)

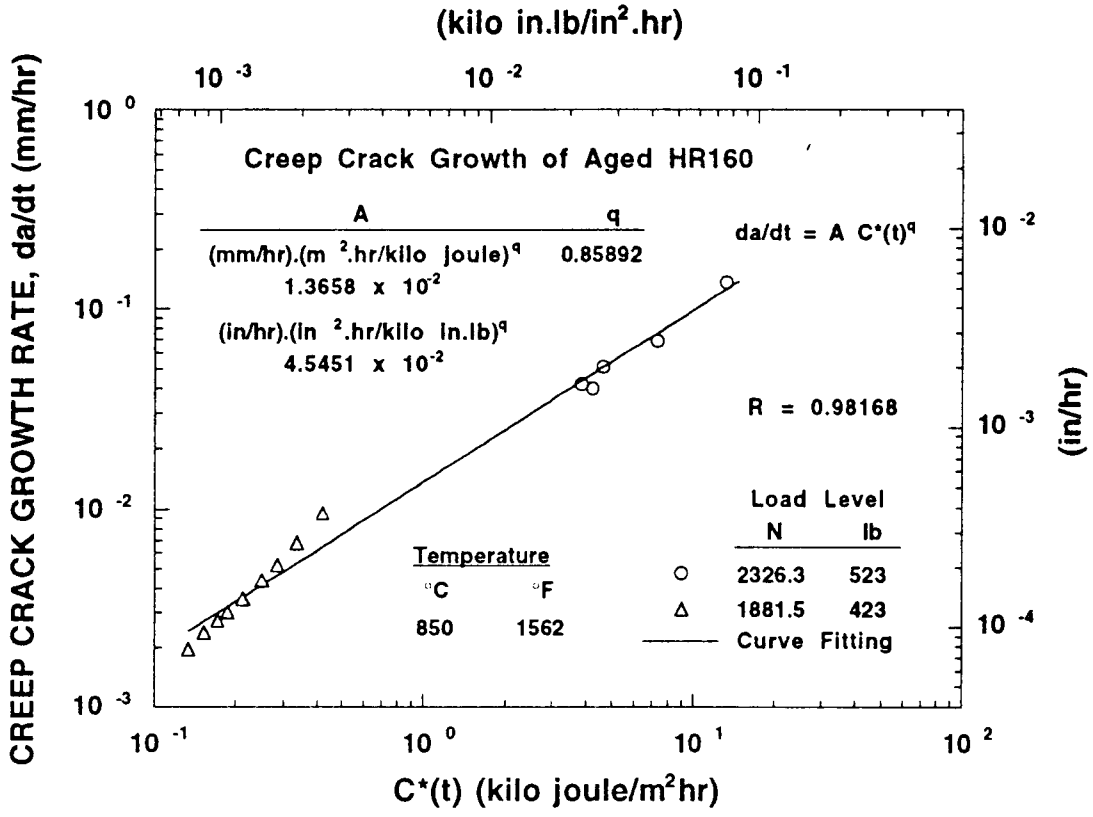

Figure 4.3-5 The Unique Correlation Between the Creep Crack Propagation Rate of the Aged HR160 and the Time-Dependent Fracture Mechanics Parameter C*(t)

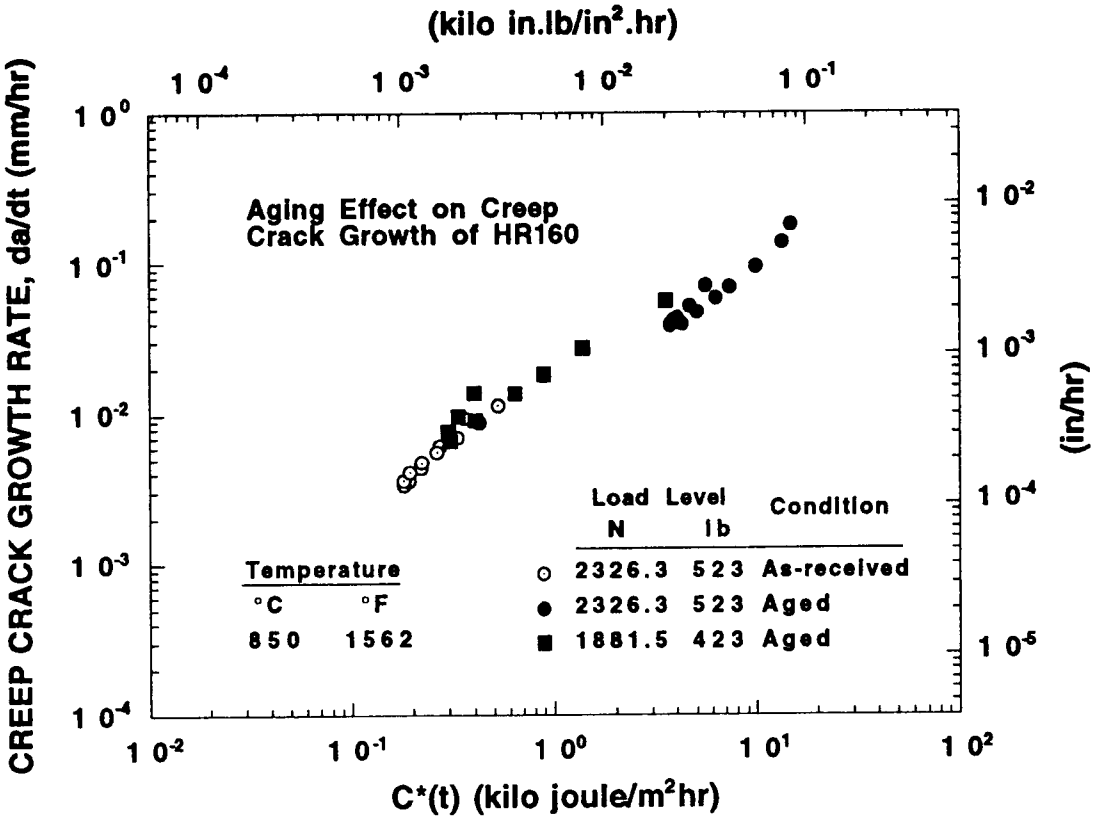

Figure 4.3-6 A Comparison Between the Creep Crack Propagation Rates of the Aged and the As-received HR160 Characterized with the Time-Dependent Fracture Mechanics Parameter C*(t)

lb) was aged at high temperature under stress for more than 7,000 hours during testing, and still no evident decrease in creep crack propagation resistance has been observed.

It is known from the microstructural analysis of the creep deformation test samples that precipitation and grain growth occur in HR160 during its exposure to elevated temperatures. Precipitates along the grain boundaries have been found to deflect the growing creep cavities into the grains, making difficult propagation paths. Furthermore, grain coarsening can usually decrease the grain boundary area, and thus, decreases the opportunities for creep cavitation to occur along the grain boundaries. It seems that these mechanisms can help keep up the creep crack propagation resistance of the material. Although the aging time in this investigation is still too short compared to the service periods of real engineering components, which usually last for decades and may greatly degrade the material properties, the results from the longest aging time of more than 7000 hours (10 months) in this investigation have shown a good possibility that HR160 is a aging resistant material from the standpoint of creep crack resistance.

4.3.3 Welded Condition

A typical plot of the creep crack propagation rate of HR160 weldment characterized with the time-dependent fracture mechanics parameter, C*(t), is given in Figure 4.3-7. It is evident that the trend of the data points is different from that of the HR160 in other material conditions. The high initial creep crack propagation rate caused by the primary creep observed in the other material conditions is not observed in this figure. In Figure 4.3-7, the data points reach the minimum rate soon after the starting point, and then increases because of the decreasing load-bearing uncracked ligament. This trend well matches the prediction made in Section 4.1.2 from the creep deformation test results. As discussed in Section 4.1.2, because the creep deformation test results of the HR160 weld showed no primary creep in the entire creep deformation process, as it is

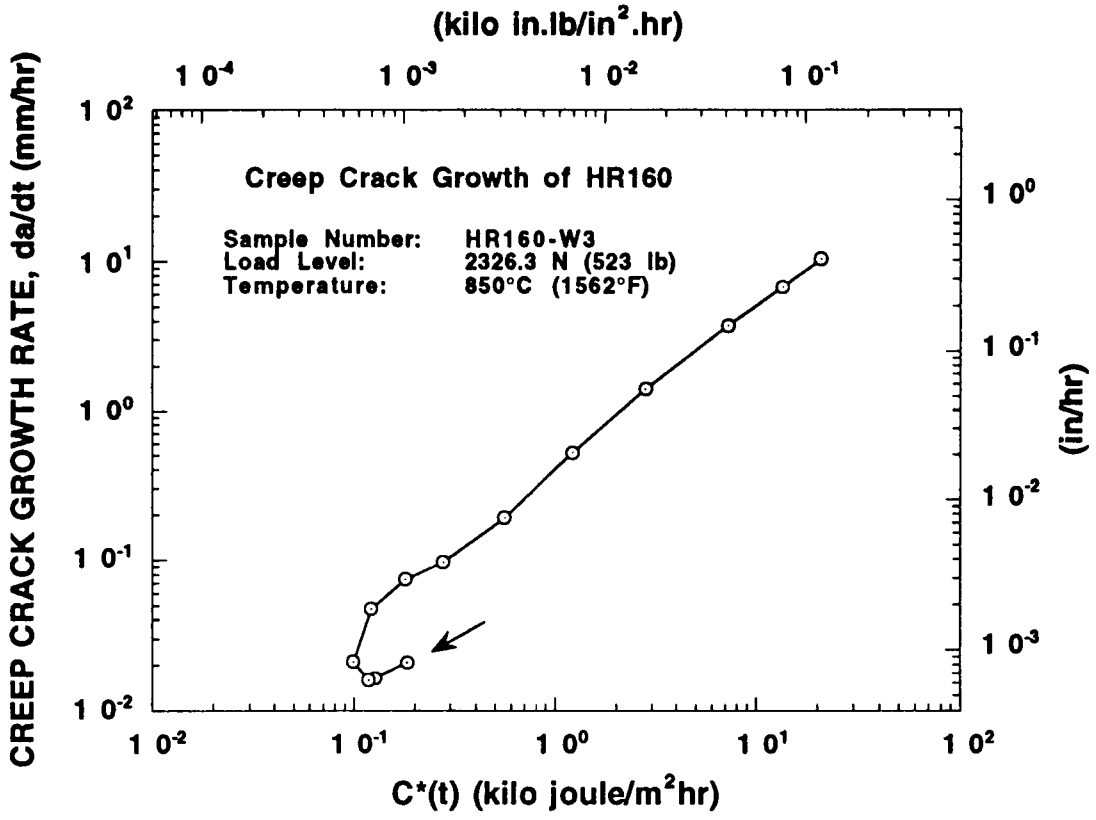

Figure 4.3-7 A Typical Plot of the Creep Crack Propagation Rate of the HR160 Weldment Characterized with the Time-Dependent Fracture Mechanics Parameter C*(t)

seen in Figure 4.1-8 b), the crack should not have a high initial propagation rate in the creep crack growth tests. The curve of the creep crack length versus time should resemble that of the creep strain versus time. Such a curve for the test shown in Figure 4.3-7 is given in Figure 4.3-8. Same as in Figure 4.1-8 b), no high initial crack propagation can be found in Figure 4.3-8. Figure 4.3-8 clearly shows that the crack length increased very slowly for approximately 90 hours before fast growing began. The initial creep crack propagation rate that was slightly higher than the minimum rate shown in Figure 4.3-7 is believed to be caused by precracking damage.

Because of the lack of primary creep, the rupture strain for the welded HR160 can be smaller than that of the as-received HR160. This has been shown in Table 4.1-5. This means that the local material at a crack tip in the weldment is much easier to rupture than that in the as-received HR160. Therefore, the creep crack propagation rate can be higher in the weld than in the as-received HR160. The developed data of creep crack propagation rate versus the time-dependent fracture mechanics parameter C*(t) for the weld are plotted in Figure 4.3-9. The values of A and q are 1.5131×10^{-1} $(mm/hr)(m^2 \cdot hr/kilo\ joule)^q$, i. e., 2.768 $(in/hr)(in^2 \cdot hr/kilo\ in.lb)^q$, and 1.1889, respectively. Compared to the A of 1.7464×10^{-2} $(mm/hr)(m^2 \cdot hr/kilo\ joule)^q$, i. e., 6.06996×10^{-2} $(in/hr)(in^2 \cdot hr/kilo\ in.lb)^q$, and q of 0.86734 for the as-received HR160, it is obvious that the values of A and q for the weld are higher than those of the as-received material. The results in Figure 4.3-9 indicate that under the same working conditions, the welds can be weaker than the base metal in creep crack propagation resistance. In addition, Figure 4.3-9 also shows that scattering of the weld data is more severe than that in any other material conditions. This can be explained by the non-uniformity in the material structures of the weld. Since the C(T) specimens employed for this investigation on welding effect contained weld and base metal, the relative percentage of the weld, HAZ and base metal could hardly be the same on the path of the crack propagation for

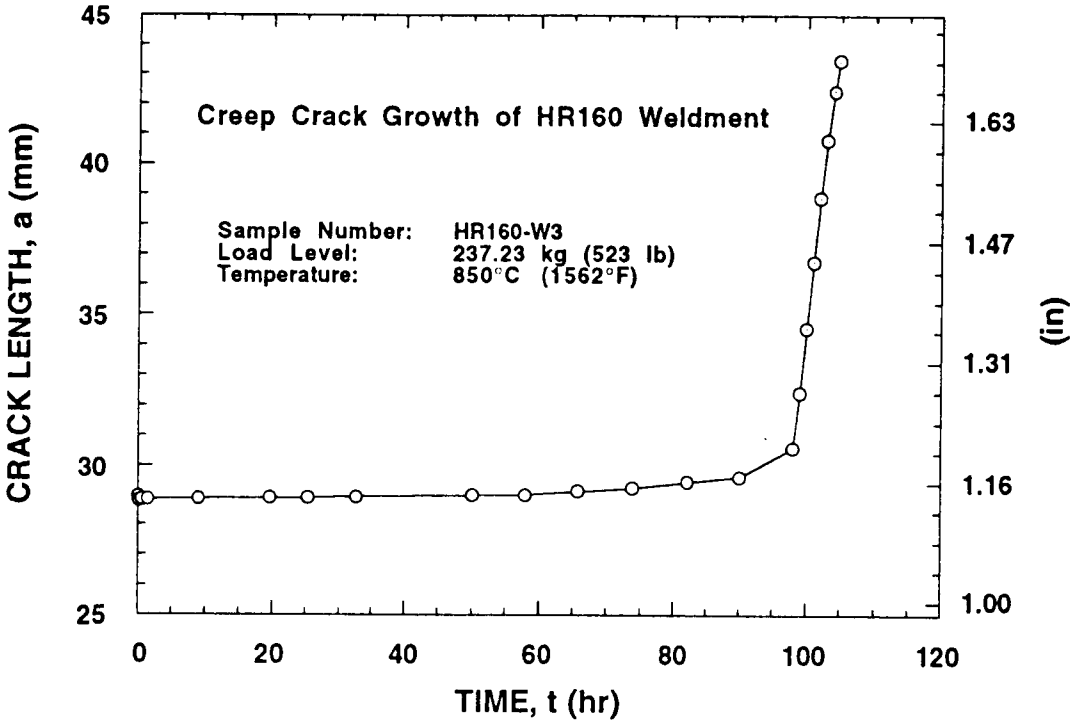

Figure 4.3-8 The Creep Crack Propagation of HR160 Weldment as a Function of Time Showing No High Initial Crack Propagation Rate

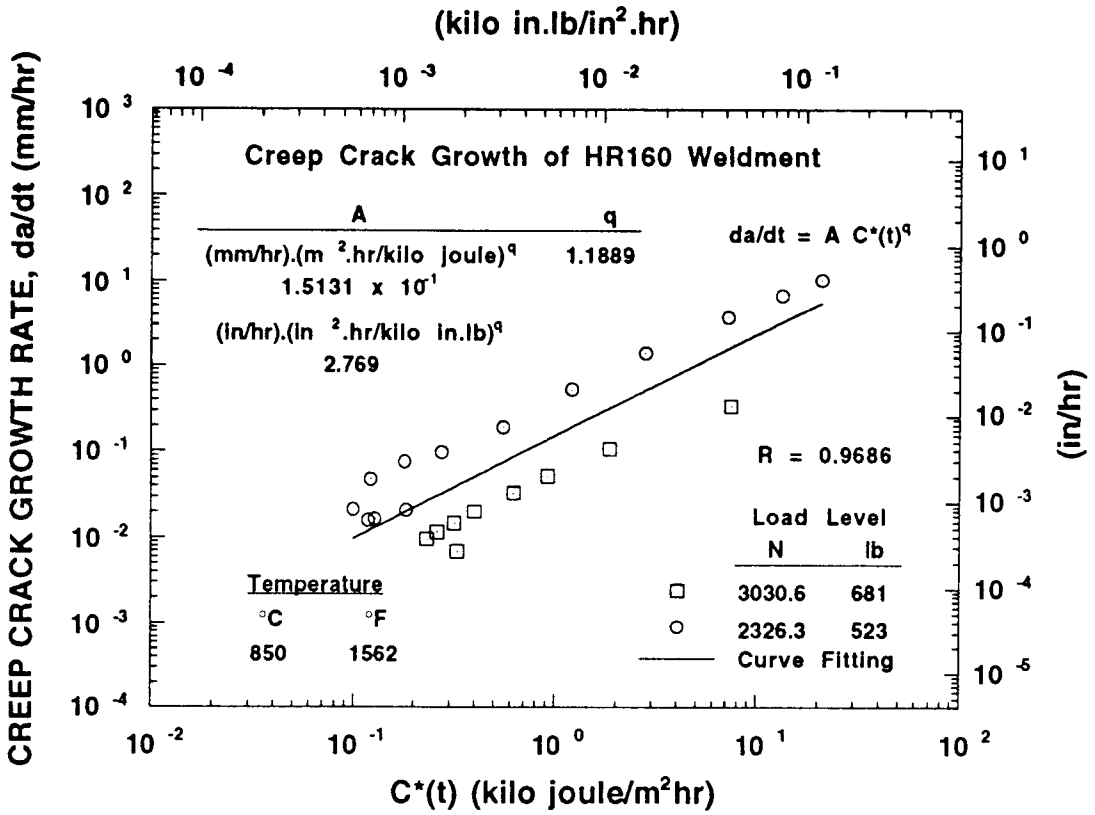

Figure 4.3-9 The Correlation Between the Creep Crack Propagation Rate of the Welded HR160 and the Time-Dependent Fracture Mechanics Parameter C*(t)

each specimen. Therefore, a variation of the creep crack propagation rate from individual specimens should be expected.

It should be pointed out that the value of q obtained from Figure 4.3-9 may contain certain error. As it has been discussed in Section 4.2.3 that only the q values obtained from at least two tests with certain span between their individual covering range of C*(t) are accurate and can be used for life prediction. In Figure 4.3-9, the two tests cover completely the same C*(t) range without any span between their covering C*(t) values. More tests should be conducted when high accuracy of the q value is required. However, the current results do not prevent us from comparing the creep crack propagation behavior on the C*(t) range covered by these two tests. The comparison of the creep crack propagation rate of the welded and the as-received HR160 is given in Figure 4.3-10. The weakness of the weld is well shown in this figure. The clear symbols represent the result of the as-received material and the solid ones represent that of the weld. The tests were conducted at the same temperatures and load levels. It is evident in this figure that at the same values of C*(t), the creep crack propagation rate of the weld is approximately 12 to 15 times higher than that of the as-received material. This makes the welds the weak parts in an industrial component made of HR160 from the standpoint of creep crack propagation resistance.

All the test results of the different material conditions obtained in this investigation are compared with that of the as-received condition in Figure 4.3-11. The straight line is the fit line of the results from the as-received HR160, while the point symbols represent those from the coarse grain size, aged and welded material conditions. As discussed above, it is obvious that the weld is the weakest part of all. The coarse grain and the aged HR160 are relatively stable in creep crack propagation resistance.

The reason for the weakness of HR160 weldment has been revealed by microstructural analysis. Figure 4.3-12 shows a creep crack fracture surface of the weld.

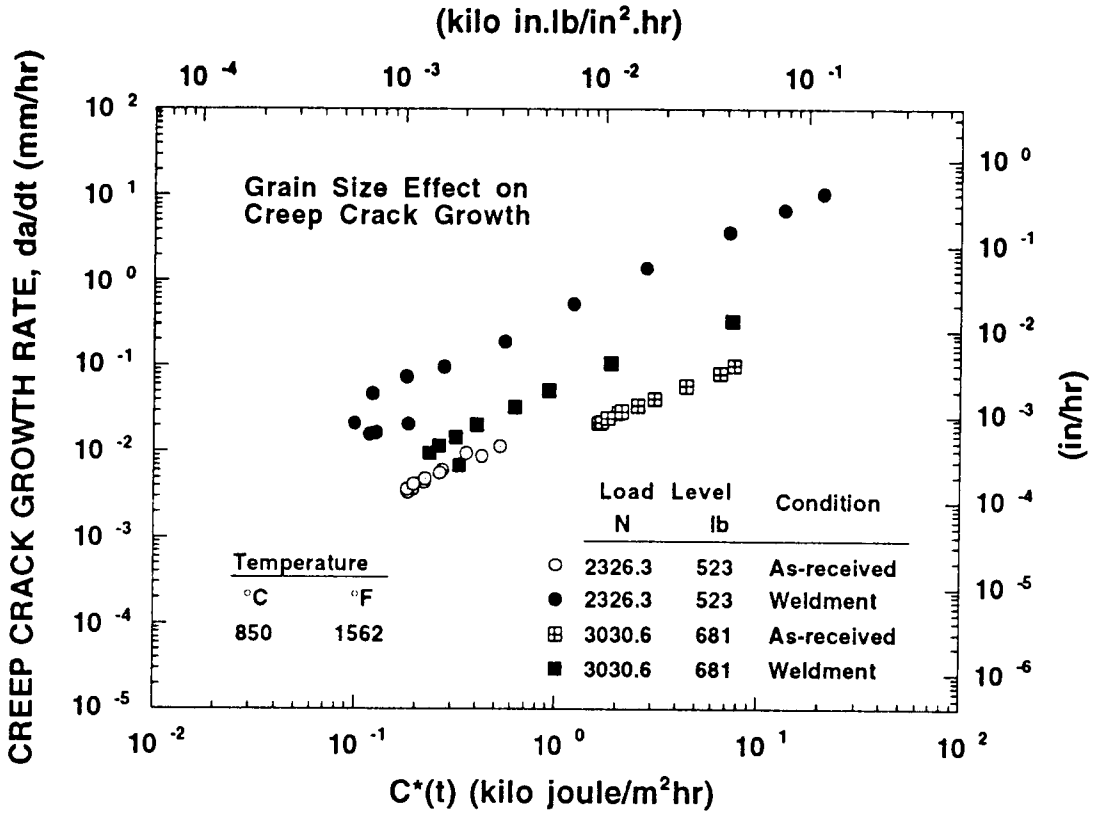

Figure 4.3-10 A Comparison Between the Creep Crack Propagation Rates of the Welded and the As-received HR160 Characterized with the Time-Dependent Fracture Mechanics Parameter C*(t)

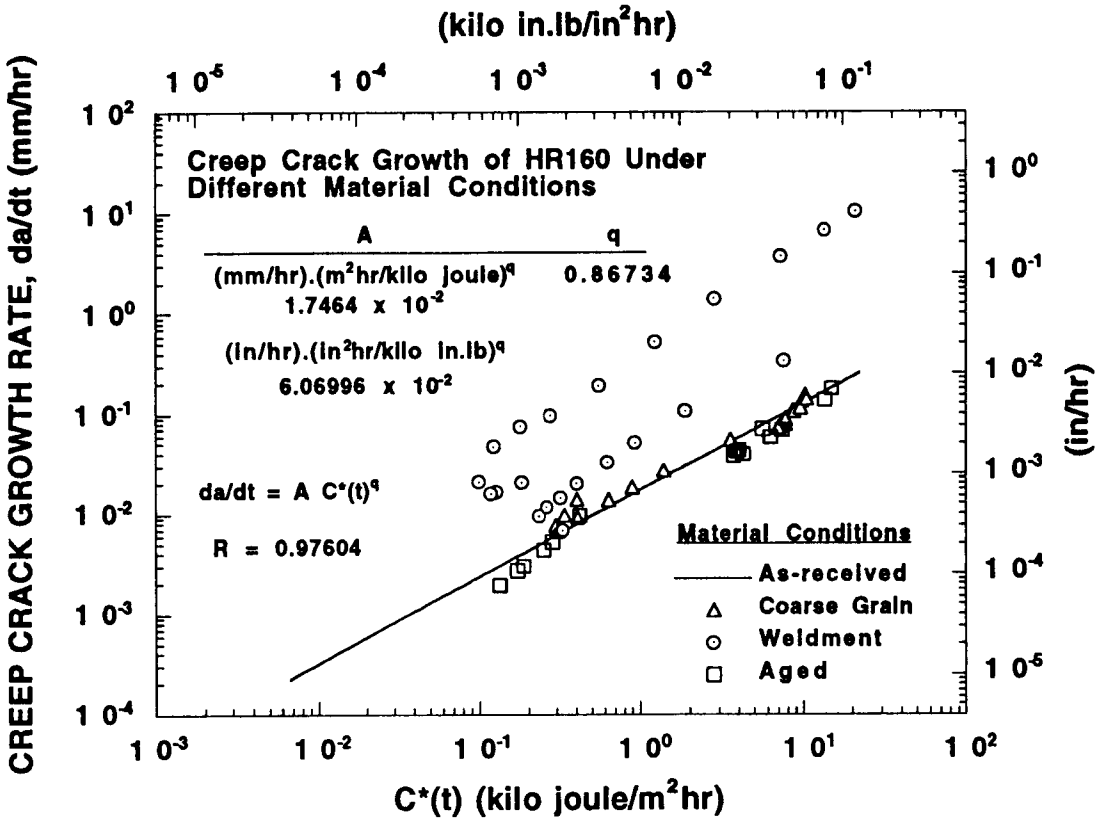

Figure 4.3-11 A Comparison Between the Creep Crack Propagation Rates of HR160 in the As-received and the Other Different Material Conditions Characterized with the Time-Dependent Fracture Mechanics Parameter C*(t)

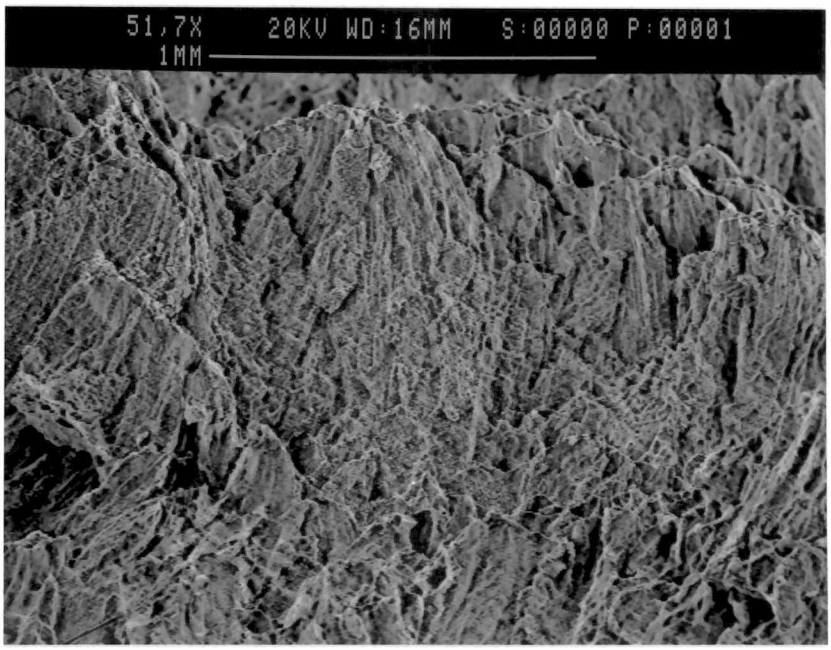

Figure 4.3-12 The Creep Crack Fracture Surface of a HR160 Weld Showing Dendrites, Typical of Casting Microstructure.

It is evident that the weld is dendritic, typical of a casting microstructure. This structure is likely to have a high crack propagation rate. The vast grain boundaries of the dendrites provide large areas of high energy as the nature of its non-equilibrium state. This feature obviously promotes creep process along the dendritic grain boundaries. Moreover, microsegregation is commonly found in dendritic microstructures. Brittle second phases usually form along the dendritic grain boundaries. Exposed to elevated temperatures, the grain boundaries can become very weak. In addition, residual stress can also worsen the situation. All these explains the decrease in both tensile and creep ductility as well as the creep crack resistance in HR160 weldment. Figure 4.3-13 shows the uncracked ligament of the weld fatigue-ruptured at room temperature after the testing. The fracture is evidently intergranular in the dendritic microstructure. Such an intergranular fracture can only be produced by fatigue at room temperature in a material with weakened grain boundaries. It can be concluded that the weld is weak because its dendritic casting microstructure provides significant amount of weak grain boundaries. This conclusion is strongly supported by Figure 4.3-14, which is the microstructure perpendicular to the dendrites of the weld after the creep crack propagation test. The lamellar cracks clearly indicate the vast weakened dendritic grain boundaries.

The observation in this section has shown that the welds of HR160 are the weak parts against creep crack propagation, the grain coarsening and aging do not have obvious effects on the creep crack propagation behavior of HR160. The aged material was prepared by re-annealing at 649°C (1200°F) for 1000 hours followed by air cooling, and the coarse grain size was obtained by re-annealing at 1204°C (2200°F) for 20 minutes followed by water quench. The fact that they do not show obvious negative effects on the creep crack propagation behavior provides a possibility to cure the weak dendritic casting structure in the weldment. It is possible to change the dendritic structure in the welds by

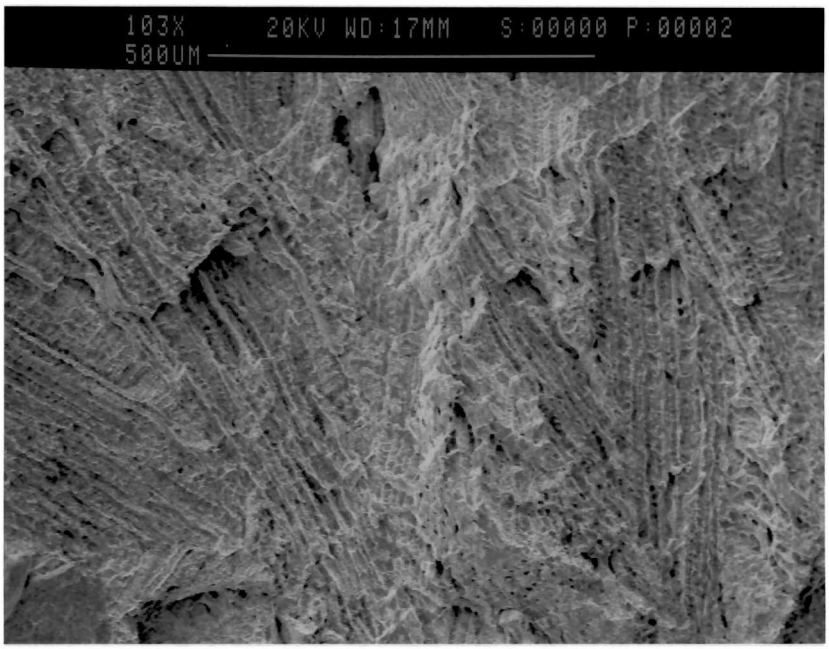

Figure 4.3-13 The Uncracked Ligament of the HR160 Weld Fatigue-Ruptured at Room Temperature After the Testing, Showing the Dendrite Interfaces Weakened at the Elevated Temperature

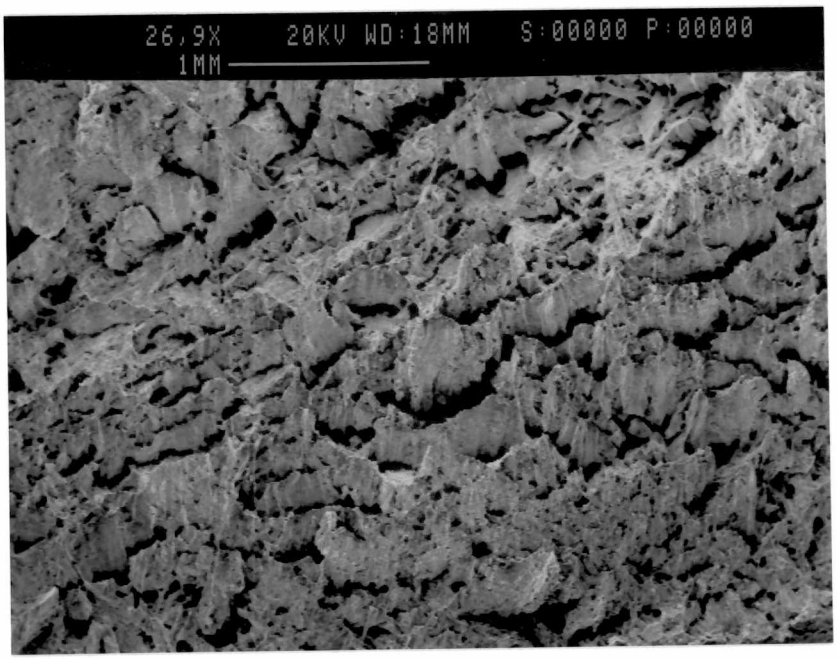

Figure 4.3-14 A Transverse Section of the Dendrites in the HR160 Weld After Creep Crack Propagation Test, Showing Lamellar Cracks Along the Weakened Dendritic Grain Boundaries

conducting localized post heating without worrying about negative effects caused by grain coarsening or aging on creep crack propagation behavior of the material.

4.4 Time-Dependent Fracture Mechanics Characterization Under Different Fatigue Conditions

4.4.1 The Crack Propagation Rate Under Cyclic Loading Conditions

As discussed in Chapter III, the average creep crack propagation rate during the hold time $(da/dt)_{avg}$ was calculated with Equation (3.3-10) and Equation (3.3-11) for time-dependent fracture mechanics characterization. The subscript, ΔK, in Equation (3.3-10) indicates that the subtraction between the measured creep-fatigue and fatigue crack propagation rates should be conducted at the same values of the stress intensity factor range. To conduct this preliminary analysis on the creep-fatigue test data, da/dN versus ΔK, developed from the results of tests with hold times of 0, 10, 100 and 3600 seconds are plotted in Figure 4.4-1.

In Figure 4.4-1, all the test results show a "hook" shape. The stress intensity factor range, ΔK, obviously does not provide a unique correlation of the data. The "hooks" indicate that, like in some other materials [63] [106], a transient trend exists for HR160 during the early period of the fatigue and creep-fatigue tests. One explanation about the hooks may be found in the decrease of the crack propagation rate during the first period of time of the tests. At the beginning of such a test, the crack starts to grow from the precrack tip introduced at room temperature. The initial crack growth rate is high because the heavy fatigue damage at the precrack tip has already weakened the local material. It then slows down into a less and less damaged area until reaching the non precrack-damaged area. The propagation rate rises again when the uncracked ligament becomes smaller and smaller. Furthermore, the crack closure phenomenon may also contribute to the deceleration and acceleration of the crack propagation [107].

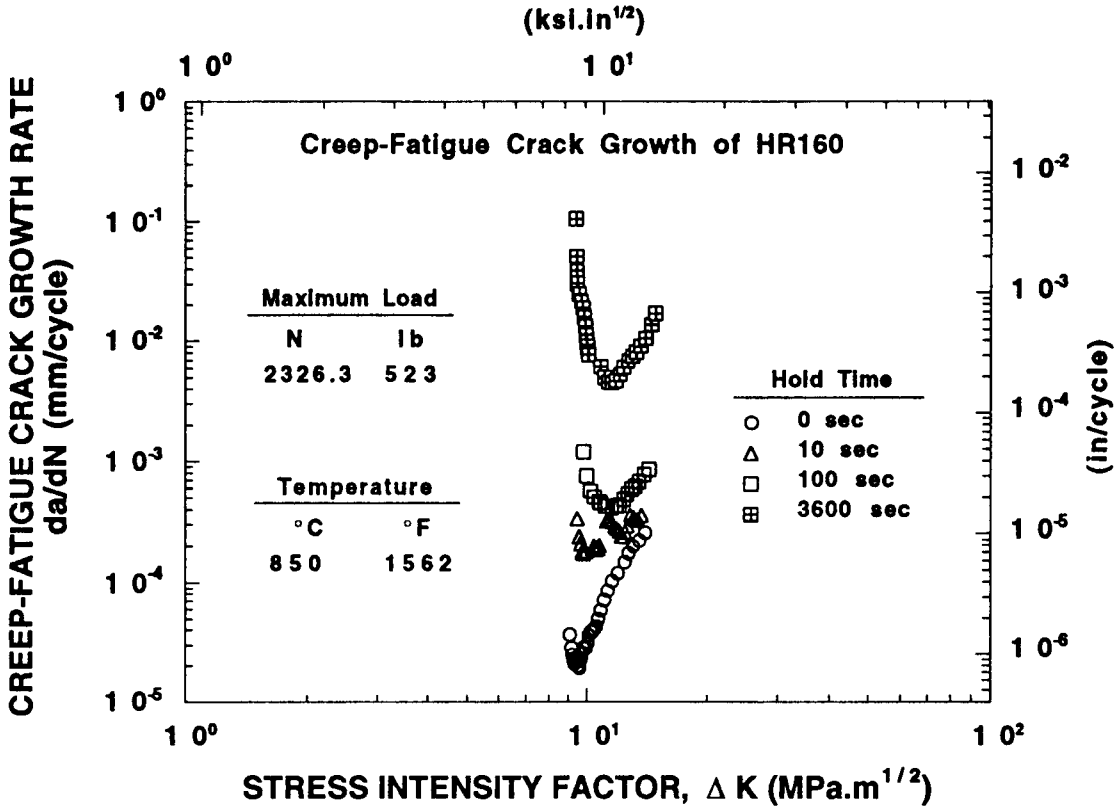

Figure 4.4-1 Fatigue and Creep-Fatigue Crack Propagation Rates Versus Stress Intensity Factor Range ΔK

However, in the curve for the 10 second hold time test, two hooks can be observed. Further explanation has to be found for this observation. The second hook was caused by an interruption of the testing. The testing system was turned off and the test sample was cooled down to room temperature at the interrupted point. The appearance of the second hook after restarting the testing is an indication that the transient phenomenon in the tests with hold time may be mainly caused by the transition from the small-scale creep to the extensive creep conditions. After the test was interrupted, the reversed plastic deformation during cooling helped partially recover the accumulated creep deformation at the crack tip. When the test was resumed, the crack tip material had to go through again the transition from the small-scale to extensive scale creep conditions, as if it were a new test. Other mechanisms, such as the primary and secondary creep conditions, may also contribute to the transient trend in a much less degree. Because of the length of the explanations of these mechanisms, interested readers can refer to Reference [36] for the details.

In order to insert Equation (3.3-11) into Equation (3.3-10), only the stabilized linear portion of the fatigue test data was used to obtain the fitting parameters C and n_f. The curve fitting of these data is given in Figure 4.4-2. It is evident in Figure 4.4-1 that the average crack propagation rates determined this way will be higher at the beginning of the tests. This is because when Equation (3.3-11) is inserted into Equation (3.3-10), the subtraction is conducted between the hooked creep-fatigue data curves and the straight fit line of the fatigue test data. The differences between the hooked data curves and the straight fit line are much greater at the beginning because of the hooks. This may be one of the reasons that hooks appear when $(da/dt)_{avg}$ is characterized with the $(C_t)_{avg}$ in some literature papers mentioned in Reference [36].

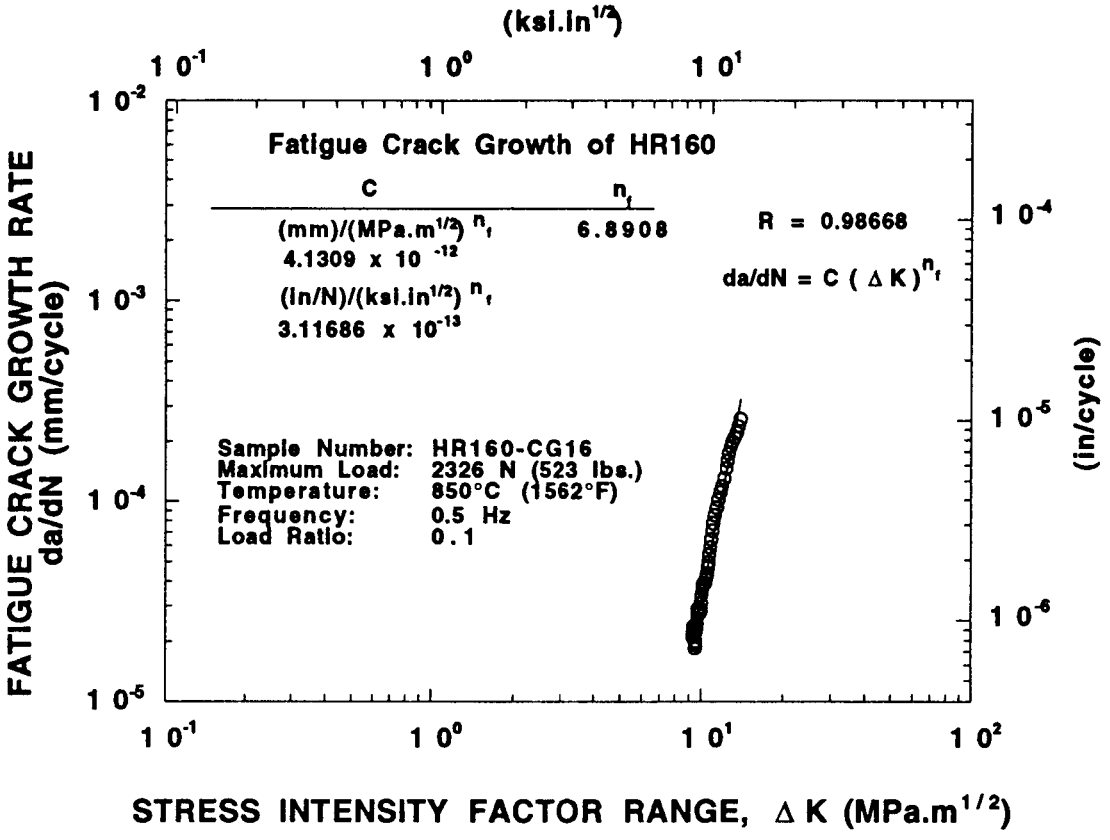

Figure 4.4-2 Parameters of the Paris Law for HR160 at 850°C (1562°F)

4.4.2 The Calculation of Time-Dependent Fracture Mechanics Parameters Under Cyclic Loading Conditions

For creep-fatigue conditions, the average creep crack propagation rate during the hold time $(da/dt)_{avg}$ has been successfully correlated to the average time-dependent fracture mechanics parameter $(C_t)_{avg}$, as proposed by Saxena and Gieseke [63]. A correlation between the creep crack and creep-fatigue crack propagation rates is desired when characterized with C*(t) (or C_t), and $(C_t)_{avg}$, respectively.

Theoretically, $(C_t)_{avg}$ should be estimated as:

$$(C_t)_{avg} = \frac{1}{t_h}\int_0^{t_h} C_t dt \qquad (4.4\text{-}1)$$

To determine $(C_t)_{avg}$ in Equation (4.4-1), the integral can be either calculated with an analytical equation of C_t [62] [64] or from Equation (2.2-40) with $\dot{V}_c$ obtained from the numerical analysis result of the loadline deflection as a function of time. There are some disadvantages in both methods. With the analytical equation of C_t, the accuracy of the calculation depends on that of the equation. Furthermore, the large number of parameters in the equation complicate the calculation. In the second method, loadline deflection as a function of time has to be recorded continuously with high resolution in order to conduct the numerical analysis. This also entails a significant amount of work in the further estimation. Therefore, approximations are obviously desired for practical purpose. In this study, $(C_t)_{avg}$ was approximated with $(C_t)_{0.5th}$ to simplify the calculation. The determination of $(C_t)_{0.5th}$ is described as follows:

From the Mean-Value Theorem for Integrals, it is known that since C_t is a continuous function of time (t) on the closed interval $[0, t_h]$, there is at least one point t' within $[0, t_h]$ such that:

$$\int_0^{t_h} C_t dt = C_t(t') \times t_h \qquad (4.4\text{-}2)$$

Substituting Equation (4.4-2) into Equation (4.4-1), we have:

$$(C_t)_{avg} = C_t(t') \qquad (4.4\text{-}3)$$

It is obvious from Equation (2.2-40) that during the hold time, C_t varies with time through the change of the loadline creep deflection rate ($\dot{V}_c$), the crack length (a) and creep crack propagation rate ($\dot{a}$). In this study, the hold time interval [0, t_h] ranged from 10 to 3600 seconds. The continuous curve of the loadline deflection as a function of time obtained in each test of this study shows that the transition period for the deflection at the beginning of each cycle was less than 1 second. Upon reloading, the deflection was recovered to more than 99% of the value at the end of the previous cycle within less than 0.1 seconds. During the hold time, no sudden or great change was observed in either the deflection or the potential drop curves. Therefore, it is reasonable to assume that there should not be any sudden or great change in C_t during the hold time. In other words, during the hold time, the curve of C_t as a function of time should be smooth and d^2C_t/dt^2 approach zero. Based on this assumption and the fact that the deflection rates were greater within the short transition period upon reloading, the time t' in Equation (4.4-3) should be very close to $0.5t_h$ in the interval $(0, 0.5t_h]$. As a practical approximation, $0.5t_h$ was chosen as the value for t'. $(C_t)_{0.5th}$ was calculated from Equation (2.2-40) with the values of crack length, crack propagation rate and loadline deflection at $0.5t_h$ of the cycles. From the above argument, we have:

$$(C_t)_{0.5th} \approx C_t(t') = (C_t)_{avg} \qquad (4.4\text{-}4)$$

For the same reason, $[C^*(t)]_{0.5th}$ was also calculated from Equation (3.3-3) for comparison:

$$[C^*(t)]_{0.5th} \approx [C^*(t')] = [C^*(t)]_{avg} \qquad (4.4\text{-}5)$$

The results developed from Equation (3.3-10), Equation (3.3-11), Equation (4.4-4) and Equation (4.4-5) have been plotted with the data of Figure 4.2-7 a) to compare with the results of the static loading tests. This comparison is presented in Figure 4.4-3. It should be pointed out that only the data points of the stabilized periods, i.e., the data points after the minimum points of the hooks, have been plotted in Figure 4.4-3. This treatment can avoid the error introduced by the great differences between the "hooks" of the creep-fatigue data and the straight fit line of the fatigue data at low $(C_t)_{avg}$, as described in the discussion of Equation (3.3-11) in Section 4.4-1.

Figure 4.4-3 shows that the stabilized creep-fatigue crack propagation rates with different hold times fall in the same trend of the creep crack propagation rates. Increasing the hold time shifts the data points along the straight fit line toward the direction of low average crack propagation rates. This indicates that a correlation exists between the creep crack propagation behavior and the combination of the creep-fatigue crack and the fatigue crack propagation behavior.

In Figure 4.4-3, a slight difference exists between the average crack propagation rates $(da/dt)_{avg}$ characterized with $(C_t)_{0.5th}$ (open symbols) and $[C^*(t)]_{0.5th}$ (filled symbols). This behavior raises a question. Which of $(C_t)_{0.5th}$ and $[C^*(t)]_{0.5th}$ is the more reasonable parameter for the characterization under cyclic loading conditions?

In the test with a hold time of 3600 seconds, the average crack propagation rates $(da/dt)_{avg}$ characterized with $[C^*(t)]_{0.5th}$ are better fitted to the straight line of the static loading test results than those characterized with $(C_t)_{0.5th}$. The reason for this behavior

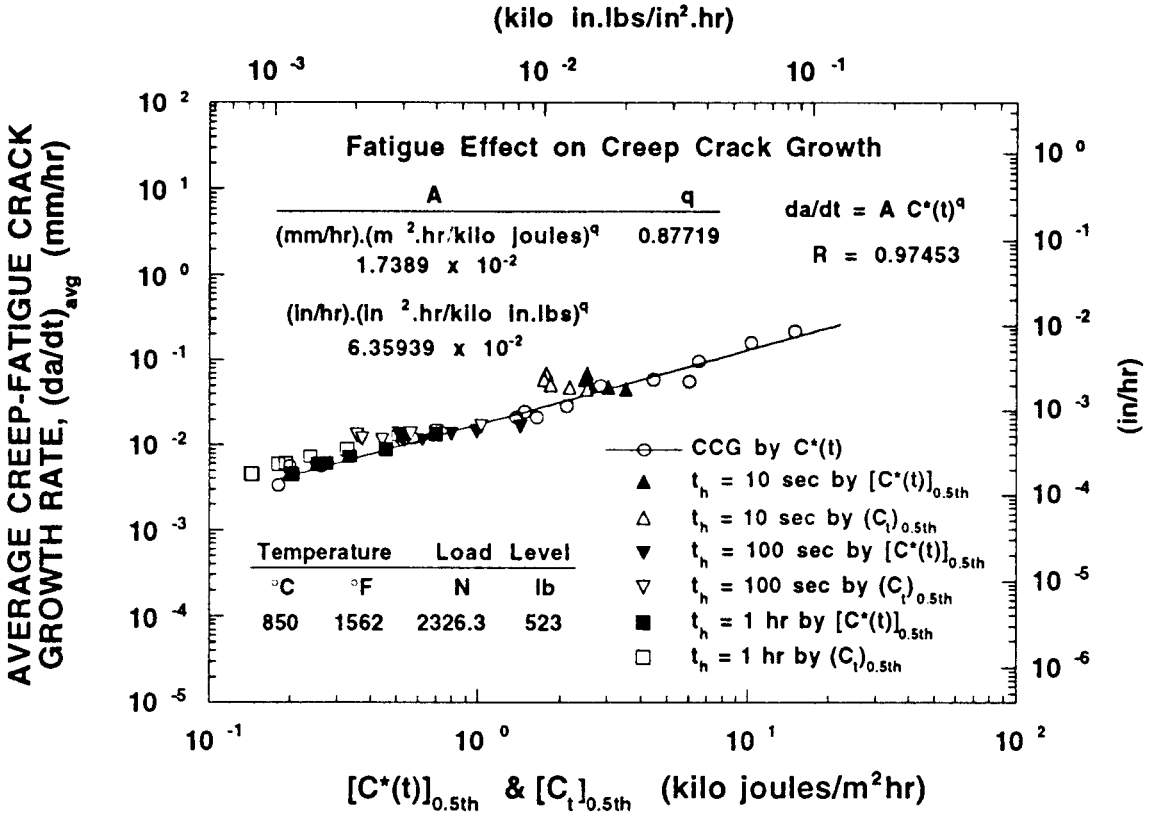

Figure 4.4-3 A Comparison Between the Test Results from Cyclic Loading and Static Loading

can be found in the transition time. The temperature and maximum load level for all the cyclic tests in this study were 850°C (1562°F) and 2326 N (523 lb). From the static loading test of the same temperature and load level, it is known that the transition time from small-scale creep to extensive creep conditions was 1918 seconds. For the hold time of 3600 seconds, the time $0.5t_h$ at which $[C^*(t)]_{0.5th}$ has been calculated was 1800 seconds. Since the transition from small-scale to extensive creep conditions is a continuous process, it is possible that after the first several cycles, the real condition at $0.5t_h$ was extensive instead of small-scale or transient creep conditions. This can be confirmed by the fact mentioned previously that all the cyclic test results plotted in Figure 4.4-3 were from the data points beyond the hooks. At such a point, the fatigue process zone could be much smaller than the creep zone [108]. During each unloading and reloading process, the reversed elastic or plastic deformation might recover a part of the creep deformation at the crack tip, but the creep process occurred beyond the scope of the elastic or plastic zone could still accumulate during each hold time. Upon reloading, the small recovered zone could be engulfed by the creep zone very quickly and the creep zone continued to extend. This is very different from the large recovered creep zone situation of the 10 second hold time test discussed in Figure 4.4-1 in Section 4.4.1. In that situation, the creep zone was largely recovered and the specimen had to go through the transition from small-scale to extensive creep conditions when the test was restarted. That was because at the turning off point, the specimen was not only unloaded, but also cooled down to room temperature. The contraction of the specimen and the testing system during the cooling process greatly recovered the creep zone. However, in the present discussion, the specimen was cyclically loaded at a constantly high temperature, the creep zone could accumulatively extend. The accumulative expanding phenomenon of creep zone was confirmed by the creep damage found in the uncracked ligament far

from the crack tip in the microstructural analysis of the tested creep-fatigue samples which will be discussed later.

The above argument also applies to the tests with short hold times of 10 and 100 seconds. Since the cycling does not completely recover the creep deformation and the creep zone continues to extend during the subsequent hold time, the transition time should be accumulatively counted from the beginning of the test instead of each load cycle. Therefore, $[C^*(t)]_{0.5th}$ seems to be a more appropriate parameter than $(C_t)_{0.5th}$ for the characterization of the average creep-fatigue crack propagation rate. Since $[C^*(t)]_{0.5th}$ and $(C_t)_{0.5th}$ are the approximations of $[C^*(t)]_{avg}$ and $(C_t)_{avg}$, respectively, $[C^*(t)]_{avg}$ should be a more appropriate parameter than $(C_t)_{avg}$ when the accumulative time exceeds a certain transition time. Using $(C_t)_{avg}$ without considering the accumulative transition time in many published papers is incorrect.

It should be pointed out that although the approximation with t' being $0.5t_h$ is successful in this study, t' shifts from $0.5t_h$ toward 0 as the transition period increases. This may happen when the load level becomes very low or the temperature becomes very high. The limit beyond which such an approximation can cause great error depends on the transition period and the accuracy requirement. When the transition period is very long, Equation (4.4-1) should be used to ensure the accuracy.

Since the data obtained from the creep-fatigue crack propagation tests fall on the fit line of the as-received HR160 when characterized with $[C^*(t)]_{0.5th}$, as shown in Figure 4.4-3, and $[C^*(t)]_{0.5th}$ has been proved to be a good approximation of $[C^*(t)]_{avg}$, the following relationship between creep-fatigue crack propagation rate and the time-dependent fracture mechanics parameter exists:

$$(da/dt)_{avg} = A\{[C^*(t)]_{avg}\}^q \qquad (4.4\text{-}6)$$

From Figure 4.4-3, it is known that decreasing the hold time, in other words, increasing the fatigue frequency, shifts the data points along the fit line toward the direction of high $(da/dt)_{avg}$ and $[C^*(t)]_{avg}$. This trend indicates that increasing shut-downs or stress fluctuations in components operating at elevated temperatures decreases their lives.

4.4.3 Microstructural Characterization of Creep-Fatigue Crack Propagation Process

Figure 4.4-4 shows the crack tip of the C(T) sample tested under cyclic loading with 0 second hold time. The crack propagated mainly in a transgranular mode. No creep cavitation at the crack tip is observed. However, the fracture surface of this crack presented in Figure 4.4-5 suggests that creep have occurred at the elevated test temperature although the sample was subjected to a cyclic loading with 0 second hold time. In Figure 4.4-5, the outline of grain boundary surfaces can be observed in a relatively flat transgranular fracture surface covered with the protective oxide layer, indicating an intergranular mode and possible creep contribution during the fatigue crack propagation process. The creep effect has been further confirmed by the observation of the uncracked ligament ruptured at room temperature by fatigue after the testing. Two SEM micrographs are given in Figure 4.4-6 and Figure 4.4-7. It is evident that the fracture surface is mainly intergranular instead of being mainly transgranular typically found in a pure fatigue fracture. Microcracks along the grain boundaries formed by the coalescence of creep cavities can also be observed.

Comparing Figure 4.4-6 and Figure 4.4-7 shows the scopes of creep and fatigue effects during the testing at elevated temperature. The position of Figure 4.4-6 in the uncracked ligament is much closer to the crack tip than that of Figure 4.4-7. More areas of transgranular fracture feature can be seen in Figure 4.4-6 than in Figure 4.4-7. This indicates that, in addition to the intergranular creep damage to the entire uncracked

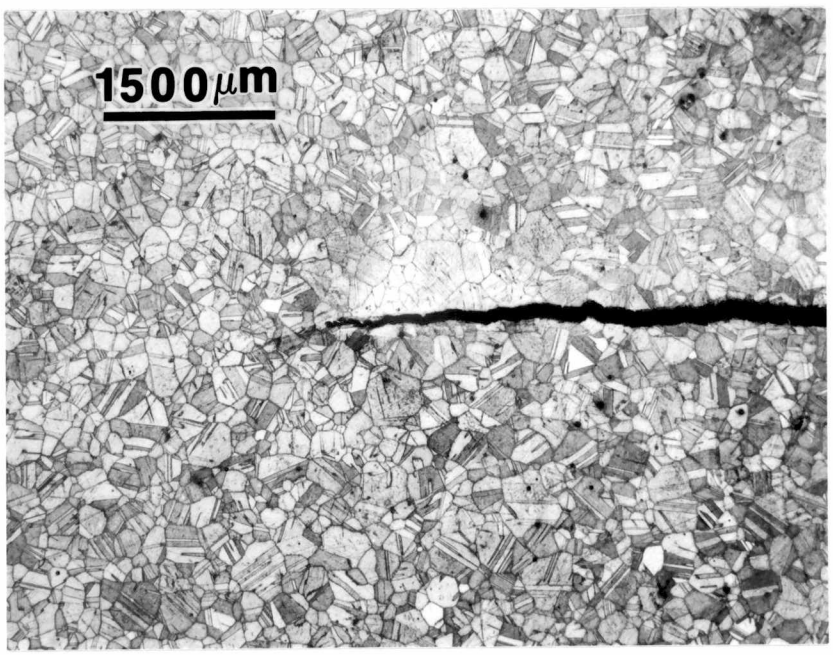

Figure 4.4-4 The Crack Tip of a Haynes HR160 Specimen Tested Under Cyclic Loading with 0 Second Hold Time at 850°C (1562°F) Showing Transgranular Nature of Crack Propagation

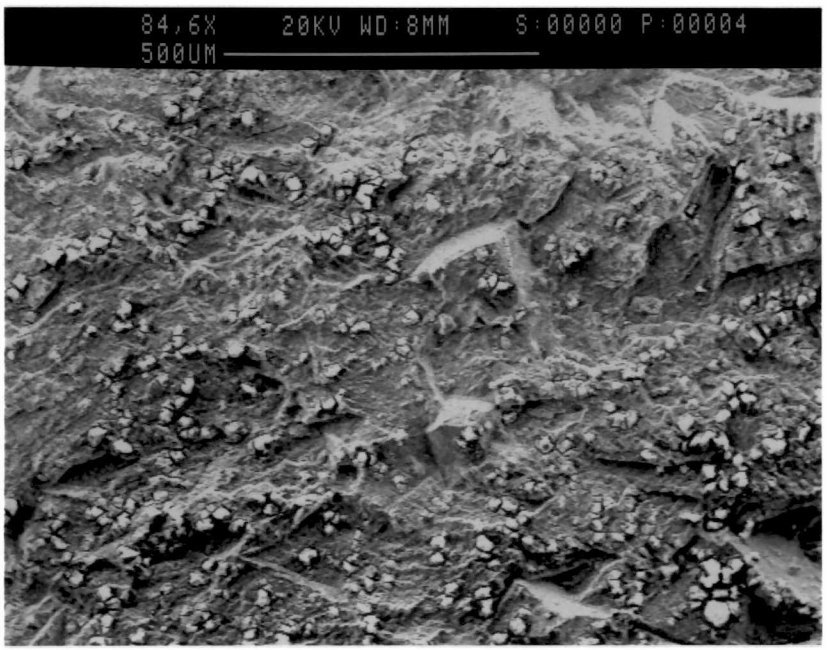

Figure 4.4-5 Fracture Surface of the Fatigue Crack in Figure 4.4-4 Showing Mainly Transgranular Nature of Crack Propagation with Some Intergranular Areas Contributed by Creep

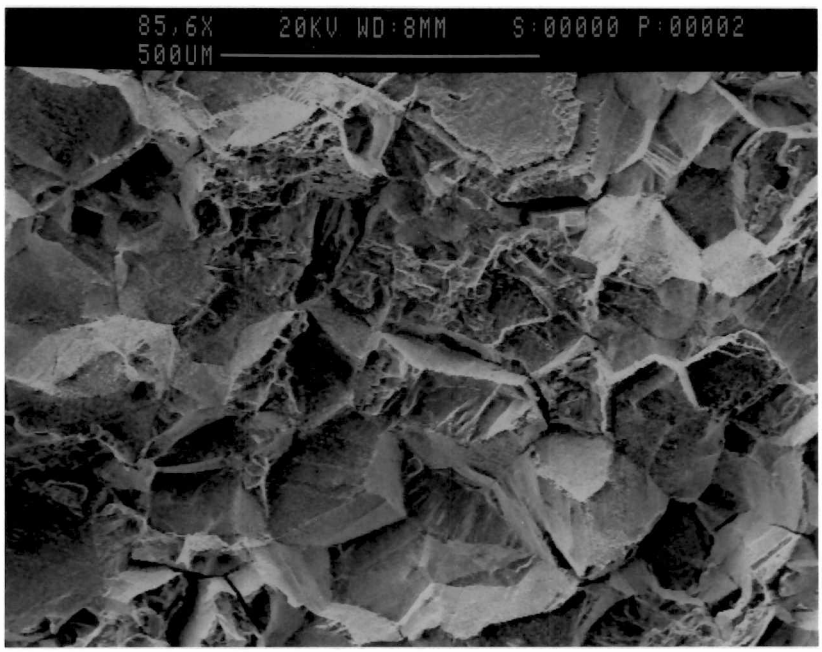

Figure 4.4-6 Uncracked Region at the Crack Tip of the Sample Shown in Figure 4.4-4, Ruptured by Fatigue at Room Temperature

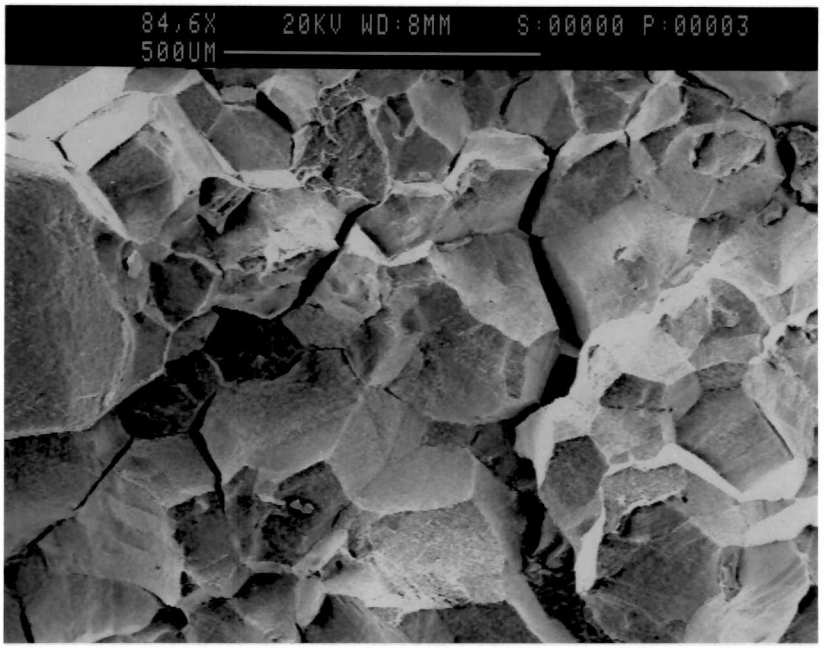

Figure 4.4-7 Uncracked Region away from the Crack Tip of the Sample Shown in Figure 4.4-4, Ruptured by Fatigue at Room Temperature

ligament, the grains close to the crack tip were weakened transgranularly in a greater degree by cyclic loading than those far from the crack tip at the elevated temperature. When the specimen was cooled to room temperature after the testing and ruptured by fatigue, the crack propagated along the weakened paths, exposing the transgranular and intergranular damage inherited from the elevated temperature testing. It is not hard to conclude from this observation that, because the fatigue process zone is within the creep process zone [109], fatigue makes damage more severe but to a smaller extent than creep does under the conditions of this investigation.

In Section 4.4.2, it was discussed that creep accumulated during the hold time periods, and therefore, $[C^*(t)]_{0.5th}$ and $[C^*(t)]_{avg}$ should be more appropriate parameters than $(C_t)_{0.5th}$ and $(C_t)_{avg}$ when the accumulative test time exceeds a certain transition time. This argument is supported by the observations discussed in the last paragraph. Creep did accumulate during the hold time periods and extended to the entire uncracked ligament. Since creep contributed to the crack propagation under cyclic loading even with 0 second hold time, as discussed above, its effect should be taken into consideration when mechanical property characterization is conducted.

Figure 4.4-8 shows the crack tip of the C(T) sample tested under cyclic loading with a hold time of 100 seconds. It is evident that the crack propagated in a mixed intergranular and transgranular mode with the intergranularity dominating the crack propagation. The fracture surface of this crack given in Figure 4.4-9 is in agreement with this observation. The mainly intergranular crack propagation had exposed the grain boundaries, which were soon covered by a protective oxide layer formed at the elevated testing temperature. The fracture surface of the uncracked ligament of this sample fatigue-ruptured at room temperature given in Figure 4.4-10 shows that the grain boundaries had been weakened by creep cavitation during the hold time. Grain

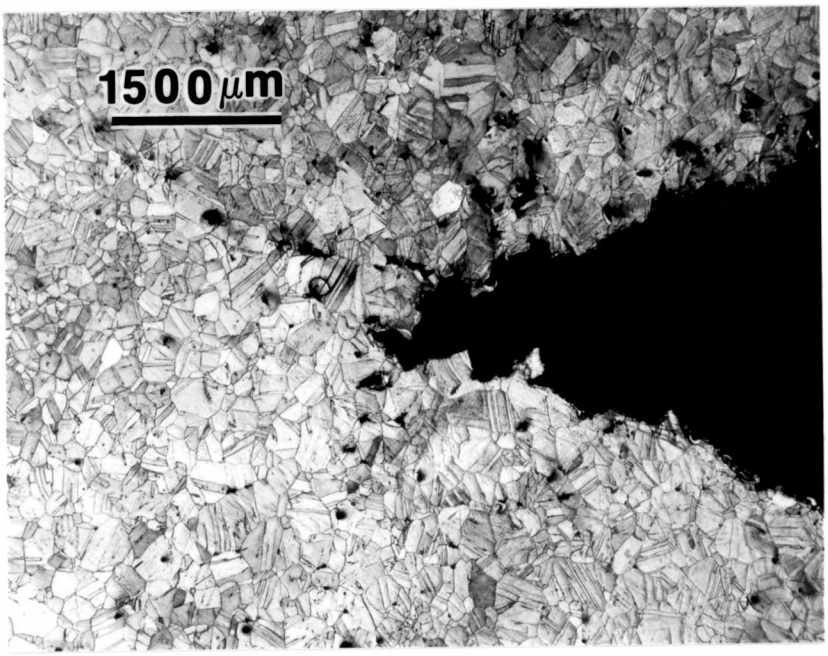

Figure 4.4-8 The Crack Tip of a Haynes HR160 Specimen Tested Under Cyclic Loading with 100 Second Hold Time at 850°C (1562°F) Showing a Mixed Nature of Mainly Intergranular with Some Transgranular Crack Propagation

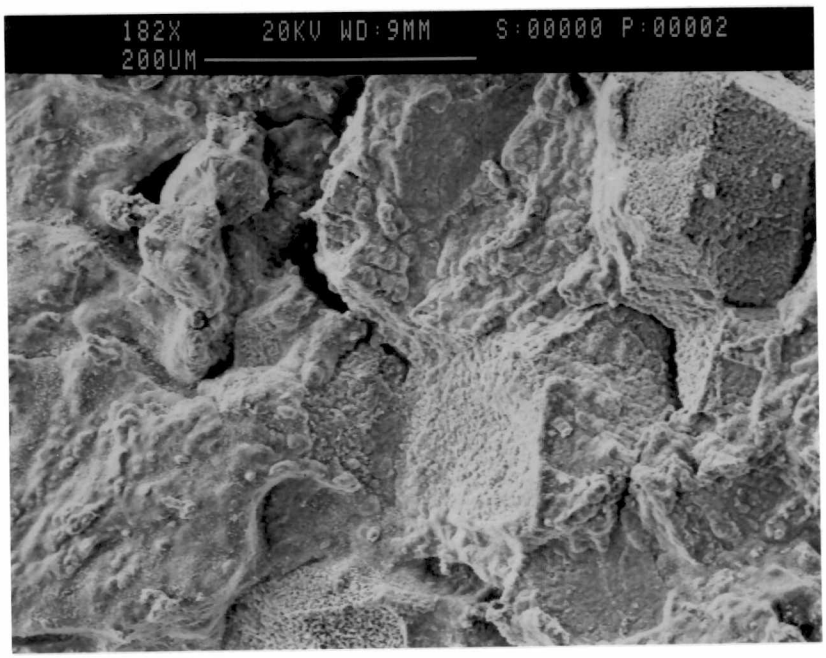

Figure 4.4-9 Fracture Surface of the Creep-Fatigue Crack in Figure 4.4-8 Showing a Mainly Intergranular Nature of Crack Propagation

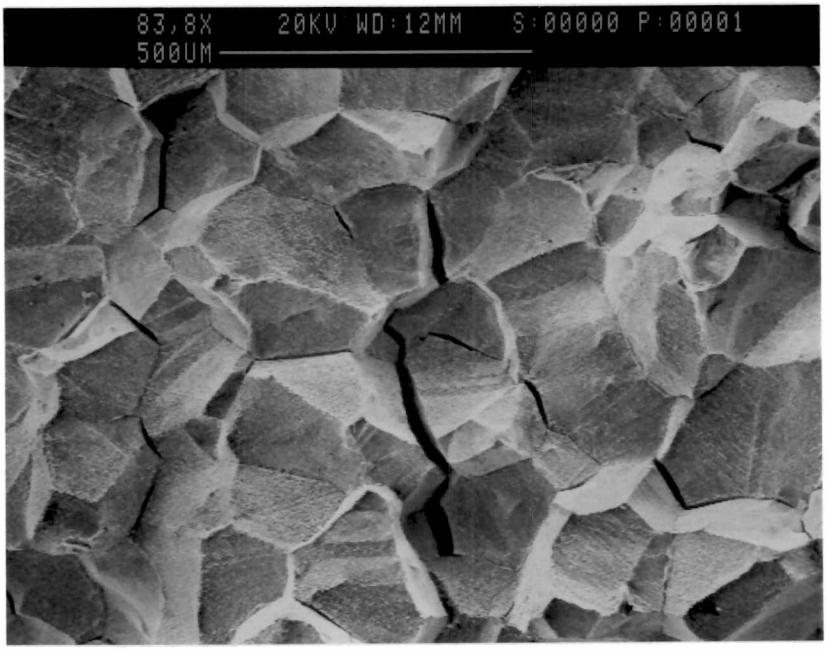

Figure 4.4-10 Uncracked Region of the Creep-Fatigue Crack in Figure 4.4-8, Ruptured by Fatigue at Room Temperature

boundaries and intergranular microcracks that resulted from creep cavitation are clearly evident.

For discussion, static loading is regarded as cyclic loading with infinite hold time. The cracks propagated under cyclic loading with 0, 100 and infinite second hold times are given in Figure 4.4-4, Figure 4.4-8 and Figure 4.2-11, respectively. It is obvious that as the hold time changes from infinite to 0 second, the crack opening decreases as well as the creep cavitation. Meanwhile, the crack propagation changes from intergranular to mainly transgranular modes. From the discussion on the fracture surfaces of these samples, it is known that creep cavitation occurred in each sample along the grain boundaries. It can be concluded that creep caused intergranular crack propagation, fatigue caused transgranular crack propagation in a much small extent within the creep zone, and thus, accelerated the total crack propagation process. Therefore, a component's life can be greatly shortened because of the fatigue effect. This can be clearly seen in Table 4.4-1. Under the same conditions, as the hold time (t_h) is decreased from infinite to 0 second and the number of loading cycles per hour is increased from 0 to 1800, the average time spent per unit crack length, $(dt/da)_{avg}$, decreases from 168 hr/mm (4271 hr/in) to 10 hr/mm (253 hr/in) because of the increasing fatigue effect.

4.5 Theoretical Modeling of Creep Crack Propagation Process

4.5.1 Creep Crack Propagation Process

Since creep crack propagation is originated from creep deformation, creep deformation testing has to be conducted first to obtain the necessary data for calculating the time-dependent fracture mechanics parameters. It is desirable that these data can be used to model the creep crack propagation process. Such an attempt has been made in this study.

Table 4.4-1 Fatigue Effect on the Average Creep Crack Propagation Time of Unit Crack Length

t_h sec	t_{test} hr	N_{cycle} 1/hr	Δa mm	Δa in	$(dt/da)_{avg}$ hr/mm	$(dt/da)_{avg}$ hr/in
∞	823	0	4.8946	0.1927	168	4271
3600	820	1	7.1489	0.2815	115	2914
100	295	35	6.4209	0.2528	46	1167
10	71	300	5.0106	0.1973	14	360
0	64	1800	6.4237	0.2529	10	253

Previous discussion [110] has shown that the macro-process of a stabilized creep crack propagation can be described as follows: (1) Creep deformation occurs at the crack tip and the local material near the crack tip elongates in the loading direction; and (2) when the local deformation at the crack tip exceeds a certain strain value, the material ruptures locally and the crack propagates. This process repeats continuously as the creep deformation at the crack tip goes on.

To model this process, the material at the crack tip is imagined as a small creep deformation sample as shown in Figure 4.5-1 a). Since the creep deformation test results of this study have shown that HR160 spends most of its creep deformation in the secondary creep, it can be assumed that the imaginary sample creeps at the secondary creep rate ($\dot{e}$). When a unit length section in the imaginary sample reaches the rupture strain, rupture occurs and the crack propagates, as shown in Figure 4.5-1 b). The next imaginary sample repeats the same process, and thus, the crack keeps growing. Let the diameter of the imaginary sample approach zero, the whole process can be described by a continuous movement of the imaginary sample, creeping at the rate of $\dot{e}$, towards the right at the crack propagation rate (da/dt) as shown in Figure 4.5-1 c).

The model proposed in this study is presented in Figure 4.5-2. Figure 4.5-2 a) shows a cracked plate and its imaginary creep deformation sample. Two points, b and c, very close to each other on a horizontal line unit distance (h) away from the central line, are selected for observation. Figure 4.5-2b) shows the definition of the parameters used in this model. The e_c is the critical strain at which the imaginary creep deformation sample starts to move towards the right. The actual value of e_c can be the strain at which the current imaginary sample no longer continues to bear the load, such as the rupture strain or the tertiary creep strain. The crack propagation process is described in Figure 4.5-3. Figure 4.5-3 a) shows that at time $t = 0$, point b reaches the critical strain, and the crack length is a. Figure 4.5-3 b) shows that after a time elapse of Δt, point c reaches the

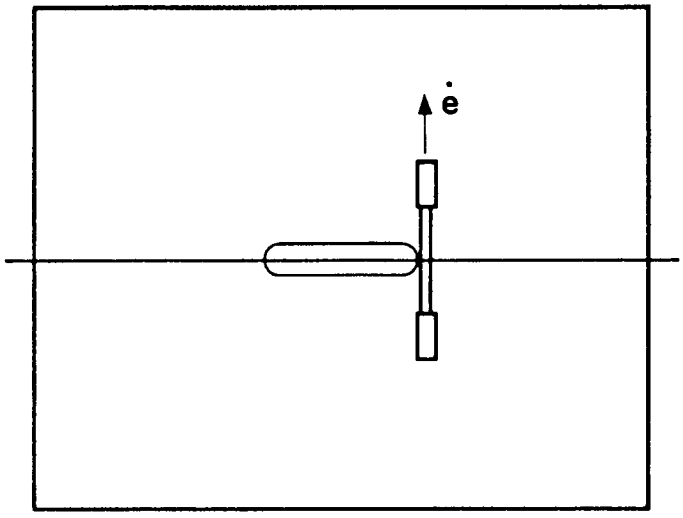

a) The Imaginary Sample Creeping at the
Minimum Creep Rate at the Crack Tip

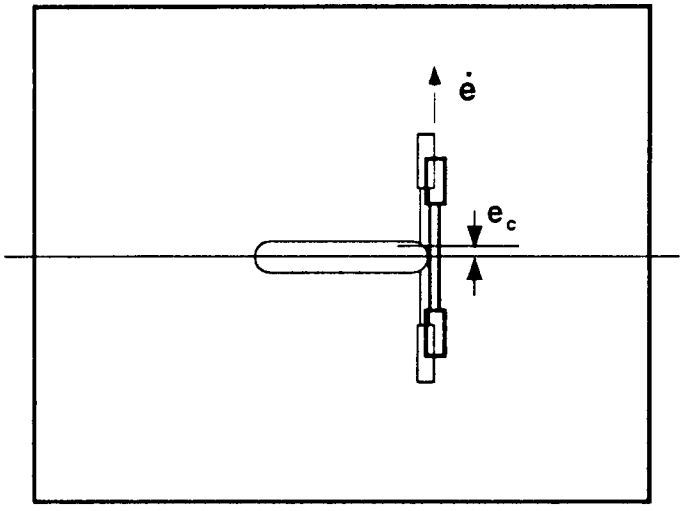

b) The Imaginary Sample Rupturing at the Critical Strain

Figure 4.5-1 Schematics Showing the Movement of the Imaginary Creep Deformation Sample at a Crack Tip as the Creep Crack Propagates

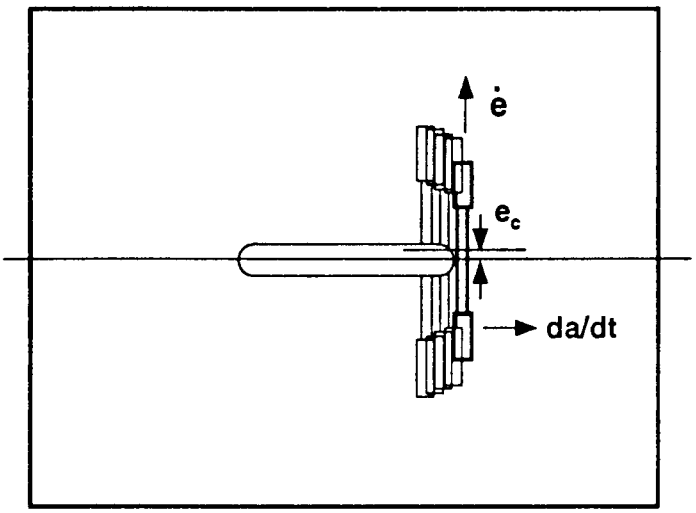

c) The Imaginary Sample Moving at the Creep Crack Propagation Rate

Figure 4.5-1 (Continued)

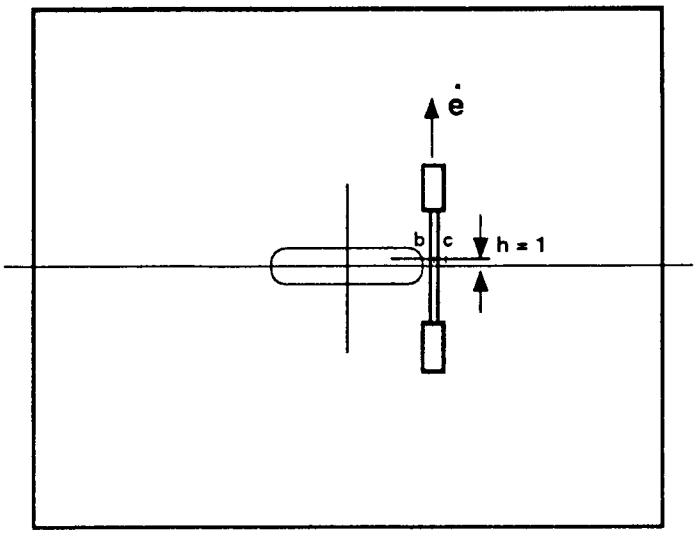

a) A Cracked Plate and Its Imaginary Creep Deformation Sample

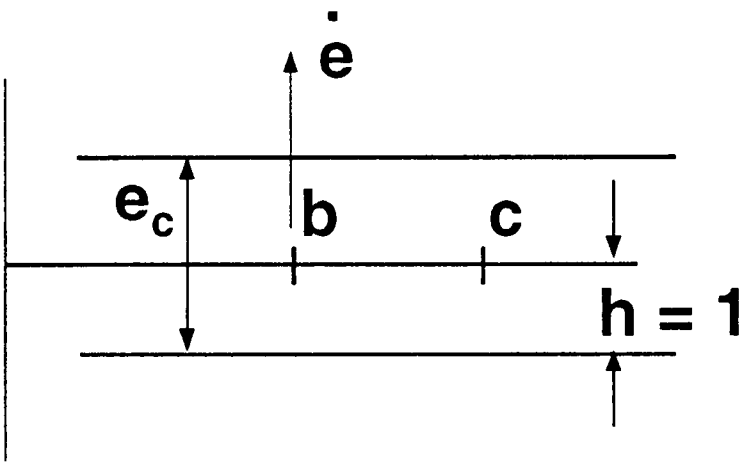

b) Definitions of the Model Parameters Before Creep Occurs

Figure 4.5-2 Parameter Definitions of the Model for Creep Crack Propagation

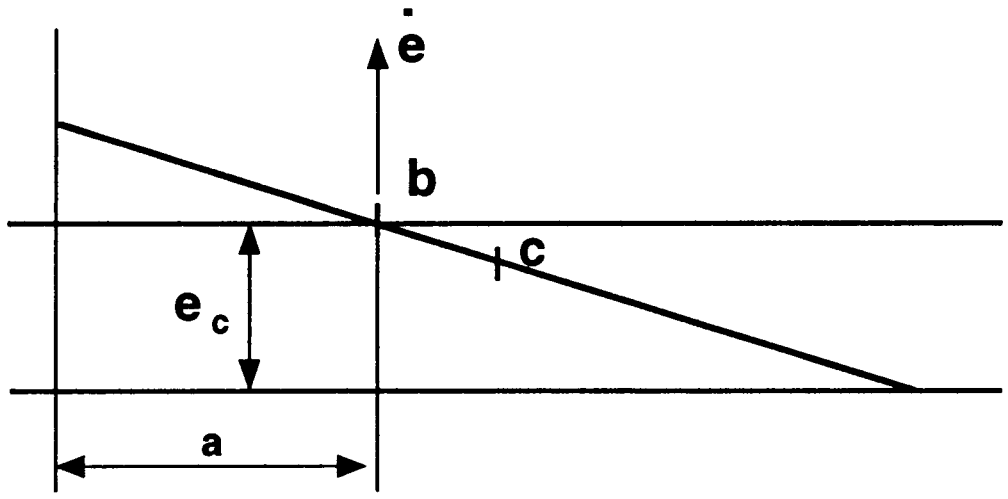

a) Creep Crack Propagation at time t = 0

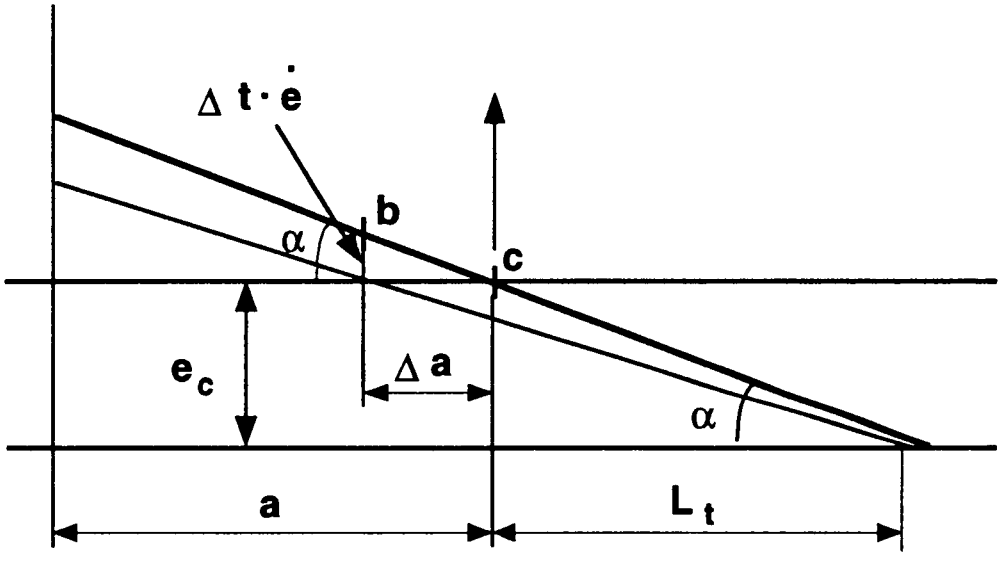

b) Creep Crack Propagation at Time t = Δt

Figure 4.5-3 Modeling of the Creep Crack Propagation Process

critical strain and the crack has propagated for a length of Δa. L_t is the distance from the crack tip to the neutral axis, i. e., the axis at which the stress changes from tension to compression. L_t is a function of time. From Figure 4.5-3 b), the following relationship can be obtained:

$$\tan\alpha = \frac{\Delta t \cdot \dot{e}}{\Delta a} = \frac{e_c + \Delta t \cdot \dot{e}}{\Delta a + L_t} \tag{4.5-1}$$

After some simple derivation of Equation (4.5-1), we have:

$$\lim_{\Delta t \to 0} \frac{\Delta a}{\Delta t} = \frac{da}{dt} = \frac{\dot{e} L_t}{e_c} \tag{4.5-2}$$

Note that e_c and $\dot{e}$ are not constants at the crack tip. They are functions of load and temperature. In order to simplify the calculation of Equation (4.5-2), a relationship between e_c and $\dot{e}$ has been found from the creep deformation test results at temperatures ranging from 850 to 950°C (1562 to 1742°F). In this study, the rupture strain, e_r, is chosen as the critical strain (e_c). The relationship found between e_r and $\dot{e}$ can be expressed as:

$$e_r = B(\dot{e})^p \tag{4.5-3}$$

where, $B = 1.4759$

$p = 0.15039$

Equation (4.5-3) is plotted in Figure 4.5-4. Inserting Equation (4.5-3) into Equation (4.5-2), we obtain:

$$\frac{da}{dt} = \frac{L_t}{B}(\dot{e})^{(1-p)} \qquad (4.5\text{-}4)$$

Equation (4.5-4) indicates that creep crack propagation rate depends on the creep rate of the material at the crack tip, the geometry of the creep zone and the rupture strain implied in B and p.

4.5.2 Rate Estimation Number R_{en}

Although Equation (4.5-4) shows that creep crack propagation rate depends on the creep rate of the local material at the crack tip, the geometry of the creep zone and the rupture strain implied in B and p, a question still remains. Because the creep rate of the local material at the crack tip is not a constant, then, what is the most essential controlling factor for the creep rate ($\dot{e}$), and thus, the creep crack propagation rate (da/dt)? As materials deform because of creep, energy has to be consumed. It is possible that how fast energy can be input in the creeping body determines the creep deformation rate ($\dot{e}$), and thus, the creep crack propagation rate (da/dt). If this is true, a relationship should exist between the power input in a creeping body and its creep deformation rate. In the case of HR160, a large portion of the total creep strain is spent at the minimum creep rate. Therefore, it is a reasonable assumption that the minimum creep rate is a function of the power input, and for a creep deformation sample of unit length, the following relationship exists:

$$\dot{e} = f(\sigma \dot{e}) \qquad (4.5\text{-}5)$$

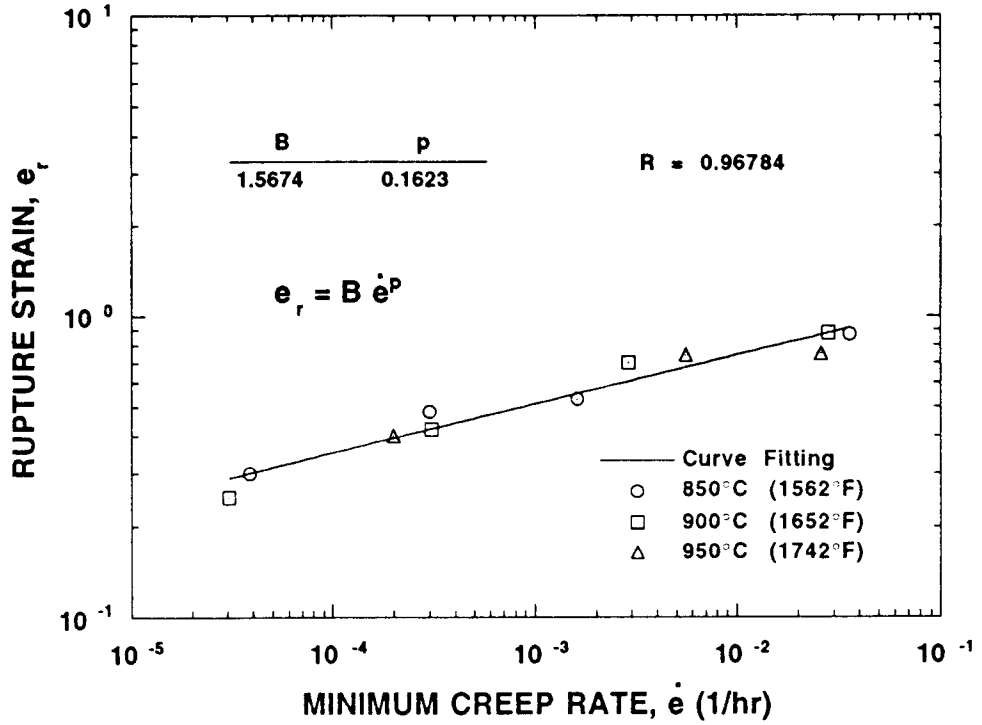

Figure 4.5-4 The Minimum Creep Rate Versus the Rupture Strain of HR160 at Temperatures of 850, 900 and 950°C (1562, 1652 and 1742°F)

Since the true stress (σ) is difficult to measure, a new parameter, the Rate Estimation Number (R_{en}), is introduced as an approximation:

$$(R_{en}) = (1 + e_r) \cdot s \cdot \dot{e} \qquad (4.5\text{-}6)$$

where, s = initial engineering stress

When necking is not greatly localized during the creep deformation process, the term $(1+e_r)\cdot s$ can be a good approximation of the true stress near rupture strain. The physical significance of R_{en} is an approximation of the power input near the rupture strain in a creeping body. The relationship between the secondary creep rate and the rate estimation number of HR160 has been found by Ren [110] to be of the form:

$$\dot{e} = M(R_{en})^{q'} \qquad (4.5\text{-}7)$$

A schematic of Equation (4.5-7) and the creep deformation test results obtained in this study is presented in Figure 4.5-5. It shows that $M = 7.9524 \times 10^{-5}$ (1/hr)$(m^3/watt)^{q'}$ [1.6193×10^{-1} (1/hr)$(s\cdot in^3/in.lb)^{q'}$] and $q' = 0.86207$ in Equation (4.5-7). Recall the value of A and q in Equation (4.2-1) obtained from the as-received HR160 in this study, it is obvious that the value of q', 0.86207, is very close to the value of q, 0.86734. This similarity is no accident. Scrutiny of Equation (3.3-3) reveals that C*(t), which has been used to correlate to the creep crack propagation rate in Equation (4.2-1), is actually an estimation of the power input in the creep zone resulting from creep deformation at the crack tip. It is obvious that the similarity between the values of q and q' originates from the essential relationship of the power input with both the creep deformation rate and the creep crack propagation rate. Further investigations are needed to confirm this similarity

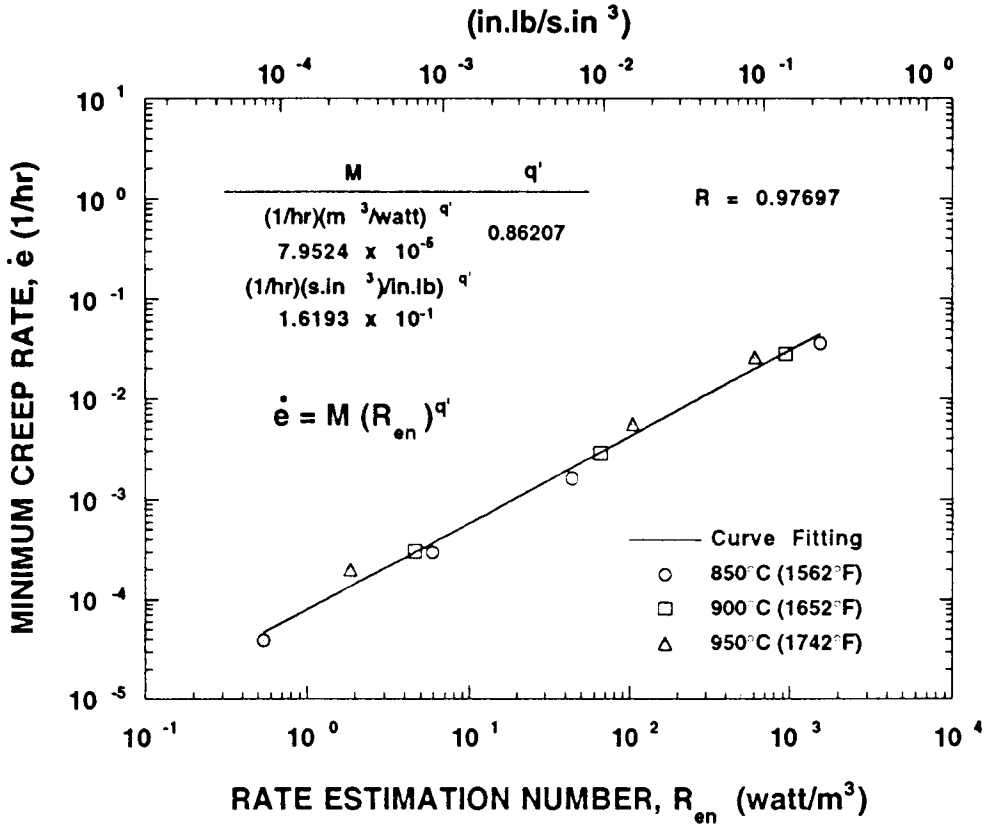

Figure 4.5-5 The Minimum Creep Rate Versus the Rate Estimation Number (R_{en}) of HR160

in more materials. If this similarity is generally true, q' obtained from creep deformation tests can be used as a good approximation for q. Because creep deformation tests have to be conducted before crack propagation tests, and usually cover a wide range of power input in terms of R_{en}, this may help overcome the scattering problem of q values obtained from individual creep crack propagation tests discussed in Section 4.2.3. Such practice can obviously save experimental materials and time.

It should be pointed out that the above modeling and the proposed life prediction methodology presented in Figure 2.3-1 are based on the secondary creep. Many materials and their weldment have very little primary creep, especially at very high temperatures. When materials are subject to conditions that they have significant amount of primary creep, a large amount of the useful lives may be spent in primary creep. The prediction based on only secondary creep may become conservative under such conditions.

CHAPTER V

SUMMARY AND CONCLUSIONS

In this investigation, a candidate material for the next generation of fossil energy systems, Haynes HR160, has been characterized with time-dependent fracture mechanics parameters. Tensile, creep deformation, creep crack propagation and creep-fatigue crack propagation tests were conducted on this material at elevated temperatures up to 950°C (1742°F). The tests were performed under different testing and material conditions. The testing conditions included different load levels, temperatures, sample sizes and fatigue hold times, while the material conditions included different heats and the as-received, aged, coarse grain size and welded conditions. A sound database has been developed through these tests for the material selection of the next generation of fossil energy systems. Some interested issues of the time-dependent fracture mechanics have been studied. Theoretical modeling has also been conducted on the dynamic process of creep crack propagation. Several new parameters have been introduced to help the characterization and the understanding of the dynamics of creep crack propagation.

After mechanical characterization, the tested specimens were examined through microstructural analyses. The scenario of the creep crack growth behavior of HR160 can be summarized as the following: At elevated temperatures, creep takes place at the precrack tip where the stress is high due to the stress concentration. The combination of diffusion and stress starts to form micro-cavities on the grain boundaries and twin boundaries. Precipitation also starts to occur on the grain boundaries, twin boundaries and some precipitation habit planes. As the creep zone expands in size, the precrack tip becomes blunted and the crack opening becomes larger. Creep mechanisms occur to accommodate the overall creep strain. Some micro creep cavities coalesce during this

process to form microcracks. When the creep enters the secondary creep stage, observable grain deformation occurs and the micro creep cracks become larger. Some of these cracks are deflected from the grain boundaries into the grain matrix by large boundary precipitates during this growing process. As the crack tip approaches a group of microcracks or cavities, the stress around these microcracks or cavities becomes even greater. Some microcracks further coalesce. Air gets in through these cracks and oxidizes the exposed grain boundaries. As the micro-cracks become larger and larger by coalescence, the remaining grain boundaries and twin boundaries can not hold the load any more and rupture occurs, and the creep crack propagates. The newly exposed grain boundaries quickly become oxidized. In cases in which the stress fluctuates periodically during the process of nucleation, growth and coalescence of creep cavities, transgranular damage can be made in addition to the intergranular creep damage because of the fatigue effect. This greatly increases the crack propagation rate and decreases the life of the cracked body.

The present work has reached the six goals proposed for this investigation. Conclusions can be drawn as follows:

I This investigation has provided a sound database for the candidate material, Haynes HR160, for the next generation of fossil energy systems.

- The creep crack propagation rate of HR160 can be uniquely correlated to the time-dependent fracture mechanics parameter, C*(t), by using an expression of the form: $da/dt = A[C^*(t)]^q$.
- For the as-received HR160, A has a value of 1.7464×10^{-2} (mm/hr)(m^2·hr/kilo joule)^q [6.06996×10^{-2} (in/hr)(in^2·hr/kilo in·lb)^q] and q of 0.86734.
- Over the C*(t) range of 0.1 to 10 (kilo joule/m^{2}hr), the values of A and q for the weld of HR160 are approximately 1.5131×10^{-1} (mm/hr)(m^2·hr/kilo joule)^q [2.769 (in/hr)(in^2·hr/kilo in·lb)^q] and 1.1889, respectively .

- The A and q values for the aged and coarse grain material conditions studied in this investigation are essentially the same as those for the as-received HR160.
- Under fatigue condition at 850°C (1562°F), the crack propagation rate of HR160 follows the Paris Law, $da/dN = C(\Delta K)^{n_f}$. At a frequency of 0.5 Hz and a minimum to maximum load ratio of 0.1, C has a value of 4.1309×10^{-12} $(mm/cycle)(MPa \cdot m^{1/2})^{n_f}$ [3.11686×10^{-13} $(in/cycle)(ksi.in^{1/2})^{n_f}$], and n_f has a value of 6.8908.
- Under creep-fatigue conditions, the average crack propagation rate of HR160 during the hold time can be uniquely correlated to the average of the time-dependent fracture mechanics parameter C*(t) by using an expression of the form: $(da/dt)_{avg} = A\{[C^*(t)]_{avg}\}^q$. The values of A and q are the same as those of the as-received HR160.
- Tensile and creep deformation data from different heats and the as-received, aged, coarse grain size and welded material conditions have been generated and given in tables.

II The time-dependent fracture mechanics parameter C*(t) has been studied under various testing conditions.

- It is confirmed that the correlation between da/dt and C*(t) in this high alloy HR160 at a high temperature, such as 850°C (1562°F), is independent of applied load. Changing the load level only shifts the data points up or down along the straight fit line of da/dt versus C*(t) in a logarithmic coordinate system.
- Different from an early report by other researchers on type 316 stainless steel, the testing temperature has been found to have no effect on the correlation between da/dt and C*(t) in HR160.

- Reducing the standard sample size to half does not affect the correlation between da/dt and C*(t) in HR160.
- This investigation shows that the unique correlation between da/dt and C*(t) can be obtained by manipulating the temperature, load level and sample size, and thus, save experimental time and materials. Based on the results from high load, low temperature and small size specimens, this correlation can be used to obtain crack growth rates of lower load, higher temperature and larger size specimens.
- When short-term test results are used to predict long-term test results, the accuracy of such a prediction increases with the spans between C*(t) ranges of individual tests.

III The creep-fatigue crack propagation behavior of HR160 has been studied and correlated to the creep crack propagation.

- The creep zone at the crack tip accumulatively expands during the hold time periods. Therefore, $[C^*(t)]_{avg}$ is a more appropriate parameter than $(C_t)_{avg}$ for characterizing the creep-fatigue crack propagation rate after the test time exceeds a certain transition time. The usage of $(C_t)_{avg}$ without considering the accumulative transition time in many literature papers is incorrect.
- When the transition period is relatively short compared to the hold time, $(C_t)_{avg}$ and $[C^*(t)]_{avg}$ can be approximated by $(C_t)_{0.5th}$ and $[C^*(t)]_{0.5th}$ respectively in characterizing the average creep-fatigue crack propagation rate $(da/dt)_{avg}$. The results of such characterization follow the same trend of the creep crack propagation rate da/dt versus C*(t).
- Decreasing hold time during creep-fatigue tests increases $(da/dt)_{avg}$. Therefore, increasing shut-downs or stress fluctuations in components operating at elevated temperatures decreases their lives.

- The hook in a plot of creep-fatigue crack propagation rate versus the stress intensity factor range is caused mainly by the transition from small-scale to extensive, plus primary to secondary creep conditions in HR160 investigated.

IV The effects of material treatments and chemical composition on the time-dependent fracture mechanics behavior and the related mechanical properties of HR160 have been studied through testing under different material conditions.

- No heat effect has been observed on the tensile, creep deformation and creep crack propagation properties of HR160.
- The strength of HR160 at the elevated temperature of 850°C (1562°F) is slightly decreased by grain coarsening, aging and welding treatments
- Tensile and creep ductility of HR160 are greatly decreased by welding, but not affected by the grain coarsening and aging in this study.
- The minimum creep rate of HR160 is not obviously affected by aging, grain coarsening and welding conducted in this investigation. However, the primary creep does not occur in the welded HR160. This may be the reason for the decrease in the creep ductility and creep crack resistance of the HR160 weldment.
- The creep crack propagation rate of HR160 is increased to approximately 12 to 15 times in the weld, but not obviously changed in the aged and coarse grain conditions.
- The increase in creep crack propagation rate in the weld is caused by the lack of creep ductility in the casting structure of the weld.
- Because the grain coarsening and aging in this study have shown little effect on the creep crack propagation rate, this feature of HR160 provides the possibility to change the casting structure in HR160 weldment by localized post heating, and thus, improve its creep crack propagation resistance.

V Creep crack and creep-fatigue crack propagation mechanisms of HR160 have been investigated through microstructural characterization.

- Under static loading, cavitation occurs in the creep zone mainly along grain boundaries and twin boundaries. Creep cracks propagate mainly in an intergranular mode by the coalescence of creep cavities.
- Cavities have been observed grown into grains from grain boundaries. This mixed growth process may increase the creep crack resistance of HR160.
- Load cycling causes a transgranular crack propagation mode within the creep zone of a cracked component at elevated temperatures. This induces a mixed intergranular and transgranular crack propagation. It increases the total crack propagation rate and decreases the component's life.
- Increasing hold time increases the extent of intergranular crack propagation under cyclic loading conditions.
- A creep contribution to the crack propagation has been observed under the condition of cyclic loading without hold time. The fracture surface of the uncracked ligament fatigue-ruptured at room temperature after the testing shows a mainly intergranular surface with some transgranular area. This observation supports statement that $[C^*(t)]_{avg}$ is a more appropriate parameter than $(C_t)_{avg}$ after the test time exceeds the accumulative transition time.

VI Theoretical modeling has been conducted and insights of the dynamic process of creep crack propagation has been studied

- A model has been established showing that the creep crack propagation rate depends on the creep deformation rate at the crack tip, the creep zone geometry and the rupture strain of the material.
- The rate estimation number, R_{en}, has been introduced to approximate the power input in the crack tip. R_{en} can be uniquely correlated to the minimum

creep rate. The q' in this relationship is numerically close to the q in the da/dt versus C*(t) relationship for superalloy HR160. Therefore, the value of q' can be used as a reference when long-term test results are predicted from short-term tests without covering wide spans between C*(t) ranges.

REFERENCES

REFERENCES

[1] P. K. Liaw, A. Saxena, and J. Schaefer, Engineering Fracture Mechanics, Vol. 32, p. 675, 1989.

[2] P. K. Liaw, A. Saxena, and J. Schaefer, Engineering Fracture Mechanics, Vol. 32, p. 709, 1989.

[3] P. K. Liaw and A. Saxena, "Remaining-Life Estimation of Boiler Pressure Parts-Crack Growth Studies", EPRI (Electric Power Research Institute) CS-4688, Project 2253-7, Final Report, July 1986.

[4] P. K. Liaw, M. G. Burke, A. Saxena and J. D. Landes, Metallurgical Transactions A, 22A, p. 455, 1991.

[5] P. K. Liaw, G. V. Rao and M. G. Burke, Materials Science and Engineering, A131, p. 187, 1991.

[6] P. K. Liaw, M. G. Burke, A. Saxena, and J. D. Landes, ASTM STP 1131, p. 756, 1992.

[7] P. K. Liaw and A. Saxena, International Journal of Fracture, Vol. 54, p. 329, 1992.

[8] R. Viswanathan, "Damage Mechanisms and Life Assessment of High-Temperature Components", ASM International Publication, Metals Park, OH, 1989.

[9] P. K. Liaw, A. Saxena, and J. Schaefer, J. of Metals, February Issue, p. 43, 1992.

[10] P. K. Liaw, J. of Metals, February Issue, p. 32, 1992.

[11] E. A. Logsdon, P. K. Liaw, A. Saxena, and V. E. Hulina, Engineering Fracture Mechanics, Vol. 25, p. 259, 1986.

[12] A. Saxena, P. K. Liaw, W. A. Logsdon, and V. E. Hulina, Engineering Fracture Mechanics, Vol. 25, p. 289, 1986.

[13] V. P. Swaminathan, N. S. Cheruvu, A. Saxena, and P. K. Liaw, "An Initiation and Propagation Approach for the Life Assessment of an HP-IP Rotor", Proceedings of Electric Power Research Institute [EPRI] Conference on Life Extension and Assessment of Fossil Plants, Session 4: Turbine Components, Sponsored by EPRI, EEI [Edison Electric Institute], ASME and ASM, Washington, DC, June 2-4, 1986.

[14] N. S. Cheruvu, Metallurgical Transactions A, 20A, p. 87, 1989.

[15] C. E. Jaske, Chemical Engineering Progress, p. 37, April 1987.

[16] P. K. Liaw, R. E. Shannon, and A. Saxena, "Life Extension Technology for Steam Pipe Systems", Final Report Contract No. P1-093-047, Westinghouse Science & Technology Center, Pittsburgh, PA, 1989.

[17] P. K. Liaw, B. K. Park, M. G. Burke, R. E. Shannon, and A. Saxena, "Life Extension Technology for Steam Pipe Systems - Part I. Materials Properties", Final Report, Contract No. P1-355488, Westinghouse Science & Technology Center, Pittsburgh, PA, 1991.

[18] A. Saxena and P. K. Liaw, "Life Extension Technology for Steam Pipe Systems - Part II. Fatigue Life Analysis and Computer Program", Final Report, Contract No. P1-355488, Westinghouse Science & Technology Center, Pittsburgh, PA, 1991.

[19] P. K. Liaw, R. E. Shannon, A. Saxena, and J. Perrin, "Life Extension Technology for Steam Pipe Systems - Part I. Nondestructive Evaluation of Steam Pipe Wall Thickness", Westinghouse Science & Technology Center, 1991.

[20] P. K. Liaw, B. K. Park, M. G. Burke, R. E. Shannon, A. Saxena, and J. Perrin, "Life Extension Technology for Steam Pipe Systems - Part II. Development of Materials Properties", Westinghouse Science & Technology Center, 1991.

[21] P. K. Liaw, A. Saxena, and J. Perrin, "Life Extension Technology for Steam Pipe Systems - Part III. Development of Life Prediction Methodology", Westinghouse Science & Technology Center, 1991.

[22] P. K. Liaw, R. Viswanathan, K. L. Murty, D. Frear and E. P. Simonen, "Microstructures and Mechanical Properties of Aging Materials", First International Conference Proceedings, TMS-AIME, Warrendale, PA, 1993.

[23] P. K. Liaw, A. Saxena, and J. S. Perrin, Engineering Fracture Mechanics, Vol. 45, p. 759, 1993.

[24] P. K. Liaw, A. Saxena, and J. S. Perrin, Engineering Fracture Mechanics, Vol. 45, p. 787, 1993.

[25] P. K. Liaw, A. Saxena and J. Schaefer, "Creep Crack Growth Behavior of Steam Pipe Steels: Effects of Inclusion Content and Primary Creep", submitted to International J. of Fracture.

[26] K. B. Yoon, A. Saxena and P. K. Liaw, International J. of Fracture, Vol. 59, p. 95, 1993.

[27] S. C. Jani and A. Saxena, "Influence of Thermal Aging on the Creep Crack Growth Behavior of Cr-Mo Steel", Proceedings of the TMS-AIME Symposium, TMS-AIME, October 1987.

[28] P. K. Liaw, A. Saxena and J. Schaefer, "Estimating Remaining Life of Elevated-Temperature Steam Pipes, Part I: Materials Properties", Engineering Fracture Mechanics, Vol. 32, p. 675-708, 1989.

[29] P. K. Liaw, A. Saxena and J. Schaefer, "Estimating Remaining Life of Elevated-Temperature Steam Pipes, Part II: Fracture Mechanics Analyses", Engineering Fracture Mechanics, Vol. 32, p. 709-722, 1989.

[30] H. Riedel and J. R. Rice. "Tensile Cracks in Creep Solids", Fracture Mechanics: Twelfth Conference, American Society for Testing and Materials, ASTM STP 700, p. 112-130, 1980.

[31] M. Okazaki, I. Hattori, F. Shiraiwa, and T. Koizumi. "Effect of Strain Wave Shape on Low-cycle Fatigue Crack Propagation of SUS 304 Stainless Steel at Elevated Temperatures", Met. Trans., 14A, p. 1649-1659, 1983.

[32] C. M. Antony, G. Y. Lai, J. W. Tackett and E. J. Bickel, A New "Structural Metallic Material for High Temperature Corrosive Environments", 1993 ASME Pressure Vessel and Piping Conference Proceedings, PVP Vol. 262, July 1993 in Denver.

[33] G. E. Dieter, "Mechanical Metallurgy", McGraw-Hill Book Company, p.352, 1986.

[34] R. O. Ritchie, Trans. ASME, J. Eng. Mater. Tech., Vol. 105, p. 1-7, 1983.

[35] J. R. Rice, Trans. ASME, Ser. E, J. Appl. Mech., Vol. 90, p. 379-386, 1968.

[36] A. Saxena, "Fracture Mechanics Approaches for Characterizing Creep-fatigue Crack Growth", JSME International Journal, Series A, Vol. 36, No. 1, p. 15-16, 1993.

[37] A. Saxena. "Creep Crack Growth Under Non Steady-State Conditions", Fracture Mechanics: Seventeenth Volume, ASTM STP 905, American Society for Testing and Materials, p. 185-201, 1986.

[38] "Standard Test Method for Measurement of Creep Crack Growth Rates in Metals", E 1457-92, Annual book of ASTM Standards, Vol. 03.01, 1993.

[39] J. D. Landes and J. A. Begley. "A Fracture Mechanics Approach to Creep Crack Growth", Mechanics of Crack Growth, American Society for Testing an Materials, ASTM STP 590, p. 128-148, 1976.

[40] K. M. Nikbin, G. A. Webster, and C. E. Turner, "Relevance of Nonlinear Fracture Mechanics to Creep Cracking", Cracks and Fracture, American Society for Testing and Materials, ASTM STP 601, p. 47-62, 1976.

[41] S. Taira, R. Ohtani and T. Kitamura, "Application of J-integral to High-Temperature Crack Propagation", Transactions of ASME Journal of Engineering Materials and Technology, Vol. 101, p. 154, 1979.

[42] V. Kumar, M. D. German, and C. F. Shih. "An Engineering Approach to Elastic-Plastic Analysis", technical Report EPRI NP-1931, Electric Power Research Institute, 1981.

[43] J. Hutchinson. "Singular Behavior at the End of a Tensile Crack in a Hardening Material", J. of Mech. and Phys. of Solids, Vol. 16, p. 13, 1968.

[44] J. Rice and G. F. Rosengren. "Plane Strain Deformation near a Crack Tip in a Power-law Hardening Material", J. of Mech and Phys. of Solids, Vol. 16, p. 1-12, 1968.

[45] N. L. Goldman and J. W. Hutchinson. "Fully Plastic Crack Problems: The Center-cracked Strip Under Plane Strain", International Journal of Solids and Structure, Vol. 11, p. 575-591, 1975.

[46] C. P. Leung, D. L. McDowell and A. Saxena, "Consideration of Primary Creep at Stationary Crack Tips: Implications for the C_t Parameter", International Journal of Fracture. Vol. 36, 1988.

[47] A. Saxena, "Creep Crack Growth in Creep-Ductile Materials", Engineering Fracture Mechanics, Vol. 40, No. 4/5, p. 721, 1991.

[48] P. K. Liaw, A. Saxena and J. Schaefer, "Estimating Remaining Life of Elevated Temperature Steam Pipes-Part I-Material Properties", Engineering Fracture Mechanics, Vol. 32, p. 675, 1989.

[49] H. Riedel, "Creep Deformation at Crack Tips in Elastic-Visoelastic Solids", Journal of Mechanics and Physics of Solids, Vol. 29, p. 35, 1981.

[50] K. Ohji, K. Ogura and S. Kubo, "Stress-Strain Field and Modified J-Integral in the Vicinity of a Crack Tip Under Transient Creep Conditions", Japan Society of Mechanical Engineers, 790-13, p. 18, 1979.

[51] J. D. Bassani and F. A. McClintock, "Creep Relaxation of Stress Around a Crack Tip", International Journal of Solids and Structures, Vol. 7, p. 479, 1981.

[52] R. Ehlers and H. Riedel, "A Finite Element Analysis of Creep Deformation in a Specimen Containing a Macroscopic Crack", Advances in Fracture Research, Proceedings of the fifth International Conference of Fracture, ICF-5, Pergamon Press, Vol. 2, p.691-698, 1981.

[53] H. Riedel and V. Hetampel, "Creep Crack Growth in Ductile, Creep Resistant Steels", International Journal of Fracture, Vol. 34, p. 179, 1987.

[54] D. L. McDowell and C. P. Leung, "Implication of Primary Creep and Damage for Creep Crack Extension Criteria", Structural Design for Elevated Temperature Environments-Creep, Ratchet, Fatigue and Fracture, Pressure Vessel and Piping Division PVP Vol. 163, American Society of Mechanical Engineers, Honolulu, HI, 23-27, July, 1989.

[55] J. L. Bassani, K. E. Hawk and A. Saxena, "Evaluation of the Ct Parameter for Characterizing Creep Crack Growth Rate in the Transient Regime", Nonlinear Fracture Mechanics, Vol. I Time-dependent fracture, American Society for Testing and Materials, ASTM STP 995, p. 7-26, 1986.

[56] C. E. Jaske and J. A. Begley, "An Approach to Assessing Creep/Fatigue Crack Growth", Ductileity and Toughness Considerations in Elevated Temperature Service, MPC-8, ASTM, p. 391, 1978.

[57] S. Taira, R. Ohtani and T. Komatsu, "Application of J-Integral to High Temperature Crack Propagation-Part II-Fatigue Crack Propagation", Tansactions of ASME, Journal of Engineering Materials Technology, Vol. 101, p. 162, 1979.

[58] R. Ohtani, T. Kitamura, A. Nitta and K. Kuwabara, "High-Temperature Low Cycle Fatigue Crack Propagation and Life Laws of Smooth Specimens Derived from the Crack Propagation Laws", ASTM STP 942, H. Solomon, G. Halford, L. Kaisand and B. Leis eds. American Society for Testing and Materials, p. 1163, 1988.

[59] K. Kuwabara, A. Nitta, T. Kitamura and T. Ogala, "Effect of Small-Scale Creep on Crack Initiation and Propagation Under Cyclic Loading", ASTM STP 924, edited by R. Wei, and R. Gangloff, American Society for Testing and Materials, p. 41, 1988.

[60] R. Ohtani, T. Kitamura and K. Yamada, "A Nonliear Fracture Mechanics Approach to Crack Propagation in the Creep-Fatigue Interaction Range" Fracture Mechanics of Tough and Ductile Materials and Its Application to Energy Related Structures, edited by H. Liu, I. Kunio and V. Weiss, Materials Nijhoff Publishers, p. 263, 1981.

[61] K. Ohji, "Fracture Mechanics Approach to Creep-Fatigue Crack Growth in Role of Fracture Mechanics in Modern Technology", Fukuoka, Japan, 1986.

[62] K. B. Yoon, A. Saxena and D. L. McDowell, "Influence of Crack-Tip Cyclic Plasticity on Creep-Fatigue Crack Growth", Fracture Mechanics: Twenty Second Symposium, ASTM STP 1131, American Society for Testing and Materials, p. 367, 1992.

[63] A. Saxena and B. Gieseke, "Transients in Elevated Temperature Crack Growth", International Seminar on High Temperature Fracture Mechanics and Mechanics, EGF-6 Elseveir Publications, p. III-19, 1990.

[64] N. Adefris, A. Saxena and D. L. McDowell, "Creep-Fatigue Crack Growth Behavior in 1Cr-1Mo-0.25V Steels I: Estimation of Crack Tip Parameters", Journal of Fatigue of Materials and Structures, 1993.

[65] A. Saxena and P. K. Liaw, "Remaining Life Estimation of Boiler Pressure Parts-Crack Growth Studies", Technical Report RP 2253-7, Electric Power Research Institute, Palo Alto, CA, January, 1986.

[66] R. L. Orr, O. D. Sherby and J. E. Dorn, Trans. ASM, Vol. 46, p. 113, 1954.

[67] O. D. Sherby, R. L. Orr and J. E. Dorn, Trans. AIME, Vol. 200, P. 71, 1954.

[68] F. R. N. Nabarro, "Deformation of Crystals by the Motion of Single Ions", Report of a Conference on Strength of Solids, Physical Society, London, p. 75, 1948.

[69] C. Herring, J. Appl. Phys., Vol. 21, p. 437, 1950.

[70] R. L. Coble, J. Appl. Phys., Vol. 34, p. 1679, 1963.

[71] J. Harper and J. E. Dorn, Acta Met., Vol. 5, p. 654, 1957.

[72] I. Le May, "Priniples of Mechanical Metallurgy", Elsevier, New York, p. 354, 1981.

[73] J. Weertman, J. Appl. Phys., Vol. 26, p. 1213, 1955.

[74] J. Weertman, J. Appl. Phys., Vol. 28, p. 362, 1957.

[75] R. Raj and M. F. Ashby, Met. Trans., 2A, p. 1113, 1971.

[76] R. Raj and M. F. Ashby, Acta Met., Vol. 23, p. 653, 1975.

[77] P. G. Shewmon, "Diffusion in Solids", McGraw-Hill Book Company, 1963.

[78] K. Sadananda and P. Shahinian, "Application of Fracture Mechanics Techniques to High Temperature Crack Growth", Fracture Mechanics, University Press of Virginia, p. 685-703, 1978.

[79] M. J. Siverns and A. T. Price, "Crack Propagation Under Creep Conditions in A Quenched 2 1/2 Chromium 1 Molybdenum Steel", Int. Journal of Fracture Mechanics, 9:199, 1973.

[80] T. Chuang and J. R. Rice, "The Shape of Intergranular Creep Cracks Growing by Surface Diffusion", Acta Met. Vol. 26, p. 1625, 1973.

[81] S. H. Goods and W. D. Nix. Acta Met. Vol. 21, p. 753, 1978.

[82] J. L. Bassani and F. A. McClintock, "Creep Relaxation of Stress Around a Crack Tip", International Journal of Solids and Structures. Vol. 17, p. 479-492, 1981.

[83] C. Y. Hui, and H. Riedel, "The Asymptotic Stress and Strain Field near the Tip of a Growing Crack Under Creep Conditions", International Journal of Fracture, Vol. 17, p. 409, 1981.

[84] J. L. Bassani and V. Vitek, "Propagation of Cracks Under Creep Conditions", Nonlinear Fracture Mechanics", Proceedings of the 9th National Conference of Applied Mechanics Symposium on Nonlinear Fracture Mechanics, Vol. III, p.19, October, 1981.

[85] R. Raj and S. Baik, "Creep Crack Propagation by Cavitation near Crack Tips", Metal Science, p. 385-393, August, 1980.

[86] J. R. Rice, "Constraints on the Diffusive Cavitation of Isolated Grain Boundary Facets in Creeping Polycrystals", Acta Met. Vol. 29, p. 675, 1981.

[87] Chun-Pok Leung, "Estimation of the Ct Parameter for Primary Creep", Ph.D. dissertation, Georgia Institute of Technology, Atlanta, July, 1988.

[88] D. M. R. Taplin, T. H. Topper and N. Y. Tang, Proceedings, ICG Special Symposium on Fracture, Beijing, China, p. 816-831, 1983.

[89] A. L. Wingrove and D. M. R. Taplin, Journal of Materials Science, Vol. 4, p. 789, 1969.

[90] J. O. Stiegler, K. Farrell, B. T. H. Loh, and H. E. McCoy, "Nature of Creep in Tungsten", Transactions of the ASM, Vol. 60, p. 494-503, 1967.

[91] K. Farrell, B. T. H. Loh, and J. O. Stiegler, "Morphologies of Bubbles and Voids in Tungsten", Transactions of the ASM, Vol. 60, p. 485-493, 1967.

[92] R. Lagneborg, "Creep and Fatigue in High Temperature Alloys", Applied Science Publishers, London, p. 41-72, 1981.

[93] R. J. Fields and M. F. Ashby, "Finger-like Crack Growth in Solids and Liquids", Philosophical Magazine, Vol. 33(1), p. 33-48, 1976.

[94] K. M. Nikbin and G. A. Webster, "Micro and Macro Mechanics of crack growth", Conference Proc. Metall. Soc., AIME, edited by K. Sadananda, B. B. Rath and D. J. Miehel, p. 137-147, 1982.

[95] K. M. Nikbin, D. J. Smith and G. A. Webster, "Advances in Life Prediction Methods at Elevated Temperatures", Conf. Proc. ASME, edited by D. A. Woodford and J. R., Whitehead, p. 249-258, 1983.

[96] A. C. F. Cocks and M. G. Ashby, Scr. Metall., Vol. 16, p. 109-114, 1982.

[97] R. K. Penny and D. L. Marriott, "Design for Creep", McGraw-Hill, London, 1971.

[98] Y. N. Rabotov, "Creep Problems in Structural Members", North-Holland, Amsterdam, 1969.

[99] K. M. Nikbin, D. J. Smith and G. A. Webster, "An Engineering Approach to the Prediction of Creep Crack Growth", Journal of Engineering Materials and Technology, Vol. 108, p. 186-191, 1986.

[100] K. M. Nikbin, D. J. Smith and G. A. Webster, "Prediction of Creep Crack Growth from Uniaxial Creep Data", Proc. R. Soc. Lond. A Vol. 396, p. 183-197, 1984.

[101] T. S. P. Austin and G. A. Webster, "Prediction of Creep Crack Growth Incubation Periods", Engineering Materials Structure", Vol. 15, No. 11, p. 1081-1090, 1992.

[102] G. A. Webster and R. A. Ainsworth, "High Temperature Component Life Assessment", Champman and Hall, 1994.

[103] "Standard Practice for Conducting Creep, Creep Rupture, and Stress-Rupture Tests of Metallic Materials", E139-83, Annual book of ASTM Standards, Vol. 03.01, 1993.

[104] H. H. Johnson, Calibrating the Electric Potential Method for Studying Slow Crack Growth. Materials Research Standards, 5(9): p. 442-445, 1956.

[105] C. E. Jaske, "Long-Term Creep Crack Growth Behavior of Type 316 Stainless Steel", Fracture Mechanics: Eighteenth Symposium, STP 945, ASTM, Philadephia, p. 867-877, 1988.

[106] K. Ohji and S. Kubo, "Crack Growth Behavior and Fractographs Under Creep-Fatigue Conditions Including the Near Threshold Regime", Fractography, Publication of the Society of Materials Science, Japan, Elsevier Applied Science, p. 105, 1990.

[107] P. K. Liaw and W. A. Logsdon, "Crack Closure: An Explanation for Small Fatigue Crack Growth Behavior", Engineering Fracture Mechanics, Vol. 22, p. 115-121, 1985.

[108] C. E. Jaske, "A Crack-Tip-Zone Interaction Model for Creep-Fatigue Crack Growth", Fatigue of Engineering Materials and Structures, Vol. 6, No. 2, p. 159-166, 1983.

[109] C. E. Jaske, "Creep-Fatigue -Crack Growth in Type 316 Stainless Steel", Advances in Life Prediction Methods, ASME, New York, p. 93-103, 1983.

[110] W. Ren, P. K. Liaw, R. W. Swindeman, B. G. Gieseke, and G. Y. Lai, "Creep Crack Behavior of Haynes HR160", Presentation at 1994's Materials Week, Rosemont, Illinois, October, 3-7 1994.

APPENDICES

Appendix A

Program for Creep Strain Rate Calculation

Instructions:

1. This program, named "2RATE.FOR", is written for calculating creep rate as a function of time and determining the minimum creep rate. This program should be used with a FORTRAN data file named "CREEP.DAT".
2. The results will be given on the screen and a file named "DSDT.DAT".
3. The algorithm of this program is the 7 point incremental polynomial method and differentiation of the polynomial with respect to time.

```
      DIMENSION DSDT(0:1000)
      COMMON TIME(0:1000), STN(0:1000)

C (1) READ IN THE TIME AND STRAIN STN
      OPEN(5,FILE='CREEP.DAT',STATUS='OLD')
      I=-1
20    I=I+1
      READ(5,*) TIME(I),STN(I)
      IF(TIME(I).GT.-1.0) GOTO 20
      N=I-1

C (2) INCREMENTAL POLYNOMIAL METHOD FOR CORRECTING STAIN C
      VALUES STN(I) AND CALCULATING STRAIN RATE DSDT(I)
      WRITE(*,*) 'TIME      STRAIN      DS/DT'
      DO I=3,N-3
      CALL PARABOLA(BAZ,BA1,BA2,I)
      STN(I)=BAZ+BA1*TIME(I)+BA2*TIME(I)*TIME(I)
      DSDT(I)=BA1+2*BA2*TIME(I)
      WRITE(*,*) TIME(I),' ',STN(I),' ',DSDT(I)
      END DO

C (3) CALCULATE THE MINIMUM STRAIN RATE
      BOX=DSDT(3)
      DO I=4,N-3
```

```
      IF(DSDT(I)-BOX) 30, 40, 40
30    BOX=DSDT(I)
40    END DO
      WRITE(*,*) 'MINIMUM STRAIN RATE =',BOX
      OPEN(10,FILE='DSDT.DAT',STATUS='NEW')
      DO I=0,N
      WRITE(10,60) TIME(I),STN(I),DSDT(I)
      END DO
      WRITE(10,*) 'MINIMUM STRAIN RATE =',BOX
      CLOSE(10)
60    FORMAT(1X,F7.2,4X,F8.6,4X,F8.5)
      PAUSE
      STOP
      END

C     SUBROUTINE FOR CALCULATION THE REGRESSION PARAMETERS C
      BY LEAST SQUARES METHOD
      SUBROUTINE PARABOLA(BAZ,BA1,BA2,I)
      COMMON TIME(0:1000), STN(0:1000), DSDT(0:1000)
      AL1=TIME(I-3)
      AASZ1=STN(I-3)
      DO J=I-3,I+2
      AL1=AL1+TIME(J+1)
      AASZ1=AASZ1+STN(J+1)
      END DO
      ALFA1=AL1/7.0
      AASZ=AASZ1/7.0
      ALU2=TIME(I-3)*(TIME(I-3)-ALFA1)**2
      ALD2=(TIME(I-3)-ALFA1)**2
      AAS1U=STN(I-3)*(TIME(I-3)-ALFA1)
      DO J=I-3, I+2
      ALU2=ALU2+TIME(J+1)*(TIME(J+1)-ALFA1)**2
      ALD2=ALD2+(TIME(J+1)-ALFA1)**2
      AAS1U=AAS1U+STN(J+1)*(TIME(J+1)-ALFA1)
      END DO
```

```
      ALFA2=ALU2/ALD2
      BETA1=ALD2/7.0
      AAST1=AAS1U/ALD2
      AAS2U=STN(I-3)*(TIME(I-3)**2-(ALFA1+ALFA2)
     1  *TIME(I-3)+ALFA1*ALFA2-BETA1)
      AS2D=(TIME(I-3)**2-(ALFA1+ALFA2)
     1  *TIME(I-3)+ALFA1*ALFA2-BETA1)**2
      DO J=I-3, I+2
      AAS2U=AAS2U+STN(J+1)*(TIME(J+1)**2
     1  -(ALFA1+ALFA2)*TIME(J+1)+ALFA1*ALFA2-BETA1)
      AS2D=AS2D+(TIME(J+1)**2
     1  -(ALFA1+ALFA2)*TIME(J+1)+ALFA1*ALFA2-BETA1)**2
      END DO
      AAST2=AAS2U/AS2D
      BAZ=AASZ-AAST1*ALFA1+AAST2*(ALFA1*ALFA2-BETA1)
      BA1=AAST1-AAST2*(ALFA1+ALFA2)
      BA2=AAST2
      RETURN
      END
```

Appendix B

Program for Creep Crack Propagation Rate Calculation

Instructions:

1. This program, named "CREEP CRACK", is written in accordance with the procedures in ASTM standard E-1457 (1993) [37] for convenient reviewing. Each step numbered in [ ] in this program corresponds to the procedure with the same number in ASTM E-1457. Modification can be made to increase the calculation speed. This program should be used with another 4 FORTRAN data files named: "AZERO.DAT", "AFINAL.DAT", "CCG.DAT" and "H1.DAT"

2 "AZERO.DAT" and "AFINAL.DAT" are data files containing the initial and final crack lengths respectively. The initial and final crack lengths are measured directly from the fracture after the testing.

3. "CCG.DAT" is the data file containing time, potential drop and deflection values. "CCG.DAT" is prepared from a customized EXCEL worksheet in which the original test data have been processed so that the time and potential values start from 0 and potential drop values do not include thermal effect.

4. The units in "CCG.DAT" file is hour for time, volt for potential drop and inch for deflection. The last row of the data in this file should be -1.0000 as a sign of ending the file.

5. "H1.DAT" is a data file for calculating h1 function [37].

6. Input the initial parameters with right units before each calculation. Their definitions can be found in Reference [37].

7. Three files named "RST1.DAT", RST2.DAT" and "ASTM.DAT" respectively will be generated as the results of running "CREEP CRACK". File "RST1.DAT" contains the calculated values of crack length and deflection from the equations recommended in ASTM standard [37]. File "RST2.DAT" contains the fitted values of crack length, loadline deflection, creep crack growth rate and loadline deflection rate. File "ASTM.DAT" contains the values of C*(t), C_t, J_p and K calculated with the equations recommended in ASTM standard E-1457 (93) [37].

C W the defined specimen width (inch)

C Yo the half distance between the voltage measuring points (inch)

C FROE the full range of the extensometer (inch)

C B the thickness of the C(T) specimens (inch)

```
C       BN      the grooved thickness of the C(T) specimens (inch)
C       P       the applied load (kips)
C       E       the elastic modulus (ksi)
C       XM,D    true strain = true stress/E + D x (true stress/yield
C               stress)^m. XM is m here.
C       YS      the yield strength (ksi)
C       XN      strain rate =A x stress^n, XN is n here
C       MU      Poisson's ratio

        DIMENSION V(0:1000), DADT(0:1000), DDLDT(0:1000)
        DIMENSION DVCDT(0:1000), CST(0:1000), YK(0:1000)
        DIMENSION CT(0:1000), FF(0:1000)
        COMMON TIME(0:1000), A(0:1000), DL(0:1000)
        REAL JP(0:1000)
        CHARACTER*4 TAB
        TAB=CHAR(9)
        PI=4.0*ATAN(1.0)
C       INITIAL PARAMETERS:
        W=?
        Y=?
        FROE=?
        BN=?
        B=?
        P=?
        E=?
        XM=?
        XN=?
        D=?
        YS=?
        MU=?

C [9.5.3] CALCULATING THE ORIGINAL CRACK LENGTH Ao AND THE C
        FINAL CRACK SIZE Af
C(1)    CALCULATE THE MEASURED INITIAL CRACK LENGTH Ao
        OPEN(5,FILE='AZERO.DAT',STATUS='OLD')
```

```
      CALL AIF(X,*1000)
      CLOSE (5)
      Ao=X
      WRITE(*,*) 'Ao = ', X
      PAUSE

C(2)  CALCULATE THE MEASURED FINAL CRACK LENGTH Af
10    OPEN(5,FILE='AFINAL.DAT',STATUS='OLD')
      CALL AIF(X,*1005)
      CLOSE (5)
      Af=X

C [10.1] DETERMINATION OF CRACK LENGTH
C(3)  READ IN THE TIME, DISPLACEMENT DL AND POTENTIAL DROP C
      V DATA
      OPEN(5,FILE='CCG.DAT',STATUS='OLD')
      I=-1
20    I=I+1
      READ(5,*) TIME(I),V(I),DL(I)
      IF(TIME(I).GT.-1.0) GOTO 20
      N=I-1

C(4)  CALCULATE THE CRACK LENGTH a(i) FROM Vo AND Vi
      Z1=(W+W)/PI
      Z2=(EXP(Y/Z1)+EXP(-Y/Z1))/2.0
      Z3=COS(Ao/Z1)
      Z4=Z2/Z3
      Z5=ALOG(Z4+SQRT(Z4**2-1))

      DO I=0,N
      Z6=V(I)*Z5/V(0)
      Z7=(EXP(Z6)+EXP(-Z6))/2.0
      A(I)=Z1*ACOS(Z2/Z7)
      END DO
      OPEN(10,FILE='RST1.DAT',STATUS='NEW')
```

```
      WRITE(10,*) '   time (hrs.)      a (in.)
     1     dL (in.)       V (volts)'
      WRITE(10,*) '-----------------------------------------------
     1-------------------------'
      WRITE(10,*) '  '

      DO I=0,N
      WRITE(10,30) TIME(I),A(I),DL(I),V(I)
      END DO
30    FORMAT(5X,F7.2,8X,F8.4,8X,E12.3,8X,F10.8)
      WRITE(10,*) '  '
      WRITE(10,*) '-----------------------------------------------
     1-------------------------'
      WRITE(10,*) '    Ao=',Ao
      WRITE(10,*) '    Af=',Af
      CLOSE(10)

C [10.2.1] CHECK THE VALIDITY OF a(i) DATA
      Z6=(A(N)-Ao)/(Af-Ao)
      IF(Z6.GT.1.15.AND.Z6.LT.0.85) GOTO 1008

C [10.2.2] &[10.2.3] ARE INCLUDED IN THE SUBROUTINE FOR (1) AND (2)

C [10.3] DETERMINATION OF CRACK GROWTH RATE AND LOADLINE
      DISPLACEMENT RATE
C [10.3.1] PICK OUT DA TOO CLOSED TO THE PREVIOUS ONES
      I=0
      J=0
      JM=0
      XW=0.02*W
      XFROE=0.001*FROE
40    I=I+1
      IF(I.GT.N) GOTO 50
42    DA=A(I)-A(J)
      IF(DA.LT.0.01) GOTO 40
```

```
      IF(DA.LE.XW) GOTO 45
      WRITE(*,*) 'WARNING: da > 0.02W OCCURED'
      PAUSE
45    DDL=DL(I)-DL(J)
      IF(DDL.LT.XFROE) GOTO 40
      JM=JM+1
      TIME(JM)=TIME(I)
      A(JM)=A(I)
      DL(JM)=DL(I)
      J=I
      GOTO 40
50    N=JM

C [10.3.2] CALCULATING da/dt AND dV/dt (DDL/DT HERE)

C (5) INCREMENTAL POLYNOMIAL METHOD FOR CORRECTING A(I)
C     AND DL(I) VALUES
C     AND CALCULATE da/dt and dL/dt
      DO I=3,N-3
      CALL PARABOLA(BAZ,BA1,BA2,BDLZ,BDL1,BDL2,I)
      A(I)=BAZ+BA1*TIME(I)+BA2*TIME(I)*TIME(I)
      DL(I)=BDLZ+BDL1*TIME(I)+BDL2*TIME(I)*TIME(I)
      DADT(I)=BA1+2*BA2*TIME(I)
      DDLDT(I)=BDL1+2*BDL2*TIME(I)
      END DO

      OPEN(10,FILE='RST2.DAT',STATUS='NEW')
      WRITE(10,*) '  time (hrs.)   a(fit) (in.)   da/dt (in/hr)
     1   dL (in.)      dL/dt (in/hr)'
      WRITE(10,*) '-----------------------------------------------
     1-------------------------------'
      WRITE(10,*) '  '

      DO I=3,N-3
      WRITE(10,60) TIME(I),A(I),DADT(I),DL(I),DDLDT(I)
```

```
      END DO
60    FORMAT(3X,F7.2,7X,F8.4,5X,E12.3,5X,E12.3,5X,E12.3)
      WRITE(10,*) '  '
      WRITE(10,*) '-----------------------------------------
     1-------------------------------'
      CLOSE(10)

C [10.4] CALCULATION OF CREEP DISPLACEMENT RATE dVc/dt
C     ([10.4.1] ~ [10.4.3])
C (6) CALCULATE K, h1, Jp, dVc/dt AND F'/F (YK,H1,JP,DVCDT AND FF
C     RESPECTFULLY HERE)
      XK=P/(SQRT(B*BN*W))
      DO I=3,N-3
      AW=A(I)/W
      YK(I)=XK*(2.0+AW)*F(AW)/(SQRT(1-AW))**3.0
      CALL H1(HH1, XM, AW)
      PHI=2.0*A(I)/(W-A(I))
      ALFA=SQRT(PHI*PHI+2.0*PHI+2.0)-(PHI+1.0)
      D1=D*(YS*1.002)**XM
      JP(I)=(D1*HH1/(((YS*1.002)*(W-
     1 A(I)))**XM))*((P/(1.455*BN*ALFA))**(XM+1))
      DVCDT(I)=DDLDT(I)-(DADT(I)*BN/P)
     1 *(2.0*YK(I)*YK(I)/E+(XM+1)*JP(I))
      FF(I)=(1.0/(2.0+AW)+3.0/(2.0*(1.0-AW)))+FP(AW)/F(AW)
      END DO

C [10.5] DETERMINATION OF C*(t)-INTEGRAL AND Ct (C*(t) = CST,
C     Ct=CT HERE)

      OPEN(10,FILE='ASTM.DAT',STATUS='NEW')
      WRITE(10,*) '  time     da/dt      C*(t)      Ct
     1       Jp         K'
      WRITE(10,*) '  ----------------------------------------
     1-------------------------------'
      WRITE(10,*) '  '
```

```
      TT=0.0
      DO I=3, N-3
      CS1=P*DVCDT(I)/(BN*(W-A(I)))
      CS2=XN/(XN+1.0)
      CS3=2.0+0.522*(W-A(I))/W
      CST(I)=CS1*CS2*CS3
      CT(I)=P*DVCDT(I)*FF(I)/((SQRT(B*BN))*W)

C [10.6] VALIDITY CRITERIA

C [10.6.2] CALCULATE TRANSITION TIME
      TPT=YK(I)*YK(I)*(1-MU*MU)/(E*(XN+1)*CST(I))
      IF(TPT-TT) 66, 66, 65
65    TT=TPT
66    WRITE(10,70) TIME(I),DADT(I),CST(I),CT(I),JP(I),YK(I)
      END DO
70    FORMAT(1X,F7.2,2X,E12.5,2X,E12.5,2X,E12.5,2X,
     1  E12.5,2X,E12.5)
      WRITE(10,*) '  '
      WRITE(10,*) '  ----------------------------------------
     1---------------------------------'
      WRITE(10,*) 'TRANSITION TIME tT = ', TT, 'hrs.'
      WRITE(10,*) 'ONLY C*(t) AT t > tT AND Ct AT t < tT ARE VALID'
      CLOSE(10)

C ANOTHER "IF" OUTLET OF (1) AND (2)
      GOTO 1010
1000WRITE(*,*) 'DATA OF Ao NOT VALID'
      CLOSE (5)
      GOTO 10
1005WRITE(*,*) 'DATA OF Af NOT VALID'
      CLOSE (5)
1008WRITE(*,*) 'DATA OF Ai NOT VALID'
1010PAUSE
      STOP
```

```
      END

C     SUBROUTINE OF (1) & (2)
      SUBROUTINE AIF(X,*)
C     CALCULATE THE MEASURED INITIAL OR FINAL CRACK LENGTH C
      Ao OR Af
      DIMENSION AM(0:10)
      DO I=1,9
      READ(5,10) AM(I)
      WRITE(*,*) AM(I), I
10    FORMAT(1X,F8.4)
      END DO
      X=(AM(1)+AM(9)+2*(AM(2)+AM(3)+AM(4)+AM(5)+AM(6)+AM(7
     1 )+AM(8)))/16
      WRITE(*,*) 'X=',X
      PAUSE
C     CHECK THE VALIDITY OF THE MEASURED INITAL OR FINAL
C     CARCK LENGTH
      DO I=1,9
      B=(ABS(X-AM(I)))/X
      IF(B.GT.0.05) RETURN 1
      END DO
      RETURN
      END

C     SUBROUTINE FOR CALCULATION THE REGRESSION PARAMETERS C
      BY LEAST SQUARES METHOD
      SUBROUTINE PARABOLA(BAZ,BA1,BA2,BDLZ,BDL1,BDL2,I)
      COMMON TIME(0:1000), A(0:1000), DL(0:1000)

      AL1=TIME(I-3)
      AASZ1=A(I-3)
      DLAZ1=DL(I-3)
      DO J=I-3,I+2
      AL1=AL1+TIME(J+1)
```

```
      AASZ1=AASZ1+A(J+1)
      DLAZ1=DLAZ1+DL(J+1)
      END DO
      ALFA1=AL1/7.0
      AASZ=AASZ1/7.0
      DLASZ=DLAZ1/7.0

      ALU2=TIME(I-3)*(TIME(I-3)-ALFA1)**2
      ALD2=(TIME(I-3)-ALFA1)**2
      AAS1U=A(I-3)*(TIME(I-3)-ALFA1)
      DLA1U=DL(I-3)*(TIME(I-3)-ALFA1)
      DO J=I-3, I+2
      ALU2=ALU2+TIME(J+1)*(TIME(J+1)-ALFA1)**2
      ALD2=ALD2+(TIME(J+1)-ALFA1)**2
      AAS1U=AAS1U+A(J+1)*(TIME(J+1)-ALFA1)
      DLA1U=DLA1U+DL(J+1)*(TIME(J+1)-ALFA1)
      END DO
      ALFA2=ALU2/ALD2
      BETA1=ALD2/7.0
      AAST1=AAS1U/ALD2
      DLAT1=DLA1U/ALD2

      AAS2U=A(I-3)*(TIME(I-3)**2-(ALFA1+ALFA2)
     1  *TIME(I-3)+ALFA1*ALFA2-BETA1)
      DLA2U=DL(I-3)*(TIME(I-3)**2-(ALFA1+ALFA2)
     1  *TIME(I-3)+ALFA1*ALFA2-BETA1)
      AS2D=(TIME(I-3)**2-(ALFA1+ALFA2)
     1  *TIME(I-3)+ALFA1*ALFA2-BETA1)**2
      DO J=I-3, I+2
      AAS2U=AAS2U+A(J+1)*(TIME(J+1)**2
     1  -(ALFA1+ALFA2)*TIME(J+1)+ALFA1*ALFA2-BETA1)
      DLA2U=DLA2U+DL(J+1)*(TIME(J+1)**2
     1  -(ALFA1+ALFA2)*TIME(J+1)+ALFA1*ALFA2-BETA1)
      AS2D=AS2D+(TIME(J+1)**2
     1  -(ALFA1+ALFA2)*TIME(J+1)+ALFA1*ALFA2-BETA1)**2
```

```
      END DO
      AAST2=AAS2U/AS2D
      DLAT2=DLA2U/AS2D

      BAZ=AASZ-AAST1*ALFA1+AAST2*(ALFA1*ALFA2-BETA1)
      BA1=AAST1-AAST2*(ALFA1+ALFA2)
      BA2=AAST2
      BDLZ=DLASZ-DLAT1*ALFA1+DLAT2*(ALFA1*ALFA2-BETA1)
      BDL1=DLAT1-DLAT2*(ALFA1+ALFA2)
      BDL2=DLAT2

      RETURN
      END

C     f(a/W) FUNCTION
      FUNCTION F(X)
      F=0.866+4.64*X-13.32*X*X+14.72*X*X*X-5.6*X*X*X*X
      RETURN
      END

C     f'(a/W) FUNTION
      FUNCTION FP(X)
      FP= 4.64-26.64*X+44.16*X*X-22.4*X*X*X
      RETURN
      END

C     SUBROUTINE FOR CALCULATING H1 VALUES
      SUBROUTINE H1(HH1,XX,AW)
      DIMENSION X(0:15), Y(0:15), YY(0:15)
      DIMENSION H(6,15), XM(0:15), YAW(0:15)

C     READ IN THE NODE VALUES Hij
      OPEN(5,FILE='H1.DAT',STATUS='OLD')

      DO J=0,9
```

```
      READ(5,10) XM(J)
      END DO

      DO I=0,5
      READ(5,10) YAW(I)
      END DO

      DO J=0, 9
      DO I=0, 5
      READ(5,10) H(I,J)
      END DO
      END DO
10    FORMAT(6F7.4)
C     FIND OUT THE INTERVAL [XMj, XMj+1] FOR THE INPUT m
C     AND INTERVAL [YAWi, YAWi+1] FOR THE INPUT A/W
      J=-1
30    J=J+1
      IF(XX.GE.XM(J)) GOTO 30
      JN=J-1
      I=-1
40    I=I+1
      IF(AW.GE.YAW(I)) GOTO 40
      IN=I-1

C     CALCULATE H1 = f(A/W, m)
      DO I=0,5
      DO J=0,9
      X(J)=XM(J)
      Y(J)=H(I,J)
      END DO
      NS=JN
      N=9
      CALL NCSPLINE(X,Y,BJN,CJN,DJN,NS,N)
      YY(I)=Y(JN)+BJN*(XX-X(JN))+CJN*(XX-X(JN))**2.0+DJN*(XX-
     1 X(JN))**3.0
```

```
      END DO

      DO I=0,5
      X(I)=YAW(I)
      Y(I)=YY(I)
      END DO
      NS=IN
      N=5
      CALL NCSPLINE(X,Y,BJN,CJN,DJN,NS,N)
      HH1=Y(IN)+BJN*(AW-X(IN))+CJN*(AW-X(IN))**2.0+DJN*(AW-
     1  X(IN))**3.0
      RETURN
      END

      SUBROUTINE NCSPLINE(X,Y,BJN,CJN,DJN,NS,N)
      REAL MU(0:10),L(0:10)
      DIMENSION X(0:10), Y(0:10)
      DIMENSION ALFA(0:10), H(0:10)
      DIMENSION Z(0:10), B(0:10), C(0:10)
      DIMENSION D(0:10)

      DO I=0, N-1
      H(I)=X(I+1)-X(I)
      END DO

      DO I=1, N-1
      ALFA(I)=3.0*(Y(I+1)*H(I-1)-Y(I)*(X(I+1)
     1  -X(I-1))+Y(I-1)*H(I))/(H(I-1)*H(I))
      END DO

      L(0)=1
      MU(0)=0
      Z(0)=0

      DO I=1, N-1
```

```
      L(I)=2.0*(X(I+1)-X(I-1))-H(I-1)*MU(I-1)
      MU(I)=H(I)/L(I)
      Z(I)=(ALFA(I)-H(I-1)*Z(I-1))/L(I)
      END DO

      L(N)=1
      Z(N)=0
      C(N)=0
      J=N
10    J=J-1
      C(J)=Z(J)-MU(J)*C(J+1)
      B(J)=(Y(J+1)-Y(J))/H(J)-H(J)*(C(J+1)+2.0*C(J))/3.0
      D(J)=(C(J+1)-C(J))/(3.0*H(J))
      IF(J.GT.NS) GOTO 10

      CJN=C(J)
      BJN=B(J)
      DJN=D(J)

      RETURN
      END
```

Appendix C

Program for Fatigue Crack Propagation Rate Calculation

Instructions:

1. Prepare data files "AZERO.DAT" and "AFINAL.DAT"
2. Prepare data file "FC.DAT" from the EXCEL file "FC/DAT". The units in this file are hour for time, volt for potential drop and inch for loadline deflection, respectively. The last row of the data in this file should be -1.0000 as a sign of ending the file. The time and loadline deflection dL must start from 0.
3. Input the following parameters with right units by hand. See ASTM E1457 for their definitions.
4. The file "RST1.DAT" contains the first calculation of crack length and deflection from the equations recommended in ASTM standard. File "RST2.DAT" contains the fitted values of crack length and dL, da/dN, dL/dt. File "ASTM.DAT" contains the values of N, C_t, a, da/dN, K and delta K.

```
C     W     the defined width (inch)
C     Yo    the half voltage measuring point distance (inch)
C     FROE  the full range of extensometer (inch)
C     B     the thickness of the C(T) sample (inch)
C     BN    the grooved thickness of the C(T) sample (inch)
C     P     maximum applied load (kips)
C     E     elastic modulus (ksi)
C     XM,D  true strain = true stress/E + D x (true stress/yield
            stress)^m.  XM is m here.
C     YS    the yield strength (ksi)
C     XN    strain rate =A x stress^n, XN is n here
C     MU    Poisson ratio
C     NC    number of cycles
C     PD    period = 1/frequency (second)
C     R     load ratio = Pmin/Pmax

      DIMENSION V(0:1000), DADN(0:1000), DDLDT(0:1000)
      DIMENSION DVCDT(0:1000), CST(0:1000), YK(0:1000)
      DIMENSION CT(0:1000), FF(0:1000), DK(0:1000)
```

```
      COMMON TIME(0:1000), A(0:1000), DL(0:1000)
      REAL JP(0:1000)
      CHARACTER*4 TAB
      TAB=CHAR(9)
      PI=4.0*ATAN(1.0)

      W=?
      Y=?
      FROE=?
      BN=?
      B=?
      P=?
      E=?
      XM=?
      XN=?
      D=?
      YS=?
      MU=?
      PD=?
      R=?

C (1) CALCULATE THE MEASURED INITIAL CRACK LENGTH Ao
      OPEN(5,FILE='AZERO.DAT',STATUS='OLD')
      CALL AIF(X,*1000)
      CLOSE (5)
      Ao=X
      WRITE(*,*) 'Ao = ', X
      PAUSE

C (2) CALCULATE THE MEASURED FINAL CRACK LENGTH Af
10    OPEN(5,FILE='AFINAL.DAT',STATUS='OLD')
      CALL AIF(X,*1005)
      CLOSE (5)
      Af=X
```

```
C (3)   READ IN THE TIME, DISPLACEMENT DL AND POTENTIAL DROP
        V DATA
        OPEN(5,FILE='FC.DAT',STATUS='OLD')
        I=-1
20      I=I+1
        READ(5,*) TIME(I),V(I),DL(I)
        IF(TIME(I).GT.-1.0) GOTO 20
        N=I-1
C (4)   CALCULATE THE CRACK LENGTH a(i) FROM Vo AND Vi
        Z1=(W+W)/PI
        Z2=(EXP(Y/Z1)+EXP(-Y/Z1))/2.0
        Z3=COS(Ao/Z1)
        Z4=Z2/Z3
        Z5=ALOG(Z4+SQRT(Z4**2-1))

        DO I=0,N
        Z6=V(I)*Z5/V(0)
        Z7=(EXP(Z6)+EXP(-Z6))/2.0
        A(I)=Z1*ACOS(Z2/Z7)
        END DO

        OPEN(10,FILE='RST1.DAT',STATUS='NEW')
        WRITE(10,*) '   time (hrs.)      a (in.)
     1    dL (in.)       V (volts)'
        WRITE(10,*) '-----------------------------------------
     1-------------------------'
        WRITE(10,*) '  '

        DO I=0,N
        WRITE(10,30) TIME(I),A(I),DL(I),V(I)
        END DO
30      FORMAT(5X,F7.2,8X,F8.4,8X,E12.3,8X,F10.8)

        WRITE(10,*) '  '
        WRITE(10,*) '-----------------------------------------
```

```
     1------------------------'
          WRITE(10,*) '    Ao=',Ao
          WRITE(10,*) '    Af=',Af
          CLOSE(10)

C         CHECK THE VALIDITY OF a(i) DATA
          Z6=(A(N)-Ao)/(Af-Ao)
          IF(Z6.GT.1.15.AND.Z6.LT.0.85) GOTO 1008

C         DETERMINATION OF CRACK GROWTH RATE AND LOADLINE
          DISPLACEMENT RATE
C         PICK OUT DA TOO CLOSED TO THE PREVIOUS ONES
          I=0
          J=0
          JM=0
          XW=0.02*W
          XFROE=0.001*FROE
40        I=I+1

          IF(I.GT.N) GOTO 50
42        DA=A(I)-A(J)
          IF(DA.LT.0.01) GOTO 40
          IF(DA.LE.XW) GOTO 45
          WRITE(*,*) 'WARNING: da > 0.02W OCCURED'
          PAUSE
45        DDL=DL(I)-DL(J)
          IF(DDL.LT.XFROE) GOTO 40
          JM=JM+1
          TIME(JM)=TIME(I)
          A(JM)=A(I)
          DL(JM)=DL(I)
          J=I
          GOTO 40
50        N=JM
```

```
C       CALCULATING da/dN AND dV/dt (DDL/DT HERE)

C (5)   INCREMENTAL POLYNOMIAL METHOD FOR CORRECTING A(I)  AND
DL(I) VALUES
C       AND CALCULATE da/dt and dL/dt
        DO I=3,N-3
        CALL PARABOLA(BAZ,BA1,BA2,BDLZ,BDL1,BDL2,I)
        A(I)=BAZ+BA1*TIME(I)+BA2*TIME(I)*TIME(I)
        DL(I)=BDLZ+BDL1*TIME(I)+BDL2*TIME(I)*TIME(I)
        DADN(I)=(BA1+2.0*BA2*TIME(I))*PD/3600.0
        DDLDT(I)=BDL1+2.0*BDL2*TIME(I)
        END DO

        OPEN(10,FILE='RST2.DAT',STATUS='NEW')
        WRITE(10,*) '  time (hrs.)   a(fit) (in.)   da/dN (in/N)
    1    dL (in.)      dL/dt (in/hr)'
        WRITE(10,*) '-----------------------------------------------
    1-------------------------------'
        WRITE(10,*) '  '

        DO I=3,N-3
        WRITE(10,60) TIME(I),A(I),DADN(I),DL(I),DDLDT(I)
        END DO
60      FORMAT(3X,F7.2,7X,F8.4,5X,E12.3,5X,E12.3,5X,E12.3)
        WRITE(10,*) '  '
        WRITE(10,*) '-----------------------------------------------
    1-------------------------------'
        CLOSE(10)

C (6)   CALCULATE da/dN, K, DELTAK and F'/F (DADN, YK, DK, AND FF
        RESPECTFULLY HERE)
        XK=P/(SQRT(B*BN*W))
        DO I=3,N-3
        AW=A(I)/W
        YK(I)=XK*(2.0+AW)*F(AW)/(SQRT(1-AW))**3.0
```

```
      DK(I)=YK(I)*(1.0-R)
      FF(I)=(1.0/(2.0+AW)+3.0/(2.0*(1.0-AW)))+FP(AW)/F(AW)
      END DO

      OPEN(10,FILE='ASTM.DAT',STATUS='NEW')
      WRITE(10,*) '  time     N        a        da/dN
     1         K         DK'
      WRITE(10,*) '  ----------------------------------------
     1---------------------------------'
      WRITE(10,*) '  '
      TT=0.0

      DO I=3, N-3
      TN=TIME(I)*3600.0/PD
66    WRITE(10,70) TIME(I),TN,A(I),DADN(I),YK(I),DK(I)
      END DO

70    FORMAT(1X,F7.2,2X,F9.2,2X,F8.4,2X,E12.5,2X,
     1  E12.5,2X,E12.5)
      WRITE(10,*) '  '
      WRITE(10,*) '  ----------------------------------------
     1---------------------------------'
      CLOSE(10)

C ANOTHER "IF" OUTLET OF (1) AND (2)
      GOTO 1010
1000WRITE(*,*) 'DATA OF Ao NOT VALID'
      CLOSE (5)
      GOTO 10
1005WRITE(*,*) 'DATA OF Af NOT VALID'
      CLOSE (5)
1008WRITE(*,*) 'DATA OF Ai NOT VALID'
1010PAUSE
      STOP
      END
```

```
C       SUBROUTINE OF (1) & (2)
        SUBROUTINE AIF(X,*)
C       CALCULATE THE MEASURED INITIAL OR FINAL CRACK LENGTH
        Ao OR Af
        DIMENSION AM(0:10)
        DO I=1,9
        READ(5,10) AM(I)
        WRITE(*,*) AM(I), I
10      FORMAT(1X,F8.4)
        END DO
        X=(AM(1)+AM(9)+2*(AM(2)+AM(3)+AM(4)+AM(5)+AM(6)
     1  +AM(7)+AM(8)))/16
        WRITE(*,*) 'X=',X
        PAUSE

C       CHECK THE VALIDITY OF THE MEASURED INITAL OR FINAL
        CARCK LENGTH
        DO I=1,9
        B=(ABS(X-AM(I)))/X
        IF(B.GT.0.05) RETURN 1
        END DO
        RETURN
        END
C       SUBROUTINE FOR CALCULATION THE REGRESSION PARAMETERS
        BY LEAST SQUARES METHOD
        SUBROUTINE PARABOLA(BAZ,BA1,BA2,BDLZ,BDL1,BDL2,I)
        COMMON TIME(0:1000), A(0:1000), DL(0:1000)

        AL1=TIME(I-3)
        AASZ1=A(I-3)
        DLAZ1=DL(I-3)
        DO J=I-3,I+2
        AL1=AL1+TIME(J+1)
        AASZ1=AASZ1+A(J+1)
        DLAZ1=DLAZ1+DL(J+1)
```

```
      END DO
      ALFA1=AL1/7.0
      AASZ=AASZ1/7.0
      DLASZ=DLAZ1/7.0

      ALU2=TIME(I-3)*(TIME(I-3)-ALFA1)**2
      ALD2=(TIME(I-3)-ALFA1)**2
      AAS1U=A(I-3)*(TIME(I-3)-ALFA1)
      DLA1U=DL(I-3)*(TIME(I-3)-ALFA1)
      DO J=I-3, I+2
      ALU2=ALU2+TIME(J+1)*(TIME(J+1)-ALFA1)**2
      ALD2=ALD2+(TIME(J+1)-ALFA1)**2
      AAS1U=AAS1U+A(J+1)*(TIME(J+1)-ALFA1)
      DLA1U=DLA1U+DL(J+1)*(TIME(J+1)-ALFA1)
      END DO
      ALFA2=ALU2/ALD2
      BETA1=ALD2/7.0
      AAST1=AAS1U/ALD2
      DLAT1=DLA1U/ALD2

      AAS2U=A(I-3)*(TIME(I-3)**2-(ALFA1+ALFA2)
     1  *TIME(I-3)+ALFA1*ALFA2-BETA1)
      DLA2U=DL(I-3)*(TIME(I-3)**2-(ALFA1+ALFA2)
     1  *TIME(I-3)+ALFA1*ALFA2-BETA1)
      AS2D=(TIME(I-3)**2-(ALFA1+ALFA2)
     1  *TIME(I-3)+ALFA1*ALFA2-BETA1)**2
      DO J=I-3, I+2
      AAS2U=AAS2U+A(J+1)*(TIME(J+1)**2
     1  -(ALFA1+ALFA2)*TIME(J+1)+ALFA1*ALFA2-BETA1)
      DLA2U=DLA2U+DL(J+1)*(TIME(J+1)**2
     1  -(ALFA1+ALFA2)*TIME(J+1)+ALFA1*ALFA2-BETA1)
      AS2D=AS2D+(TIME(J+1)**2
     1  -(ALFA1+ALFA2)*TIME(J+1)+ALFA1*ALFA2-BETA1)**2
      END DO
      AAST2=AAS2U/AS2D
```

```
      DLAT2=DLA2U/AS2D

      BAZ=AASZ-AAST1*ALFA1+AAST2*(ALFA1*ALFA2-BETA1)
      BA1=AAST1-AAST2*(ALFA1+ALFA2)
      BA2=AAST2
      BDLZ=DLASZ-DLAT1*ALFA1+DLAT2*(ALFA1*ALFA2-BETA1)
      BDL1=DLAT1-DLAT2*(ALFA1+ALFA2)
      BDL2=DLAT2

      RETURN
      END

C f(a/W) FUNCTION
      FUNCTION F(X)
      F=0.866+4.64*X-13.32*X*X+14.72*X*X*X-5.6*X*X*X*X
      RETURN
      END

C f'(a/W) FUNTION
      FUNCTION FP(X)
      FP= 4.64-26.64*X+44.16*X*X-22.4*X*X*X
      RETURN
      END

      SUBROUTINE NCSPLINE(X,Y,BJN,CJN,DJN,NS,N)
      REAL MU(0:10),L(0:10)
      DIMENSION X(0:10), Y(0:10)
      DIMENSION ALFA(0:10), H(0:10)
      DIMENSION Z(0:10), B(0:10), C(0:10)
      DIMENSION D(0:10)

      DO I=0, N-1
      H(I)=X(I+1)-X(I)
      END DO
```

```
      DO I=1, N-1
      ALFA(I)=3.0*(Y(I+1)*H(I-1)-Y(I)*(X(I+1)
    1 -X(I-1))+Y(I-1)*H(I))/(H(I-1)*H(I))
      END DO

      L(0)=1
      MU(0)=0
      Z(0)=0

      DO I=1, N-1
      L(I)=2.0*(X(I+1)-X(I-1))-H(I-1)*MU(I-1)
      MU(I)=H(I)/L(I)
      Z(I)=(ALFA(I)-H(I-1)*Z(I-1))/L(I)
      END DO

      L(N)=1
      Z(N)=0
      C(N)=0

      J=N
   10 J=J-1
      C(J)=Z(J)-MU(J)*C(J+1)
      B(J)=(Y(J+1)-Y(J))/H(J)-H(J)*(C(J+1)+2.0*C(J))/3.0
      D(J)=(C(J+1)-C(J))/(3.0*H(J))
      IF(J.GT.NS) GOTO 10

      CJN=C(J)
      BJN=B(J)
      DJN=D(J)

      RETURN
      END
```

Appendix D

Program for Creep-Fatigue Crack Propagation Rate Calculation

Instructions:

1. Prepare data files "AZERO.DAT" and "AFINAL.DAT"
2. Prepare data file "CFG.DAT" from the EXCEL "CFG/DAT" file by copy and paste. The units in this file is in hr. for time, volt for potential drop and in for deflection. The last row of datum in this file should be -1.0000 as a sign for the ending of the file. The time and dL must be counted from 0.
3. Input the following parameters with right units by hand. (see ASTM E1457 for their definitions).
4. The file "RST1.DAT" is the first calculation of crack length and deflection from the equations recommended in ASTM standard. File "RST2.DAT" is the fit values of crack length and dL, da/dN, dL/dt. File "ASTM.DAT" is the values of C*(t), Ct, Jp and K calculated with the equations in ASTM standard E-1457 (93).

C	W	the defined width (inch)
C	Yo	the half voltage measuring point distance (inch)
C	FROE	the full range of extensometer (inch)
C	B	the thickness of the Ct sample (inch)
C	BN	the grooved thickness of the Ct sample (inch)
C	P	maximum applied load (kips)
C	E	elastic modulus (ksi)
C	XM,D	true strain = true stress/E + D x (true stress/yield stress)^m, XM is m here.
C	YS	the yield strength (ksi)
C	XN	strain rate =A x stress^n, XN is n here
C	MU	Poisson ratio
C	NC	number of cycles
C	PD	period = 1/frequency (second)
C	R	load ratio = Pmin/Pmax
C	FRN	fraction of the hold time subtracted from t of Pmax to approximate the t for average deflection and deflection rate. FRN = 0.0 ~ 0.5.
C	TH	hold time (second)

```
C       CC      coefficient C of the Paris Law: da/dN = C x delta K **nf
                ([in/(ksi.in1/2)]**nf)
C       XNF  exponent nf of the Paris Law

      DIMENSION V(0:1000), DADN(0:1000), DDLDT(0:1000)
      DIMENSION DADT(0:1000), ATH(0:1000),TN(0:1000)
      DIMENSION DVCDT(0:1000), CST(0:1000), YK(0:1000)
      DIMENSION CT(0:1000), FF(0:1000), DK(0:1000)
      COMMON TIME(0:1000), A(0:1000), DL(0:1000)
      REAL JP(0:1000)

      CHARACTER*4 TAB
      TAB=CHAR(9)

      PI=4.0*ATAN(1.0)

      W=?
      Y=?
      FROE=?
      BN=?
      B=?
      P=?
      E=?

      XM=?
      XN=?
      D=?
      YS=?
      MU=?
      PD=?
      R=?
      FRN=?
      TH=?

C     pure fatigue parameter:
```

```
      CC=?
      XNF=?

C     Calculating the Original Crack Length Ao and the Final Crack     Size Af

C (1) CALCULATE THE MEASURED INITIAL CRACK LENGTH Ao
      OPEN(5,FILE='AZERO.DAT',STATUS='OLD')
      CALL AIF(X,*1000)
      CLOSE (5)
      Ao=X
      WRITE(*,*) 'Ao = ', X
      PAUSE

C  (2) CALCULATE THE MEASURED FINAL CRACK LENGTH Af
10    OPEN(5,FILE='AFINAL.DAT',STATUS='OLD')
      CALL AIF(X,*1005)
      CLOSE (5)
      Af=X

C     Determination of Crack Length
C (3) READ IN THE TIME, DISPLACEMENT DL AND POTENTIAL DROP
      V DATA

      OPEN(5,FILE='CFG.DAT',STATUS='OLD')
      I=-1
20    I=I+1
      READ(5,*) TIME(I),V(I),DL(I)
      IF(TIME(I).GT.-1.0) GOTO 20
      N=I-1

C (4) CALCULATE THE CRACK LENGTH a(i) FROM Vo AND Vi
      Z1=(W+W)/PI
      Z2=(EXP(Y/Z1)+EXP(-Y/Z1))/2.0
      Z3=COS(Ao/Z1)
      Z4=Z2/Z3
```

```
      Z5=ALOG(Z4+SQRT(Z4**2-1))

      DO I=0,N
      Z6=V(I)*Z5/V(0)
      Z7=(EXP(Z6)+EXP(-Z6))/2.0
      A(I)=Z1*ACOS(Z2/Z7)
      END DO

      OPEN(10,FILE='RST1.DAT',STATUS='NEW')
      WRITE(10,*) '   time (hrs.)      a (in.)
     1    dL (in.)       V (volts)'
      WRITE(10,*) '-----------------------------------------------
     1------------------------'
      WRITE(10,*) '  '

      DO I=0,N
      WRITE(10,30) TIME(I),A(I),DL(I),V(I)
      END DO
30    FORMAT(5X,F7.2,8X,F8.6,8X,E12.6,8X,F10.6)

      WRITE(10,*) '  '
      WRITE(10,*) '-----------------------------------------------
     1------------------------'
      WRITE(10,*) '    Ao=',Ao
      WRITE(10,*) '    Af=',Af
      CLOSE(10)
C     CHECK THE VALIDITY OF a(i) DATA

      Z6=(A(N)-Ao)/(Af-Ao)
      IF(Z6.GT.1.15.AND.Z6.LT.0.85) GOTO 1008

C     Determination of Crack Growth rate and Load-Line Displacement Rate
C     PICK OUT DA TOO CLOSED TO THE PREVIOUS ONES
C     (Seting time=0 and DL=0 for Ao was done when preparing data file CFG.DAT
      with excel)
```

```
      I=0
      J=0
      JM=0
      XW=0.02*W
      XFROE=0.001*FROE
40    I=I+1

      IF(I.GT.N) GOTO 50
42    DA=A(I)-A(J)
      IF(DA.LT.0.01) GOTO 40
      IF(DA.LE.XW) GOTO 45
      WRITE(*,*) 'WARNING: da > 0.02W OCCURED'
      PAUSE
45    DDL=DL(I)-DL(J)
      IF(DDL.LT.XFROE) GOTO 40
      JM=JM+1
      TIME(JM)=TIME(I)
      A(JM)=A(I)
      DL(JM)=DL(I)
      J=I
      GOTO 40
50    N=JM

C     Calculating da/dN and (dV/dt)fth (DDL/DT here)

C (5) INCREMENTAL POLYNOMIAL METHOD FOR CORRECTING A(I) AND
C     DL(I) VALUES
C     AND CALCULATE (a)fth, da/dN and (dL/dt)fth. (a)fth and (dL/dt)fth
C     are the a and dL/dt values at the time tfh during the hold time.
C     ATH is for (a)fth and DDLDT for (dL/dt)fth, respectively.

      DO I=3,N-3
      CALL PARABOLA(BAZ,BA1,BA2,BDLZ,BDL1,BDL2,I)
      A(I)=BAZ+BA1*TIME(I)+BA2*TIME(I)*TIME(I)
      ATH(I)=BAZ+BA1*(TIME(I)-FRN*TH/3600.0)
```

```
     1    +BA2*(TIME(I)-FRN*TH/3600.0)*(TIME(I)-FRN*TH/3600.0)
          DL(I)=BDLZ+BDL1*TIME(I)+BDL2*TIME(I)*TIME(I)
          DADN(I)=(BA1+2.0*BA2*TIME(I))*PD/3600.0
          DDLDT(I)=BDL1+2.0*BDL2*(TIME(I)-FRN*TH/3600.0)

          END DO

          OPEN(10,FILE='RST2.DAT',STATUS='NEW')
          WRITE(10,*) '  time (hr)  a(fit) (in)  da/dN (in/cycle)
     1    dL (in.)    (dL/dt)fth (in/hr)'
          WRITE(10,*) '-----------------------------------------------
     1----------------------------------'
          WRITE(10,*) '  '

          DO I=3,N-3
          WRITE(10,60) TIME(I),A(I),DADN(I),DL(I),DDLDT(I)
          END DO
    60    FORMAT(3X,F7.2,7X,F8.6,5X,E12.6,5X,E12.6,5X,E12.6)

          WRITE(10,*) '  '
          WRITE(10,*) '-----------------------------------------------
       1----------------------------------'

          CLOSE(10)

    C     Calculation of Creep Displacement Rate dVc/dt

    C (6) CALCULATE (da/dt)avg.(DADT here). YK and DK are K and     deltaK at the
    C     time of Pmax during the hold time, respectfully here)
    C     (da/dt)avg.=[da/dN-(C.deltaK**nf)]/th

          XK=P/(SQRT(B*BN*W))
          DO I=3,N-3
          AW=A(I)/W
          YK(I)=XK*(2.0+AW)*F(AW)/(SQRT(1-AW))**3.0
```

```
      DK(I)=YK(I)*(1.0-R)
      DADT(I)=(DADN(I)-CC*(DK(I))**XNF)*3600.0/TH

C (7) CALCULATE (dVc/dt)fth (DVCDT here)
C     K, Jp, AND F'/F (YK,JP, and FF respectfully here) are the values
C     at certain time 'tfh' during the hold time to approximate the      average
C     dVc/dt during the hold time. H1 is the value of h1 function,

      XK=P/(SQRT(B*BN*W))
      AWTH=ATH(I)/W
      YK(I)=XK*(2.0+AWTH)*F(AWTH)/(SQRT(1-AWTH))**3.0
      CALL H1(HH1, XM, AWTH)
      PHI=2.0*ATH(I)/(W-ATH(I))
      ALFA=SQRT(PHI*PHI+2.0*PHI+2.0)-(PHI+1.0)
      D1=D*(YS*1.002)**XM
      JP(I)=(D1*HH1/(((YS*1.002)*(W-ATH(I)))**XM))
     1 *((P/(1.455*BN*ALFA))**(XM+1))
      DVCDT(I)=DDLDT(I)-(DADT(I)*BN/P)
     1 *(2.0*YK(I)*YK(I)/E+(XM+1)*JP(I))
      FF(I)=(1.0/(2.0+AWTH)+3.0/(2.0*(1.0-AWTH)))+FP(AWTH)/F(AWTH)
      END DO

C     Determination of (C*(t)-Integral)fth and (Ct)fth
C     (C*(t)fth = CST, (Ct)fth = CT there)
      OPEN(10,FILE='ASTM.DAT',STATUS='NEW')
      WRITE(10,*) '  time     N      afth    (da/dt)avg
     1 C*(t)fth    (Ct)fth      Kfth      deltaK'
      WRITE(10,*) '  ----------------------------------------
     1-----------------------------------------------'
      WRITE(10,*) '  '

      TT=0.0
      DO I=3, N-3

      CS1=P*DVCDT(I)/(BN*(W-ATH(I)))
```

```
      CS2=XN/(XN+1.0)
      CS3=2.0+0.522*(W-ATH(I))/W
      CST(I)=CS1*CS2*CS3
      CT(I)=P*DVCDT(I)*FF(I)/((SQRT(B*BN))*W)

C     Calculate Transition Time

      TN(I)=TIME(I)*3600.0/PD
66    WRITE(10,70) TIME(I),TN(I),ATH(I),DADT(I),
     1 CST(I),CT(I),YK(I),DK(I)

      END DO

70    FORMAT(1X,F7.2,1X,F8.1,1X,F8.4,1X,E12.5,1X,
     1 E12.5,1X,E12.5,1X,E12.5,1X,E12.5)

      WRITE(10,*) ' '
      WRITE(10,*) ' ----------------------------------------
     1-------------------------------------------------'
      CLOSE(10)

C     ANOTHER "IF" OUTLET OF (1) AND (2)
      GOTO 1010
1000WRITE(*,*) 'DATA OF Ao NOT VALID'
      CLOSE (5)
      GOTO 10
1005WRITE(*,*) 'DATA OF Af NOT VALID'
      CLOSE (5)
1008WRITE(*,*) 'DATA OF Ai NOT VALID'
1010PAUSE
      STOP
      END

C SUBROUTINE OF (1) & (2)
```

```
      SUBROUTINE AIF(X,*)

C     CALCULATE THE MEASURED INITIAL OR FINAL CRACK LENGTH
      Ao OR Af
      DIMENSION AM(0:10)
      DO I=1,9
      READ(5,10) AM(I)
      WRITE(*,*) AM(I), I
10    FORMAT(1X,F8.4)
      END DO
      X=(AM(1)+AM(9)+2*(AM(2)+AM(3)+AM(4)+AM(5)+AM(6)+AM(7
      )+AM(8)))/16
      WRITE(*,*) 'X=',X
      PAUSE
C     CHECK THE VALIDITY OF THE MEASURED INITAL OR FINAL
      CARCK LENGTH
      DO I=1,9
      B=(ABS(X-AM(I)))/X
      IF(B.GT.0.05) RETURN 1
      END DO
      RETURN
      END

C     SUBROUTINE FOR CALCULATION THE REGRESSION PARAMETERS
      BY LEAST SQUARES METHOD

      SUBROUTINE PARABOLA(BAZ,BA1,BA2,BDLZ,BDL1,BDL2,I)
      COMMON TIME(0:1000), A(0:1000), DL(0:1000)

      AL1=TIME(I-3)
      AASZ1=A(I-3)
      DLAZ1=DL(I-3)
      DO J=I-3,I+2
      AL1=AL1+TIME(J+1)
      AASZ1=AASZ1+A(J+1)
```

```
      DLAZ1=DLAZ1+DL(J+1)
      END DO
      ALFA1=AL1/7.0
      AASZ=AASZ1/7.0
      DLASZ=DLAZ1/7.0

      ALU2=TIME(I-3)*(TIME(I-3)-ALFA1)**2
      ALD2=(TIME(I-3)-ALFA1)**2
      AAS1U=A(I-3)*(TIME(I-3)-ALFA1)
      DLA1U=DL(I-3)*(TIME(I-3)-ALFA1)
      DO J=I-3, I+2
      ALU2=ALU2+TIME(J+1)*(TIME(J+1)-ALFA1)**2
      ALD2=ALD2+(TIME(J+1)-ALFA1)**2
      AAS1U=AAS1U+A(J+1)*(TIME(J+1)-ALFA1)
      DLA1U=DLA1U+DL(J+1)*(TIME(J+1)-ALFA1)
      END DO
      ALFA2=ALU2/ALD2
      BETA1=ALD2/7.0
      AAST1=AAS1U/ALD2
      DLAT1=DLA1U/ALD2

      AAS2U=A(I-3)*(TIME(I-3)**2-(ALFA1+ALFA2)
     1  *TIME(I-3)+ALFA1*ALFA2-BETA1)
      DLA2U=DL(I-3)*(TIME(I-3)**2-(ALFA1+ALFA2)
     1  *TIME(I-3)+ALFA1*ALFA2-BETA1)
      AS2D=(TIME(I-3)**2-(ALFA1+ALFA2)
     1  *TIME(I-3)+ALFA1*ALFA2-BETA1)**2
      DO J=I-3, I+2
      AAS2U=AAS2U+A(J+1)*(TIME(J+1)**2
     1  -(ALFA1+ALFA2)*TIME(J+1)+ALFA1*ALFA2-BETA1)
      DLA2U=DLA2U+DL(J+1)*(TIME(J+1)**2
     1  -(ALFA1+ALFA2)*TIME(J+1)+ALFA1*ALFA2-BETA1)
      AS2D=AS2D+(TIME(J+1)**2
     1  -(ALFA1+ALFA2)*TIME(J+1)+ALFA1*ALFA2-BETA1)**2
      END DO
```

```
      AAST2=AAS2U/AS2D
      DLAT2=DLA2U/AS2D

      BAZ=AASZ-AAST1*ALFA1+AAST2*(ALFA1*ALFA2-BETA1)
      BA1=AAST1-AAST2*(ALFA1+ALFA2)
      BA2=AAST2
      BDLZ=DLASZ-DLAT1*ALFA1+DLAT2*(ALFA1*ALFA2-BETA1)
      BDL1=DLAT1-DLAT2*(ALFA1+ALFA2)
      BDL2=DLAT2

      RETURN
      END

C     f(a/W) FUNCTION

      FUNCTION F(X)
      F=0.866+4.64*X-13.32*X*X+14.72*X*X*X-5.6*X*X*X*X
      RETURN
      END

C     f'(a/W) FUNTION

      FUNCTION FP(X)
      FP= 4.64-26.64*X+44.16*X*X-22.4*X*X*X
      RETURN
      END

C     SUBROUTINE FOR CALCULATING H1 VALUES

      SUBROUTINE H1(HH1,XX,AW)

      DIMENSION X(0:15), Y(0:15), YY(0:15)
      DIMENSION H(6,15), XM(0:15), YAW(0:15)

C  (2)READ IN THE NODE VALUES Hij
```

```
      OPEN(5,FILE='H1.DAT',STATUS='OLD')

      DO J=0,9
      READ(5,10) XM(J)
      END DO

      DO I=0,5
      READ(5,10) YAW(I)
      END DO

      DO J=0, 9
      DO I=0, 5
      READ(5,10) H(I,J)
      END DO
      END DO

10    FORMAT(6F7.4)

C  (3)FIND OUT THE INTERVAL [XMj, XMj+1] FOR THE INPUT m
C     AND INTERVAL [YAWi, YAWi+1] FOR THE INPUT A/W

      J=-1
30    J=J+1
      IF(XX.GE.XM(J)) GOTO 30
      JN=J-1

      I=-1
40    I=I+1
      IF(AW.GE.YAW(I)) GOTO 40
      IN=I-1

C  (4)CALCULATE H1 = f(A/W, m)

      DO I=0,5
      DO J=0,9
```

```
X(J)=XM(J)
Y(J)=H(LJ)
END DO
NS=JN
N=9
CALL NCSPLINE(X,Y,BJN,CJN,DJN,NS,N)
YY(I)=Y(JN)+BJN*(XX-X(JN))+CJN*(XX-X(JN))**2.0+DJN*(XX-
X(JN))**3.0
END DO

DO I=0,5
X(I)=YAW(I)
Y(I)=YY(I)
END DO
NS=IN
N=5
CALL NCSPLINE(X,Y,BJN,CJN,DJN,NS,N)
HH1=Y(IN)+BJN*(AW-X(IN))+CJN*(AW-X(IN))**2.0+DJN*(AW-
X(IN))**3.0
RETURN
END

SUBROUTINE NCSPLINE(X,Y,BJN,CJN,DJN,NS,N)

REAL MU(0:10),L(0:10)
DIMENSION X(0:10), Y(0:10)
DIMENSION ALFA(0:10), H(0:10)
DIMENSION Z(0:10), B(0:10), C(0:10)
DIMENSION D(0:10)

DO I=0, N-1
H(I)=X(I+1)-X(I)
END DO

DO I=1, N-1
```

```
      ALFA(I)=3.0*(Y(I+1)*H(I-1)-Y(I)*(X(I+1)
     1 -X(I-1))+Y(I-1)*H(I))/(H(I-1)*H(I))
      END DO

      L(0)=1
      MU(0)=0
      Z(0)=0

      DO I=1, N-1
      L(I)=2.0*(X(I+1)-X(I-1))-H(I-1)*MU(I-1)
      MU(I)=H(I)/L(I)
      Z(I)=(ALFA(I)-H(I-1)*Z(I-1))/L(I)
      END DO

      L(N)=1
      Z(N)=0
      C(N)=0

      J=N
   10 J=J-1
      C(J)=Z(J)-MU(J)*C(J+1)
      B(J)=(Y(J+1)-Y(J))/H(J)-H(J)*(C(J+1)+2.0*C(J))/3.0
      D(J)=(C(J+1)-C(J))/(3.0*H(J))
      IF(J.GT.NS) GOTO 10

      CJN=C(J)
      BJN=B(J)
      DJN=D(J)

      RETURN
      END
```

VITA

Weiju Ren was born in Chengdu, Mainland China in 1957. Inspired by the spirit of democracy and freedom of the American people, his father, a history teacher, name him Weiju (means Great Torch in Chinese) after the torch of the Statue of Liberty. Born in a big city full of great historic and cultural heritage, he was interested in liberal arts in his early ages. During his high school education, he spent one year at a school owned by one of the three biggest turbine companies of China, where he became also interested in engineering. Unfortunately, because of political and social chaos, formal higher education was not available in China when he graduated form high school. He spent time performing in a band, wandering in streets, visiting farms and factories, and finally, with the help of his parents, relatives and friends, he obtained an opportunity to audit courses in the Foreign Language Department of Sichuan University, where he learned some English and Japanese. In 1977, China resumed her formal higher education. After a tough, nation wide examination in 1978, he was enrolled into Tsinghua University in Beijing, one of the best universities in China. He finished the required 5 year courses and obtained his B.S. in mechanical engineering from Tsinghua University in 1983. In September 1983, he went to the graduate school of Tianjin University in Tianjin, the oldest university and also one of the best in China. He conducted his research under the direction of Professor Wenyie Zhang, a famous Chinese researcher in welding engineering. During his study and research in Tianjin University, he independently designed and built with his own hands a computer-control welding simulation system, and obtained his M.S. in mechanical engineering in May, 1986. He stayed in Tianjin University as a research associate, helping Professor Zhang in directing graduate students in the welding simulation system program. Then he started to take some courses required for a Ph.D. program. In February 1989, he came to the University of Tennessee as a visiting research associate, conducting research in welding and microwave processing of ceramics. In Fall of 1990, he registered as a

graduate student in the Department of Materials Science and Engineering, the University of Tennessee, for his Ph.D. degree with Dr. P. K. Liaw and Dr. T. T. Meek as his advisors. He performed his Ph.D. dissertation research in the time-dependent fracture mechanics at the Metals and Ceramics Division, Oak Ridge National Laboratory, Oak Ridge, Tennessee, and obtained his Ph.D. degree in metallurgical engineering in Spring of 1995. He will continue his research in the Oak Ridge National Laboratory.